CHEMICALLY MEDIATED PLANKTON INTERACTIONS – PREVALENCE, UPTAKE, AND TARGETS OF POLYUNSATURATED ALDEHYDES

DISSERTATION

(KUMULATIV)

zur Erlangung des akademischen Grades doctor rerum naturalium

(Dr. rer. nat.)

vorgelegt dem Rat der Chemisch-Geowissenschaftlichen Fakultät

der Friedrich-Schiller-Universität Jena von Diplom-Chemikerin

Stefanie Wolfram

geboren am 11.04.1985 in Pößneck

To my family

TABLE OF CONTENTS

DANKSAGUNG

Abstract/Kurzzusammenfassung

Abstract: Diatoms are key players in the aquatic ecosystem as they significantly contribute to photosynthetic carbon assimilation and transfer of energy to higher trophic levels. Some of these single celled algae produce polyunsaturated aldehydes (PUAs), which are derived from enzymatic oxidation of fatty acids. These aldehydes are known to interfere with the reproduction of their predators and have been suggested to act as info- and allelochemicals.

Compared to the biological functions of PUAs, their mechanisms of action have been less investigated. Here, I present PUA quantification data for plankton communities and provide experimental results for an enhanced mechanistic understanding of these oxylipins.

To perform the studies, I established fluorescent probes according to the activity-based protein profiling (ABPP) strategy on the basis of PUAs and bioinactive saturated aldehydes. I developed key methodological approaches (feeding and two-step incubation protocols, procedures for fluorescence microscopy) and a novel probe reporter that is a useful and universal tool in chemical biology. Uptake studies showed that the PUA-derived probe entered algal cells and accumulated in the gonads of a predator. Moreover, investigation of targets based on covalent reactions with PUAs revealed several labeled proteins in a diatom. This first proteomic approach suggests that key metabolic pathways are affected by PUAs.

Kurzzusammenfassung: Diatomeen nehmen in aquatischen Ökosystemen eine Schlüsselrolle ein, da sie bedeutend zur Kohlenstoffassimilation durch Photosynthese und zum Energietransfer zu höheren trophischen Stufen beitragen. Einige dieser einzelligen Algen produzieren polyungesättigte Aldehyde (PUA), die durch die enzymatische Oxidation von Fettsäuren entstehen. Diese Aldehyde beeinträchtigen die Reproduktion ihrer Fraßfeinde und wirken möglicherweise als Info- und Allelochemikalien.

Verglichen mit den biologischen Wirkungen der PUA sind ihre Wirkmechanismen weniger untersucht worden. In dieser Arbeit habe ich PUA in Planktongemeinschaften quantifiziert und stelle experimentelle Ergebnisse für ein verbessertes mechanistisches Verständnis dieser Oxylipine vor.

Für die Untersuchungen etablierte ich fluoreszierende Sonden nach der aktivitätsbasierten Protein-Profiling (ABPP)-Strategie auf Basis eines PUA und eines bioinaktiven gesättigten Aldehyds. Außerdem entwickelte ich zentrale methodische Ansätze (Fütterungs- und zweistufige Inkubationsprotokolle, Abläufe für die Fluoreszenzmikroskopie) und einen neuartigen Reporter für Sonden, der ein hilfreiches und universelles Instrument in der chemischen Biologie darstellt. Die PUA-abgeleitete Sonde wurden in Algenzellen aufgenommen und reicherte sich in den

Gonaden eines Fraßfeindes an. Die Untersuchung von Targets auf Basis kovalenter Reaktionen mit PUA ergab zudem verschiedene markierte Proteine in einer Diatomee. Dieser erste proteomische Ansatz weist darauf hin, dass wichtige Stoffwechselvorgänge durch PUA beeinflusst werden.

ABBREVIATIONS

ABP	activity-based probe	EPA	eicosapentaenoic acid
ABPP	activity-based protein profiling	ESI	electrospray ionization
ATP	adenosine triphosphate	GC-MS	gas chromatography coupled to mass spectrometry
AtpA	gene name of ATP synthase subunit alpha	gDNA	genomic DNA
AtpB	gene name of ATP synthase subunit beta	HD	2*E*,4*Z*-heptadienal
		HNE	4-hydroxy-2-nonenal
BNS	*N*-(3-azidopropyl)-6-bromo-5-(dimethylamino)naphthalene-1-sulfonamide	HSAB	hard and soft acids and bases
		HSF1	heat shock factor 1
		Hsp	heat shock protein
BODIPY	dipyrromethene boron difluoride	IAP	inhibitor of apoptosis protein
		ICAT	isotope-coded affinity tags
BPT	4-(3-azidopropoxy)-5-(4-bromophenyl)-2-(pyridin-2-yl)thiazole	IDBEST	isotope-differentiated binding energy shift tags
BrdU	bromodeoxyuridine	iTRAQ	isobaric tags for relative and absolute quantitation
CAS	cellular apoptosis susceptibility protein	LC-MS	liquid chromatography coupled to mass spectrometry
CE	capillary electrophoresis	LC-MS/MS	liquid chromatography/ tandem mass spectrometry
CuAAC	Cu(I)-catalyzed azide-alkyne cycloaddition	LHC	light harvesting complex
Cy	cyanine	LOX	lipoxygenase
Cdk1	cyclin-dependent kinase 1	MALDI	matrix-assisted laser desorption/ionization
DD	2*E*,4*E/Z*-decadienal		
DDA	data-dependent acquisition	MRSA	methicillin-resistant *Staphylococcus aureus*
DDY	2*E*,4*E*-decadien-9-ynal		
DIA	data-independent acquisition	MudPIT	multidimensional protein identification technology
DIGE	difference gel electrophoresis		
DNS	*N*-(3-azidopropyl)-5-(dimethylamino)naphthalene-1-sulfonamide	NBD	*N*-(3-azidopropyl)-7-nitrobenzo[*c*][1,2,5]oxadiazol-4-amine
DT	2*E*,4*E/Z*,7*Z*-decatrienal	NBD-Cl	4-chloro-7-nitrobenzo[*c*][1,2,5]oxadiazole
DMSP	β-dimethylsulfoniopropionate		

NHS	*N*-hydroxysuccinimide	SA	5-hexynal
NIR	near infrared	SDS-PAGE	sodium dodecyl sulfate poly-acrylamide gel electrophoresis
NO	nitric oxide		
OD	2*E*,4*Z*-octadienal	SPME	solid phase microextraction
OT	2*E*,4*Z*,7*Z*-octatrienal	TAMRA	tetramethylrhodamine
PFB	*O*-2,3,4,5,6-pentafluorobenzyl	TAMRA-SA	SA coupled to TAMRA
PRK	phosphoribulokinase	TAMRA-PUA	DDY coupled to TAMRA
PUA	polyunsaturated aldehyde	TEV	tobacco etch virus
PUFA	polyunsaturated fatty acid	TOP	tandem orthogonal proteolysis
RG	reactive group	TUNEL	terminal deoxynucleotidyl trans-ferase-mediated deoxyuridine triphosphate nick-end labeling
ROS	reactive oxygen species		
RPE	ribulose-phosphate-3-epimerase		

LIST OF FIGURES

1 INTRODUCTION

1.1   Chemical defense of marine phytoplankton

Oceans contain a great diversity of life and harbor the habitat for plankton, which comprises all free-floating organisms. Autotrophic bacteria, microalgae, and dinoflagellates form the basis of phytoplankton and contribute to this diversity. Numerically, the most abundant phytoplankton group is represented by the prokaryotic cyanobacteria [1]. The three dominant eukaryotic phyto-plankton clades are diatoms, dinoflagellates, and coccolithophores [1]. Diatoms, a class of unicellular algae with silicified cell walls and a huge variety of shapes (Figure 1), are found in marine and fresh water and can be either free-living in the water column or form biofilms on a solid substratum [1]. They are key players in the marine food web (Figure 2) as they contribute to almost 40% of global oceanic primary productivity [2].
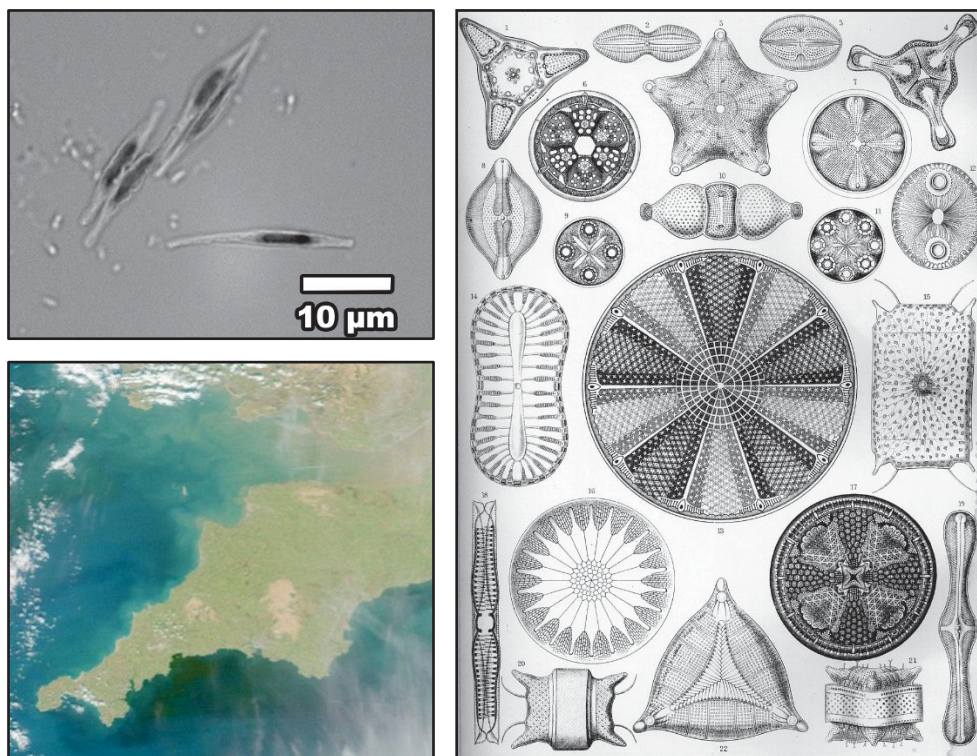
Figure 1.   **Light microscopy image of the diatom *Phaeodactylum tricornutum* (top left), algal bloom of *Skeletonema costatum* around Cornwall and the south of Wales in March 2011 [3] (bottom left), and different diatom structures drawn 1904 by Ernst Haeckel [4] (right).**

A characteristic feature for some diatom species is the formation of algal blooms around coasts and in the open water. In the north-east Atlantic and associated coasts they typically occur as spring blooms when the nutrient intake is high and the herbivorous grazer population and activity is low (Figure 1, bottom left) [5]. Among the grazers copepods, a class of small crustaceans with a usual length of 1 to 2 mm [6], belong to the main predators of diatoms (Figure 2).
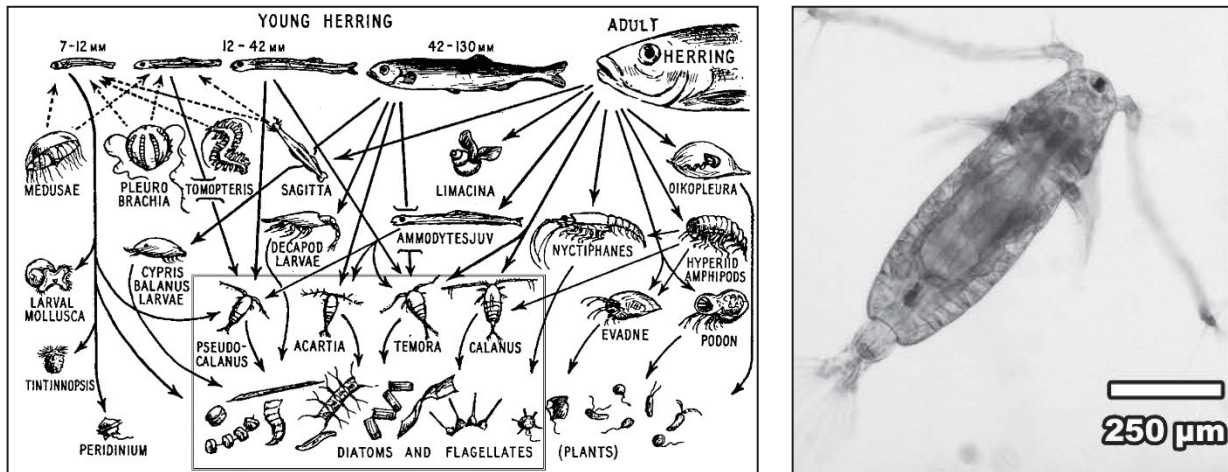
Figure 2.   **The classical view of the marine food web after Hardy, 1956 [7] (left) and light microscopy image of the copepod *Acartia tonsa* (right).** The box inside the marine food web highlights the predator-prey relation of copepods and phytoplankton including diatoms.

Different defense strategies of the phytoplankton have been developed during evolution including morphological features such as mechanical defense in form of silicified cell walls of diatoms [8] (Figure 1, right) or formation of large colonies concentrated in voluminous polysaccharide spherical shells (e.g., in *Phaeocystis pouchetii*), which cannot be ingested by the comparably small herbivores [9].

A chemical defense strategy comprises liberation of toxic substances such as domoic acid from *Pseudo-nitzschia multiseries* [10,11] or paralytic shellfish toxins (e.g., saxitoxin) of the genus *Alexandrium* (reviewed in [12,13]). This constitutive chemical defense bases on the storage of toxic substances in the cell [12]. Release of these toxins during phytoplankton blooms may threaten public health by bioaccumulation in shellfish and cause massive fish kills and thus creates economic problems for fisheries. However, the direct effects on predators are poorly understood (reviewed in [12,14]).

Recently, also indications for an induced chemical defense strategy based on domoic acid for a *Pseudo-nitzschia* species in response to copepods were presented [15]. This defense is generally characterized by perception of signals from a herbivore or pathogen that causes biosynthetic upregulation of harmful metabolites [12]. Also waterborne cues from the copepod *A. tonsa* induced production of paralytic shellfish toxins like in the dinoflagellate *Alexandrium minutum*, which correlated with increased resistance to copepod grazing [16].

By contrast, during activated chemical defense, potent compounds are produced from less potent storage forms upon cell disruption, which diminishes the risk of self-toxicity. A wide-spread proposed defense model among marine algae involves cleavage of β-dimethylsulfonio-propionate (DMSP) by the enzyme DMSP-lyase after wounding. Both of the resulting products, dimethyl sulfide and acrylate, possibly act as feeding deterrents [17,18].

Another activated defense strategy has been reported for diatoms [19,20]. Traditionally, these microalgae are considered as beneficial food source for copepods, which build the basis for top consumers and thus fisheries (Figure 2, left), but a series of studies of diatom effects on the reproductive success of copepods revealed diminished hatching success and malformations in the copepod offspring (reviewed in [21]). These effects had never been demonstrated before the initial studies of the 1990th for unicellular algae [21]. In 1999, Miralto *et al.* isolated the low molecular weight polyunsaturated aldehydes (PUAs) 2*E*,4*E*/*Z*-decadienal (DD) and 2*E*,4*E*/*Z*,7*Z*-dectrienal (DT) from the diatoms *Thalassiosira rotula*, *S. costatum*, and *Pseudo-nitzschia delicatissima* that were made responsible for arrested embryonic development in copepods and sea urchins [22] (Figure 3).
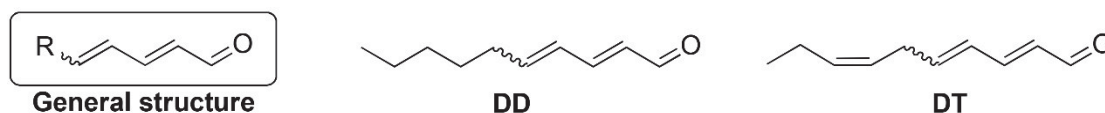
Figure 3. **General structure and examples of PUAs.** All PUAs contain the essential structural α,β,γ,δ-unsaturated aldehyde element (R = alkyl, alkenyl, alkyl/alkenoic acid) [23]. The α,β-double bond is always *trans*-constituted (see chapter 1.2.1). DD and DT were identified in marine diatoms by Miralto *et al.* [22].

PUA production occurs within seconds after wounding of diatoms [20] and involves different enzymatic processes responsible for release and transformation of fatty acids, which is summarized in the next section. The PUA production after mechanical disruption of phytoplankton (referred as particulate PUA) in surface waters ranges from zero up to picomolar concentrations in the Atlantic Ocean [24] (for cells > 10 µm) and nanomolar concentrations in the Adriatic Sea [25] (for cells > 1.2 µm), where 2*E*,4*Z*-heptadienal (HD) is the most abundant metabolite.

The production of these aldehydes was mainly attributed to marine diatoms, in which PUA production is wide-spread; the metabolites have been found in pelagic species, floating in the open ocean, and benthic diatoms, living on the sediment or sub-sediment layers [26]. PUAs have also been detected in freshwater diatoms [26,27], other microalga species [28], and macroalgae [29,30]. In addition, PUA production and occasionally proposed ecological and biological functions (e.g., pheromone activity, chemical defense against predators, increase of inflammatory processes) are known from other organisms such as mosses [31,32], higher plants [33-35], insects [36,37], and mammals [38]. Occurrence of these aldehydes in food products (e.g., bread, fish) [39-41] and heated oil [42] is known as well.

1.2   Biosynthesis, biological functions, targets, and mode of action of (poly)unsaturated aldehydes

1.2.1   Biosynthesis of PUAs

PUAs biosynthetically derive from oxidative transformation of free polyunsaturated fatty acids (PUFAs, Figure 4) [20,43] and thus belong to the class of oxylipins. PUA-production in diatoms is highly species- and even isolate-dependent [23] and limited by the availability of substrate fatty acids [44].
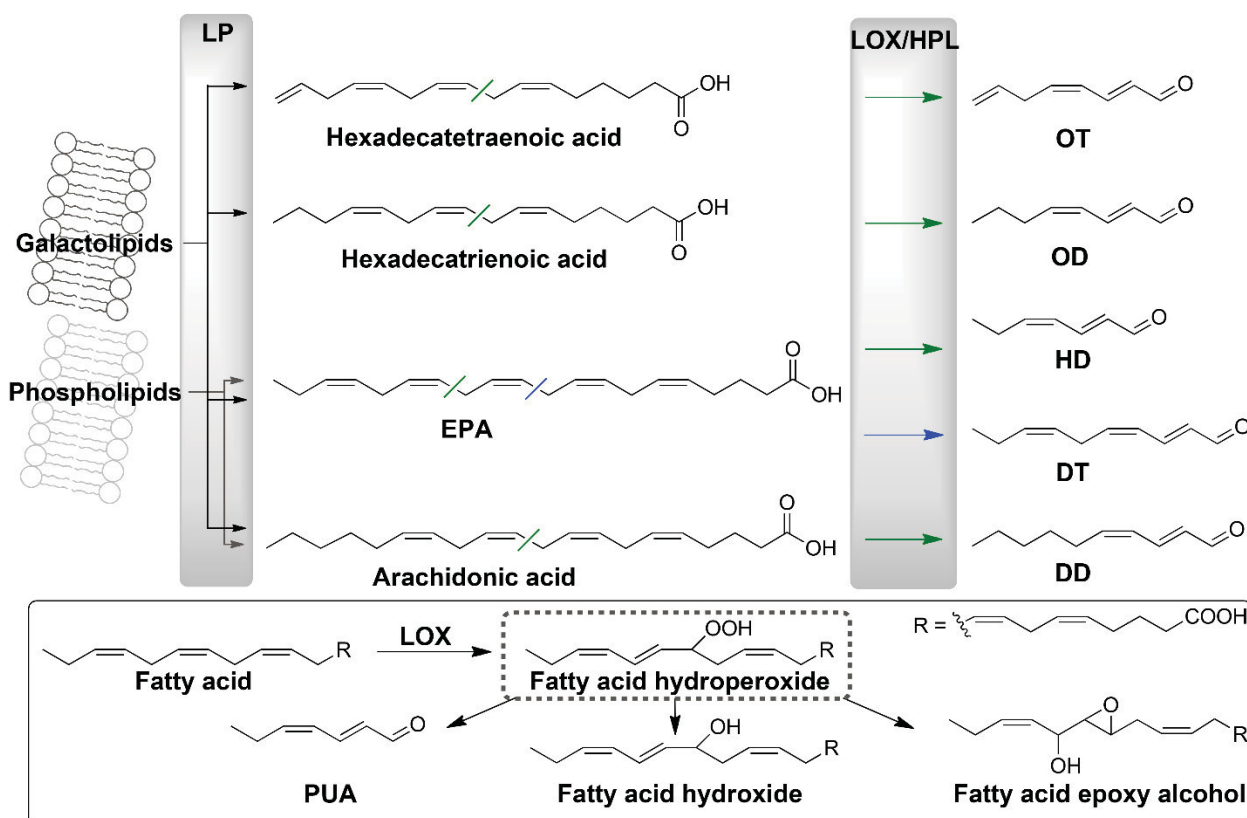
Figure 4.   Biosynthesis of volatile PUAs in *S. costatum/T. rotula* (top) and sketch for the biosynthesis of different oxylipins in *S. costatum/Chaetoceros affinis* after [45] (bottom). Enzyme activities are marked in gray boxes and formal bond cleavage of fatty acids are labeled with green/blue lines (top). Biosynthesis of PUAs and other oxylipins is preceded by formation of fatty acid hydroperoxides from fatty acids (here exemplarily presented for EPA; stereochemistry is not considered; bottom). PUAs have not been detected in *Chaetoceros affinis* [45]. (Abbreviations – HPL: hydroperoxide lyase; LOX: lipoxygenase; LP: lipase)

In *T. rotula*, DD and DT originate from the fatty acids arachidonic acid (C20:4ω6[I]) and eicosapentaenoic acid (EPA, C20:5ω3), respectively [20]. EPA was also confirmed to be converted into the shorter chain PUA HD in *S. costatum* [46]. 2*E*,4*Z*-octadienal (OD) is derived from hexadecatrienoic acid (C16:3ω4) in *S. costatum* [47] and *T. rotula* [48] and 2*E*,4*Z*,7*Z*-octatrienal (OT) from the

---

[I] **Fatty acid nomenclature**: in the example C20:4ω6, C20 refers to the number of carbon atoms of the fatty acid, 4 indicates the number of C-C double bonds and ω6 the position of the first double bond counted from the methyl end.

corresponding tetraenoic fatty acid (C16:4ω1) in the same species [46,49] (Figure 4). The dienals and trienals are presumably released as 2E,4Z- and 2E,4Z,7Z-structures but isomerize to the corresponding 2E,4E- and 2E,4E,7Z-isomers [47,50]. 4E- and 4Z-dienals and trienals show the same antiproliferative activity [51]. Besides volatile, also polar oxo-acids like 9-oxo-nona-5Z,7E-dienoic acid derived from EPA in the diatom *P. tricornutum* and 12-oxo-dodeca-5Z,8Z,10E-trienoic acid[II] (not shown in Figure 4) are known [23].

The precursor fatty acids are released from phospho- and galactolipids immediately after cell disruption upon wounding. Whereas hexadecatrienoic and hexatetraenoic acids originate almost exclusively from chloroplastic galactolipids via galactolipase activity [46,52], phospholipase A$_2$ and galactolipase activities release arachidonic acid and EPA from the hydrolysis of the corresponding lipids [19,46] in *S. costatum* and/or *T. rotula*. In a first step, lipoxygenase (LOX)-mediated oxidation of PUFAs leads to hydroperoxides (Figure 4, bottom) followed by a species-dependent bifunctional LOX- or hydroperoxide lyase- or halolyase-mediated cleavage to the corresponding PUAs [43,53,54].

1.2.2   Biological functions of PUAs

Since the identification of the first diatom-derived PUAs by Miralto *et al*. in 1999 [22] (Figure 3), diatom-copepod interactions evolved to a highly investigated research area. The effects of PUA-producing diatom diets on copepod reproduction in field and laboratory studies revealed negative effects on copepod gametogenesis, gamete functionality, embryogenesis and egg hatching success as well as impaired development and induced malformations in the copepod offspring (reviewed in [21,43,55]). PUAs were made responsible for these anti-proliferative and teratogenic effects[III] [22,56] that enable a diatom defense strategy against predators (Figure 5).
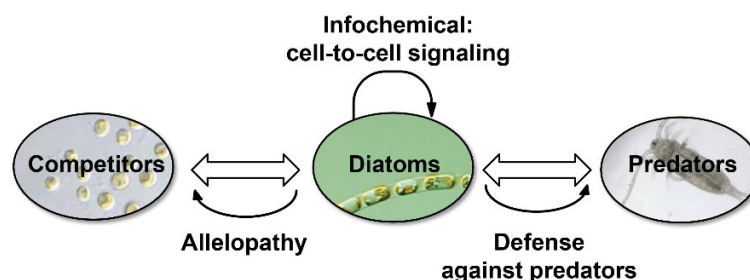
Figure 5. **Schematic representation of the ecological roles of PUAs in diatom-plankton interactions after Leflaive and Ten-Hage [57].** White arrows indicate interactions between diatoms and grazing predators or competitors, whereas some of which are probably mediated by PUAs (black arrows). The main effects include reproductive failure in predators (PUAs as defense metabolites), growth inhibition of competing organisms (PUAs as allelochemicals), and control of degenerative processes (PUAs as infochemicals in cell-to-cell communication).

[II] In the alga *Asterionella formosa* 12-oxo-dodeca-5Z,8Z,10E-trienoic acid derives from EPA or arachidonic acid [20]

[III] **Teratogens** are substances that cause congenital defects in the offspring of organisms when they are exposed during gestation [21].

A worldwide laboratory study indicated the wide distribution of teratogenic effects: 16 different copepod species showed a response in egg production and egg viability when fed with 16 out of 17 diatom diets compared to non-diatom controls [58]. Not the single diatom cell but rather the community benefits from this defense strategy by reducing the grazing pressure of subsequent generations of copepods [21].

In physiological studies, the direct role of PUAs revealed teratogenic effects on copepods [56,59], polychaetes, sea urchins and other organisms (reviewed in [21]). Among PUAs, DD is the best studied metabolite. Besides being teratogenic to copepods, it is cytotoxic and inhibits the growth of bacteria and fungi [60] and induces apoptosis in a human cancer cell line [22].

PUAs of different chain lengths and side chain polarities are bioactive; thus activity is structure specific and depends on the presence of an α,β,γ,δ- or at least an α,β-unsaturated aldehyde motive, whereas saturated aldehydes are not active [51,60].

While PUAs can explain several studies of poor copepod reproduction in response to diatom diets, their adverse effect is not universal. Some laboratory and especially field studies [61-65] failed to show a direct correlation between PUA production and reproductive failure in copepods and thus, the anti-proliferative role of PUAs remains contradictory [21,43,44].

A couple of alternative explanations, including lipid peroxidation products other than PUAs, were made responsible for the observed teratogenic effects [45]: LOX-induced higher molecular weight oxylipins like fatty acid hydroperoxides (these include the precursors of PUAs), hydroxides, and epoxy alcohols (Figure 4, bottom) [44,45,66] as well as highly reactive oxygen species (ROS), such as the hydroxyl radical [45], have been considered as trigger. Also depletion of PUFAs [44], differences in the nutritional quality of unicellular algae in general [67], poor nutrient uptake due to rapid gut passage time of certain diatom species [68], and combinations of these metabolites and effects were considered.

The most investigated function of diatom-derived PUAs is their role in chemical defense against copepods. However, evidence for their function in intra- and other interspecific interactions has been suggested (reviewed in [57], Figure 5). This concept was supported by Vidoudez and Pohnert [69], who described for the first time a release of PUAs by intact *S. costatum* cells in laboratory studies. Thereby it was demonstrated that PUAs do not only occur upon wounding of diatom cells but are also actively released in the late stationary phase of the intact algae [69]. Later, the active release was confirmed in mesocosm (large enclosures filled with sea water) and field studies [25,70]. This may point towards PUAs' potential to initiate termination of algal blooms by cell lysis [25,69,71,72]. During a bloom, stress and cell lysis rates increase and PUA concentration may exceed a threshold and trigger population-level cell death [71]. Vardi *et al.* suggested a cell-to-cell signaling mechanism for *Thalassiosira weissflogii* and *P. tricornutum* [71]. Thereby, DD triggered intracellular calcium transients and rapid formation of nitric oxide (NO) by

a calcium-dependent NO-synthase-like activity. DD-caused stress could be transmitted to non-exposed cells by a diffusible NO-inducing signal from stressed cells in *P. tricornutum*, demonstrating the existence of a sophisticated stress surveillance system. Pretreatment with sublethal concentrations of DD stimulated resistance to subsequent lethal doses. This additionally supports the idea that PUAs may play a role as infochemicals[IV] in mediating plankton interactions [71]; the same phenomenon was also presented for the diatom *S. costatum* [69].

PUAs may act as allelochemicals[V] in interspecific phytoplankton interactions (Figure 5) by suppressing the growth of other species. DD is the most potent growth inhibitor among PUAs, affecting the diatoms *T. weissflogii* [74] and *S. costatum* [28], the chlorophyte *Dunaliella tertiolecta* [75], the dinoflagellate *Amphidinium carterae* [75], the prymnesiophyte *Isochrysis galbana* [75], and some marine bacteria [76]. Besides PUAs, also PUFAs may have an allelopathic effect on bacteria (reviewed in [57]).

1.2.3   Targets and mode of action of (poly)unsaturated aldehydes

Acrolein, 4-hydroxy-2-nonenal (HNE), and crotonaldehyde are the most reactive and toxic α,β-unsaturated aldehydes [77]. These substances contribute to electrophilic stress and disrupt normal cellular functions [77]. Unsaturated aldehydes, particularly the above mentioned, have been shown to covalently react with nucleophilic centers of diverse biomolecules such as amino acids, peptides, proteins, DNA, RNA, lipids, and phospholipids [78,79].

The activity of unsaturated aldehydes (2-enals) and PUAs containing a 2,4-dienal motive (with optional non-conjugated double bonds) can be attributed to the electrophilic Michael acceptor structural element that reacts with accessible nucleophiles such as thiol and amine groups of proteins or amine groups of the bases of DNA and RNA [80]. In contrast to saturated aldehydes, conjugation of the alkene with the carbonyl group makes the β-carbon positively polarized. Thus, the β-carbon becomes the preferred site of nucleophilic attack of soft nucleophiles such as thiols [81,82]. In this 1,4-Michael-type addition[VI], the arising enol is rapidly tautomerized to a Michael-type product [82] (Figure 6, right top). For $\alpha,\beta,\gamma,\delta$-unsaturated aldehydes like DD, a 1,6-addition is also possible [84] (Figure 6, right bottom). According to Pearson's concept of hard and soft acids and bases (HSAB), primary amines are hard electrophiles and preferentially react with the

---

[IV] **Infochemicals** carry information in the chemical interaction between organisms, evoking in the receiver a behavioral or physiological response that is adaptive to one or both of the interaction partners [73].

[V] **Allelochemicals** are secondary metabolites of plants or microorganisms that affect the growth or development of competitors commonly in a negative manner [57].

[VI] The **Michael addition** is a reaction between a C-H acidic compound that is enolizable as Michael donor and a vinylogous carbonyl compound as Michael acceptor [83]. In a broader sense also reactions with other nucleophiles like thiols belong to this reaction type and are referred to as **Michael-type addition** [80]; this term is also used here.

aldehyde moiety to unstable hemiaminals that are converted to imines, also known as Schiff bases [79] (Figure 6, left).
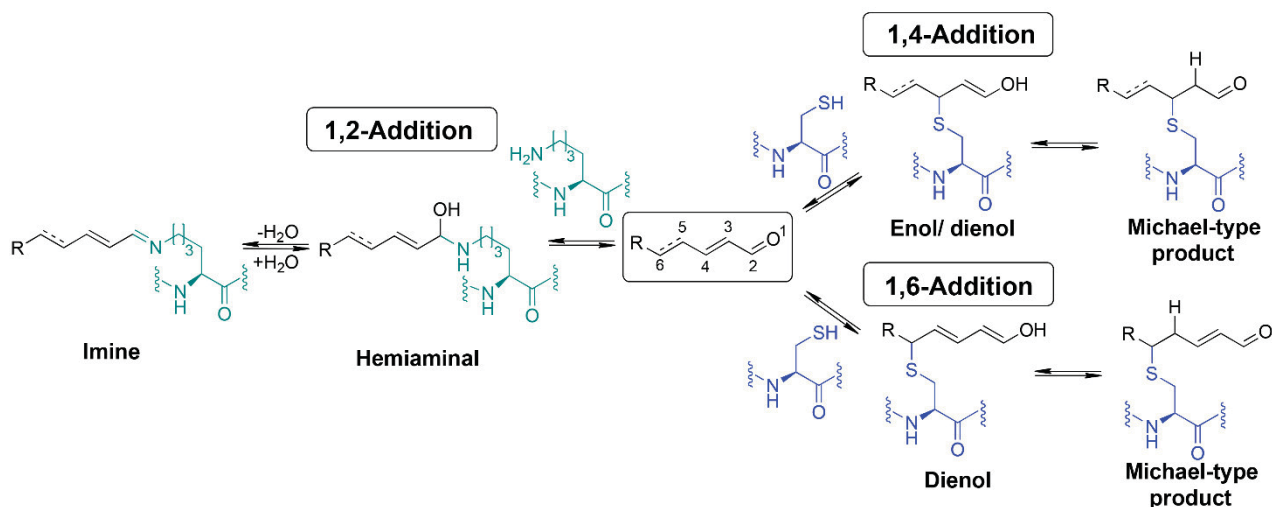
Figure 6. **Reaction of an α,β- or α,β,γ,δ-unsaturated aldehyde (dotted double bond) with a thiol group of cysteine (blue) or amine group of lysine (green) that are incorporated in a protein modified after [80,84].** For simplicity only one imine stereoisomer is drawn. (Abbreviation – R: residue)

In proteins, Michael adduct formation with thiol and amine groups, imine formation with amines, as well as diverse cyclization and several subsequent reactions have been identified for unsaturated aldehydes [85]. In detail, DD formed imines with isolated cytochrome c and ribonuclease, cysteine Michael-type adducts with β-lactoglobulin, and pyridinium adducts with lysine [86,87]. For DNA and RNA, 1,2-additions of amine groups of nucleobases on α,β-unsaturated aldehydes including DD and 1,4-Michael-type additions both followed by intramolecular cyclization reactions were reported [81,88,89]. These covalent modifications by unsaturated aldehydes may alter the structure and biological function of proteins, cause mutations in DNA, block replication, and influence gene expression [78]. Moreover, they have been shown to trigger a wide range of adverse effects including general toxicity, diseases, allergic reactions, mutagenicity, and carcinogenicity [84,90].

Despite the well-researched biological functions of PUAs in plankton communities, their mechanisms of action[VII] leading to the observed PUA-induced phenotypes are still poorly understood [55]. The few available information about PUAs' mode of action[VII] are summarized in the next section. However, most of the literature is restricted to a descriptive level. The complex linkage between interactions on a molecular level and cellular and physiological responses is insufficiently characterized.

[VII] The **mode of action** is defined as a biologically plausible series of key events and processes leading to a functional or anatomical change at the cellular level. It starts with exposure of a chemical to a living organism. In contrast, the **mechanism of action** implies a more comprehensive description of events on a molecular level and includes a molecular target [91,92].

The mode of action of PUAs in planktonic organisms may be ascribed to three effects: (I) disruption of intracellular calcium signaling, (II) induction of cytoskeletal instability, and (III) promotion of apoptotic pathways[VIII] (reviewed by Caldwell [55]).

In eukaryotic organisms, change of the intracellular free-calcium concentration is a common signal particularly related to reproductive and developmental processes [55]. DD and DT reduced the voltage-gated calcium current activity of the plasma membrane in ascidian embryos and acted as fertilization channel blockers [93]. Besides interference in calcium signaling, PUAs have also been reported to affect the cytoskeleton [60,93], which is essential to almost all cellular functions including mitotic events and cytokinesis [55]. Hansen *et al.* demonstrated negative effects of DD on key events of mitotic cell division and complete inhibition of the key cell cycle regulator cyclin B/cyclin-dependent kinase 1 (Cdk1) complex in sea urchin embryos; Cdk1 was not able to maintain its kinase activity by phosphorylating the histone H1 after covalent reaction with DD [94]. Staining of antibodies against α-tubulin revealed that DD-incubated eggs never formed a distinct mitotic spindle [94]. In the ascidian *Ciona intestinalis*, DD affected the reorganization of actin filaments and mitochondrial migration leading to a disturbance in cell cleavage and induction of larval teratogenicity [93].

Cell death as a consequence of apoptosis and sometimes necrosis[VIII] has been reported in copepod adult tissue, in particular gonads, as well as in early copepod and sea urchin embryonic stages and larvae in response to diatoms or DD (reviewed in [55]). Typical hallmarks of apoptosis include DNA laddering, chromatin dispersal, activation/release of certain proteins (e.g., caspases, cytochrome *c*) as well as change of their gene expression, and characteristic morphological changes that have been shown in sea urchin embryos [94-96], adult copepods, and copepod embryos and larvae [56,59,64,95].

In humans and animal models, unsaturated aldehydes derived from lipid peroxidation interfered with calcium homeostasis and the functional protein network of the cytoskeleton [90] and thus overlap with the observed effects in planktonic organisms.

A recently increasing number of studies addresses the influence of PUAs or PUA-producing diatoms on regulation of gene expression [96-101]. As introduced before, Vardi *et al.* demonstrated altered calcium concentration and NO generation in *P. tricornutum* in response to DD [71]. A subsequent transcriptome analysis [97] revealed that the gene *PtNOA*, which encodes a protein of the guanosine triphosphate-binding protein subfamily thought to play a role in NO generation, is upregulated in response to DD. *PtNOA* overexpressing cell lines are hypersensitive to DD with altered expression of superoxide dismutase and metacaspases; these proteins are involved in

---

[VIII] **Apoptosis** is a physiological mechanism, which belongs to programmed cell death. It occurs in organisms to maintain their function through elimination of unwanted cells. In contrast, **necrosis** is an uncontrolled form of cell death linked to pathological, inflammatory conditions [55].

activation of programmed cell death [97]. In contrast, HD, OD, and DD lead to NO decrease in *S. costatum* and except DD also in *P. tricornutum*, suggesting a species- and PUA-dependent mode of action [102]. Besides NO [71] also ROS, which are produced in response to OD in *Skeletonema tropicum* [103] and in *S. costatum* [104], have been attributed to be key components of the molecular cascade leading to cell death. Lauritano *et al.* [98] explored changes in expression levels of different genes in the copepod *Calanus helgolandicus* in response to strong and weak oxylipin-producing diatoms (*Skeletonema marinoi* vs. *Chaetoceros socialis*). Apoptosis regulation proteins like the inhibitor of apoptosis protein (IAP) that probably contributes to resistance to apoptosis and the cellular apoptosis susceptibility protein (CAS) were downregulated [100]. Induction of cytoskeletal instability, another mode of action of PUAs classified by Caldwell [55], was affirmed in a study with *C. helgolandicus* [98]. In this copepod, molecular downregulation of α- and β-tubulins in response to *S. marinoi* compared to a control diet occurred [98]. Only recently, Varrella *et al.* [101] even proposed effects of different PUAs on gene networks in the sea urchin *Paracentrotus lividus*. PUAs do not only act on their target genes but also indirectly influence other genes [101].

Remarkably, some diatom predator species and populations, bacteria, and PUA- and non-PUA-producing algae are less inhibited and influenced by those oxylipins than others, which is possibly the result of efficient detoxification mechanisms [57].

Lauritano *et al.* [99] explored the population-specific response of *C. helgolandicus* of different origin in response to a PUA-producing *S. marinoi* and a control diet. Antioxidant defense genes (encoding for glutathione S-transferase, superoxide dismutase, and catalase) and more specific detoxification systems (aldehyde dehydrogenases) were activated after 24 hours in the Atlantic Ocean and North Sea populations, whereas *C. helgolandicus* coming from the Mediterranean Sea is probably more susceptible to toxic diatom diets due to less exposure to long-lasting spring diatom blooms [99]. Also members of the aldo-keto reductase family [90] may degrade PUAs, but relevant genes were not selected in this study. In the PUA-producing *S. marinoi*, the synthesis of carotenoids to maintain photosynthetic performance [102] was enhanced during PUA exposure as a potential protection mechanism. Low molecular weight peptides like glutathione contributed to PUA detoxification in model investigations [84] and probably also act as detoxifying substances in planktonic organisms.

Besides clues of the potential mode of action of PUAs and altered gene expression, most of the research addressed the biological outcome of effects of PUAs on several organisms (chapter 1.2.2). Frequently, authors suggested potential covalent bond formations of PUAs with proteins and DNA (e.g.,[55,60,94]), but no verified covalently modified targets in the context of diatom-copepod interactions or function of PUAs as info- or allelochemicals in marine plankton have been identified so far.

1.3   Activity-based protein profiling (ABPP) and reporter tags

1.3.1   Probe design and functional principle of ABPP

To discover targets of drugs, toxins, or natural products, transcriptomic, metabolomic, or proteomic studies can be applied. In the last chapter the influence of DD on the transcriptome of certain planktonic species was introduced. Additionally, nucleophilic moieties of proteins offer a direct target of PUAs due to their electrophilic character. Thus, proteomic methods are a reasonable tool to study these oxylipins.

In particular, the activity-based protein profiling (ABPP), a method to target active enzymes, is of considerable interest to study covalent interactions of proteins with electrophiles. Pioneered by Bogyo [105] and Cravatt [106], this strategy was developed to investigate enzyme classes in an activity-based rather than an abundance-based manner. This is important since the activity of enzymes is regulated by diverse post-translational regulations; these include presence of inactive enzyme precursors, covalent modifications, subcellular compartmentation, and interactions with proteins and small-molecule inhibitors [107].

Small-molecule activity-based probes (ABPs) are the core of this profiling strategy (Figure 7, top and center). They covalently react with enzymes, mostly at the active site in an inhibitory manner. Since their introduction in the late 1990th, ABPs for diverse enzyme classes including proteases, glucosidases, kinases, phosphatases, oxidoreductases, and others have been developed (reviewed in [108,109]).

An ABP consists of two core elements: (I) the reactive group (RG) is responsible for covalent modification of the nucleophilic active site of a protein. It usually contains structures of known enzyme inhibitors or substrates to profile specific classes of enzymes in a directed manner; general electrophilic motives (e.g., α-chloroacetamide, Michael acceptors, epoxides, sulfonate esters [110]) have been utilized to profile multiple enzymes in a non-directed way. Furthermore, ABPs contain (II) a reporter tag, which is usually a dye for fluorescence-based visualization or an affinity tag like biotin for isolation and purification. Additional elements may involve a flexible spacer (e.g., a polyethylene glycol chain; Figure 7, top right) and/or a binding group (e.g., short-chain peptides, alkyl and aryl motives), which directs the probe reactivity to the enzyme active site [107,108,111].

Depending on the analytical platform used for detection (see chapter 1.3.2) also bifunctional reporter units, containing, for example, a fluorophore and biotin [112], cleavable structures like the tobacco etch virus (TEV) protease cleavage site [113], or photo-cleavable structures [114] can be introduced in the reporter unit.
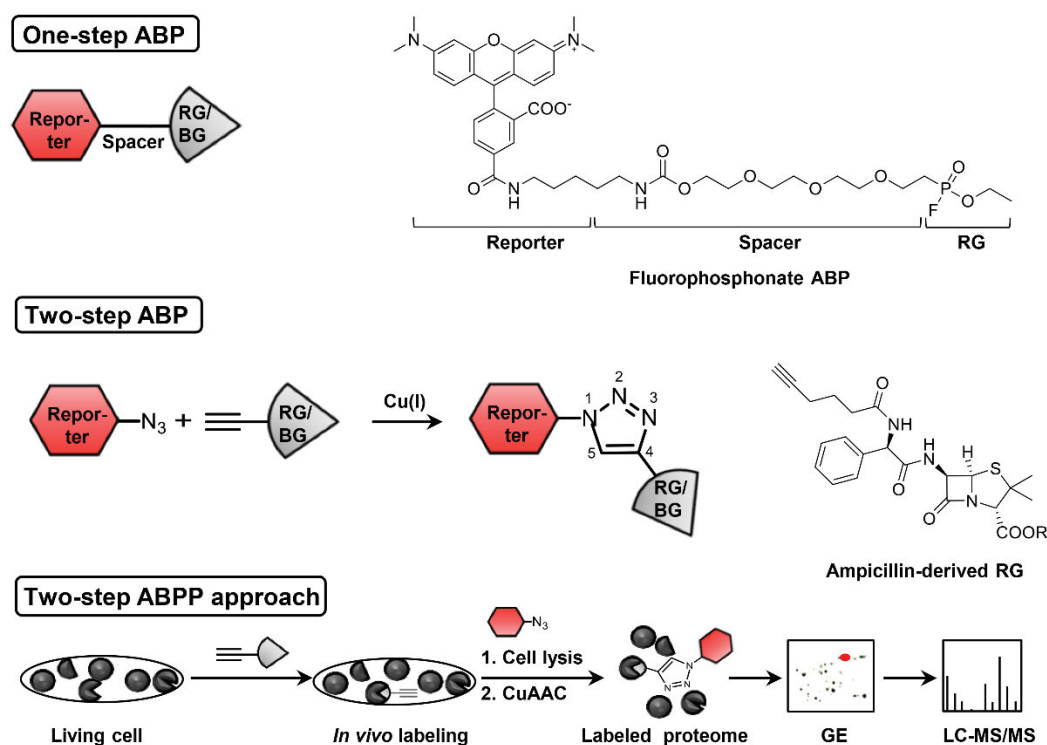
Figure 7.   General structure and examples of a one-step (top) and a two-step ABP (center) and application principle of two-step ABPP (bottom). The fluorophosphonate ABP (top right) was introduced by Cravatt and co-workers to selectively inhibit enzymes of the serine hydrolase family; the hydrophilic spacer separates the RG from the fluorophore [111]. The β-lactam-containing RG (center right) is part of a two-step ABP that was used to label penicillin-binding proteins in different bacteria; inhibition of these proteins by antibiotics (e.g., ampicillin) stops bacterial growth by interference of cell wall biosynthesis [115]. In a typical two-step approach (bottom), intact cells are labeled with the RG and the reporter is introduced after cell lysis. Labeled proteins are visualized by gel electrophoresis and fluorescence detection and analyzed by mass spectrometry after digestion of proteins excised from gels or enriched by immunoprecipitation [107,116]. (Abbreviations – ABP: activity-based probe; ABPP: activity-based protein profiling; BG: binding group; CuAAC: Cu(I)-catalyzed azide-alkyne cycloaddition; GE: gel electrophoresis; LC-MS/MS: liquid chromatography/ tandem mass spectrometry; RG: reactive group)

The presence of a bulky reporter group (Figure 7, top) might interfere with cell permeability and thus application of one-step ABPs is usually restricted to homogenized cells and tissue. In this *in vitro* application, proteins are removed from their native environment, which changes the complex regulatory system of cells and tissue [117]. Additionally, bulky groups might interfere with active site interactions.

To overcome these issues, a new generation of probes, namely two-step ABPs (Figure 7, center) that exploit „click chemistry[IX]" to connect the reporter to the RG, was introduced. Among click chemistry, the bioorthogonal Cu(I)-catalyzed azide-alkyne cycloaddition (CuAAC) is often consid-

---

[IX]Sharpless and co-workers [118] published a number of modular, "*spring-loaded*" reactions that are "*wide in scope, give very high yields, generate only inoffensive byproducts . . . and [are] stereospecific*", which they term **click chemistry**; these reactions include e.g., nucleophilic ring opening of epoxides, cycloadditions like the Diels-Alder reaction etc.

ered as prototypical reaction, which results in the formation of a 1,4-substituted 1,2,3-triazol (Figure 7, center).

Other bioorthogonal strategies, which enable formation of a specific product without interfering with other biomolecules, comprise copper free click chemistry with cyclooctynes and azides [119], the Staudinger ligation between azides and triarylphosphines [120], inverse electron-demand Diels-Alder reactions of tetrazines with alkenes [121], and others [119,121]. Compared to CuAAC, those reactions are less frequently used for ABPs [116].

Two-step ABPP was particularly developed for *in vivo* or *in situ* utilization. Therefore, the terminal alkyne (or azide)-containing RG is applied to the biological system (Figure 7, bottom). Subsequent CuAAC in cell lysates enables introduction of the reporter. In-gel fluorescence detection in 1D or less frequently 2D gels or affinity enrichment in combination with liquid chromatography coupled to mass spectrometry (LC-MS) are applied to separate and identify labeled proteins (see chapter 1.3.2) [122].

ABPP also has become a powerful method to study protein targets of natural products [111,122], especially if the interaction of these compounds and the protein targets are covalent in nature [122]. Therefore, natural product derivatives that are tagged with a bioorthogonal handle (e.g., alkyne, azide) are usually applied in form of two-step ABPP.

As an example, two-step ABPs helped to identify resistance mechanisms in bacteria. It is well known that β-lactam-containing natural products such as penicillin block bacterial growth by inhibition of enzymes responsible for cell wall biosynthesis. By developing a RG based on the semi-synthetic ampicillin [115] (Figure 7, center right) and applying improved β-lactam RGs, Sieber and co-workers identified resistance-associated enzymes that were unique to antibiotic-resistant *Staphylococcus aureus* strains (methicillin-resistant *S. aureaus*, MRSA) [115,123]. These enzymes displayed the ability to hydrolyze β-lactam antibiotics and thus ABPs have improved the understanding of the mechanisms of resistance of MRSA. This example demonstrates the value of ABPP to characterize and identify new target proteins and biochemical pathways, which could be useful in drug development [111].

Today, natural product-derived ABPs have evolved as the method of choice in the identification of the comprehensive natural product target spectrum and are also very well suited to identify off-targets of drugs, which may cause undesirable side effects [122].

1.3.2   Analytical platforms for protein identification in ABPP

Conventional proteomic methods profile protein abundance but fail to report on changes in protein activities. Therefore, combination of certain analytical protein techniques and specific analy-

tical platforms developed for ABPP are utilized; they are divided into gel-based and gel-free techniques (reviewed in [107,116]).

The most frequently applied gel-based technique to separate proteins labeled with a fluorescent or biotin-containing ABP is sodium dodecyl sulfate polyacrylamide gel electrophoresis (SDS-PAGE). After proteins are separated according to their size, in-gel fluorescence detection enables visualization of fluorescently labeled proteins, whereas avidin blotting is used for biotin-containing ABPs [107,116]. SDS-PAGE is a robust and fast method but suffers from restricted resolution leading to co-migrated proteins. 2D gel electrophoresis additionally resolves proteins according to their isoelectric point in the first dimension prior to SDS-PAGE in the second step and thus offers enhanced resolution [116].

The identity of proteins is revealed by excising the labeled proteins out of the gel followed by an optional in-gel reduction and alkylation step of cysteins, in-gel trypsin digestion, and analysis of peptides by liquid chromatography/tandem mass spectrometry (LC-MS/MS). During reversed phase chromatographic separation, peptides are eluted in order of their hydrophobicity. After passing the column, the peptides are usually ionized by electrospray ionization (ESI) and transferred to the mass spectrometer, which cycles for instance between two sequences [124]: a first sequence obtains the mass spectrum of the peptides, in a second sequence the tandem mass spectra composed of fragments of single preselected precursor peptides (data-dependent acquisition, DDA) or precursor peptides without or less preselection (data-independent acquisition, DIA) are recorded. Different types of suitable mass spectrometers and tandem techniques (acquisition cycles) are available (reviewed in [125]). Finally, depending on the acquisition mode, the peptide-sequencing data are processed by algorithms and searched against protein databases [125].

A series of gel-free, LC-MS/MS-based platforms for the analysis of probe-labeled proteomes have been developed that offer higher sensitivity than gel-based techniques. Among these platforms, tandem orthogonal proteolysis (TOP), antibody-based methods, as well as the multidimensional protein identification technology (MudPIT) are broadly distributed [107,116].

A strategy that quantifies labeled proteins and determines the site of labeling is TOP-ABPP [113,117]. Thereby, the proteome is labeled in a two-step approach by an alkyne-containing RG and then subjected to CuAAC to attach a biotin-azide reporter that contains a TEV protease cleavage site. Biotin-labeled proteins are enriched by incubation with (strept)avidin beads. After on-bead trypsin digestion, the released peptides are analyzed by LC-MS/MS to provide information on the entire protein sequences. The remaining probe-labeled peptides that are bound to the beads are released by a TEV protease and analyzed by LC-MS/MS to provide information on the labeling site [113,117].

Another platform uses capillary electrophoresis (CE) to separate probe-modified active site peptides with high reproducibility and resolution [126]. Therefore, fluorescent probe-labeled proteins are digested with trypsin. The fluorophore-containing peptides are enriched and collected by immunoprecipitation through use of anti-fluorophore antibodies, which specifically recognize small organic fluorophores, and are measured by CE with laser-induced fluorescence. Identification of proteins is done separately by LC-MS/MS experiments [126].

Furthermore, microarrays offer isolation, detection, and identification of ABP-labeled proteins in one step [107,108,127]. Therefore, antibodies that specifically recognize proteins are arrayed on glass slides. Fluorescently ABP-labeled proteins bind to their specific antibodies and can be detected by fluorescence scanning [127].

1.3.3   Reporter tags

Reporter tags[X] responsible for visualization, detection, or enrichment of molecules have become a valuable tool in chemical biology, proteomics, and metabolomics. Bioorthogonal labeling techniques enable two-step approaches, which allow introduction of sterically demanding reporter tags, such as fluorophores or affinity tags, like shown before in ABPP (chapter 1.3.1). Besides ABPP, other tagging strategies make use of tags to image and retrieve nucleic acids, proteins, glycans, lipids, and other metabolites *in vitro* and *in vivo* (reviewed in [119]).

The great diversity of commercially available fluorophores with a broad range of absorption and emission spectra have increased their field of application [130] and almost completely replaced radioisotopes. Most commonly used fluorophores in ABPs comprise fluorescein, rhodamine, dansyl, 4-chloro-7-nitrobenzo[*c*][1,2,5]oxadiazole (NBD-Cl), dipyrromethene boron difluoride (BODIPY), and cyanine (Cy) dyes [130], but a huge variety of other organic fluorophores is available [131]. Also other techniques, like distance-dependent fluorescence by combination of fluorophores using Förster resonance energy transfer or fluorescence quenching and bioluminescent imaging, are possible (reviewed in [132]).

Besides fluorescence detection, also mass spectrometry is used to monitor biomolecules. Not only bioorthogonal coupling enables introduction of a tag, many strategies make use of the presence of a functional group in the biomolecule to introduce a reporter tag. For instance,

---

[X] The term **reporter tag** is used according to the definition of Cravatt and co-workers [109, 128] and Sieber and co-workers [111,122] as molecule for visualization and enrichment in ABPP. The term bioorthogonal **chemical reporter** can also have another meaning which is not intended here: a bioorthogonal chemical reporter can be defined as a non-native, non-perturbing chemical handle that contains a bioorthogonal group (e.g., an alkyne for modification with exogenous molecules such as fluorophores); the chemical reporter is incorporated into the target biomolecule by using the cell's own biosynthetic machinery (e.g., alkyne-modified nucleosides that are incorporated into DNA and RNA) [119,129].

labeling of amine groups via *N*-hydroxysuccinimide (NHS)-esters [133] or thiols with iodoacet-amide derivatives [134] have been utilized to compare expression levels of proteins via stable isotope labels. Among these labels, isotope-coded affinity tags (ICAT) comprise heavy and light reporters for labeling of different protein samples followed by mass spectrometric quantification of labeled peptides in the combined samples [134]. These isotope-coded probes have also been used in the field of ABPP in form of heavy and light azide reporter tags [135]. Isobaric tags for relative and absolute quantitation (iTRAQ) show identical mass spectra of peptide fragments but possess distinguishable MS/MS signatures depending on the utilized tag [133].

Mass tags that contain bromine [136-138] and chlorine [136,139] have been reported in prote-omics related applications; they can increase recognition of peptides by generating a characteris-tic peptide isotopic pattern.

Small metabolites have been covalently labeled with tags that target distinct classes of small molecules carrying common chemical functionalities (e.g., amines, alcohols, acids, thiols, ketones/aldehydes). Charged tags like ammonium [140,141] or phosphonium [142] enhance ionization in ESI positive mode and improve retention behavior during chromatographic separa-tion. The latter was also reported for bromine- and chlorine-containing tags that additionally offered characteristic isotopic patterns in LC-MS approaches [141,143-145].

2   SCOPE OF THE STUDY

Almost two decades ago, polyunsaturated aldehydes (PUAs) produced by diatoms came into focus of chemical ecologists. Since then, these aldehydes have been demonstrated to act against reproduction of diatom grazers and proposed to mediate other planktonic interactions (reviewed in [21,55,57], see chapter 1.2.2).

This work aimed to contribute to available quantification data (Figure 8) and to provide data that can be related to biological effects of PUAs in a mesocosm study. The main emphasis of the thesis was to deepen the mechanistic understanding of effects of PUAs. So far, PUA targets and their mechanisms of action are only poorly investigated. I strived to unveil PUA uptake and targets of these oxylipins that are covalently modified with emphasis on proteins (Figure 8). However, the precise assurance of a molecular target in accordance with pharmaceutical practice was not the aim of this work, rather a screening of putative targets and derived from these findings, the disclosure of potentially affected biological pathways and molecular functions. Besides PUA target identification, I aimed to design a new reporter molecule for probes and other applications in the field of chemical biology (Figure 8).
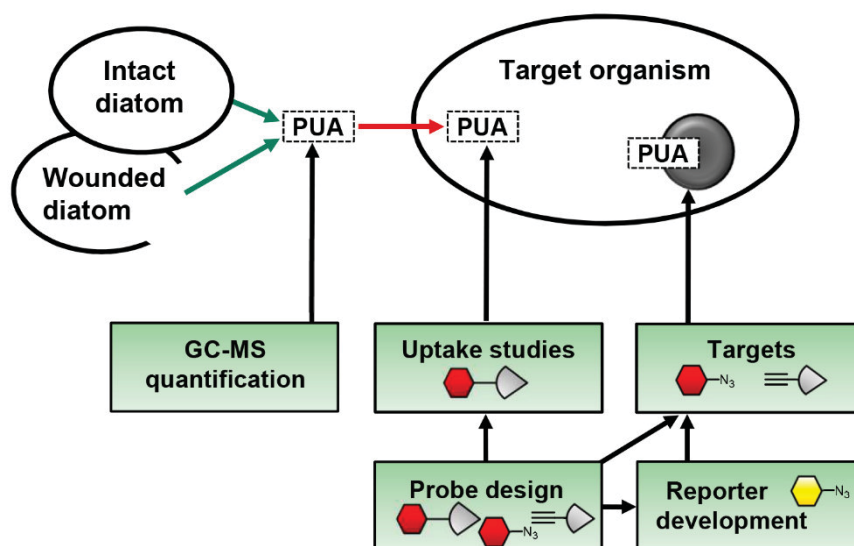
Figure 8. **Summary of the aims of this thesis.** Diatoms produce PUAs upon wounding, cell lysis, and by intact cells (green arrows) [20,69,70,146]. Besides quantification of these metabolites, their uptake (red arrow) and covalent reactions with molecular targets (gray circle, e.g., proteins) are to be investigated to extend the general understanding of mechanistic effects of PUAs in conjunction with a few already available information of gene expression regulation [98-101]. Rectangular boxes and black arrows demonstrate the experimental aspects of this work. (Abbreviation – GC-MS: gas chromatography coupled to mass spectrometry)

In detail, this work comprises the following elements:

Quantification of PUAs in a mesocosm study and their impact on grazing experiments

Blooms of the PUA-producing algal species *Skeletonema marinoi* and *Phaeocystis pouchetii* are to be observed in a mesocosm experiment in collaboration with other researchers. During this study, dilution experiments were planned to examine microzooplankton community grazing on phytoplankton. We attempted to enlighten previous unexplainable results of grazing experiments through support by chemical analysis of bioactive PUAs. I co-worked on this topic, took samples on-site, and quantified PUAs by gas chromatography coupled to mass spectrometry (GC-MS) (chapter 5.1).

Probe design and uptake of a PUA-derived probe in planktonic organisms

Visualization of uptake and accumulation of PUAs in organisms is essential to clarify mechanistic aspects of this substance class. To achieve this goal, I aimed to utilize a previously developed fluorescent probe, which I designed according to activity-based protein profiling (ABPP)[147].

With the help of the PUA-derived activity-based probe (ABP) and a saturated aldehyde control probe, I planned to establish uptake studies in model organisms.

I used the copepod *Acartia tonsa* to study delivery and distribution of both types of aldehydes by exploiting a carrier species (chapter 5.2). Furthermore, I aimed to observe probe uptake in the PUA-producing *Phaeodactylum tricornutum* (chapter 5.2). This alga is capable of cell-to-cell communication in response to 2*E*,4*E/Z*-decadienal (DD) [71] and is one of a few sequenced diatoms [148], allowing further protein target studies.

Target identification of PUAs in planktonic organisms

To unravel the mechanisms of action of PUAs, identification of molecular targets is an essential step. I aimed to develop and conduct the first screening of covalently labeled protein targets of PUAs in a planktonic organism. Thereby, I intended to develop a two-step ABPP procedure for the diatom *P. tricornutum* and derive possible consequences of covalently modified proteins for the cells. In addition, also DNA targets as well as small molecules, which potentially contribute to PUA detoxification, were addressed (chapter 5.3).

Reporter tag development for multiple detection possibilities

Besides investigations that are exclusively based on the fluorescence detection of a probe, I aimed to develop a new reporter tag for orthogonal detection possibilities including mass spectrometry and fluorescence. The reporter may contribute to the identification of small PUA-detoxifying molecules and extend the toolbox of ABPs and chemical biology. It should be connectable to terminal alkyne-containing molecules via Cu(I)-catalyzed azide-alkyne cycloaddition (CuAAC) (chapter 5.4).

3   PUBLICATION LIST AND DOCUMENTATION OF AUTHORSHIP

<div align="center">

Manuscript A:

Underestimation of microzooplankton grazing in dilution experiments due to inhibition of phytoplankton growth

</div>

Diane K Stoecker, Jens C Nejstgaard, Rakhesh Madhusoodhanan, Georg Pohnert, Stefanie Wolfram, Hans Henrik Jakobsen, Sigitas Šulčius, Aud Larsen. *Limnology and Oceanography* **2015**, *60*(4):1426–1438. doi:10.1002/lno.10106.

Summary

During an international mesocosm experiment, I quantified dissolved and particulate polyunsaturated aldehydes (PUAs) produced by the bloom forming algal species *Skeletonema marinoi* and *Phaeocystis pouchetii* under close-to-nature conditions. The data provide explanation for the results of dilution experiments that examine microzooplankton community grazing on phytoplankton. Within the experiments, net growth of phytoplankton in diluted samples was distorted resulting in unusual low grazing coefficients. We ascribed these inhibiting effects to bioactive PUAs, which were released by damaged algal cells during filtration of sea water for diluted treatments.

Author contributions

DK Stoecker	Planned the mesocosm research approach; conceived, designed, and performed the dilution grazing and laboratory experiments, analyzed the data, wrote the manuscript.
JC Nejstgaard	Designed and coordinated the mesocosm research approach, analyzed the data.
R Madhusoodhanan	Performed dilution grazing experiments and analyzed the data.
G Pohnert	Planned the mesocosm research approach, supervised SW, analyzed the PUA quantification data, and wrote the corresponding part of the manuscript.
S Wolfram	Planned and performed PUA sample preparation on-site, conducted GC-MS measurements, analyzed the data, and wrote the corresponding part of the manuscript. (Suggested publication equivalent: 0.25)
HH Jakobsen	Planned, performed, and analyzed the plankton composition.
S Šulčius	Performed dilution grazing experiments and analyzed the data.

A Larsen   Project leader and coordinator of the mesocosm experiment.

All co-authors commented on the manuscript.

<div align="center">

Manuscript B:

A metabolic probe-enabled strategy reveals uptake and protein targets of polyunsaturated aldehydes in the diatom *Phaeodactylum tricornutum*

</div>

Summary

PUAs have been shown to mediate cell-to-cell signaling. In particular, 2*E*,4*E*/*Z*-decadienal (DD) increased intracellular calcium concentration, NO generation, and transcriptional changes in the diatom *P. tricornutum*. To improve understanding of the underlying mechanistic aspects, we studied PUA uptake and targets in *P. tricornutum* by using molecular probes similar to activity-based protein profiling (ABPP). Application of the DD-derived, fluorescent probe TAMRA-PUA revealed substantial uptake in cells by fluorescence microscopy compared to a saturated aldehyde control probe. In a subsequent two-step ABPP approach, we received selective fluorescent labeling of target proteins by the PUA probe. Putative targets have roles in key biological processes such as the pentose phosphate pathway and photosynthesis, including photophosphorylation and the Calvin cycle, and may be negatively affected by covalent PUA modifications.

Author contributions

S Wolfram   Conceived, designed, and performed all experiments (except 2D gels, digestion, LC-MS/MS), analyzed the data, and wrote the manuscript. The syntheses of TAMRA-PUA/TAMRA-N$_3$/DDY are based on my diploma thesis [147]. (Suggested publication equivalent: 1.0)

N Wielsch   Performed LC-MS/MS measurements, processed the raw data, wrote the corresponding materials and methods section.

Y Hupfer   Performed 2D gel electrophoresis and in-gel digestion of proteins.

B Mönch   Advanced method development for probe labeling, protein extraction, and 2D gel electrophoresis; performed preliminary experiments.

H-W Lu-Walther   Planned, performed, and analyzed fluorescence microscopy experiments and wrote the corresponding materials and methods section. (Suggested publication equivalent: 0.25)

R Heintzmann   Involved in planning and data analysis of fluorescence microscopy.

O Werz   Conceived and designed probe labeling and 2D gel electrophoresis experiments.

A Svatoš   Supported research and data analysis.

G Pohnert   Involved in planning of the work and data analysis; wrote the manuscript.

All co-authors commented on the manuscript.

Manuscript C:
Accumulation of polyunsaturated aldehydes in the gonads of the copepod *Acartia tonsa* revealed by tailored fluorescent probes

Summary

PUAs have been shown to interfere with copepod reproduction, but PUA uptake to investigate this issue has not been addressed to date. We developed a feeding and monitoring procedure for adult females of the copepod *A. tonsa* to localize the fluorescent probe TAMRA-PUA that is based on the $\alpha,\beta,\gamma,\delta$-unsaturated aldehyde DD and the saturated aldehyde-derived TAMRA-SA as control. The feeding procedure includes the use of the heterotrophic dinoflagellate *Oxyrrhis marina* as a carrier since an active feeding procedure for delivery of the probes is required. TAMRA-PUA and TAMRA-SA attached non-covalently to the surface of this dinoflagellate and were taken up by copepods during feeding. TAMRA-PUA accumulated in a female reproductive tissue and thus explains PUAs' teratogenic activity, whereas TAMRA-SA derived from bioinactive saturated aldehydes enriched in the lipid sac.

Author contributions

S Wolfram   Conceived, designed, and performed all experiments and analyzed the data; wrote the manuscript. The synthesis of the TAMRA-PUA probe is based on my diploma thesis [147]. (Suggested publication equivalent: 1.0)

JC Nejstgaard   Conceived and designed the experiments, involved in accomplishment of the experiments, analyzed the data, wrote the manuscript.

G Pohnert   Conceived the research approach, analyzed the data, and wrote the manuscript.

Manuscript D:
A small azide-modified thiazole-based reporter molecule for fluorescence and mass spectrometric detection

Summary

The manuscript describes the synthesis, characterization and application of the reporter molecule 4-(3-azidopropoxy)-5-(4-bromophenyl)-2-(pyridin-2-yl) thiazole (BPT) that allows fluorescence and UV detection as well as mass spectrometric detection through a characteristic isotopic pattern caused by bromine. BPT carries an azide moiety that can be coupled to terminal alkyne-containing molecules via Cu(I)-catalyzed azide-alkyne cycloaddition (CuAAC). This property allows utilization of BPT as reporter unit for two-step ABPP. We demonstrate advantageous features compared to commercially available, azide-tagged fluorophores of similar mass range and a brominated one and show model reactions with a small molecule and a protein that had been prelabeled with a PUA-derived alkyne.

Author contributions

S Wolfram   Conceived and designed the experiments, synthesized the structures *N*-(3-azidopropyl)-5-(dimethylamino)naphthalene-1-sulfonamide (DNS) and *N*-(3-azidopropyl)-6-bromo-5-(dimethylamino)naphthalene-1-sulfonamide (BNS), performed all experiments (except synthesis of *N*-(3-azidopropyl)-7-nitrobenzo[*c*][1,2,5]oxadiazol-4-amine (NBD) and BPT), analyzed the data, wrote the manuscript. The synthesis of DDY is based on my diploma thesis [147]. (Suggested publication equivalent: 1.0)

H Würfel   Conceived the structure of BPT, supported design of the experiments, synthesized BPT, wrote the manuscript.

SH Habenicht   Synthesized BPT and performed UV-Vis and fluorescence spectroscopy experiments.

C Lembke   Synthesized NBD and assisted in UV-Vis spectroscopy experiments.

P Richter   Synthesized NBD and supported research.

E Birckner   Measured fluorescence quantum yields; support during research.

R Beckert   Involved in the design of BPT.

G Pohnert   Involved in planning of the work and analysis of the data, wrote the manuscript.

All co-authors commented on the manuscript.

4   PUBLICATIONS

4.1   Manuscript A

Underestimation of microzooplankton grazing in dilution experiments due to inhibition of phytoplankton growth

Diane K Stoecker, Jens C Nejstgaard, Rakhesh Madhusoodhanan, Georg Pohnert, Stefanie Wolfram, Hans Henrik Jakobsen, Sigitas Šulčius, Aud Larsen

Underestimation of microzooplankton grazing in dilution experiments due to inhibition of phytoplankton growth

Diane K. Stoecker,[*][1] **Jens C. Nejstgaard,**[†][2] **Rakhesh Madhusoodhanan,**[3] **Georg Pohnert,**[4] **Stefanie Wolfram,**[4] **Hans Henrik Jakobsen,**[5] **Sigitas Šulčius,**[6] **Aud Larsen**[2]

[1]Horn Point Laboratory, University of Maryland Center for Environmental Science, Cambridge, Maryland 21613
[2]Uni Research Environment and Hjort Centre for Marine Ecosystem Dynamics, Bergen, Norway
[3]Department of Biology, University of Bergen, N-5020 Bergen, Norway
[4]Institute of Inorganic and Analytical Chemistry, Friedrich Schiller University, Lessingstr. 8, 07743 Jena, Germany
[5]Department of Bioscience, Aarhus University, Frederiksborgvej 399, DK-4000, Roskilde, Denmark
[6]Open Access Centre for Nature Research, Nature Research Centre, LT-08412 Vilnius, Lithuania

Abstract

Microzooplankton dilution grazing experiments conducted in phytoplankton rich waters, particularly in polar and subpolar seas, often result in calculation of nonsignificant or negative grazing coefficients. We hypothesized that preparation of filtered seawater (FSW) from water containing high biomass of phytoplankton results in release of allelochemicals that inhibit phytoplankton growth, lowering the net growth of phytoplankton in the more diluted treatments. We tested this hypothesis during blooms of *Skeletonema marinoi* and *Phaeocystis pouchetii* in a nutrient-enriched mesocosm in the Raunefjord, Norway. During the *S. marinoi* bloom, inhibition of phytoplankton growth occurred in the diluted treatments. Simultaneously the concentration of total as well as dissolved polyunsaturated aldehydes (PUAs) was elevated. Passage of the FSW through a carbon cellulose cartridge to remove dissolved organic material reduced, or eliminated, the inhibition. In the early phase of the *P. pouchetii* bloom that followed the diatom bloom in the mesocosm, PUA concentration was relatively low and the untreated FSW had a less drastic, but often significant, inhibitory effect on phytoplankton growth. Laboratory experiments with cultures of *S. marinoi* and *P. pouchetii* confirmed that material present in filtrate prepared from diluted cultures was self-inhibitory. Many phytoplankters, particularly during late stages of a bloom, produce inhibitory metabolites that may be released during filtration of the relatively large volumes of seawater needed for dilution experiments. Under some conditions, dilution grazing experiments may underestimate phytoplankton growth coefficients and microzooplankton grazing coefficients.

Dilution experiments have been used extensively in coastal and oceanic waters to estimate phytoplankton growth and microzooplankton community grazing and to compare carbon cycling in the upper ocean among marine systems (Calbet and Landry 2004). However, dilution experiments in polar and subpolar seas often yield difficult to interpret results, including "0" estimates of microzooplankton grazing when microzooplankton abundances are high and "reverse" slopes that result in the calculation of "negative' estimates of grazing. This has been noted during *Phaeocystis antarctica* blooms in the Ross Sea, Antarctica

(Caron et al. 2000), *Phaeocystis pouchetii* blooms in the Arctic Ocean and Bering Sea (Calbet et al. 2011; Stoecker et al. 2014) and during ice-associated diatom blooms in the Bering Sea (Sherr et al. 2013). Low microzooplankton grazing in polar and subpolar waters has been ascribed to the effects of low water temperatures on microzooplankton grazing and growth (Rose and Caron 2007, but *see* Franzè and Lavrentyev 2014), but cannot explain negative grazing coefficients (*g*). Statistically significant negative grazing coefficients can occur even with addition of inorganic nutrients to prevent nutrient limitation in the diluted treatments (Sherr et al. 2013; Stoecker et al. 2014). Negative grazing is impossible, but negative values of "*g*" result when the net or apparent growth rate of the phytoplankton, *K*, is lower in the diluted than the undiluted treatments. In the absence of grazing, *K* should be equal in diluted and undiluted treatments. With grazing, *K* should be higher in the diluted treatments

because dilution reduces encounter rate between microzooplankton grazers and their phytoplankton prey. The opposite trend, lower K in the diluted than undiluted treatments, indicates a violation of one of the central assumptions of the dilution technique, that the instantaneous growth (μ) of phytoplankton is the same in all dilutions (Landry and Hassett 1982).

We hypothesized that inhibitory metabolites released during preparation of the filtered seawater (FSW) used for dilution of the whole seawater (WSW) can negatively affect phytoplankton growth. To test this hypothesis, we conducted dilution grazing experiments in spring 2012 during sequential blooms of *Skeletonema marinoi* and *P. pouchetii* in an in situ mesocosm in the Raunefjord at the Marine Biological Station, University of Bergen, Norway. Both *S. marinoi* and *P. pouchetii* produce polyunsaturated aldehydes (PUAs) that can inhibit growth of phytoplankton (Pohnert 2000; Hansen and Eilertson 2007) and reproduction or growth of zooplankton (Pohnert et al. 2002; Ianora and Miralto 2010). We conducted dilution experiments during the exponential, stationary, and declining phase of a *S. marinoi* bloom, and during the early and exponential stages of a *P. pouchetii* bloom in the mesocosm. We compared the net growth rate of phytoplankton in a diluted treatment in which the FSW had been passed through a carbon cellulose cartridge to reduce dissolved organic material to that in a control dilution treatment, in which the FSW was not passed through the cartridge. We measured the net growth of phytoplankton in the undiluted treatments and compared that to the daily net increase of chlorophyll *a* (Chl *a*) in the mesocosm. We later conducted laboratory dilution experiments with cultured *P. pouchetii* and *S. marinoi* to confirm our results that organic agents released during preparation of dilution water could be self-inhibitory. We thereby determined that there are conditions in which the dilution technique results in underestimation of microzooplankton grazing and explored modifications to the dilution protocol that might allow the technique to be applied under these conditions.

Methods

Mesocosm

We conducted our experiment in a nitrate and phosphate enriched large volume (10 m^3) in situ mesocosm as part of a larger mesocosm experiment conducted in the Raunefjord, western Norway (60°16′N, 05°14′E) in March 2012 at the Marine Biological Station, University of Bergen, Norway. The design of the mesocosms, filling and mixing are as described for an earlier experiment at the same location in Nejstgaard et al. (2006). On 8 March 2012 (day 0), the mesocosms were filled with unfiltered seawater from the fjord (31.8 psu) and on the following day, 9 March (day 1), the mesocosms received different control or nutrient enrichments. The mesocosm experiment ended on 30 March 2012.

For the experiments described herein, we used mesocosm M2, which was enriched with 16 μM nitrate and 1 μM phosphate to stimulate a bloom of *P. pouchetii*. Because of the high silicate concentrations in the fjord in early March, a *S. marinoi* bloom developed first, followed by a *P. pouchetii* bloom after silicate depletion. Thus, we were able to conduct dilution experiments during two types of blooms, although, unfortunately, the mesocosm experiment ended before the peak of the *P. pouchetii* bloom occurred.

Each morning a SAIV SD204 CTD was used to measure water temperature throughout the water column in the mesocosm. A 35-L carboy was filled with a subsurface sample ($\sim$ 0.5 m depth) from the mesocosm. The carboy was immediately brought to the laboratory, placed in a 4°C environmental chamber, and sampled for Chl *a*, nutrients (nitrite, nitrate, phosphate, and silicate), phytoplankton and microzooplankton. The details of Chl *a* and nutrient analyses are presented in Nejstgaard et al. (2006). The daily net growth rate (K, d^{-1}) of phytoplankton in the mesocosm was estimated from the change in Chl *a* from the previous sampling day as ln Chl a_t − ln Chl a_{t-1}.

Microzooplankton, *S. marinoi* and *P. pouchetii* were analyzed by a Flow Cam II as described in Jónasdottir et al. (2011) and in Vidoudez et al. (2011a). Briefly, images of *P. pouchetii*, *S. marinoi*, and microzooplankton were manually separated from the FlowCAM image collages. Colonial *P. pouchetii* cells were estimated by calibrating grayscale area to cell number of *P. pouchetii* images collected, whereas *S. marinoi* cell numbers were estimated from calibrated cell number to chain length relationships. In addition to the daily samples, separate 10 L samples were collected every third day for analyses of particulate and dissolved PUAs.

Determination, analysis, and quantification of particulate and dissolved PUAs

PUAs produced by *S. marinoi*, including 2,4-heptadienal, 2,4-octadienal, and 2,4,7-octatienal, were quantified as well as 2,4-decadienal, which is produced by *P. pouchetii* (Wichard et al. 2005; Hansen and Eilertson 2007). Determination of the production of PUAs by cells was performed according to a slightly modified protocol based on Vidoudez et al. (2011b). Important steps in the Vidoudez et al. protocol are briefly described, whereas steps which varied from the Vidoudez et al. (2011b) protocol are described in detail in an online supplement (Supporting Information).

Dilution grazing experiments in the mesocosm

For calculation of growth and grazing rates, we used the two-point dilution method (Landry et al. 2008), which provides similar results to the original Landry and Hassett (1982) dilution series protocol (Strom et al. 2006; Strom and Fredrickson 2008). The experiments were conducted using water from mesocosm M2 and incubated in this mesocosm. Dilution experiments were conducted on days 8, 11, 15, 19, and 21 of the mesocosm experiment (16, 19, 23, 27, and 29

Table 1. Environmental conditions in mesocosm M2, started 8 March 2012 with 31.8 psu sea water from the Raunefjord, Norway.

Day	Date	Chl a (μg L^{-1})	Temp. (°C)	NO$_3$ + NO$_2$ (μmol L^{-1})	NH$_3$ (μmol L^{-1})	P (μmol L^{-1})	Si (μmol L^{-1})
0	8 Mar	0.66	Nd	6.36	0.46	0.33	4.31
1	9 Mar	0.74	5.9	22.64	0.40	1.22	4.16
8	16 Mar	6.22	6.6	17.78	0.27	0.96	<0.01
11	19 Mar	14.16	6.3	15.72	0.54	0.85	0.66
15	23 Mar	9.05	6.9	12.62	0.73	0.71	0.64
19	27 Mar	8.32	7.4	7.87	0.86	0.51	0.39
21	29 Mar	14.39	7.5	0.11	1.42	0.27	0.68

March, Table 2). In all experiments, we included a WSW treatment and diluted (ca. 10% WSW) treatments prepared with untreated FSW and, for comparison, with FSW that had been treated by passage through a carbon cellulose (CC) filter to reduce or remove dissolved organic material (Table 2). Nutrient addition treatments were included in dilution experiments conducted after mesocosm day 11 (first Chl a peak) because of the decline in nutrient availability (Tables 1 and 2). In the final experiment (day 21), only nutrient addition treatments were used. In addition to the 10% WSW treatment, we included an intermediate dilution (25% WSW) that was not used in the two-point calculation. We included this treatment as an indicator of the shape of the response of net growth rate to dilution.

Early on the morning of a dilution experiment, WSW was collected from just below the surface of mesocosm M2 using wide mouth 35 L Nalgene polycarbonate carboys with a 200 μm mesh fitted to the top to exclude > 200 μm zooplankton. The water was immediately transported to a 4°C environmental chamber with dim lighting. Approximately 25 L of FSW was prepared in the cold room by gravity filtration through a FS-Polycap AS Whatman filter. Meanwhile, a carbon cellulose cartridge (Model CCA/CFS-CA/CFA-CA, Claes Ohlson, Sweden) was conditioned by passing 30 or more liters of FSW through it. Carbon cellulose-treated FSW (CC) was then prepared in the cold room by passing a portion of the FSW through the conditioned carbon cellulose cartridge. In independent experiments, a mixture of PUAs in 5 L FSW (2.3 nM heptadienal, 0.84 nM octadienal, and 3.9 nM decadienal) was submitted to carbon cellulose treatment as indicted above. The treated water was then submitted for the PUA quantification of diluted PUA (see above). This

Table 2. Dilution grazing experiments conducted in mesocosm M2, March 2012. Calculated dilution was 10% for all diluted treatments; achieved dilution (based on Chl a) at $t = 0$ is presented

Mesocosm Day	Date	Nutrient treatment	Treatments
8	16 March	None added	Whole SW
			13% Whole SW
			13% Whole SW (CC)
11	19 March	None added	Whole SW
			14% Whole SW
			6% Whole SW (CC)
15	23 March	None added	Whole SW
			12% Whole SW (CC)
15	23 March	Added nutrients	Whole SW (Nut)
			12% Whole SW (Nut)
			12% Whole SW (Nut) CC
19	27 March	None added	Whole SW
			8% Whole SW (CC)
19	27 March	Added nutrients	Whole SW (Nut)
			10% Whole SW (Nut)
			8% Whole SW (Nut) CC
21	29 March	Added nutrients	Whole SW (Nut)
			10% Whole SW (Nut)
			8% Whole SW (Nut) CC

Table 3. Relative composition of phytoplankton polyunsaturated aldehydes (PUAs), in mesocosm M2. Values are for dates bracketing dilution experiments

Mesocosms Day	Dilution Experiment Date	Heptadienal (%)	Octadienal (%)	Octatrienal (%)	Decadienal (%)
8	16 Mar*	65–52	16–22	20–26	0
11	19 Mar*	52–53	22–26	26–20	0–0.4
15	23 Mar*	53–58	26–22	20–19	0.4–0
19	27 Mar	100	0	0	0
21	29 Mar*	100–30	0–36	0	0–33

*16 Mar (15 and 18 Mar), 19 Mar (18 and 21 Mar), 23 Mar (21 and 24 Mar), 29 Mar (27 and 30 Mar).

procedure removes quantitatively all PUA (detection limit below 0.1 nM).

Whole SW was added to either FSW or CC in a carboy to achieve a calculated 10% WSW; use of high-dilution levels (5–10% WSW) reduces potential artifacts due to trophic cascades (Calbet and Saiz 2013). Four replicate Chl *a* samples for $t = 0$ were taken from each carboy. Water from the carboys was distributed through silicone tubing into triplicate 2.2 L incubation bottles for each treatment. When nitrate + nitrite levels were < 15 μmol L^{-1} (experiments on mesocosm day 15, 19, and 21; Tables 1 and 3), we included additional triplicate incubation bottles of WSW and diluted treatments (FSW and/or CC) to which we added nutrients (Nut treatment). The nutrient addition was a calculated 12 μM nitrate and 1.7 μM phosphate and was accomplished by adding 35 μL of Solution 1 (Hansen 1989) per liter. In addition to sodium nitrate and sodium phosphate, solution 1 contains Na$_2$EDTA and trace metals.

The incubation bottles were transported from the environmental chamber in a covered container to the mesocosm. Each bottle was suspended in situ at 0.5 m depth in the mesocosm for 24 h. At the end of the 24 h incubation, the bottles were retrieved and transported back to the laboratory. Duplicate samples for Chl *a* were taken from each bottle ($t = 24$ h samples). All Chl *a* samples were filtered onto 0.22-μm pore size 47-mm diameter polycarbonate filters using gentle vacuum filtration, extracted in 90% acetone at 4°C for 12 h, and analyzed with a precalibrated Turner Designs AU fluorometer.

Chl *a* was a proxy for phytoplankton biomass at the beginning ($t = 0$ h) and end ($t = 24$ h) of the incubation. The phytoplankton net growth, K d^{-1}, was estimated for both the diluted treatments and the WSW treatments as ln Chl a_{t24h} − ln Chl a_{t0h}. We determined the realized dilution factors for each experiment from the $t = 0$ Chl *a* values in the WSW and diluted treatments. The calculated dilution was 10% WSW but the measured dilutions varied from 5% to 14% WSW. The intrinsic growth rate of phytoplankton (μ, d^{-1}) for the two treatment methods was calculated as described in Landry et al. (2008) except that we used the

actual rather than calculated dilution factor to estimate the fraction of natural grazer density in the dilute treatments. Mortality due to microzooplankton grazing, g, was calculated as $\mu - K_{wsw}$.

Laboratory experiments with cultured phytoplankton

Laboratory experiments were conducted to determine if dilution itself or organic metabolites in filtrate made from diluted cultures influenced the growth rate of phytoplankton. All experiments were carried out in phytoplankton growth medium with nutrients in excess of what is required for growth, therefore, nutrient addition treatments were not included. We used cultures of a Norwegian isolate of *P. pouchetii* (AJ01) and a temperate isolate of *S. marinoi* (strain CCMP 3318). CCMP 3318 is a low or non-PUA producing strain (identified as the strain isolated in 2005 in Gerecht et al. 2011). Both were grown in ~30 psu seawater with *P. pouchetii* in f/2-Si medium and *S. marinoi* in L1 medium (recipes in Andersen et al. 2005) at ~200 photons m^{-2} s^{-1} on a 14:10 L:D cycle. *P. pouchetii* was cultured at 4°C and *S. marinoi* at 20°C. All experimental manipulations were performed at the respective growth temperature.

The *P. pouchetii* culture was grown to late exponential growth (4.6×10^5 cells mL^{-1}) and diluted with f/2 medium to 5.0×10^3 cells mL^{-1}, which is equivalent to a dense bloom. This diluted culture was considered the "WSW" in this experiment and stored in a 20 L carboy. In a 4°C environmental chamber, 12 L of FSW was prepared from the "WSW" using a FS-Polycap AS Whatman filter. Carbon cellulose-treated FSW (CC) was prepared by passing 6 L of the FSW through a Culligan Pentek C1 carbon-impregnated cellulose filter cartridge. In separate carboys, the following 20% dilutions were set up: 20% WSW and 80% FSW, 20% WSW and 80% CC, 20% WSW and 80% medium (f/2-Si). After mixing, triplicate samples for Chl *a* analyses were taken from the WSW and each diluted treatment. Aliquots of 250 mL from each carboy were siphoned into triplicate Corning polystyrene tissue culture flasks. The flasks were incubated at the growth irradiance and temperature for 24 h. At the end of the incubation, duplicate samples for
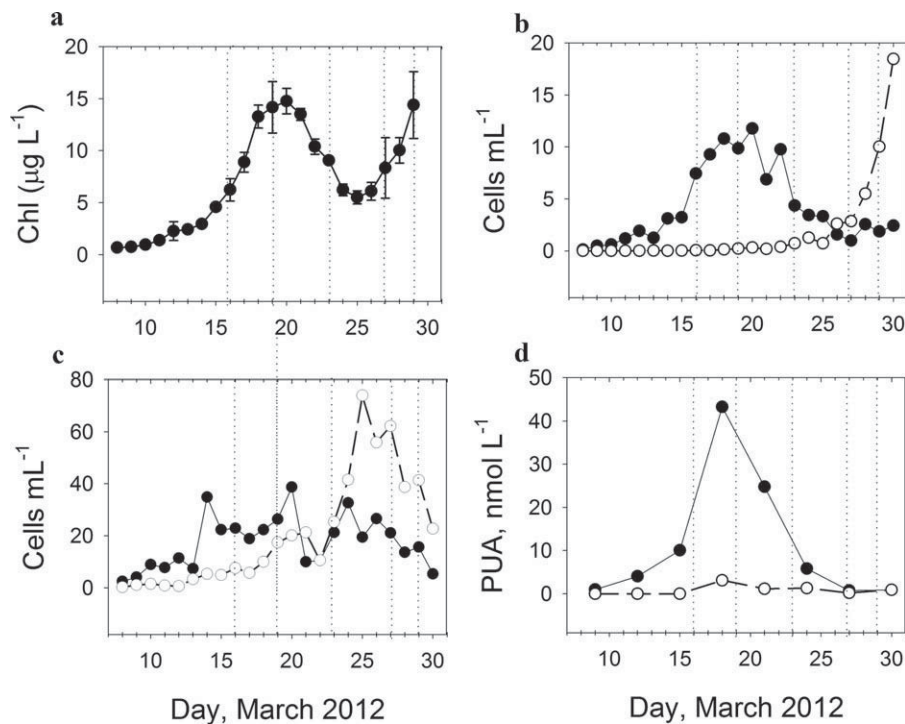
Fig. 1. Chl *a* concentration (a), abundance of colonial *Phaeocystis pouchetii* cells (1×10⁴) (open circles) and *Skeletonema marinoi* (1×10³) (solid circles) (b), microzooplankton abundance, ciliates (solid circles) and *Gyrodinium spirale* (open circles) (c), and concentration of particulate (solid circles) and dissolved (open circles) polyunsaturated aldehydes (PUAs) (d) in mesocosm M2. The vertical dotted lines indicate dates of the dilution experiments. In panel (a), error bars = 95% C.I.

Chl *a* analyses were analyzed from each incubation flask. Phytoplankton net growth (*K*) was determined from changes in Chl *a* as described in the previous section.

The experiment with *S. marinoi* was similar except that the culture was grown to midexponential phase (8.46 × 10⁵ cells mL⁻¹) and diluted with L1 medium to 5.0 × 10³ cells mL⁻¹ to make the "WSW." The experiment was conducted in a 20°C environmental chamber. The experimental manipulations and data analyses were otherwise similar to the *P. pouchetii* laboratory experiment.

Statistical methods

Single classification analysis of variance (ANOVA) was used to test for significant differences ($p < 0.05$) among mean values of treatment groups. Pairwise multiple comparisons were made with the Holm-Sidak procedure. Sigma Stat version 9.0 (Systat Software, Inc.) was used for the statistical analyses.

Results

Mesocosm

Initial values of nutrients before nutrient addition (day 0) in mesocosm M2 were relatively high, especially silicate, and after addition of nitrate and phosphate on day 1, sequential blooms developed (Table 1, Fig. 1a).

During most of the mesocosm experiments, the dominant phytoplankton was *S. marinoi*, with a bloom initiating ~12 March and peaking at ~10⁵ cells mL⁻¹ between 16 and 22 March, and then sharply declining after March 22 (Fig. 1b). During the peak of the *S. marinoi* bloom (15-23 March), ciliates, primarily large oligotrichs, were the dominant microzooplankton and they ranged in abundance from 10 to 39 cells mL⁻¹ (Fig. 1c). During this period, heterotrophic dinoflagellates were also common and one species, *Gyrodinium spirale*, dominated. It ranged in abundance from 5 to 25 cells mL⁻¹ (Fig. 1c). The *S. marinoi* bloom coincided with a peak in particulate and dissolved PUA (Fig. 1d). The PUAs detected during the *S. marinoi* bloom were primarily heptadienal, octadienal, and octratrienal (Table 3).

As the *S. marinoi* bloom declined, a *P. pouchetii* bloom developed, and was still on the rise when the mesocosm experiment ended on 30 March (Fig. 1b). Colonial *Phaeocystis* cells reached a density of over 1.5 × 10⁴ cells mL⁻¹. During the *Phaeocystis* bloom, ciliate densities decreased (Fig. 1c). *G. spirale* became the numerically dominant microzooplankton during the *Phaeocystis* bloom (Fig. 1c). During the rise of the *P. pouchetii* bloom, PUA concentrations were lower than during the *S. marinoi* peak (Fig. 1d).

Although picoplankton was present (data not shown), nano- and microphytoplantkon other than *Skeletonema* and

Table 4. Estimated phytoplankton net growth coefficient (K) in mesocosm M2 (from change in Chl a) and from dilution in experiments incubated in the mesocosm (treatment without added nutrients); phytoplankton instantaneous growth coefficient (μ) and microzoopankton grazing coefficients (g) from dilution experiments.

	Phytoplankton net growth (K, d^{-1})		Phytoplankton instantaneous growth and microzooplankton grazing from dilution experiments	
Date (Mesocosm Day)	Mesocosm*	Dilution Experiment Avg (Std Dev)	μ, d$^{-1\dagger}$	g, d$^{-1\dagger}$
16 Mar (8)	0.35	0.18 (0.01)	0.23	0.05
			0.54 (CC)‡	0.36 (CC)
19 Mar (11)	0.04	−0.08 (0.06)	−0.17	0.10
			1.07 (CC)‡	1.15
23 Mar (15)	−0.37	−0.25 (0.07)	−0.34 (Nut)	0 (Nut)
			−0.28 (Nut,CC)‡	0.06 (Nut, CC)
			−0.24 (CC)	0.01 (CC)
27 Mar (19)	0.35	−0.12 (0.04)	0 (Nut)	0.32 (Nut)
			0.22 (Nut, CC)‡	0.55 (Nut, CC)
			0.32 (CC)‡	0.44 (CC)
29 Mar (21)	0.36	−0.15(0.11)	0.79 (Nut)‡	1.14 (Nut)
			0.80 (Nut, CC)‡	1.16 (Nut,CC)

*Estimated for from change in Chl a from morning of experiment to next morning except for 29 March when estimated from previous morning to morning of experiment.

†CC=Filtered seawater treated by passage through a carbon cellulose cartridge
Nut=Nitrate and phosphate added

‡=Net growth rate in diluted treatment significantly different (p<0.05) than in corresponding whole seawater treatment (refer to Figure 2).

Phaeocystis were not abundant in the mesocosms. Estimates of phytoplankton net daily growth based on Chl a values the previous day and day of a dilution experiment were ~0.35 during the rise in *S. marinoi* (16 March) and the rise in *P. pouchetii* abundance (27 and 29 March; Table 4 and Fig. 1a and b).

Dilution grazing experiments in the mesocosm

In the dilution experiment conducted on 16 March during the rise in *Skeletonema* (Fig. 1b), the net growth rate of phytoplankton (K) in WSW treatment was positive, but the K in the untreated 10% WSW dilution was not significantly different from zero ($p > 0.05$; Fig. 2a). However, the growth rate of phytoplankton in the diluted treatment with carbon cellulose-treated FSW (CC treatment) was significantly higher ($p < 0.05$) than in the WSW or untreated FSW treatments (Fig. 2a). This resulted in an estimated phytoplankton instantaneous rate of increase (μ, d^{-1}) of 0.54 and a grazing coefficient (g, d^{-1}) of 0.36 based on the "CC" treatment (Table 4). In comparison, the estimated μ and g without the CC treatment were not statistically significant (Table 4).

In the dilution experiment conducted on 19 March, at the peak of the *Skeletonema* bloom (Fig. 1b), phytoplankton net growth (K) in the WSW treatment and in the untreated 10% WSW dilution were slightly negative and not statistically different ($p > 0.05$). In contrast, phytoplankton net growth in the CC-treated dilution was positive and high (~1 d^{-1}; Fig. 2b). This resulted in negative estimates of μ and g with the untreated filtrate and positive and significant estimates of μ and g with use of the CC-treated filtrate (Table 4).

On 23 March, during the decline of the *Skeletonoma* bloom (Fig. 1b), net growth rate of phytoplankton was negative in all treatments including the WSW and CC-treated FSW treatments with and without addition of nutrients (Fig. 2c). The only significant difference in K was between the WSW with added nutrients and the treated (+CC) treatment with added nutrients. Estimated g based on the nutrient addition treatment with the treated dilution water was 0.06, low but positive (Table 4).

On 27 March, at the end of the *Skeletonema* decline and at the beginning of the *Phaeocystis* bloom (Fig. 1b), the differences in net growth rate (K) among treatments were pronounced (Fig. 2d). In the WSW, net growth was negative, with and without nutrient addition (Fig. 2d). The phytoplankton net growth rate was highly variable in the untreated FSW dilution and positive in the carbon cellulose-treated seawater dilution experiment both with and without added nutrients (Fig. 2d). Without the CC treatment, estimates μ and g were not statistically significant, but with the CC treatment they were significant (Table 4). In the CC treatment without nutrients, phytoplankton instantaneous
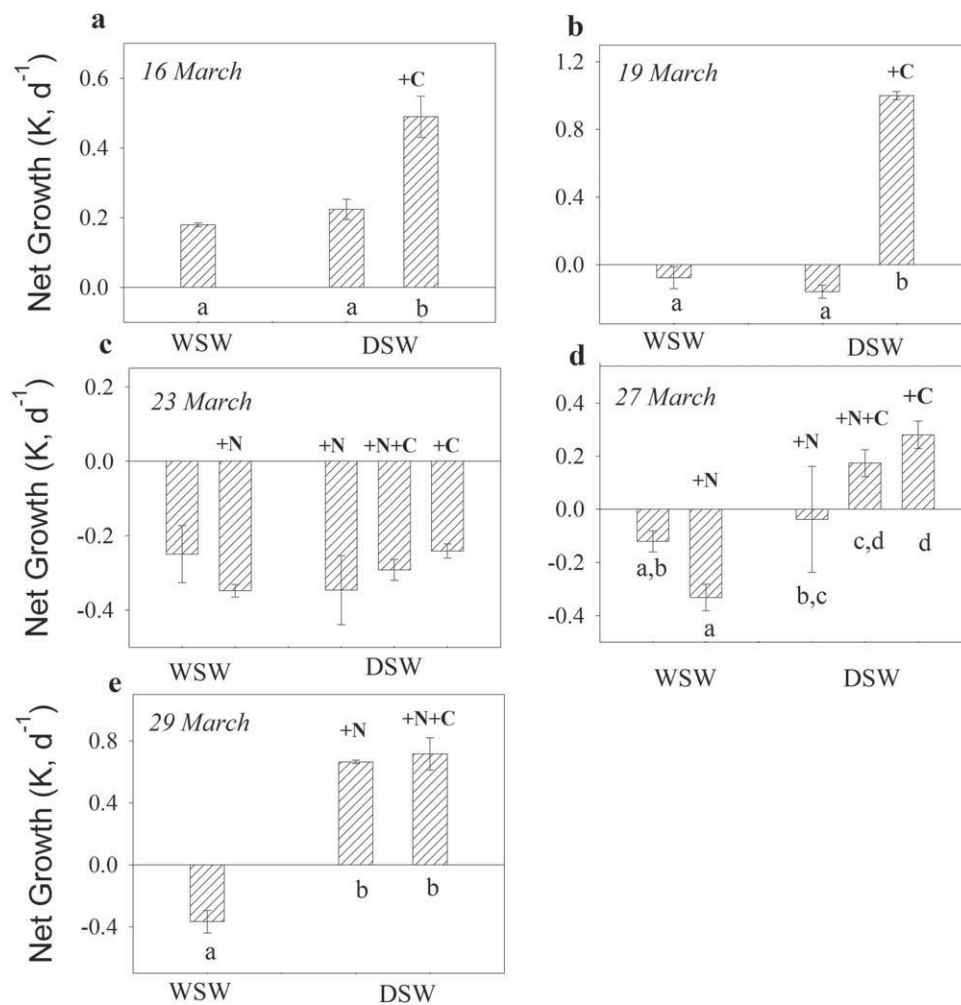
Fig. 2. Mean net growth rate (K, d^{-1}) of phytoplankton in whole seawater (WSW) and diluted treatments (DSW) in dilution experiments conducted on 16 March (a), 19 March (b), 23 March (c), 27 March (d), and 29 March (e) in mesocosm M2. $N = 3$ with Error bars = standard deviation. +C = diluted seawater treated by passage through a carbon cellulose (CC) cartridge; +N = addition of inorganic nutrients. Single Classification ANOVAs for 16 March ($F_{2,6} = 58.123$), 19 March ($F_{2,6} = 608.519$), 27 March ($F_{4,10} = 17.846$), and 29 March ($F_{2,6} = 206.074$) data sets are significant ($p < 0.001$), but 23 March ANOVA ($F_{4,10} = 2.458$) is not significant ($p > 0.05$). For panels with overall significant differences among treatments, different lowercase letters indicate bars which are statistically different ($p < 0.05$; Holm-Sidak method).

growth rate was 0.32 d^{-1} and the estimated grazing coefficient 0.44 d^{-1} (Table 4).

In the 29 March experiment, during the steep rise in *Phaeocystis*, nutrients were added to all treatments because of the low nutrient level in the mesocosm (Table 1). The net rate of growth of phytoplankton in the undiluted treatment was negative, whereas growth was positive and similar in the diluted treatments with and without the CC-treated FSW (Fig. 2e). Estimates of μ and g were 0.71 and 1.08, respectively, with the untreated FSW and 0.79 and 1.16, respectively, with the CC-treated FSW (Table 4). Differences in coefficients between the FSW and CC-treated FSW were not significant ($p > 0.05$).

The pattern of response of phytoplankton net growth rate to dilution was complex when the 25% WSW dilution was considered (Table 5). In the experiment on 16 March, the

growth rate of phytoplankton was positive in all treatments, but interestingly, the net growth rate in the 25% WSW treatment was significantly higher than in either the 10% or WSW treatments, indicating an inverted V-shaped response to dilution in this experiment. In the rest of the experiments, the net growth rate of phytoplankton in the 25% treatment was negative, and similar (19 and 23 March) or more negative (27 and 29 March) than the net growth rate of phytoplankton in the 10% WSW treatment.

Laboratory dilution experiments with algal cultures

The laboratory dilution experiments with a late exponential phase culture of *P. pouchetii* clearly indicate that dilution of a suspension of *P. pouchetii* with filtrate from that suspension dramatically changes the growth rate, with differences among treatments statistically significant (Fig. 3a). In the

Table 5. Comparison of the mean net growth rate (K, d^{-1}) of phytoplankton in the 25% WSW treatment to that in the 10% WSW and undiluted (100% WSW) treatments. On mesocosm days 8 and 11, no nutrients were added to the treatments, on days 15, 19, and 21, nutrients were added to all treatments. Means (+Standard deviation). One Way ANOVA with the Holm-Sidak Method used to compare the results from 25% treatment to the 10% and 100% WSW treatments. ns = nonsignificant.

Mesocosm Day	Date	10%	25%	100%	Statistics
8	16 Mar	0.224(0.024)	0.453(0.310)	0.179(0.004)	ANOVA: $Fs_{2,6} = 125.121$; $p < 0.001$ 25% vs.10%: $p < 0.05$ 25% vs.100%: $p < 0.05$
11	19 Mar	−0.159(0.031)	−0.204(0.017)	−0.079(0.052)	ANOVA: $Fs_{2,6} = 9.124$; $p = 0.015$ 25% vs.10%: n.s. 25% vs.100%: $p < 0.05$
15	23 Mar	−0.347(0.076)	−0.301(0.013)	−0.348(0.014)	ANOVA: $Fs_{2,6} = 1.052$; $p = 0.406$, ns
19	27 Mar	−0.038(0.163)	−0.371(0.110)	−0.332(0.041)	ANOVA: $Fs_{2,6} = 7.392$; $p = 0.024$ 25% vs.10%: $p < 0.05$ 25% vs.100%: $p < 0.05$
21	29 Mar	0.680(0.025)	−0.312(0.166)	−0.351(0.077)	ANOVA: $Fs_{2,6} = 90.086$; $p < 0.001$ 25% vs.10%: $p < 0.05$ 25% vs.100%: ns

undiluted suspension, the growth was positive but it was negative in the diluted (FSW) treatment. With CC treatment of the filtrate, growth was still negative, but the decline was less than in the untreated FSW treatment. In a control, in which the suspension was diluted with clean medium, the growth rate was similar to that in the undiluted, WSW, treatment (Fig. 3a).

Although growth was positive in all treatments with a midexponential growth phase culture of *S. marinoi* (CCMP 3318), the growth rate in the dilution was reduced compared to the undiluted WSW suspension when the cell suspension was diluted with untreated filtrate (Fig. 3b). With CC-treated filtrate or fresh medium, there was no reduction in growth rate compared to the WSW treatment (Fig. 3b). The negative effects of the untreated filtrate were not as severe as with the *P. pouchetii* cell suspension although the treatments with the two phytoplankters were at the same initial cell density (5000 mL^{-1}) in the WSW.

Discussion

Dilution experiments are widely used, and the only method available, to estimate in situ microzooplankton community grazing, however, the responses to dilution are not always linear, which can make interpretation of results difficult and may lead to over or under estimation of grazing (reviewed in Schmoker et al. 2013). Most attention has been

on factors that result in an over-estimation of grazing, such as release of microzooplankton from top down control in the absence of mesozooplankton (Dolan et al. 2000). This factor is potentially most important in warm waters in which populations of microzooplankton can double each day. Underestimation of grazing has received less attention. Trophic cascades, particularly in experiments in which maximum dilution levels are moderate ($\geq$25% WSW) can lead to V-shaped responses, nonsignificant results, and sometimes to "reverse" slopes, all of which may lead to underestimation of grazing (Calbet and Saiz 2013). We frequently obtained "reverse" slopes in mesocosm or laboratory dilution experiments with *S. marinoi* or *P. pouchetii* when the potential for trophic cascading was nonexistent (i.e., with phytoplankton cultures) or minimal (due to use of high dilution level).

The dilution experiments conducted in the mesocosm show that higher net growth rate of phytoplankton in undiluted rather than diluted treatments, resulting in "negative" or statistically nonsignificant grazing coefficients, can occur during *S. marinoi* blooms. During some, but not all stages of the mesocosm bloom, treatment of the dilution water to remove or reduce dissolved organics (CC treatment) had a large effect, and resulted in positive and significant estimates of microzooplankton grazing in experiments in which grazing estimates were negative, 0 or low without the CC treatment. Due to the physicochemical properties of charcoal, CC treatment can be considered to remove efficiently all
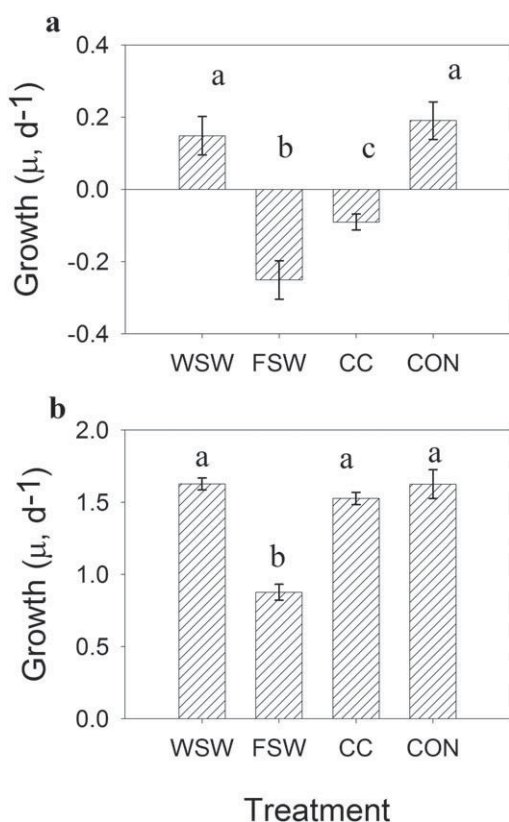
Fig. 3. Growth of phytoplankton in laboratory dilution experiments conducted with cultures. Mean growth rate (μ, d^{-1}) with $N = 3$; error bars = standard deviation. WSW = culture suspension at 5000 cells mL^{-1}. Diluted treatments (10% WSW): FSW = 90% filter seawater made from culture suspension; CC = 90% FSW treated by passage through a carbon cellulose cartridge; CON = 90% medium. Single Classification ANOVA for the *Phaeocystis pouchetii* (Panel a) ($F_{3,8} = 58.184$), and *Skeletonema marinoi* (Panel b) ($F_{3,8} = 94.889$) are both statistically significant ($p < 0.001$); different lowercase letters indicate bars which are statistically different ($p < 0.05$; Holm-Sidak method).

organic metabolites present. This was exemplary demonstrated by the quantitative removal of excess PUA from FSW. Above natural PUA concentrations were reduced to levels below the detection limit by single passage through the CC cartridge (see experimental, data not shown). Nutrient addition sometimes influenced net phytoplankton growth, but in most mesocosm dilution experiments, the carbon cellulose treatment had a more pronounced influence on phytoplankton growth than nutrient addition in the diluted treatments.

In the laboratory experiment with cultured *S. marinoi* (CCMP 3318), the inhibition of growth by the filtrate was less dramatic than in the mesocosm dilution experiments. This is not surprising since the CCMP 3318 strain that is not a high producer of PUA. Furthermore, the laboratory experiment was at a density of 5×10^3 cells mL^{-1}, but in the mesocosm, *Skeletonema* reached a higher density, 1×10^5 cells mL^{-1}, and was subject to grazing and silica limitation,

which can stimulate PUA production (Pohnert 2000; Ribalet et al. 2009). It is also possible that additional unidentified inhibitory metabolites were present in the mesocosms.

Many bloom-forming diatoms produce PUAs or other potentially toxic oxylipins (Wichard et al. 2005), with the amount and variety of compounds produced species- and strain-specific (Taylor et al. 2009; Ianora and Miralto 2010). PUAs can inhibit the growth of PUA producers, as well as of other phytoplankton (Hansen and Eilertson 2007; Paul et al. 2009; Ribalet et al. 2014). In phytoplankton, such as *S. marinoi*, the production and release of PUAs is triggered by growth phase and/or mechanical stress (Pohnert 2000; Pohnert et al. 2002; Vidoudez and Pohnert 2012). In mesocosm M2, total PUA concentration reached concentrations of over 40 nmol L^{-1}, with particulate PUA accounting for most of the total, at the height of *Skeletonema* bloom. We observed the most inhibition of phytoplankton net growth by the untreated FSW during the peak in *Skeletonema* abundance and in PUA concentrations in the mesocosm. It is likely that the mechanical stress involved in production of large volumes (~25 L) of FSW stimulated PUA production and/or release into the filtrate used for dilution.

P. pouchetii is also known to produce PUAs, but mainly decadienal, whereas *S. marinoi* mainly produces heptadienal, octdienal, and octradienal (Hansen and Eilertson 2007). However, all four PUAs inhibit mitotic cell divisions (Adolph et al. 2003). PUA concentrations were low in the mesocosm, when colonial *P. pouchetii* was dominant, although cell densities reached 10^4 cells mL^{-1}. This is perhaps because the population was still growing exponentially when the mesocosm experiment ended, and thus it was not sampled during its peak abundance or during its decline when it would have been subject to increasing stress, when it may have produced more decadienal. Alternatively, a population low in PUA could have been the dominant bloom former. In the final mesocosm dilution experiment, when *P. pouchetii* was still increasing and PUAs were low, we did not observe growth inhibition due to the FSW.

In contrast, in the laboratory experiment with cultured *P. pouchetii* at a lower concentration than in the mesocosm experiment, we observed a strong inhibition of growth due to dilution with the filtered water. The laboratory experiment was with a late growth phase culture containing single cell, whereas the *P. pouchetii* population in the mesocosm experiment was actively growing, but forming colonies. It is possible that the difference in culture and mesocosm results was due to growth form and phase. Alternatively, the culture may have been a higher PUA producing strain than the ones in the fjord and captured in the mesocosm.

In our investigation, we measured PUAs, but not other potentially inhibitory metabolites known to be produced by marine phytoplankton. We focused on PUAs because the dominant phytoplankton in the mesocosms, *S. marinoi* and *P. pouchetii*, are known PUA producers (Hansen and Eilertson

2007, Paul et al. 2009) . We think that the inhibitory effects we observed were due primarily to PUAs released from *Skeletonema* during filtration, but we cannot exclude the possibility that the effects were at least partly due to other, unidentified metabolites in the dilution water.

An important question is whether the phenomenon we observed in mesocosm and laboratory dilution experiments influences the results of field measurements of microzooplankton community grazing. *S. marinoi* reached higher concentrations in the mesocosm than usually observed in NE Atlantic and Arctic waters, where maximum abundances are ~500 cells mL^{-1} (Degerlund and Eilertsen 2010). However, many bloom forming diatoms can produce PUAs and total diatom biomass may reach the levels in our experiments. The *P. pouchetii* concentration used in the laboratory experiment was within the range observed during spring *P. pouchetii* blooms in Arctic and sub-Arctic waters (Wassmann et al. 2005; Degerlund and Eilertsen 2010).

There is evidence of negative effects on phytoplankton growth, leading to underestimation of microzooplankton grazing, in dilution experiments conducted during *Phaeocystis* and diatom blooms in cold seas. Calbet et al. (2011) observed that during a summer *P. pouchetii* bloom, microzooplankton biomass was considerable, but significant grazing was only observed in 38% of the dilution experiments. In the eastern Bering Sea during spring, Sherr et al. (2013) obtained negative slopes in 37% of the dilution experiments and estimated phytoplankton instantaneous growth rates varied from slightly negative to >0.4 d^{-1}. In the eastern Bering Sea in summer, where remnants of spring diatom blooms persisted as well as new, patchy blooms of *P. pouchetii* near the shelf edge, 39% of the grazing coefficients obtained were ≤0 and in 3% of the experiments, negative slopes were statistically significant (Stoecker et al. 2014). In the investigations discussed above, the dilutions were amended with inorganic nutrients or nutrients were shown to have no effect; thus, the negative results were not due to lack of nutrient regeneration in the diluted treatments.

Inhibition of phytoplankton growth by dilution is not a general phenomenon. Globally, average phytoplankton production estimates from dilution experiments are slightly higher than production estimated from ^{14}C uptake experiments (Calbet and Landry 2004). The two methods have been directly compared in studies in the oligotrophic Red Sea (Moigis 1999), the Arabian Sea (Brown et al. 1999, 2002) and as part of enclosure experiments in the northern Baltic Sea (Lignell et al. 2003). In these investigations, the two methods produced comparable results, indicating that dilution did not inhibit phytoplankton growth. However, to our knowledge, the results of ^{14}C uptake and dilution experiments have not been compared during dense diatom or *Phaeocystis* blooms.

To explore the potential effects of dilution on phytoplankton during *Phaeocystis* and diatom blooms, Stoecker et al. (2014) measured variable fluorescence (Fv/Fm) as part of 14 dilution grazing experiments conducted in the eastern Bering Sea in summer of 2008. In half of the experiments, variable fluorescence was lower in the diluted (20% WSW) than in the WSW treatment. Decrease in variable fluorescence in phytoplankton is an indicator of physiological stress and is usually associated with a reduction in ability of cells to photosynthesize (Chekalyuk and Hafez, 2008). Low estimates of microzooplankton grazing were associated with experiments in which variable fluorescence declined in the diluted treatment. These results suggest that phytoplankton instantaneous growth and microzooplankton grazing coefficients may be underestimated by dilution protocols in some situations due to decreased survival or growth of phytoplankton in the diluted treatments. It is not surprising that filtration, particularly of large volumes of WSW, can sometimes result in release of organic material into filtered sea water that then can inhibit phytoplankton growth and perhaps also microzooplankton grazing. However, whether or not phytoplankton growth is inhibited depends on species and strain, physiological state, and cell density of the phytoplankton as well as stresses such as grazing (Ianora and Miralto 2010). The exact protocol for producing the FSW also must matter. The concentration of metabolites released can be expected to increase with the phytoplankton biomass and the volume filtered because longer retention of phytoplankton on the filter may increase the stress on cells.

Use of a carbon cellulose cartridge to treat the FSW before use for dilution of the WSW appears to reduce or eliminate the inhibitory affect. This is useful in identifying when there is a problem with the dilution protocol. However, using this added treatment to "correct" the experiment is problematical. In dilution experiments conducted during dense blooms, there may be considerable PUAs and other metabolites free in the water that are inhibiting phytoplankton growth and, perhaps microzooplankton grazing, in the WSW. Treatment of the diluted water to remove these initial amounts, as well as the additional amounts released during filtration, could lower the concentration in the diluted treatments below that in the WSW, resulting in an overestimation of phytoplankton growth and microzooplankton grazing.

We suggest that the first step in resolving this issue is determining in which plankton communities it occurs. The dilution technique generally works very well (reviewed in Calbet and Saiz 2013). Problems are most likely to arise in applying this technique during dense blooms of phytoplankton or immediately post bloom. Production of many inhibitory allelochemcials is stimulated by nutrient stress, grazing, and/or associated with cell death and thus it is possible that the concentration of inhibitory chemicals is also high in declining blooms (Ianora and Miralto 2010, Ribalet et al. 2009, 2014). In addition to diatom blooms, these effects may also be associated with dense blooms of dinoflagellates (Tillman and Hansen 2009) and prymesiophytes (Schmidt

and Hansen 2001, Strom et al. 2003, Fredrickson and Strom 2009) since bloom forming members of these taxa are known to produce allelopathetic compounds.

In dense bloom or post bloom situations, we suggest that a full dilution series with at least five or six dilution levels (with replication), including at least one high dilution level (5 or 10% WSW) be used. At the high dilution levels, artifacts due to feeding saturation and trophic cascades are minimized (Calbet and Saiz 2013), but problems due to release of allelochemicals from phytoplankton into the dilution water should be maximum. A linear relationship between phytoplankton net growth and dilution level (Fig. 1a in Calbet and Saiz 2013) would indicate that there is not a problem and that the data could be analyzed using linear regression (Landry and Hassett 1982) or the two-point method (Worden and Binder 2002, Landry et al. 2008). An L-shaped or V-shaped response curve (Fig. 1b,c in Calbet and Saiz 2013) would indicate that saturation of grazers or trophic cascades occurred at the lower dilution levels and that the data are best analyzed using the two-point method. A positive slope is indicative of contamination of the FSW with toxic substances. Contamination may be due to release of inhibitory substances from phytoplankton during preparation of FSW, as shown herein, or possibly due to presence of toxins on the filtration apparatus. Trophic cascades may also sometimes result in a positive slope, but their effects should be alleviated at high dilution levels (Calbet and Saiz 2013). Another possibility is an inverted V-shaped response, as seen in one of our mesocosm dilution experiments; this type of response is most likely to be due to inhibitory substances in the FSW.

If filtration equipment is clean and nontoxic but dilution experiments with a plankton assemblage result in positive slopes and/or inverted V-shaped responses, what steps can be taken to understand or alleviate the problem? One step would be to modify the filtration procedure so that is gentler (i.e., results in less release of organic material from phytoplankton). The next step may be to use several intermediate dilution levels to determine if there is a range of dilution where the response is linear and to use the slope in this region to calculate the grazing coefficient.

In some bloom situations, it may not be possible to use the dilution technique to accurately estimate microzooplankton grazing, but it would be worthwhile to document the phytoplankton community involved and that the dilution water was the problem. This could involve 1) removal of dissolved organic material from the dilution water as described herein, 2) comparison of metabolomic profiles of WSW and FSW, and 3) comparison of Chl *a* specific rates of photosynthesis or of variable fluorescence (Fv/Fm) in the WSW and dilution water. These efforts would lead to a better understanding of the limitations of the dilution technique in bloom situations, of phytoplankton growth and microzooplankton grazing during blooms, and of the complex chemi-

cal interactions that can occur between phytoplankton and their grazers that may influence bloom persistence and the transfer of carbon to higher trophic levels.

References

Adolph, S., S. S. Poulet, and G. Pohnert. 2003. Synthesis and biological activity of α, β, γ, δ-unsaturated aldehydes from diatoms. Tetrahedron **59**: 3003–3008. doi:10.1016/S0040-4020(03)00382-X

Andersen, R. A., J. A. Berges, P. J. Harrison, and M. M. Watanabe. 2005. Appendix A. Recipes for freshwater and seawater Media. p. 429–532. In Andersen RA. [ed.] Algal Culturing Techniques. Elsevier Academic Press. 578 pp.

Brown, S. L., M. R. Landry, R. T. Barber, L. Campbell, D. L. Garrison, and M. M. Gowing. 1999. Picophytoplankton dynamics and production in the Arabian Sea during the 1995 Southwest Monsoon. Deep Sea Res. II **46**: 1745–1768. doi:10.1016/S0967-0645(99)00042-9

Brown, S. L., M. R. Landry, S. Christensen, D. Garrison, M. M. Gowing, R. R. Bidigare, and L. Campbell. 2002. Microbial community dynamics and taxon-specific phytoplankton production in the Arabian Sea during the 1995 monsoon seasons. Deep Sea Res. II **49**: 2345–2376. doi:10.1016/S0967-0645(02)00040-1

Calbet, A. and M. R. Landry. 2004. Phytoplankton growth, microzooplankton grazing and carbon cycling in marine systems. Limnol. Oceanogr. **49**: 51–57. doi:10.4319/lo.2004.49.1.0051

Calbet, A. and E. Saiz. 2013. Effects of trophic cascades in dilution grazing experiments: From artificial saturated feeding responses to positive slopes. J. Plank. Res. **35**: 1183–1191. doi:10.1093/plankt/fbt067

Calbet, A., and others. 2011. Low microzooplankton grazing rates in the Arctic Ocean during a *Phaeocystis pouchetii* bloom (Summer 2007): Fact or artefact of the dilution technique? J. Plank. Res. **33**: 687–701. doi:10.1093/plankt/fbq142

Caron, D. A., M. R. Dennett, D. J. Lonsdale, D. M. Moran, and L. Shalapyonok. 2000. Microzooplankton herbivory in the Ross Sea, Antarctica. Deep Sea Res. II **47**: 3249–3272. doi:10.1016/S0967-0645(00)00067-9

Chekalyuk, A. and M. A. Hafez. 2008. Advanced laser fluorometry of natural aquatic environments. Limnol. Oceanogr.: Methods **6**: 591–609. doi:10.4319/lom.2008.6.591

Degerlund, M. and H. C. Eilertsen. 2010. Main species characteristics of phytoplankton spring blooms in NE Atlantic and Arctic waters (68-80°N). Estuaries Coasts **33**: 242–269. doi:10.1007/s12237-009-9167-7

Dolan, J. R., C. L. Gallegos, and A. Moigis. 2000. Dilution effects on microzooplankton in dilution grazing experiments. Mar. Ecol. Prog. Ser. **200**: 127–139. doi:10.3354/meps200127

Franzè, G. and P. J. Laventyev. 2014. Microzooplanton growth rates examined across a temperature gradient in the Barents Sea. PLoS One **9**: e86429. doi:10.1371/journal.pone.0086429

Fredrickson, K. A. and S. L. Strom. 2009. The algal osmolyte DMSP as a microzooplankton grazing deterrent in laboratory and field studies. J. Plank. Res. **31**: 135–152. doi:10.1093/plankt/fbn112

Gerecht, A., G. Romano, A. Ianora, G. d'Ippolito, A. Cutignano, and A. Fontana. 2011. Plasticity of oxylipin metabolism among clones of the marine diatom *Skeletonema marinoi* (Bacillariophyceae). J. Phycol. **47**: 1050–1056. doi:10.1111/j.1529-8817.2011.01030.x

Hansen, P. J. 1989. The red tide dinoflagellate *Alexandrium tamarense*: Effect on behaviour and growth of a tintinnid ciliate. Mar. Ecol. Prog. Ser. **53**: 105–116. doi:10.3354/meps053105

Hansen, E. and H. C. Eilertsen. 2007. Do polyunsaturated aldehydes produced by *Phaeocystis pouchetii* (Hariot) Langerheim influence diatom growth during the spring bloom in Norway? J. Plank. Res. **29**: 87–96. doi:10.1093/plankt/fbn1065

Ianora, A. and A. Miralto. 2010. Toxigenic effects of diatoms on grazers, phytoplankton and other microbes: A review. Ecotoxicology **19**: 493–511. doi:10.1007/s10646-009-0434-y

Jónasdottir, S. H., and others. (2011). Extensive cross disciplinary analysis of biological and chemical control of *Calanus finmarchicus* reproduction and grazing response to an aldehyde forming diatom bloom in mesocosms. Mar. Biol. **158**: 1943–1963. doi:10.1007/s00227-011-1705-8

Landry, M. R., S. L. Brown, Y. M. Rii, K. E. Selph, R. R. Bidigare, E. J. Yang, and M. P. Simmons. 2008. Depth-stratified phytoplankton dynamics in Cyclone *Opal*, a subtropical mesoscale eddy. Deep Sea Res. II **55**: 1348–1359. doi:10.1016/j.dsr2.2008.02.001

Landry, M. R. and R. P. Hassett. 1982. Estimating the grazing impact of marine micro-zooplankton. Mar. Biol. **67**: 283–288. doi:10.1007/BF00397668

Lignell, R., J. Seppälä, P. Kuuppo, T. Tamminen, T. Andersen, and I. Gismervik. 2003. Beyond bulk properties: Responses of coastal summer plankton communities to nutrient enrichment in the northern Baltic Sea. Limnol. Oceanogr. **48**: 189–209. doi:10.4319/lo.2003.48.1.0189

Moigis, A. G. 1999. Photosynthetic rates in the surface waters of the Red Sea: The radiocarbon versus the non-isotopic dilution method. J. Plankton Res. **22**: 713–727. doi:10.1093/plankt/22.4.713

Nejstgaard, J. C., and others. 2006. Plankton development and trophic transfer in seawater enclosures with nutrients and *Phaeocystis pouchetii* added. Mar. Ecol. Prog. Ser. **321**: 99–121. doi:10.3354/meps321099

Paul, C., A. Barofsky, C. Vidoudez, and G. Pohnert. 2009. Diatom exudates influence metabolism and cell growth of co-cultured diatom species. Mar. Ecol. Prog. Ser. **389**: 61–70. doi:10.3354/meps08162

Pohnert, G. 2000. Wound-activated chemical defense in unicellular planktonic algae. Angew. Chem. Int. Ed. **39**: 4352–4354. Doi:10.1002/1521-3773(20001201)39:23< 4352::AID-ANIE4352>3.0.CO;2-U

Pohnert, G., O. Lumineau, A. Cueff, S. Adolph, C. Cordevant, M. Lange, and S. Poulet. 2002. Are volatile unsaturated aldehydes from diatoms the main line of chemical defense against copepods? Mar. Ecol. Prog. Ser. **245**: 33–45. doi:10.3354/meps245033

Ribalet, F., C. Vidoudez, D. Cassin, G. Pohnert, A. Ianora, A. Miralto, and R. Casotti. 2009. High plasticity in the production of diatom-derived polyunsaturated aldehydes under nutrient limitation: Physiological and ecological implications. Protist **160**: 444–451. doi:10.1016/j.protis.2009.01.003

Ribalet, F., and others. 2014. Phytoplankton cell lysis associated with polyunsaturated aldehyde release in the northern Adriatic Sea. PLoS ONE **9**(1): e85947. doi:10.1371/journal.pone.0085947

Rose, J. M. and D. A. Caron. 2007. Does low temperature constrain the growth rates of heterotrophic protists? Evidence and implications for algal blooms in cold water. Limnol. Oceanogr. **52**: 886–895. doi:10.4319/lo.2007.52.2.0886

Schmidt, E. W. and P. J. Hansen. 2001. Allelopathy in the prymnesiophyte *Chrysochromulina polylepis*: Effects of cell concentration, growth phase and pH. Mar. Ecol. Prog. Ser. **216**: 67–81. doi:10.3354/meps216067

Schmoker, C. S., Hernandez-Leon, and A. Calbet. 2013. Microzooplankton grazing in the oceans: Impacts, data availability, knowledge gaps and future directions. J. Plank. Res. **35**: 691–706. doi:10.1093/plankt/fbt023

Sherr, E. B., B. F. Sherr, and C. Ross. 2013. Microzooplankton grazing impact in the Bering Sea during spring sea ice conditions. Deep Sea Res. II **94**: 57–67. doi:10.1016/j.dsr2.2013.03.019

Stoecker, D. K., A. Weigel, and J. A. Goes. 2014. Microzooplankton grazing in the Eastern Bering Sea in summer. Deep Sea Res II **109**: 145–156. doi:10.1016/j.dsr2.2013.09.017

Strom, S. L. and K. A. Fredrickson. 2008. Intense stratification leads to phytoplankton nutrient limitation and reduced microzooplankton grazing in the southeastern Bering Sea. Deep Sea Res. II **55**: 1761–1774. doi:10.1016/j.dsr2.2008.04.008

Strom, S. L., M. B. Olson, E. L. Macri, and C. W. Mordy. 2006. Cross-shelf gradients in phytoplankton community structure, nutrient utilization, and growth rate in the coastal Gulf of Alaska. Mar. Ecol. Prog. Ser. **328**: 75–92. doi:10.3354/meps328075

Strom, S., G. Wolfe, A. Slajer, S. Lambert, and J. Cough. 2003. Chemical defense in the microplankton II:

Inhibition of protist feeding by beta-dimethylsufonioproprionate (DMSP). Limnol. Oceanogr. **48**: 230–237. doi:10.4319/lo.2003.48.1.0230

Taylor, R. L., K. Abrahamsson, A. Godhe, and S-Å. Wängberg. 2009. Seasonal variability in polyunsaturated aldehyde production potential among strains of *Skeletonema marinoi* (Bacillariophyceae). J Phycol. **45**: 46–53. doi: 10.1111/j.1529-8817.2008.00625.x

Tillman, U. and P. J. Hansen. 2009. Allelopathetic effects of *Alexandrium tamarense* on other algae: Evidence from mixed growth experiments. Aquat. Microb. Ecol. **57**: 101–112. doi:10.3354/ame01329

Vidoudez, C., R. Cascotti, M. Bastianini, and G. Pohnert. 2011b. Quantification of dissolved and particulate polyunsaturated aldehydes in the Adriatic Sea. Mar Drugs **9**: 500–513 doi:10.3390/md9040500

Vidoudez, C., J. C. Nejstgaard, H. H. Jakobsen, and G. Pohnert. 2011a. Dynamics of dissolved and particulate polyunsaturated aldehydes in mesocosms inoculated with different densities of the diatom *Skeletonema marinoi*. Mar Drugs **9**: 345–358.doi: 10.3390/md9030345

Vidoudez, C., and G. Pohnert. 2012, Comparative metabolomics of the diatoms *Skeletonema marinoi* in different growth phases. Metabolomics **8**: 654–669. doi:10.1007/s11306-011-0356-6

Wassmann, P., T. Ratkova, and M. Reigstad. 2005. The contribution of single and colonial cells of *Phaeocystis pouchetii* to spring and summer blooms in the north-eastern North Atlantic. Harmful Algae **4**: 823–840. doi:10.1016/j.hal.2004.12.009

Wichard, T., S. A. Poulet, C. Halsband-Lenk, A. Albania, R. Harris, D. Liu, and G. Pohnert. 2005. Survey of the chemical defense potential of diatoms: Screening of fifty one species for α, β, γ, δ-unsaturated aldehydes. J. Chem. Ecol. **31**: 949–958. doi:10.1007/s10886-005-3615-z

Supplement to Stoecker et al. "Underestimation of microzooplankton grazing in dilution experiments due to inhibition of phytoplankton growth"

Methods for Determination, Analysis and Quantification of particulate and dissolved PUAs

Determination of the production of PUAs by cells was performed according to a slightly modified protocol based on Vidoudez et al. (2011). Important steps in the Vidoudez et al. protocol are briefly described, whereas steps which varied from the Vidoudez et al. (2011) protocol are described in detail.

For particulate PUA, 1 to 5 L of mesocosm water depending on cell densities was concentrated on a GF/C filter (Whatman, Dassel, Germany) under vacuum (min. 500 mbar). This protocol was verified not to result in the release of PUAs from cells. The filter was rinsed with 1.5 mL of a 25 mM *O*-(2,3,4,5,6-pentafluorobenzyl) hydroxylamine hydrochloride (PFBHA, Roth, Karlsruhe, Germany) solution in 100 mM TRIS-HCl, pH 7.2. The filter and the cell suspension were transferred into a glass vial and were mixed on a vortexer, 5 µL of the internal standard (benzaldehyde 1 nM in methanol, Sigma Aldrich) was added, the vial was closed and shaken. The samples were frozen and thawed for mechanical cell disruption, incubated and subsesquently stored according to the original protocol (Vidoudez et al. 2011). PUA extraction was performed according to Vidoudez et al. (2011), but, for the first extraction step, glass spheres were added and the suspension was vortexed for 2 min. after the addition of the 750 µL methanol and 1.5 mL hexane. Finally, the hexane extracts were vacuum dried and re-dissolved in 80 µL hexane for GC-MS measurements.

For dissolved PUAs, 5 µL of internal standard (benzaldehyde, 1 mM in methanol) was added to 1 L of the mesocosm water in a PP bottle. The samples were filtrated on a GF/C filter (Whatman, Dassel, Germany) under vacuum (max. 500 mbar) and the filtrate was transferred through teflon tubing with a flow rate of circa 1 L h^{-1} to a 3 mL EASY® solid phase extraction cartridge (Macherey-Nagel, Düren, Germany) which had been pretreated with 1 mL of a PFBHA solution in 100 mM TRIS-HCl, pH 7.2. The liquid retained in the cartridge was reduced by applying overpressure from an empty syringe to the cartridge. EASY® cartridges were then washed with 2 x 2 mL deionized water, dried in vacuum (circa 600 mbar) and eluted into glass vials with 2 x 2 mL of a 5 mM solution of PFBHA in methanol. After incubation for 1 h at room temperature, samples were stored at -20°C. The PUA extraction was accomplished according to Vidoudez et al. (2011b). Finally, the hexane extracts were vacuum dried and re-dissolved in 80 µL hexane for GC-MS measurements. The identical protocol without the GF/C filtration step was followed for the determination of the purification success of charcoal cartridges (see below).

The samples were measured with GC/MS (ISQ Trace GC Ultra, Thermo Fisher, Dreieich, Germany) equipped with a 0.25 mm x 30 m DB-5MS GC column (Agilent, Böblingen, Germany) in electron impact (EI 70 eV) mode. Data were evaluated with the Xcalibur Quan Browser (2.1.0 SP1.1160). Identification of PUAs was based on the retention time compared with standards (except octatrienal that was identified based on its characteristic mass spectrum) and major fragment ions as described in Vidoudez et al. (2011). The quantification was based on the ratio between the molecular ions of the derivatized PUAs (m/z 319 for octadienal, 317 for octatrienal, 347 for decadienal) or the major fragment m/z 276 (present in all measured PUAs) for octadienal and the fragment m/z 271 of the derivatized internal standard. The following quantification standards were produced and derivatized, 0.5, 1,

2, 5, 10, 20, 50, 75 nM from heptadienal (<97%, Sigma-Aldrich), octadienal (96+%, Sigma-Aldrich) and decadienal (85%, Sigma-Aldrich) according to the original protocol (Vidoudez et al. 2011). The same calibration as for octadienal was used for octatrienal. The selected quantification curves for each standard were dependent on the detection limit of each PUA and the maximal amount found in the sample with the highest concentration. The GC temperature program for the separation was 60°C (held for 2 min) then ramped with a rate of 8°C min^{-1} to 240°C and then with a rate of 15°C min^{-1} to 300°C (held for 3 min).

Reference

Vidoudez C., R. Cascotti, M. Bastianini, and G. Pohnert. 2011. Quantification of dissolved and particulate polyunsaturated aldehydes in the Adriatic Sea. Marine Drugs 9: 500-513 doi:10.3390/md9040500.

4.2   Manuscript B

A metabolic probe-enabled strategy reveals uptake and protein targets of polyunsaturated aldehydes in the diatom *Phaeodactylum tricornutum*

Stefanie Wolfram, Natalie Wielsch, Yvonne Hupfer, Bettina Mönch, Hui-Wen Lu-Walther, Rainer Heintzmann, Oliver Werz, Aleš Svatoš, Georg Pohnert

The supporting information S1 Folder, S2 Folder, S3 Folder and S1 Table of this publication are available via the embedded DVD.

RESEARCH ARTICLE

A Metabolic Probe-Enabled Strategy Reveals Uptake and Protein Targets of Polyunsaturated Aldehydes in the Diatom *Phaeodactylum tricornutum*

Stefanie Wolfram[1], Natalie Wielsch[2], Yvonne Hupfer[2], Bettina Mönch[3], Hui-Wen Lu-Walther[4], Rainer Heintzmann[4,5], Oliver Werz[3], Aleš Svatoš[2], Georg Pohnert[1] *

1 Bioorganic Analytics, Institute for Inorganic and Analytical Chemistry, Friedrich Schiller University, Jena, Germany, 2 Department Mass Spectrometry/Proteomics, Max Planck Institute for Chemical Ecology, Jena, Germany, 3 Department of Pharmaceutical and Medicinal Chemistry, Institute of Pharmacy, Friedrich Schiller University, Jena, Germany, 4 Biomedical Imaging, Department Microscopy, Leibniz Institute of Photonic Technology e.V., Jena, Germany, 5 Institute for Physical Chemistry, Abbe Center of Photonics, Friedrich Schiller University, Jena, Germany

* Georg.Pohnert@uni-jena.de

Abstract

Diatoms are unicellular algae of crucial importance as they belong to the main primary producers in aquatic ecosystems. Several diatom species produce polyunsaturated aldehydes (PUAs) that have been made responsible for chemically mediated interactions in the plankton. PUA-effects include chemical defense by reducing the reproductive success of grazing copepods, allelochemical activity by interfering with the growth of competing phytoplankton and cell to cell signaling. We applied a PUA-derived molecular probe, based on the biologically highly active 2,4-decadienal, with the aim to reveal protein targets of PUAs and affected metabolic pathways. By using fluorescence microscopy, we observed a substantial uptake of the PUA probe into cells of the diatom *Phaeodactylum tricornutum* in comparison to the uptake of a structurally closely related control probe based on a saturated aldehyde. The specific uptake motivated a chemoproteomic approach to generate a qualitative inventory of proteins covalently targeted by the α,β,γ,δ-unsaturated aldehyde structure element. Activity-based protein profiling revealed selective covalent modification of target proteins by the PUA probe. Analysis of the labeled proteins gave insights into putative affected molecular functions and biological processes such as photosynthesis including ATP generation and catalytic activity in the Calvin cycle or the pentose phosphate pathway. The mechanism of action of PUAs involves covalent reactions with proteins that may result in protein dysfunction and interference of involved pathways.

Introduction

Oceans accommodate numerous coexisting microalga species in the plankton. Their community is shaped by different factors including nutrient limitation, predation and chemical signaling. Diatoms, a class of unicellular algae, are key players in the marine food web as they are responsible for about 40% of global marine primary productivity [1]. Some diatom species release biologically active metabolites as mediators of interactions. An intensively studied compound class in this context are oxylipins, which derive from the oxidative transformation of polyunsaturated fatty acids [2]. Of considerable interest among oxylipins are polyunsaturated aldehydes (PUAs), which have been reported to mediate various inter- and intraspecific interactions (reviewed in [2–5]). 2,4-Decadienal (DD) is the best studied metabolite of the group of PUAs, with attributed roles in grazer defense [6], allelophathy [7], cell to cell signaling [8], antibacterial activity [7,9] and bloom termination initiation [10,11]. PUA-mediated allelopathy [5,7,12,13] is impairing different phyla regarding growth and physiological performance. Sensitivity against PUAs has been reported for the prymnesiophyte *Isochrysis galbana* [7], the chlorophyte *Dunaliella tertiolecta* [7] as well as the centric diatom *Thalassiosira weissflogii* [14]. A synchronized release of PUAs from intact *Skeletonema marinoi* cells transiently before the culture changes to the decline phase supports the idea that PUAs play a role as infochemicals in mediating bloom termination [10]. Despite the well-documented biological functions of PUAs, their mechanism of action and their molecular targets are almost unknown [3,4]. Only few impaired biological processes and functions are recognized mainly involving disruption of intracellular calcium signaling, cytoskeletal instability and induction of apoptosis (reviewed in [2–4]).

PUA activity is structure-specific, since saturated aldehydes, like decanal that lack the conjugated $\alpha,\beta,\gamma,\delta$-unsaturated aldehyde motive of PUA, are not active [15,16]. Conjugated unsaturated aldehydes are reactive compounds belonging to the class of Michael acceptors. They act as electrophiles and react with proteins [17,18] and DNA [19–21]. Model investigations revealed that DD covalently modifies proteins by formation of imines (Schiff bases), pyridinium adducts and 1,4-addition products with nucleophiles [17,18]. Thus, proteins are putative targets of the electrophilic PUAs. PUAs also react with DNA resulting in apoptosis in copepods (reviewed in [22]). In algae [7], sea urchin embryos [23] and copepod embryos and nauplii [6,24] DNA laddering and chromatin dispersal or complete DNA fragmentation and dislocation is observed after PUA exposure.

The diatoms *Phaeodactylum tricornutum* [25] and *Thalassiosira pseudonana* [26] have emerged as model organisms since these were the first species with sequenced genome. *P. tricornutum* is a producer of the oxylipins 12-oxo-(5Z,8Z,10E)-dodecatrienoic acid and 9-oxo-(5Z,7E)-nonadienoic acid [27] and was reported to be affected by DD [8,28]. Exposure to this aldehyde altered the mitochondrial glutathione redox potential by oxidation of glutathione and induced cell death of *P. tricornutum* [28]. DD also triggers intracellular calcium transients and nitric oxide generation [8]. There is evidence for a sophisticated stress surveillance system in which individual diatom cells sense local DD concentration thereby monitoring the stress level of the entire population. An ortholog of the plant enzyme AtNOS1 was predicted as molecular target of PUAs [8]. Transcriptome analysis revealed that *PtNOA*, a gene with similarities to AtNOS1 [8], is upregulated in response to DD [29]. *PtNOA* overexpressing cell lines are hypersensitive to this PUA with altered expression of superoxide dismutase and metacaspases; both protein classes are involved in activation of programmed cell death [29]. Other studies on gene regulation in response to PUAs focused on copepods. In *Calanus helgolandicus* tubulin expression [30] and primary defense systems [31] were downregulated whereas detoxification genes

like glutathione S-transferase, superoxide dismutase, and catalase remained unaffected [31] in response to a diet of the PUA producer *S. costatum* compared to a control.

We report here on the uptake, accumulation and molecular targets of a molecular probe containing a DD-derived head group and a 5-tetramethylrhodamine carboxamide fluorophore (TAMRA) reporter in *P. tricornutum* using an activity-based protein profiling (ABPP) strategy (Fig 1). Such chemical probe-enabled proteome strategies have been successfully applied with mechanism-based inhibitors [32] or protein-reactive natural products [33,34]. The utilized probe consists of a reactive group mimicking DD and a fluorescent reporter tag for detection [35]. By applying 2D gel electrophoresis (GE) followed by liquid chromatography/tandem mass spectrometry (LC-MS/MS) we found specific probe-labeled proteins having important roles regarding catalytic activity and biological functions in the alga including fucoxanthin chlorophyll *a/c* proteins, ATP synthases, a ribulose-phosphate-3-epimerase (RPE) and a phosphoribulokinase (PRK).

Materials and Methods

Uptake experiments

Growth of *P. tricornutum*. *P. tricornutum* (strain UTEX 646, Segelskär, Finland) was cultivated in artificial seawater prepared as described in Maier and Calenberg [36] under a 14/10 hours light/dark cycle, at 32 to 36 mmole photons s^{-1} m^{-2} and 13°C in 580 mL Weck jars (Weck, Wehr, Germany). The 4-(2-hydroxyethyl)-1-piperazineethanesulfonic acid (HEPES)-buffered medium was adjusted to a pH of 7.8 before autoclaving. Nutrient levels were 14.5 mM phosphate, 620 mM nitrate and 320 mM silicate. Incubation experiments were done under the same conditions.

Sample preparation. A *P. tricornutum* culture (100 μL) was pipetted on ethanol pre-cleaned cover slips (Marienfeld 474030-9010-000, 18x18 mm², D = 0.17 mm +/- 0.005 mm; Carl Zeiss Canada, Toronto, ON). To prevent evaporation cover slips were placed in a Petri dish, which contained a seawater wetted filter paper and were covered. Incubation for 8 hours allowed cells to adhere to the cover slips. Subsequently, 10μM of the substances DDY coupled to TAMRA (TAMRA-PUA), 5-hexynal (SA) coupled to TAMRA (TAMRA-SA) or azide modified TAMRA (TAMRA-N_3) were added to the cell suspensions (each 0.5 mM stocks in DMSO), mixed gently with a pipette and incubated for one hour. Afterwards, the cell suspensions were removed and the cover slips were washed seven times by carefully pipetting 200 μL artificial seawater and incubated with 100 μL 4% [w/v] para-formaldehyde in artificial seawater for 25 min. The cover slips were washed twice with 200 μL artificial seawater and finally the
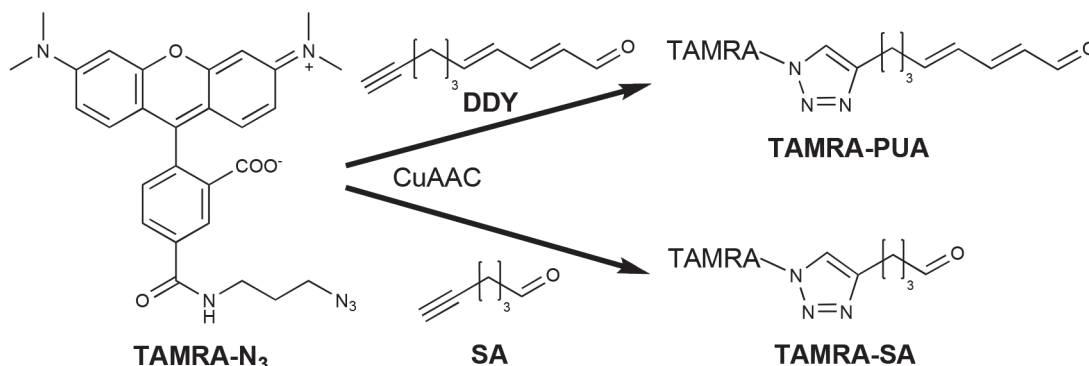
Fig 1. Synthesis of the probe TAMRA-PUA and the control TAMRA-SA. For details on the synthesis see [35].

liquid was removed. A control with the same washing and fixation steps was prepared as well. Due to extensive washing steps a part of algae cells detach from cover slips. 4 μL of 2,2'-thio-diethanol were pipetted on an ethanol pre-cleaned object slide and the treated side of the cover slip was placed on top of the object slide and slightly pressed down. Edges were fixed with nail polish and the slides were stored at 4°C until measurements on the next day. For each treatment three individual cover slips (biological replicates) were prepared out of three different *P. tricornutum* cultures. Those cultures have been prepared out of the same stock and kept under identical growth condition.

Fluorescence microscopy and analysis. *P. tricornutum* cells were observed with a structured illumination microscope (SIM), Zeiss Elyra S1 system (Carl Zeiss, Jena, Germany). Imaging was performed with an oil immersion objective lens (Plan-Apo, 63X, 1.4NA, Carl Zeiss, Jena, Germany). A 561 nm laser was used for excitation and fluorescence was filtered by a band pass filter (BP 570–620 nm) which opens up above 750 nm. 2D wide field images were acquired to compare fluorescence intensity of the different probes and treatments (TAMRA-PUA, TAMRA-SA, TAMRA-N$_3$, no probe), whereas all cells were measured using the same settings (laser intensity, gain, exposure time). 12 cells were observed per treatment distributed over three biological replicates (microscope slides), four cells each. Three dimensional SIM images of treated *P. tricornutum* providing twofold resolution improvement were taken from selected samples to confirm, that TAMRA-PUA and TAMRA-SA were taken up in the cells and did not exclusively stick onto their surfaces. 15 raw images are required for reconstructing one 2D SIM image. 3D SIM images were taken with z steps of 110 nm. All SIM images were reconstructed on ZEN software 2010 (black edition, Carl Zeiss, Jena, Germany).

For fluorescence analysis bright field and wide field fluorescence images at 561 nm excitation were exported in TIF format with the ZEN software and processed with ImageJ2x 2.1.4.7 (freeware, http://www.rawak.de/ij2x/Download.html) as follows: tonal correction of the bright field image of each cell was optimized (see S1 Folder for unmodified images), the cell was encircled by hand and this selection was laid on the corresponding fluorescence picture using the ROI manager. The mean gray value, which is defined in this software as the sum of the gray values of all the pixels in the selection divided by the number of pixels, and the mean gray value of the background were measured and subtracted. For the previously described issue we use the term mean gray value per pixel. For background analysis a region of at least 1000 pixels was used.

Probe labeling, 1D and 2D gel electrophoresis and identification of target proteins

***In vivo* labeling of *P. tricornutum* and sample preparation for gel electrophoresis.** *P. tricornutum* cultures were grown for 13 days in 580 mL Weck jars (1.0×10^6 to 1.5×10^6 cells mL^{-1}) without shaking as described before, which resulted in cells mainly sticking to the glass bottom. The overlaying artificial seawater was almost quantitatively removed with a pipette and cells were transferred into centrifuge tubes with the remaining medium.

For 1D GE samples were incubated with 100 μM DDY or 100 μM SA (each 50 mM stocks in DMSO) or DMSO for one hour.

For 2D GE the concentrated algae suspension was treated with 14 μL (250 μM) DDY stock solution (50 mM), which was added to 2.8 mL concentrated cell suspension (total cell number 48.7×10^6 resulting in 14 fmol DDY cell^{-1}) and incubated for 1 hour. During this incubation period no change in cell viability compared to untreated cells was observed by microscopy after application of Evan's Blue [37]; however, we observed that incubation of several hours increases the amount of non-viable cells. The undiluted samples were centrifuged for 2 min at

1,800 g immediately after incubation to remove DDY and salts; the supernatant was removed and the cells were washed twice with 1 mL buffer A (10 mM HEPES and 250 mM sucrose, pH 7.4) and twice with 1 mL buffer B (10 mM HEPES and 250 mM sucrose, pH 8.2). After each washing step the tubes were centrifuged at 1,800 g for 2 min and the supernatant was discarded. Application of Evan's Blue [37] and microscopy ensured that cells stayed intact during this procedure. The pellet was resuspended in buffer B and cells were treated with 1 mM dithiothreitol (20 mM stock in buffer B) to react with possibly unremoved DDY. Cells were lysed by sonication (ultrasonic probe: Bandelin sonotronic HD2070, power supply: Bandelin UW2070; Bandelin electronic, Berlin, Germany) twice for 15 s on ice.

The protein concentration was determined with the Roti®-Quant universal assay (Carl Roth, Karlsruhe, Germany) based on the biuret test using a microplate reader (Mithras LB 940, Berthold Technologies, Bad Wildbad, Germany) and bovine serum albumin as reference.

Copper(I)-catalyzed azide-alkyne cycloaddition (CuAAC). *P. tricornutum* protein samples (30μL, 30 to 50 μg proteins μL^{-1}) were diluted with 270 μL buffer B and incubated with 6 μL (0.09 mM) TAMRA-N$_3$ solution (5 mM stock in DMSO), 18 μL (0.09 mM) ligand tris [(1-benzyl-1*H*-1,2,3-triazol-4-yl)methyl]amin solution (1.7 mM stock in DMSO/*tert*-butanol, 1/4, v/v) and 12 μL (35 mM) of a freshly prepared ascorbic acid solution (1.00 M in water). Samples were vortexed and 6 μL (0.88 mM) copper sulfate solution (50 mM in water) were added. Samples were vortexed again and stored on ice for 1 hour. 1% Triton™ X-100 and protease inhibitor cocktail (M221, Amresco Inc., Solon, OH, USA) were added according to the manufacturer's protocol and after 30 min on ice samples were centrifuged at 15,000g and 3°C for 20 min. The supernatant was transferred into centrifugal filter units (vivaspin®500, 5,000 MWCO, PES, Sartorius, Göttingen, Germany) and the sample volume was reduced by centrifugation at 15,000g and 3°C. 100μL buffer B was added three times and the volume was reduced by centrifugation after each addition to give a final protein concentration of 10 to 20 μg proteins μL^{-1}.

Sodium dodecyl sulfate polyacrylamide gel electrophoresis (SDS-PAGE) and in-gel fluorescence detection. 20 μg of protein samples were mixed with 2× loading buffer [38] and heated to 95°C for 6 min. A protein ladder (PageRuler unstained protein ladder, Thermo Fischer Scientific Inc., Waltham, MA, USA) and the protein sample were loaded on a SDS mini gel containing 12% acrylamide resolving gel and 5% stacking gel prepared according to [39]. The gel was separated in a Mini-Protean® Tetra gel cell (Bio-Rad, Herculas, CA, USA) by applying 80 V for 30min followed by 180 V for 65min. A fluorescent picture was taken at 312nm irradiation using a UV transilluminator (UV star, Bio-Rad), a PowerShot A640 camera (Canon, Tokyo, Japan) and a 520 nm long pass filter. The gel was stained with RAPIDstain™ (G-Biosciences, St. Louis, MO, USA).

Difference gel electrophoresis (DIGE). DIGE was conducted in triplicates. 440 to 880 μg protein of the probe-treated sample (incubated with DDY and connected with TAMRA-N$_3$ by CuAAC as described before) and 50 μg protein of a control sample incubated with the N-hydroxysuccinimide ester of the cyanine 5 fluorophore (Cy5 NHS ester) were loaded on each of the isoelectric focusing (IEF) strips (Immobiline DryStrip, 24 cm, pH 3–11 NL, GE Healthcare Bio- Sciences, Piscataway, NJ, USA). For Cy5 labeling of the whole proteome 20 μL of the control sample were diluted with 48 μL buffer B. 3 μL Cy5 NHS ester (2 mM in DMSO) were added and the mixture was incubated with shaking at 4°C for 45 min. To stop labeling 5 μL of a 10 mM solution of L-lysine in water were added.

The IEF strip was rehydrated overnight (7 M urea, 2 M thiourea, 2% [w/v] CHAPS, 0.002% [w/v] bromophenol blue, 0.5% [v/v] IPG buffer (GE Healthcare Bio-Sciences), 10 mM dithiothreitol). Isoelectric focusing of the strips with the Ettan IPGphor II (GE Healthcare Bio-

Sciences) was carried out according to the following protocol: 4 h at 300 V (gradient), 4 h at 600 V (gradient), 4 h at 1,000 V (gradient), 4 h at 8,000 V (gradient) and 3 h at 8,000 V (step).

After isoelectric focusing the IEF strips were equilibrated for 15 min in 10 mL of equilibration buffer (6 M urea, 30% [v/v] glycerol, 2% [w/v] SDS, 75 mM tris(hydroxymethyl)aminomethane, 0.002% [w/v] bromophenol blue) containing 1% [w/v] dithiothreitol and subsequently for 15 min in 10 mL of equilibration buffer containing 2.5% [w/v] iodoacetamide. For separation of proteins in the second dimension, the Ettan DALT System (GE Healthcare Bio-Sciences) was used. SDS polyacrylamide gels 12% [w/v] of 1.0 mm thickness were casted via the Ettan DALTsix Gel caster (GE Healthcare Bio-Sciences). The separation conditions were as follows: 1 W/gel for 1 h followed by 15 W/gel for 5 h. Proteins were visualized by analyzing the gels with a Typhoon 9410 scanner (GE Healthcare Bio-Sciences) using a resolution of 100 µm. Proteins were fixed (10% [v/v] acetic acid, 50% [v,v] methanol in water), stained (0,025% [w/v] Coomassie R 250, 10% [v/v] acetic acid in water) and the gels were destained (10% [v/v] acetic acid in water; see S3 Folder for unmodified Coomassie and fluorescence images of the gels). Gels were merged with Delta2D (DECODON, Greifswald, Germany).

Protein isolation, LC-MS/MS analysis and data processing. Fluorescent TAMRA-PUA protein spots were in-gel reduced, alkylated with iodoacetamide and digested as described by Shevchenko et al. [40]. Tryptic peptides were extracted, dried down in a vacuum centrifuge and dissolved in 10 µL of water containing 0.1% formic acid.

LC-MS/MS analysis and data processing were conducted as described in S1 Information.

Results

Probe design and labeling strategy

The fluorescent α,β,γ,δ-unsaturated aldehyde-derived probe TAMRA-PUA (Fig 1) could be used successfully to investigate uptake and accumulation of PUAs in *P. tricornutum* and to monitor protein targets of these natural products. TAMRA-PUA was recently developed in our group to monitor accumulation of PUAs in copepods [35]. The probe consists of DDY as reactive group that mimics DD. The alkyne functionality allows to couple the commercially available azide modified tetramethylrhodamine TAMRA-N$_3$ (Fig 1). To identify protein targets, DDY was incubated with *P. tricornutum* cells. After work-up CuAAC allowed to covalently link the reporter TAMRA-N$_3$ to DDY (Figs 1 and 2). For uptake studies we employed the probe as already coupled construct TAMRA-PUA. For comparison of the activity of α,β,γ,δ-unsaturated aldehyde-derived probes with structurally related saturated-aldehyde-derived ones we also applied the probe TAMRA-SA (Fig 1).
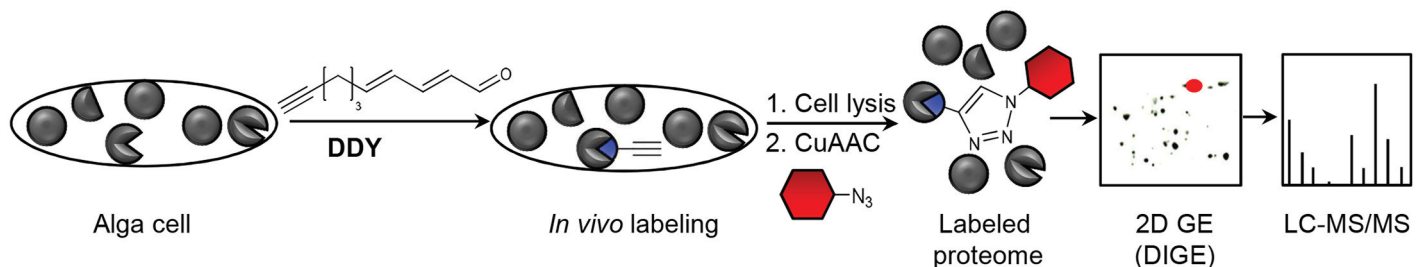
Fig 2. Schematic *in vivo* application of the probe. Living cells of *P. tricornutum* were incubated with the PUA-derivative DDY. After removal of excess DDY cell lysis followed by CuAAC enables attachment of the fluorescent reporter to covalently labeled proteins. 1D GE quickly allows detection of labeled proteins (not shown). Identification of protein targets is enabled by 2D GE. Therefore, a second *P. tricornutum* sample was treated with Cy5 NHS ester to label the whole proteome. The combined samples were separated using DIGE, labeled proteins were digested using trypsin and the resulting peptides were separated and analyzed by LC-MS/MS.

doi:10.1371/journal.pone.0140927.g002

TAMRA-PUA accumulates in *P. tricornutum*

Cell permeability and uptake of the probes by *P. tricornutum* was investigated by wide field fluorescence microscopy. Living cells were treated with TAMRA-PUA, TAMRA-SA or TAMRA-N_3 for labeling or kept as control without additional treatment. After one hour incubation probes were removed by washing seven times with artificial seawater, once with artificial seawater containing 4% paraformaldehyde for cell fixation and twice with artificial seawater. Cells were embedded in 2,2'-thiodiethanol and measured with an epifluorescence microscope in wide field mode. Images were processed with ImageJ. Cells were encircled by hand and the background corrected average mean gray value per pixel within each alga cell was calculated (Fig 3). The aldehyde containing probes TAMRA-PUA and TAMRA-SA were significantly enriched in the cells compared to TAMRA-N_3 or the control. Interestingly, TAMRA-PUA accumulation was significantly higher compared to TAMRA-SA, despite being similar in physicochemical properties.

Results were verified in additional independent experiments, also using a different embedding medium (S1 Fig). To confirm that the probes do not only appear on the surface we conducted 3D SIM showing that TAMRA-PUA and TAMRA-SA accumulate within the cells (Fig 4). Distribution of label revealed local maxima but in general nearly the entire cellular content was affected by the probe.

DDY covalently modifies proteins of *P. tricornutum*

We next tested for protein targets of PUAs in living cells using DDY as well as the saturated aldehyde derivative SA. After incubation with the probes followed by cell lysis, TAMRA-N_3 was coupled to the alkyne groups of DDY as well as SA via CuAAC (Fig 2). Proteins were
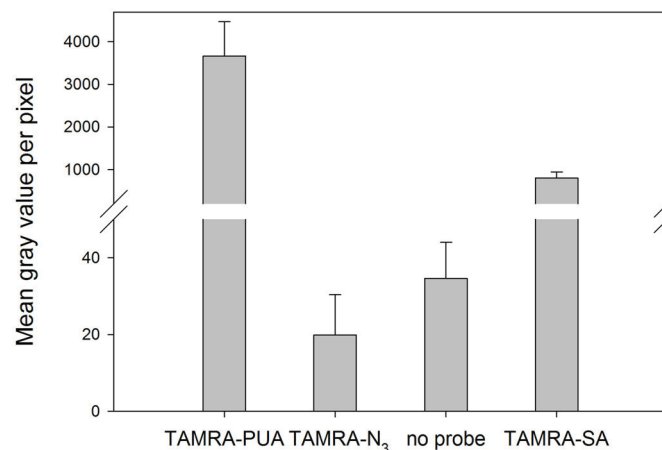
Fig 3. Fluorescence intensity of *P. tricornutum* cells treated under different conditions. Cells were either incubated with TAMRA-PUA, TAMRA-N_3, TAMRA-SA for one hour or kept under identical conditions without probe. For each treatment three microscope slides with four cells each were measured. Unmodified raw data are available in S1 and S2 Folders. Fluorescence intensities were recorded as mean gray value per pixel after data treatment as described in the main text. Averaged mean gray values per pixel of cells of each treatment are presented as bars ±SD. One way Anova comparing results of different microscope slides within one treatment revealed no statistical difference (p>0.05). Kruskal-Wallis one way analysis of variance on ranks revealed differences in the median values among the treatment groups (H = 42.436, p<0.001) and Tukey's HSD test (p<0.05) allowed classification into three groups: (a) TAMRA-PUA with the highest mean gray value per pixel of 3661±809, (b) TAMRA-SA with 800±140 and (c) TAMRA-N_3 and control with almost no emission signals (20±10 and 35±9); these controls were not significantly different to each other (Tukey's HSD test p>0.05).

doi:10.1371/journal.pone.0140927.g003
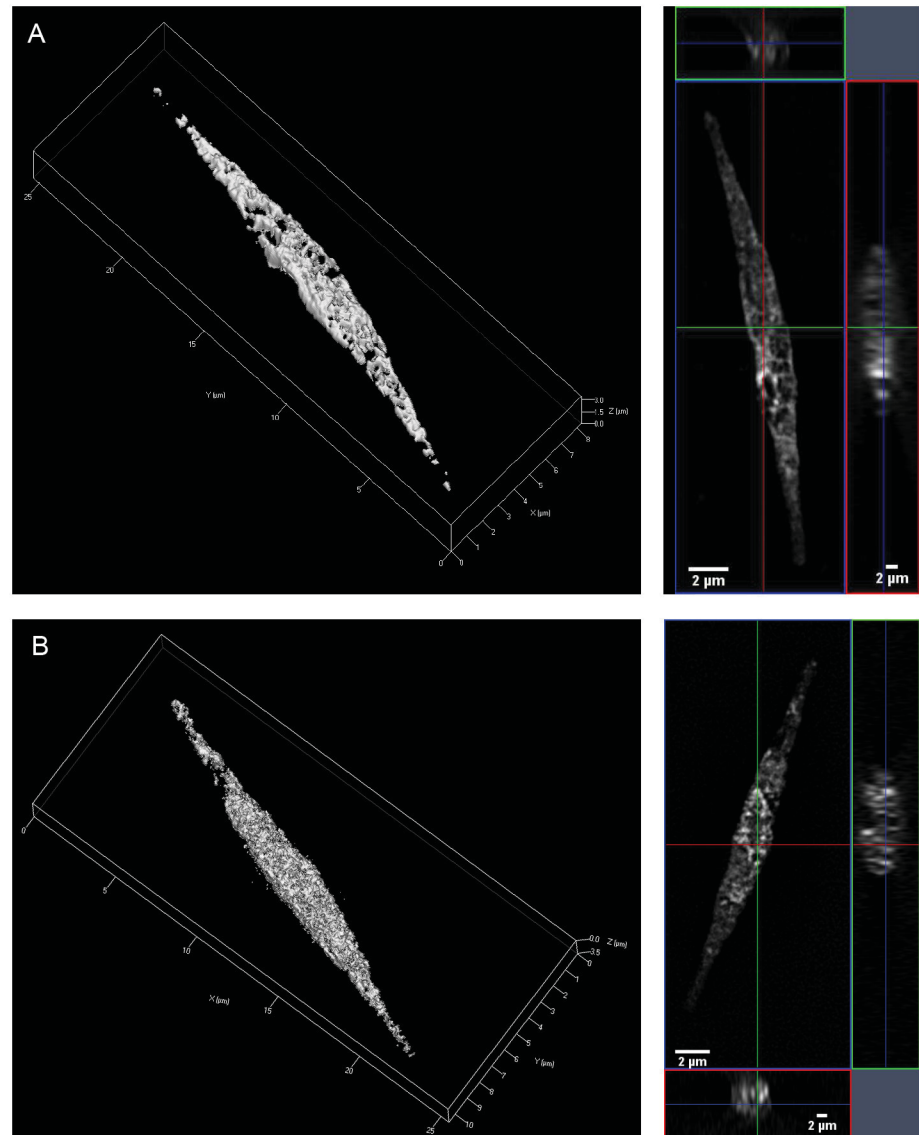
Fig 4. Fluorescence microscopy of *P. tricornutum* cells. 3D (left) and 2D (right) images of a TAMRA-PUA (A) and a TAMRA-SA (B) treated cell. Images were taken in 3D SIM mode. A 561nm laser was used for excitation, and fluorescence was filtered by a band pass filter (BP 570-620nm) which opens up above 750nm. Fluorescence is visible in the entire cells, which confirms that both probes were taken up.

doi:10.1371/journal.pone.0140927.g004

separated by 1D GE and monitored for fluorescent labeling. UV-illumination revealed exclusive labeling of proteins in DDY treated cells while SA and DMSO treatments did not result in any fluorescent bands (S2 Fig).

To unravel protein targets of DDY, protein extracts obtained after incubation of *P. tricornutum* with the probe as described above were separated by DIGE in three replicates (S3 Fig, S3 Folder for unmodified pictures). For comparison samples without probe addition were incubated with the Cy5 NHS ester to label the whole proteome. Separation was performed by isoelectric focusing and SDS-PAGE as second dimension and DDY-TAMRA labeled proteins were excised and tryptically digested. Digested peptides were separated and analyzed by LC-MS/MS (Fig 2). More precisely separation was conducted with a nano Ultra Performance

Liquid Chromatography (nanoUPLC) and analysis by tandem mass spectrometry using data-independent acquisition (MS^E analysis). In data-independent analysis the mass spectrometer cycles between low and high energy acquisition of data resulting in high sampling rate.

A list of confident target proteins classified according to their biological processes and molecular functions is shown in Table 1. Two ATP synthases, four different chlorophyll *a/c* binding proteins, different catalytic active enzymes and some predicted proteins were found to be modified by the probe. A full list of confident, probable and putative proteins (for evaluation see S1 Information) as well as an overview of all protein hits for each gel is given in S1 Table.

Discussion

While previous research mainly has reported the teratogenic and allelochemical effects of PUAs as well as their role in cell to cell signaling (reviewed in [2–5]) and PUAs influence on

Table 1. Confident target proteins found by 2D GE. [1]

Protein	Gene name	Accession No.	Mass (kDa)	Gel 1	Gel 2	Gel 3
1) Biological process						
ATP biosynthetic process						
ATP synthase subunit alpha, chloroplastic	*AtpA*	A0T0F1	54621.6	X	OO	O
ATP synthase subunit beta	*AtpB*	B7FS46	53619.2	X	OO	O
Photosynthesis						
Fucoxanthin chlorophyll a/c protein	*Lhcf10*	B7G5B6	21352.7	X	OOO	O
Fucoxanthin chlorophyll a/c protein	*Lhcf9*	B7G955	22100.5	OOO	O	X
Fucoxanthin chlorophyll a/c protein	*Lhcx2*	B7FR60	21177.4	OO	O	X
Fucoxanthin chlorophyll a/c protein	*Lhcf4*	B7FRW2	21328.5	OO	O	X
2) Molecular function						
Catalytic activity, isomerase activity						
Ribulose-phosphate 3-epimerase	*Rpe*	B7FRG3	27812.0	OO	O	O
Catalytic activity, ligase activity						
Predicted protein, family: Aspartate-ammonia ligase	*PHATRDRAFT_44902*[a]	B7FW24	43206.1	X	OO	O
Catalytic activity, oxidoreductase activity						
Predicted protein, domains: Thioredoxin-like fold, Thioredoxin domain	*PHATRDRAFT_42566*[a]	B7FNS4	24136.3	X	OOO	OOO
Predicted protein, domain: Rieske [2Fe-2S] iron-sulphur domain	*PHATRDRAFT_9046*[a]	B7FPI8	17010.4	X	OO	O
Catalytic activity, transferase activity						
Phosphoribulokinase	*Prk*	B5Y5F0	43325.4	X	OO	O
3) Predicted proteins without assignable function						
Predicted protein	*PHATRDRAFT_42612*[a]	B7FNX7	24938.5	O	OOO	OOO
Predicted protein	*PHATRDRAFT_45465*[a]/ *PHATRDRAFT_50215*[a]	B7FXS8	37645.2	O	X	OOO
Predicted protein, family: SOUL haem-binding protein	*PHATRDRAFT_37136*[a]	B7G284	46049.4	O	OOO	OOO
Predicted protein	*PHATRDRAFT_49286*[a]	B7GA37	32141.6	OO	O	O
Predicted protein, domain: NAD(P)-binding domain	*PHATRDRAFT_49287*[a]	B7GA38	126885.6	X	OO	O
Predicted protein, family: Protein of unknown function DUF1517	*PHATRDRAFT_32071*[a]	B7FQ47	33258.8	OO	X	O

[1]Proteins in this table were found in at least two of the three gels, a full list of labeled proteins can be found in S1 Information. OOO—only one protein per excised gel spot was found, OO—identification of probe labeled protein besides other unlabeled proteins in a gel spot, O—more than one labeled protein per excised gel spot, X—no hit.

[a]Names are temporarily ascribed to an open reading frame (ORF) by a sequencing project [41].

doi:10.1371/journal.pone.0140927.t001

gene regulation [30,31], almost nothing is known about underlying mechanistic aspects regarding covalent protein interactions. Therefore, we applied a PUA-derived as well as control probe to *P. tricornutum*.

Probe design and labeling strategy

PUAs are known to have diverse effects on planktonic organisms but defined molecular targets are hitherto almost unidentified. Especially their function in cell to cell communication of diatoms has attracted much attention [7,8,10,14]. We undertook a labeling study to obtain a deeper insight into the mechanism of action of these metabolites to reveal potential PUA-uptake of phytoplankton and to identify protein targets of the compounds. Following previous structure activity studies we addressed the specific activity of PUAs by comparison of probes derived from the active unsaturated aldehyde (TAMRA-PUA) and the inactive saturated aldehyde (TAMRA-SA) [16,35]. The design of the probes allowed to employ them in two different modes. For uptake studies we could use the TAMRA coupled molecules as described earlier for the monitoring of PUA-targeting in copepods [35]. Interestingly, the different effects of unmodified saturated aldehydes and PUAs observed in previous studies [16] were also mirrored in the effect of our different TAMRA-constructs. This indicates that the TAMRA substitution has no significant influence on the action of the aldehydes. However we cannot exclude that permeability is altered by the substitution.

Probe concentration was set to 10μM, a value for which different algae showed response to DD regarding cell membrane permeability of SYTOX Green [7], but *P. tricornutum* did not [8]. For identification of protein targets we developed a two-step protocol involving incubation with unmodified SA or DDY and, after work-up, coupling with the TAMRA-N_3. This approach allows to minimize the influence of bulky groups during *in vivo* interaction with target proteins. The well-established CuAAC coupling allowed to covalently link the dye to DDY-labeled proteins [42,43]. As fluorescent reporter we selected the tetramethylrhodamine fluorophore as it is relatively cheap, pH insensitive, photostable, cell permeable and easily excitable with common lasers and filter sets [44]. Compared to experimental design of fluorescence microscopy where physiological conclusions were relevant, probe concentration in the mechanistic gel electrophoretic experiments was increased to 250μM DDY ensuring an adequate detection of labeled proteins.

TAMRA-PUA accumulates in *P. tricornutum*

Fluorescence microscopy clearly shows an uptake and accumulation of the DD derived probe by *P. tricornutum* (Fig 3). In contrast, TAMRA-SA, the probe derived from an almost inactive aldehyde with otherwise similar physicochemical properties, compared to TAMRA-PUA, did not substantially accumulate in the cells. Apparently the α,β,γ,δ-unsaturated structure element found in PUAs is responsible for uptake and/or accumulation within diatom cells. A potential mechanism explaining the accumulation could be an inhibited exfiltration due to covalent adduct formation with cellular components such as proteins [17,18] as verified below or DNA [19–21]. In contrast, the weaker fluorescence signal of TAMRA-SA is consistent with the much lower reactivity of the underlying structure hexanal for which only few covalent reactions with proteins have been reported [45,46]. By applying the hexanal derived TAMRA-SA to a *P. tricornutum* culture we did not observe any covalently modified proteins in the corresponding 1D gel (S2 Fig).

The intracellular accumulation can explain the specific elicitation of effects by PUAs [8]. We can exclude that the dye itself accumulates unspecifically in cells since TAMRA-N_3 treated *P. tricornutum* showed no different fluorescence signals compared to untreated controls

(Tukey's HSD test p>0.05 between TAMRA-N₃ and no probe), confirming the effective washing procedure to remove TAMRA [47]. 3D SIM images (Fig 4) reveal that fluorescence after application of the TAMRA-PUA probe is distributed over almost the entire cell. The lack of intracellular compartmentation can be explained with the high reactivity of such types of electrophilic Michael acceptors [16,48,49]. Apparently no preferred shuttling of the probe into specific compartments occurs but also the cell walls and membranes do not represent a barrier for this compound class. PUA-uptake might thus be a way to facilitate diatoms´ perception of this compound class. Efficient uptake of essential metabolites has been earlier observed in diatoms but specific uptake mechanisms of primary and secondary metabolites involving transporters are not yet identified [50]. However, transporters of glucose that can support mixotrophic growth of *P. tricornutum* are known, supporting the note of the capability of the alga to actively take up organic metabolites from its environment [51]. This further supports the notion of a possible cell to cell communication mechanism based on PUAs that requires cellular uptake. To unravel potential molecular targets within the proteome of *P. tricornutum* we undertook further labeling studies.

DDY covalently modifies proteins of *P. tricornutum*

We performed an *in vivo* labeling of *P. tricornutum* with a PUA-derived probe to identify target proteins and to deduce affected molecular functions and biochemical pathways. We hypothesize that modified proteins may lose their function and that PUAs thereby interrupt or disturb metabolic pathways. These changes on a molecular level probably lead to observed effects of PUAs like growth inhibition and cell death [4,8].

Whereas Vardi et al. used a transcriptome analysis to search for DD affected genes and gene products by screening for up- and downregulated transcripts [29], we performed a direct investigation on the covalent modification of the proteome by DDY. Thus, we discover interactions with proteins, which do not necessarily have an influence on the transcript level but a direct influence on the functionality of these proteins.

Although the unsaturated aldehyde group of PUAs is universally reactive against nucleophilic amino acid side chains, we received moderate specific labeling of proteins (Table 1). This agrees with previous findings that DD preferentially attacks distinct proteins and specific nucleophilic sites if incubated with isolated purified proteins [17]. Underneath the confident target proteins we found four fucoxanthin chlorophyll *a*/*c* proteins, which are part of the light harvesting complex (LHC), responsible for the delivery of excitation energy between photosystem I and II [52]. Compared to higher plants, LHCs of diatoms named fucoxanthin-chlorophyll-proteins bind chlorophyll *c* instead of *b* and fucoxanthin instead of lutein [53]. Three groups of LHCs regarding their sequence and function are known, the found target proteins (see Table 1) belong to two groups of them: *Lhcx* gene products are needed for protection against surplus light and thus photoprotection and *Lhcf* gene products, the main antenna proteins, function in light harvesting (reviewed in [54]). Effects of DD on photosystem efficiency have already been shown for the diatoms *Thalassiosira weissflogii* [14] and a transgenic *P. tricornutum* [29] and our findings now provide a mechanistic explanation for this action of PUAs.

The energy harvested during light reaction is mainly stored by forming adenosine triphosphate (ATP). We identified two probe labeled ATP synthase subunits (see Table 1) belonging to the extrinsic catalytic sector, CF1 [55] of the chloroplastic ATP synthase. ATP synthase, located either in the mitochondria inner membrane or chloroplast thylakoid membrane, are responsible for cellular ATP production from adenosine diphosphate and inorganic phosphor in the presence of a proton gradient across the membrane [56]. The two PUA-targets ATP

synthase subunit alpha (*AtpA*) and ATP synthase subunit beta (A*tpB*) are located in the water soluble CF1 complex of the chloroplastic ATP synthase. In the green algae *Chlamydomonas reinhardtii* in the absence of the mitochondrial beta-subunit (gene name *Atp2*), ATP synthase could not be assembled into an enzyme complex leading to decreased mitochondrial respiration [57]. In conjunction with the finding of impairment of enzymes involved in light harvesting the identified ATP synthase targets support the notion of a profound modulation of the energy household under the influence of PUAs.

Enzymes from the Calvin cycle are also PUA-targets connected to photosynthetic activity. Two PUA-targets, the kinase PRK and the epimerase RPE were found to be labeled after DDY incubation. These enzymes are involved in carbon dioxide assimilation during the dark reaction. RPE reversibly catalyzes the reaction of D-xylulose 5-phosphate to D-ribulose 5-phosphate in the Calvin cycle and pentose phosphate pathway [58]. The product D-ribulose-5-phosphate is under ATP consumption further converted by PRK to D-ribulose-1,5-bisphosphate, which acts as acceptor for CO_2 in photosynthetic carbon assimilation [59]. In the Calvin cycle glyceraldehyde-3-phosphate dehydrogenase, the small protein CP12 and PRK form a multi-enzyme complex, the redox state of PRK is regulated by thioredoxin-mediated thiol-disulfide exchange in a light-dependent manner [59,60]. PRK is not active in the oxidized form where cysteine residues at positions 16 and 55 in land plants and green algae form an intramolecular disulfide bridge [61]. By reaction of those thiols with a PUA inactivation of PRK due to spatial changes and loss of redox behavior is conceivable. Also labeling on other sites, such as Lys may lead to loss of activity. Examples for alkylations were shown for PRK of different origin [62,63] and accordingly, alkylation of thiols and other nucleophilic residues by PUAs might change activity of enzymes.

It is striking that metabolic pathways such as the pentose phosphate pathway, photosynthesis including photophosphorylation and Calvin cycle that are involved in the energy household are specifically affected by PUA-treatment. The response is more immediate than transcriptomic regulation since proteins are the direct target of a covalent modification.

Conclusion

In this study we investigate the structure specificity of the uptake of PUA-derived probes and analogues in *P. tricornutum*. We could also reveal PUA probe targets within the proteome of the alga. Uptake experiments show a clear enrichment of TAMRA-PUA within the cells compared to TAMRA-SA. Chemoproteomics allowed the identification of target proteins of TAMRA-PUA. Interestingly, preferential targets have important roles in biological processes covering photosynthesis including ATP generation, conversion in Calvin cycle or the pentose phosphate pathway. Besides three *Lhcf*- and one *Lhcx*-coding proteins important for light harvesting and photoprotection we found two ATP synthases. Generation of ATP is of major importance since it supports nearly all cellular activities that require energy and its synthesis is the most frequent chemical reaction in the biological word [56]. PRK, another PUA target catalyzes the only reaction by which intermediates in the Calvin cycle can be contributed for further CO_2 assimilation [64]. RPE is important for both, the Calvin cycle and the reverse pentose phosphate pathway. Loss of molecular functions of these proteins as it might occur through covalent reactions of the nucleophilic protein residues with a PUA would immediately interfere with the homeostasis of algae cells, explaining the fast adverse effect of PUAs.

Supporting Information

S1 Fig. Relative fluorescence intensity of *P. tricornutum* cells treated under different conditions in two independent experiments. Cells were either incubated with TAMRA-PUA,

TAMRA-N$_3$, TAMRA-SA (only experiment 2) for one hour or kept under identical conditions without probe. For each experiment one microscope slide per treatment with five cells (experiment 1) or seven cells (experiment 2) was measured. For experiment 1, all microscope slides were embedded in 2,2'-thiodiethanol as described in the materials and methods section, for experiment 2 a poly (vinyl alcohol)/ n-propyl gallate antifade embedding medium [See Lu-Walther H-W, Kielhorn M, Förster R, Jost A, Wicker K, Heintzmann R. fastSIM: a practical implementation of fast structured illumination microscopy. Methods Appl Fluoresc. 2015;3 (1):014001] was used. Fluorescence intensities were recorded as mean gray value per pixel after data treatment as described in the main text. To compare both experiments results were normalized to "no probe". Normalized averaged mean gray values per pixel of cells of each treatment are presented as bars ±SD. Kruskal-Wallis one way analysis of variance on ranks revealed differences in the median values among the treatment groups of each experiment (No. 1 H = 12.500, No. 2 H = 22.902; p<0.05). Tukey's HSD test (p<0.05) attested significant differences between TAMRA-PUA and all other treatments within each experiment.
(TIF)

S2 Fig. SDS-PAGE of *in vivo* treated samples of *P. tricornutum*. *P. tricornutum* was incubated with 100µM of the reactive group (RG) DDY or SA or DMSO as control. After one hour incubation cells were lysed, CuAAC with TAMRA-N$_3$ was applied and SDS-PAGE and in-gel fluorescence detection were accomplished (see also Fig 2). Only the DDY treated sample shows specific fluorescent bands.
(TIF)

S3 Fig. 2D GE images. Position of excised spots with identified proteins in the three 2D gels (1, 2 and 3) presented in the Coomassie stained gels (A) and fluorescence images excited at 532nm for TAMRA-PUA detection (B). The positions of the spots were computed by Delta 2D for each image by considering the Coomassie stained gel image as well as TAMRA-PUA and Cy5 fluorescence images (for raw data of each image see S3 Folder). Slightly shifted positions of spots between Coomassie and fluorescence images of each gel are due to change of gel dimensions during Coomassie staining.
(TIF)

S1 Folder. Unmodified wide field fluorescence images of *P. tricornutum* treated with TAMRA-PUA, TAMRA-SA, TAMRA-N$_3$ or without addition of a substance as control for uptake experiments. Cells were measured with a Zeiss Elyra S1 system in wide field mode. A 561 nm laser was used for excitation, and fluorescence was filtered by a band pass filter (BP 570–620 nm) which opens up above 750 nm. WF—wide field.
(ZIP)

S2 Folder. Unmodified bright field images of *P. tricornutum* treated with TAMRA-PUA, TAMRA-SA, TAMRA-N$_3$ or without addition of a substance as control for uptake experiments. Cells were measured with a Zeiss Elyra S1 system in bright field mode. Before data analysis tonal correction was optimized. BF—bright field.
(ZIP)

S3 Folder. Unmodified 2D GE images. Fluorescence images of TAMRA-PUA and Cy5 labeled protein gels and images of Coomassie stained gels.
(ZIP)

S1 Information. LC-MS/MS analysis and data processing.
(DOCX)

S1 Table. Target proteins found by 2D GE. Proteins were classified into confident, labeled and putative proteins subject to guidelines described in S1 Information and separated according to their biological processes and molecular functions.
(XLSX)

Acknowledgments

Author Contributions

Conceived and designed the experiments: SW GP BM OW. Performed the experiments: SW NW YH BM HWLW. Analyzed the data: SW NW GP. Contributed reagents/materials/analysis tools: SW NW RH OW AS. Wrote the paper: SW GP.

References

1. Nelson DM, Tréguer P, Brzezinski MA, Leynaert A, Quéguiner B. Production and dissolution of biogenic silica in the ocean: Revised global estimates, comparison with regional data and relationship to biogenic sedimentation. Global Biogeochem Cycles. 1995; 9(3):359–72.

2. Pohnert G. Diatom/Copepod interactions in plankton: The Indirect chemical defense of unicellular algae. ChemBioChem. 2005; 6(6):946–59. PMID: 15883976

3. Caldwell G. The influence of bioactive oxylipins from marine diatoms on invertebrate reproduction and development. Mar Drugs. 2009; 7(3):367–400. doi: 10.3390/md7030367 PMID: 19841721

4. Ianora A, Bentley MG, Caldwell GS, Casotti R, Cembella AD, Engström-Öst J, et al. The relevance of marine chemical ecology to plankton and ecosystem function: An emerging field. Mar Drugs. 2011; 9(9):1625–48. doi: 10.3390/md9091625 PMID: 22131962

5. Ianora A, Miralto A. Toxigenic effects of diatoms on grazers, phytoplankton and other microbes: a review. Ecotoxicology. 2010; 19(3):493–511. doi: 10.1007/s10646-009-0434-y PMID: 19924531

6. Ianora A, Miralto A, Poulet SA, Carotenuto Y, Buttino I, Romano G, et al. Aldehyde suppression of copepod recruitment in blooms of a ubiquitous planktonic diatom. Nature. 2004; 429(6990):403–7. PMID: 15164060

7. Ribalet F, Berges JA, Ianora A, Casotti R. Growth inhibition of cultured marine phytoplankton by toxic algal-derived polyunsaturated aldehydes. Aquat Toxicol. 2007; 85(3):219–27. PMID: 17942163

8. Vardi A, Formiggini F, Casotti R, De Martino A, Ribalet F, Miralto A, et al. A stress surveillance system based on calcium and nitric oxide in marine diatoms. PLoS Biol. 2006; 4(3):411–9.

9. Balestra C, Alonso-Sáez L, Gasol JM, Casotti R. Group-specific effects on coastal bacterioplankton of polyunsaturated aldehydes produced by diatoms. Aquat Microb Ecol. 2011 Mar 31; 63(2):123–31.

10. Vidoudez C, Pohnert G. Growth phase-specific release of polyunsaturated aldehydes by the diatom Skeletonema marinoi. J Plankton Res. 2008; 30(11):1305–13.

11. Vidoudez C, Casotti R, Bastianini M, Pohnert G. Quantification of dissolved and particulate polyunsaturated aldehydes in the adriatic sea. Mar Drugs. 2011; 9(4):500–13. doi: 10.3390/md9040500 PMID: 21731545

12. Ribalet F, Wichard T, Pohnert G, Ianora A, Miralto A, Casotti R. Age and nutrient limitation enhance polyunsaturated aldehyde production in marine diatoms. Phytochemistry. 2007; 68(15):2059–67. PMID: 17575990

13. Casotti R, Mazza S, Ianora A, Miralto A. Growth and cell cycle progression in the diatom Thalassiosira weissflogii is inhibited by the diatom aldehyde 2-trans-4-trans-decadienal. ASLO Aquatic Sciences 2001 Meeting, Special Session 22—Strategies to reduce mortality in marine and freshwater phytoplankton; 2001 Oct 24–27, Albuquerque, USA.

14. Casotti R, Mazza S, Brunet C, Vantrepotte V, Ianora A, Miralto A. Growth inhibition and toxicity of the diatom aldehyde 2-trans,4-trans-decadienal on Thalassiosira weissflogii (bacillariophyceae) J Phycol. 2005; 41(1):7–20.

15. Adolph S, Poulet SA, Pohnert G. Synthesis and biological activity of α,β,γ,δ-unsaturated aldehydes from diatoms. Tetrahedron. 2003; 59(17):3003–8.

16. Adolph S, Bach S, Blondel M, Cueff A, Moreau M, Pohnert G, et al. Cytotoxicity of diatom-derived oxylipins in organisms belonging to different phyla. J Exp Biol. 2004; 207(17):2935–46.

17. Zhu X, Tang X, Zhang J, Tochtrop GP, Anderson VE, Sayre LM. Mass spectrometric evidence for the existence of distinct modifications of different proteins by 2(E),4(E)-decadienal. Chem Res Toxicol. 2010; 23(3):467–73. doi: 10.1021/tx900379a PMID: 20070074

18. Sigolo CAO, Di Mascio P, Medeiros MHG. Covalent modification of cytochrome *c* exposed to *trans*, *trans*-2,4-decadienal. Chem Res Toxicol. 2007; 20(8):1099–110. PMID: 17658762

19. Carvalho VM, Asahara F, Di Mascio P, de Arruda Campos IP, Cadet J, Medeiros MHG. Novel 1,N^6-etheno-2'-deoxyadenosine adducts from lipid peroxidation products. Chem Res Toxicol. 2000; 13 (5):397–405. PMID: 10813657

20. Loureiro APM, Di Mascio P, Gomes OF, Medeiros MHG. *trans*,*trans*-2,4-Decadienal-induced 1,N^2-etheno-2'-deoxyguanosine adduct formation. Chem Res Toxicol. 2000; 13(7):601–9. PMID: 10898592

21. Loureiro APM, de Arruda Campos IP, Gomes OF, Di Mascio P, Medeiros MHG. Structural characterization of diastereoisomeric ethano adducts derived from the reaction of 2'-deoxyguanosine with *trans*, *trans*-2,4-decadienal. Chem Res Toxicol. 2004; 17(5):641–9. PMID: 15144221

22. Buttino I, Hwang J-S, Sun C-K, Hsieh C-T, Liu T-M, Pellegrini D, et al. Apoptosis to predict copepod mortality: state of the art and future perspectives. Hydrobiologia. 2011; 666(1):257–64.

23. Hansen E, Even Y, Genevière A-M. The α,β,γ,δ-unsaturated aldehyde 2-*trans*-4-*trans*-decadienal disturbs DNA replication and mitotic events in early sea urchin embryos. Toxicol Sci. 2004; 81(1):190–7. PMID: 15201434

24. Romano G, Russo GL, Buttino I, Ianora A, Miralto A. A marine diatom-derived aldehyde induces apoptosis in copepod and sea urchin embryos. J Exp Biol. 2003; 206(19):3487–94.

25. Bowler C, Allen AE, Badger JH, Grimwood J, Jabbari K, Kuo A, et al. The *Phaeodactylum* genome reveals the evolutionary history of diatom genomes. Nature. 2008 Nov 13; 456(7219):239–44. doi: 10.1038/nature07410 PMID: 18923393

26. Armbrust EV, Berges JA, Bowler C, Green BR, Martinez D, Putnam NH, et al. The genome of the diatom *Thalassiosira pseudonana*: Ecology, evolution, and metabolism. Science. 2004 Oct 1; 306 (5693):79–86. PMID: 15459382

27. Pohnert G, Lumineau O, Cueff A, Adolph S, Cordevant C, Lange M, et al. Are volatile unsaturated aldehydes from diatoms the main line of chemical defence against copepods? Mar Ecol Prog Ser. 2002; 245:33–45.

28. Graff van Creveld S, Rosenwasser S, Schatz D, Koren I, Vardi A. Early perturbation in mitochondria redox homeostasis in response to environmental stress predicts cell fate in diatoms. The ISME journal. 2015 Feb; 9(2):385–95. doi: 10.1038/ismej.2014.136 PMID: 25083933

29. Vardi A, Bidle KD, Kwityn C, Hirsh DJ, Thompson SM, Callow JA, et al. A diatom gene regulating nitric-oxide signaling and susceptibility to diatom-derived aldehydes. Curr Biol. 2008; 18(12):895–9. doi: 10.1016/j.cub.2008.05.037 PMID: 18538570

30. Lauritano C, Borra M, Carotenuto Y, Biffali E, Miralto A, Procaccini G, et al. First molecular evidence of diatom effects in the copepod *Calanus helgolandicus*. J Exp Mar Biol Ecol. 2011; 404(1–2):79–86.

31. Lauritano C, Borra M, Carotenuto Y, Biffali E, Miralto A, Procaccini G, et al. Molecular evidence of the toxic effects of diatom diets on gene expression patterns in copepods. PLoS ONE. 2011; 6(10):e26850. doi: 10.1371/journal.pone.0026850 PMID: 22046381

32. Evans MJ, Cravatt BF. Mechanism-based profiling of enzyme families. Chem Rev. 2006; 106(8):3279–301. PMID: 16895328

33. Gersch M, Kreuzer J, Sieber SA. Electrophilic natural products and their biological targets. Nat Prod Rep. 2012; 29(6):659–82. doi: 10.1039/c2np20012k PMID: 22504336

34. Böttcher T, Pitscheider M, Sieber SA. Natural products and their biological targets: Proteomic and metabolomic labeling strategies. Angew Chem Int Ed. 2010; 49(15):2680–98.

35. Wolfram S, Nejstgaard JC, Pohnert G. Accumulation of polyunsaturated aldehydes in the gonads of the copepod Acartia tonsa revealed by tailored fluorescent probes. PLoS One. 2014; 9(11):e112522. doi: 10.1371/journal.pone.0112522 PMID: 25383890

36. Maier I, Calenberg M. Effect of extracellular Ca2+ and Ca2+-antagonists on the movement and chemoorientation of male gametes of Ectocarpus siliculosus (Phaeophyceae). Bot Acta. 1994; 107 (6):451–60.

37. Gaff DF, Okong'o-Ogola O. The use of non-permeating pigments for testing the survival of cells. J Exp Bot. 1971; 22(3):756–8.

38. Laemmli UK. Cleavage of structural proteins during the assembly of the head of bacteriophage T4. Nature. 1970; 227(5259):680–5. PMID: 5432063

39. Carl Roth GmbH. Karlsruhe: Polyacrylamide gel electrophoresis (PAGE). Available: http://www.carlroth.com/website/fr-fr/pdf/PAGE_E.pdf. Accessed 2012 Sep 15.

40. Shevchenko A, Tomas H, Havlis J, Olsen JV, Mann M. In-gel digestion for mass spectrometric characterization of proteins and proteomes. Nat Protoc. 2006; 1(6):2856–60. PMID: 17406544

41. UniProt consortium [Internet]. Universal Protein Resource cornsortium; 2002–2015 [updated 2015 Feb 5]; Gene names. Available: http://www.uniprot.org/help/gene_name. Accessed 2015 Mar 30.

42. Baskin JM, Bertozzi CR. Bioorthogonal click chemistry: Covalent labeling in living systems. QSAR Comb Sci. 2007; 26(11–12):1211–9.

43. Best MD. Click chemistry and bioorthogonal reactions: Unprecedented selectivity in the labeling of biological molecules. Biochemistry. 2009 Jul 21; 48(28):6571–84. doi: 10.1021/bi9007726 PMID: 19485420

44. Haugland RP. Handbook of fluorescent probes and research products. 9th ed. Eugene: Molecular Probes Inc: 2002.

45. Meynier A, Rampon V, Dalgalarrondo M, Genot C. Hexanal and t-2-hexenal form covalent bonds with whey proteins and sodium caseinate in aqueous solution. Int Dairy J. 2004; 14(8):681–90.

46. O'Keefe SF, Wilson LA, Resurreccion AP, Murphy PA. Determination of the binding of hexanal to soy glycinin and β-conglycinin in an aqueous model system using a headspace technique. J Agric Food Chem. 1991; 39(6):1022–8.

47. Cunningham CW, Mukhopadhyay A, Lushington GH, Blagg BSJ, Prisinzano TE, Krise JP. Uptake, distribution and diffusivity of reactive fluorophores in cells: Implications toward target identification. Mol Pharm. 2010; 7(4):1301–10. doi: 10.1021/mp100089k PMID: 20557111

48. Schwöbel JAH, Wondrousch D, Koleva YK, Madden JC, Cronin MTD, Schüürmann G. Prediction of Michael-type acceptor reactivity toward glutathione. Chem Res Toxicol. 2010; 23(10):1576–85. doi: 10.1021/tx100172x PMID: 20882991

49. Witz G. Biological interactions of α,β-unsaturated aldehydes. Free Radic Biol Med. 1989; 7(3):333–9. PMID: 2673948

50. Spielmeyer A, Gebser B, Pohnert G. Investigations of the uptake of dimethylsulfoniopropionate by phytoplankton. ChemBioChem. 2011 Oct 17; 12(15):2276–9. doi: 10.1002/cbic.201100416 PMID: 21853511

51. Zheng Y, Quinn A, Sriram G. Experimental evidence and isotopomer analysis of mixotrophic glucose metabolism in the marine diatom *Phaeodactylum tricornutum*. Microb Cell Fact. 2013 Nov 14; 12 (1):1–17.

52. Liu XD, Shen YG. NaCl-induced phosphorylation of light harvesting chlorophyll a/b proteins in thylakoid membranes from the halotolerant green alga, *Dunaliella salina*. FEBS Lett. 2004 Jul 2; 569(1–3):337–40.

53. Veith T, Büchel C. The monomeric photosystem I-complex of the diatom Phaeodactylum tricornutum binds specific fucoxanthin chlorophyll proteins (FCPs) as light-harvesting complexes. Biochim Biophys Acta (BBA)—Bioenergetics. 2007 Dec; 1767(12):1428–35.

54. Gundermann K, Schmidt M, Weisheit W, Mittag M, Büchel C. Identification of several sub-populations in the pool of light harvesting proteins in the pennate diatom *Phaeodactylum tricornutum*. Biochim Biophys Acta. 2013 Mar; 1827(3):303–10. doi: 10.1016/j.bbabio.2012.10.017 PMID: 23142526

55. Groth G, Strotmann H. New results about structure, function and regulation of the chloroplast ATP synthase (CF0CF1). Physiol Plant. 1999; 106(1):142–8.

56. Yoshida M, Muneyuki E, Hisabori T. ATP synthase—a marvellous rotary engine of the cell. Nat Rev Mol Cell Biol. 2001; 2:669–77. PMID: 11533724

57. Lapaille M, Thiry M, Perez E, Gonzalez-Halphen D, Remacle C, Cardol P. Loss of mitochondrial ATP synthase subunit beta (Atp2) alters mitochondrial and chloroplastic function and morphology in *Chlamydomonas*. Biochim Biophys Acta. 2010 Aug; 1797(8):1533–9. doi: 10.1016/j.bbabio.2010.04.013 PMID: 20416275

58. Sprenger GA. Genetics of pentose-phosphate pathway enzymes of *Escherichia coli* K-12. Arch Microbiol. 1995 Nov; 164(5):324–30. PMID: 8572885

59. Brandes HK, Hartman FC, Lu T-YS, Larimer FW. Efficient expression of the gene for spinach phosphoribulokinase in *Pichia pastoris* and utilization of the recombinant enzyme to explore the role of regulatory cysteinyl residues by site-directed mutagenesis. J Biol Chem. 1996; 271(11):6490–6. PMID: 8626451

60. Graciet E, Lebreton S, Gontero B. Emergence of new regulatory mechanisms in the Benson—Calvin pathway via protein—protein interactions: a glyceraldehyde-3-phosphate dehydrogenase/CP12/phosphoribulokinase complex. J Exp Bot. 2004; 55(400):1245–54. PMID: 15047759

61. Maberly SC, Courcelle C, Groben R, Gontero B. Phylogenetically-based variation in the regulation of the Calvin cycle enzymes, phosphoribulokinase and glyceraldehyde-3-phosphate dehydrogenase, in algae. J Exp Bot. 2010 Mar, 2010; 61(3):735–45. doi: 10.1093/jxb/erp337 PMID: 19926682

62. Porter MA, Hartman FC. Commonality of catalytic and regulatory sites of spinach phosphoribulokinase: Characterization of a tryptic peptide that contains an essential cysteinyl residue. Biochemistry. 1986 Nov; 25(23):7314–8.

63. Lebreton S, Graciet E, Gontero B. Modulation, via protein-protein interactions, of glyceraldehyde-3-phosphate dehydrogenase activity through redox phosphoribulokinase regulation. J Biol Chem. 2003; 278(14):12078–84. PMID: 12556449

64. Michels AK, Wedel N, Kroth PG. Diatom plastids possess a phosphoribulokinase with an altered regulation and no oxidative pentose phosphate pathway. Plant Physiol. 2005; 137(3):911–20. PMID: 15734914

S1 Supporting Information. LC-MS/MS analysis and data processing

A metabolic probe-enabled strategy reveals uptake and protein targets of polyunsaturated aldehydes in the diatom *Phaeodactylum tricornutum*

Stefanie Wolfram[1], Natalie Wielsch[2], Yvonne Hupfer[2], Bettina Mönch[3], Hui-Wen Lu-Walther[4], Rainer Heintzmann[4,5], Oliver Werz[3], Aleš Svatoš[2], Georg Pohnert[1]*

[1]Bioorganic Analytics, Institute for Inorganic and Analytical Chemistry, Friedrich Schiller University, Jena, Germany

[2]Department Mass Spectrometry/Proteomics, Max Planck Institute for Chemical Ecology, Jena, Germany

[3]Department of Pharmaceutical and Medicinal Chemistry, Institute of Pharmacy, Friedrich Schiller University, Jena, Germany

[4]Biomedical Imaging, Department Microscopy, Leibniz Institute of Photonic Technology e.V., Jena, Germany

[5]Institute for Physical Chemistry, Abbe Center of Photonics, Friedrich Schiller University, Jena, Germany

* Corresponding author
E-mail: Georg.Pohnert@uni-jena.de

LC-MS/MS analysis

After protein reduction, alkylation and digestion, 1 to 8 µL of the peptide mixture depending on staining intensity were injected onto a nanoAcquity nanoUPLC system (Waters, Milford, MA, USA) online coupled to a Q-ToF HDMS mass spectrometer (Waters). Peptides were desalted using a Symmetry C18 trap-column (20 x 0.18 mm, 5 µm particle size) at a flow rate of 15 µL min^{-1} (0.1% aqueous formic acid (FA)) and then eluted onto a nanoAcquity C18 analytical column (200 mm × 75 µm ID, BEH 130 material, 1.7 µm particle size) at a flow rate of 350 nl/min. The gradient used for peptide separation was 1–30% B over 13 min, 30–50% B over 5 min, 50–95% B over 5 min, isocratic at 95% B for 4 min, and a return to 1% B over 1 min (phases A and B composed of 0.1% [v/v] FA in water and 0.1% [v/v] FA in 100% acetonitrile, respectively); the analytical column was re-equilibrated for 9 min prior to the next injection. The eluted peptides were transferred via the NanoLockSpray ion source into a Synapt HDMS tandem mass spectrometer (Waters) operated in V-mode with a resolving power of at least 10,000 full width at half height. The source temperature was set to 80°C, cone gas flow 20 L/h, and the nanoelectrospray voltage was 3.2 kV. A 650 fmol/µL human Glu-Fibrinopeptide B in 0.1% aqueous FA/acetonitrile [1:1, v/v] was infused at a flow rate of 0.5 µL min^{-1} through the reference sprayer every 30 seconds to compensate for mass shifts in MS and MS/MS fragmentation mode.

LC-MS data were collected using MassLynx v4.1 software (Waters) under data-independent acquisition that utilizes alternating scanning in low (MS) and elevated energy (MS^{E}) mode. In low energy mode, data were collected at constant collision energy of 6 eV. In elevated MS^{E} mode, collision energy was ramped from 15 to 40 eV. MS and MS^{E} data were acquired over 1.5 sec intervals in the mass range of 50-1700 *m/z*.

Data processing

The acquired data were processed using ProteinLynx Global Server Browser v.2.5.2 software (Waters) using the ion accounting algorithm as [1]. For processing of the raw-data following thresholds for low/high energy scan ions and peptide intensity were used: 150, 10, and 750 counts, respectively. The peptide fragment spectra were searched against the *Phaeodactylum tricornutum* database combined with Viridipantae database, both were downloaded on March 3, 2014 from http://www.uniprot.org/. Database searching was restricted to tryptic peptides with a

variable carbamidomethyl modification for Cys residues. To investigate possible probe modifications we specified the following variable modifications based on previous findings of Cys Michael adducts with 2,4-decadienal (DD) [2], imine formation of Lys with DD [2,3] and DDY [4], Lys Michael adduct formation with unsaturated aldehydes [5,6] and imidazole adduct formation between Arg and 4-oxo-2-nonenal [7]:

- for TAMRA-PUA and arising Michael adducts of Cys or Lys 661.314 Da (named: TAMRA-PUA_Cys_Michaelreaction or TAMRA-PUA_Lys_Michaelreaction),
- for TAMRA-PUA and arising imine formation with Lys or imidazole formation with Arg with loss of H_2O 643.303 Da (named: TAMRA-PUA_Lys or TAMRA-PUA_Arg),
- for DDY and arising Michael adducts of Cys or Lys 148.089 Da (named: DDY_Cys_Michaelreaction or DDY_Lys_Michaelreaction),
- for DDY and arising imine formation with Lys or imidazole formation with Arg with loss of H_2O 130.078 Da (named: DDY_Lys or DDY_Arg).

Further, default searching parameter specifying mass measurement accuracy were used, minimum number of product ion matches per peptide (3), minimum number of product ion matches per protein (5), minimum number of peptide matches (1), and maximum number of missed tryptic cleavage sites (2). Maximum false positive rate was set to 4% and all peptides matched under the 4% FDR were considered as correct assignments. For data processing only conclusive proteins were considered.

Proteins of each gel (gel 1, gel 2, gel 3) were classified according to the following results:
- confident target protein: protein found as single hit in an excised gel spot,
- labeled target protein: protein labeled by DDY or TAMRA-PUA in an excised gel spot besides other unlabeled proteins,
- putative target protein: protein found in an excised gel spot with more than one protein hit.

Additional classification into proteins with assigned biological processes or molecular functions or predicted proteins without assignable function was made by using InterPro (http://www.ebi.ac.uk/interpro).

Results of all 3 gels were included in S1 Table and Table 1. Therefore proteins were classified according the following procedure:
- confident target proteins:

- A) target proteins: the protein was found in at least two different gels, at least in one excised gel spot the protein occurred as single hit
- B) target proteins labeled: the protein was found in at least two different gels, at least in one excised gel spot the DDY or TAMRA-PUA labeled protein was identified
- probable target proteins
  - C) probable target proteins: the protein was only found in one gel as single hit in an excised gel spot
  - D) probable target proteins labeled: the protein was found in only one gel and is labeled by DDY or TAMRA-PUA
  - E) probable target proteins: the protein was found in at least two different gels with more than one protein hit per excised gel spot
- putative target proteins
  - F) putative target proteins: the protein was found in only one gel with more than one protein hit per excised gel spot.

References

1. Li GZ, Vissers JP, Silva JC, Golick D, Gorenstein MV, Geromanos SJ. Database searching and accounting of multiplexed precursor and product ion spectra from the data independent analysis of simple and complex peptide mixtures. Proteomics. 2009 Mar;9(6):1696-719.

2. Zhu X, Tang X, Zhang J, Tochtrop GP, Anderson VE, Sayre LM. Mass spectrometric evidence for the existence of distinct modifications of different proteins by 2(*E*),4(*E*)-decadienal. Chem Res Toxicol. 2010;23(3):467–73.

3. Sigolo CAO, Di Mascio P, Medeiros MHG. Covalent modification of cytochrome *c* exposed to *trans*,*trans*-2,4-decadienal. Chem Res Toxicol. 2007;20(8):1099–110.

4. Wolfram S, Würfel H, Habenicht SH, Lembke C, Richter P, Birckner E, et al. A small azide-modified thiazole-based reporter molecule for fluorescence and mass spectrometric detection. Beilstein J Org Chem. 2014;10:2470–9.

5. Isom AL, Barnes S, Wilson L, Kirk M, Coward L, Darley-Usmar V. Modification of cytochrome *c* by 4-hydroxy- 2-nonenal: evidence for histidine, lysine, and arginine-aldehyde adducts. J Am Soc Mass Spectrom. 2004 Aug;15(8):1136–47.

6. Ichihashi K, Osawa T, Toyokuni S, Uchida K. Endogenous formation of protein adducts with carcinogenic aldehydes: implications for oxidative stress. J Biol Chem. 2001;276(26):23903-13.

7. Oe T, Lee SH, Silva Elipe MV, Arison BH, Blair IA. A novel lipid hydroperoxide-derived modification to arginine. Chem Res Toxicol. 2003 Dec;16(12):1598–605.
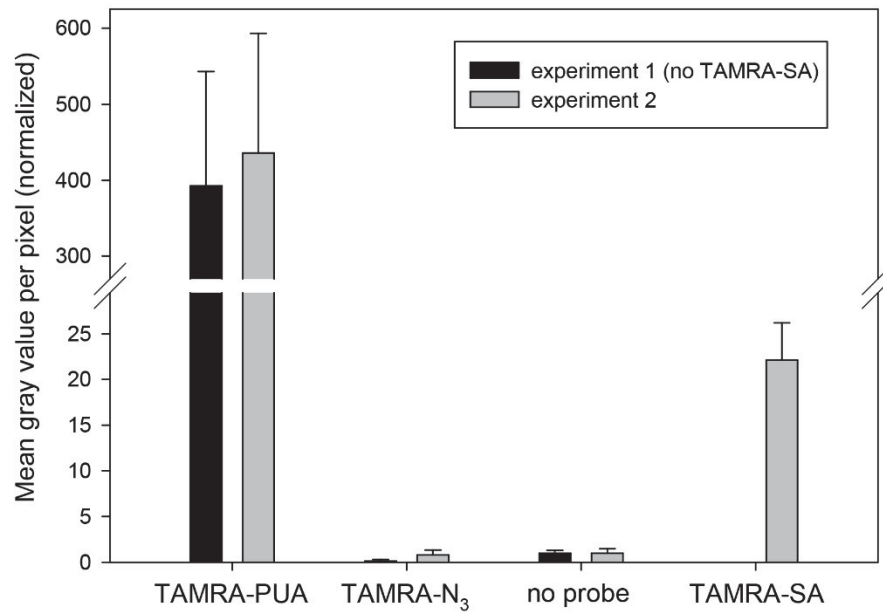
S1 Fig
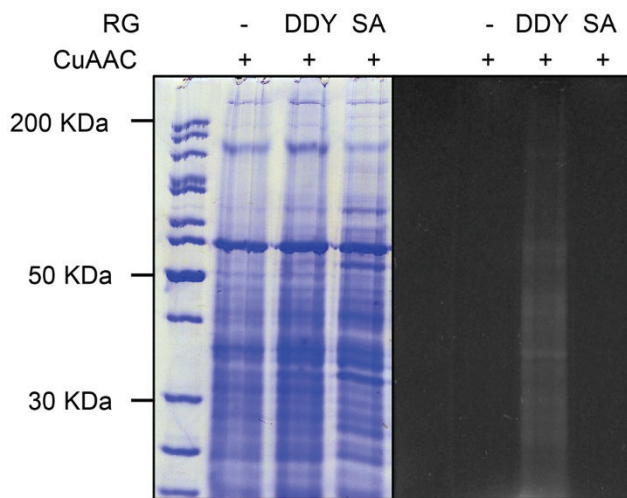
S2 Fig
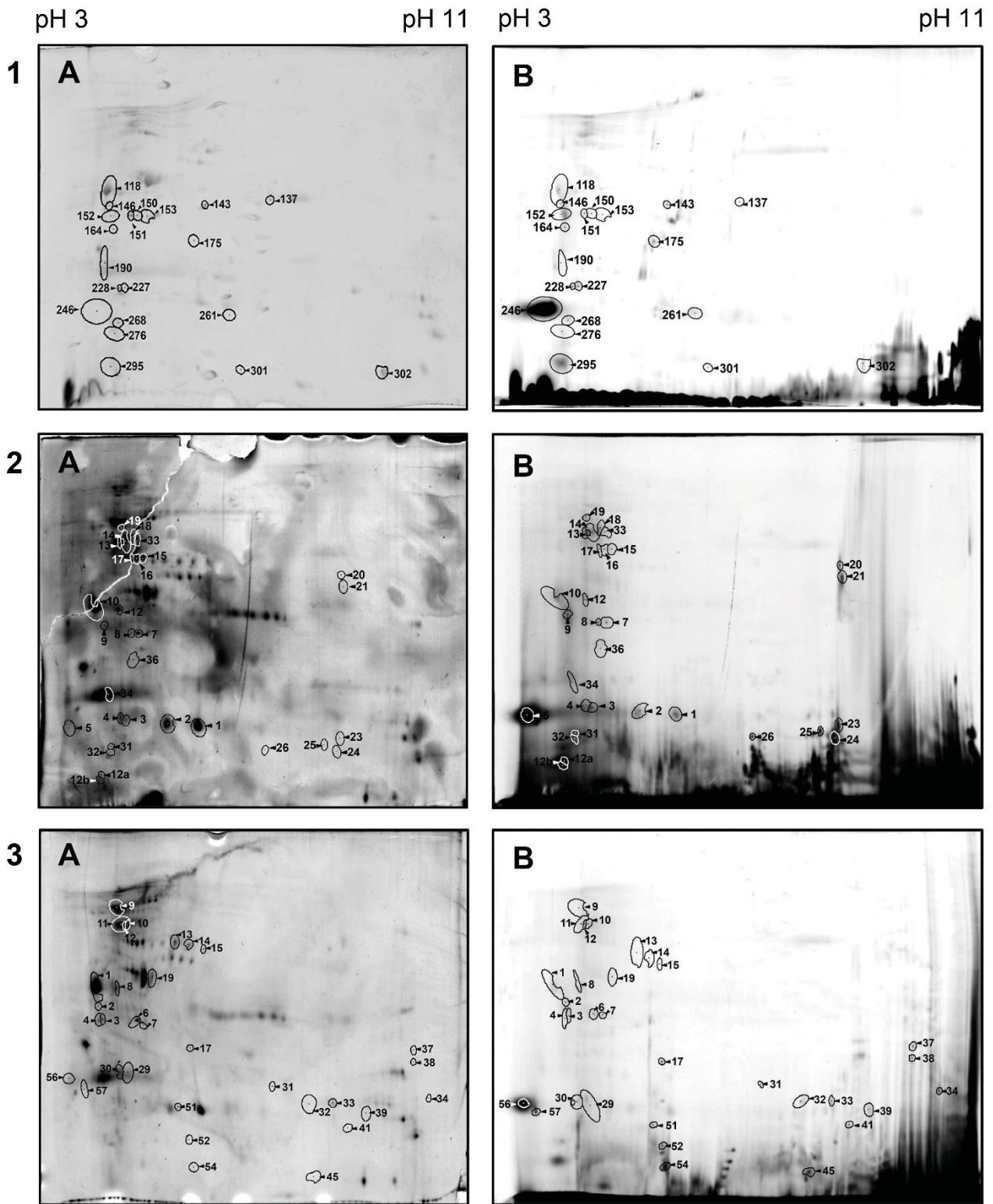
S3 Fig

4.3   Manuscript C

Accumulation of polyunsaturated aldehydes in the gonads of the copepod *Acartia tonsa* revealed by tailored fluorescent probes

Stefanie Wolfram, Jens C Nejstgaard, Georg Pohnert

Folder S1 of this publication is available via the embedded DVD.

PLOS ONE

Accumulation of Polyunsaturated Aldehydes in the Gonads of the Copepod *Acartia tonsa* Revealed by Tailored Fluorescent Probes

Stefanie Wolfram[1], Jens C. Nejstgaard[2,3]*, Georg Pohnert[1]*

1 Institute for Inorganic and Analytical Chemistry, Friedrich Schiller University, Jena, Germany, **2** Skidaway Institute of Oceanography, Savannah, GA, United States of America, **3** Department of Experimental Limnology, Leibniz-Institute of Freshwater Ecology and Inland Fisheries (IGB), Department 3 Experimental Limnology, Stechlin, Germany

Abstract

Polyunsaturated aldehydes (PUAs) are released by several diatom species during predation. Besides other attributed activities, these oxylipins can interfere with the reproduction of copepods, important predators of diatoms. While intensive research has been carried out to document the effects of PUAs on copepod reproduction, little is known about the underlying mechanistic aspects of PUA action. Especially PUA uptake and accumulation in copepods has not been addressed to date. To investigate how PUAs are taken up and interfere with the reproduction in copepods we developed a fluorescent probe containing the $\alpha,\beta,\gamma,\delta$-unsaturated aldehyde structure element that is essential for the activity of PUAs as well as a set of control probes. We developed incubation and monitoring procedures for adult females of the calanoid copepod *Acartia tonsa* and show that the PUA derived fluorescent molecular probe selectively accumulates in the gonads of this copepod. In contrast, a saturated aldehyde derived probe of an inactive parent molecule was enriched in the lipid sac. This leads to a model for PUAs' teratogenic mode of action involving accumulation and covalent interaction with nucleophilic moieties in the copepod reproductive tissue. The teratogenic effect of PUAs can therefore be explained by a selective targeting of the molecules into the reproductive tissue of the herbivores, while more lipophilic but otherwise strongly related structures end up in lipid bodies.

Data Availability: The authors confirm that all data underlying the findings are fully available without restriction. All relevant data are within the paper and its Supporting Information files.

Competing Interests: The authors have declared that no competing interests exist.

* Email: nejstgaard@igb-berlin.de (JN); Georg.Pohnert@uni-jena.de (GP)

Introduction

Diatoms are highly abundant marine phytoplankton and considered to be among the most important food sources for the dominating zooplankton such as copepods. Diatoms are thus at the bottom of the marine food web and also play central roles in climate functioning [1]. The beneficial role of diatoms as food source was however questioned due to evidence of decreased reproductive success in copepods feeding on diatom rich diets, compared to various non-diatom prey types (reviewed in [2,3]). Since these initial studies the effect of diatoms on copepod reproduction has been intensively investigated in field and laboratory experiments (reviewed in [4–6]). The production of teratogenic $\alpha,\beta,\gamma,\delta$-polyunsaturated aldehydes (PUAs) was made responsible for the reduced hatching success of copepod eggs and apoptotic malformations of copepod offspring [5,7,8]. While PUAs can explain several instances of poor copepod reproduction, their negative impact is not universal. Several field and laboratory assays gave no evidence of adverse PUA effects [9–13] while others did (reviewed in [5]). Higher molecular weight oxylipins and other toxins might provide additional explanations for observed teratogenic effects of diatoms on copepods [4,5]. Nutritional

inadequacies of some diatom species [14] and poor nutrient uptake due to rapid gut passage time [15] were also discussed. Most reports fuelling the debate about PUA toxicity focus on observations of the outcome of feeding experiments, while very few mechanistic studies address the origin of these findings and the mode of action of PUAs [9,16]. Data is especially lacking on how the metabolites are delivered to and distributed in feeding copepods.

Production of PUAs is initiated when diatom cells are wounded in the feeding organs of the herbivores and is even observed in the guts of the animals [17,18]. Thus proper experiments on uptake and targeting of PUAs would have to involve an active feeding process for delivery. Few PUA carriers have been introduced for feeding experiments that mimic the situation in the plankton. Buttino et al. [19] delivered the PUA 2,4-decadienal (DD) encapsulated in giant liposomes and observed reduced egg hatching success as well as induction of apoptosis in female tissue and copepod embryos of *Temora stylifera* and *Calanus helgolandicus*. Ianora et al. [7] incubated the non PUA-producing dinoflagellate *Prorocentrum minimum* as neutral living carrier with DD that was then delivered to copepods in feeding

experiments. But no feeding protocols using living food sources that allow detection of fluorescently labeled probes without interfering photosynthetic pigments have been available to date. This has hampered a mechanistic evaluation of PUA delivery in the animals.

Here we introduce a feeding protocol that allows delivery of fluorescent probes using the heterotrophic dinoflagellate *Oxyrrhis marina* as a vector. We use this procedure to deliver novel fluorescent molecular probes to adults of *Acartia tonsa*. This calanoid copepod is commonly found in coastal waters in a wide geographical range including the Antlantic, Indian and Pacific Oceans, the Baltic, Mediterranean and North Seas [20,21]. For *Acartia spp.* first experiments on the effects of diatoms in general as well as PUA producers were performed. No teratogenic effect was observed with *A. tonsa* feeding on a diatom rich natural diet but no information about the PUA content of this mixed diet was reported [22]. In specific feeding experiments the PUA producer *Thalassiosira rotula* caused reduced egg production and hatching success and led to blockage of egg development in *Acartia clausi* [23].

The applied probe for monitoring the targeting of PUA consists of a head group containing the $\alpha,\beta,\gamma,\delta$-unsaturated aldehyde motive and a tetramethylrhodamine based fluorescent reporter (TAMRA-PUA in Figure 1). The general layout follows concepts of activity-based protein profiling that allow delivery of nucleophilic target molecules to biological matrices [24]. According to previous results saturated aldehydes (SAs) that are structurally very similar to PUAs are not active and represent ideal controls due to their physicochemical resemblance to the antiproliferative metabolites [25]. We therefore applied a SA derived probe (TAMRA-SA in Figure 1) with otherwise identical properties compared to TAMRA-PUA. These probes proved to be valuable tools to monitor PUA uptake and to answer the question if accumulation takes place in specific organs of the copepods. Indeed, accumulation of TAMRA-PUA was visible in the gonads of *A. tonsa* while TAMRA-SA enriched in the lipid sac.

Materials and Methods

Synthesis of the probe and other molecules

A DD derived synthetic probe (TAMRA-PUA) synthesized from 2*E*,4*E*-decadien-9-ynal (DDY) containing the fluorophore 5-tetramethylrhodamine, a hexanal derived probe containing 5-tetramethylrhodamine (TAMRA-SA) and 5-tetramethylrhodamine-azide (TAMRA-N$_3$) were synthesized (Figure 1, Information S1).

Culturing of *O. marina* and incubation with the probes

Oxyrrhis marina (Dujardin) CCMP605, obtained from the Provasoli-Guillard National Center for Marine Algae and Microbiota, (NCMA, East Boothbay, Maine, USA), was used as food for copepods and carrier of the molecular probes. Cultures were kept with *Dunaliella tertiolecta* (Butcher) CCMP1320 as food source. Before copepod feeding experiments *O. marina* cultures (9.4×10^3 cells in 10 mL f/2) were fed with *D. tertiolecta* (500 µL of a 728×10^3 cells mL^{-1} culture) and kept for six days at 22°C without light in f/2 medium [26]. For experiments with copepods only cultures with low *D. tertiolecta* content (cell number lower than one tenth of *O. marina*) were used. To load *O. marina* with molecular probes, these cultures were incubated in the dark at 22°C for 2 h (experiment **I**) or 1 h (experiments **II**, **III**) with 10 µM TAMRA-PUA, TAMRA-N$_3$ or TAMRA-SA, respectively (for structures see Figure 1). Probes were administered as 5 mM stock solutions in DMSO at *O. marina* cell densities of 12.5×10^3

cells mL^{-1} (**I**, **II**) and 5.0×10^3 cells mL^{-1} (**III**). A schematic representation of the experiments is given in Figure 2.

Sampling and selection of *A. tonsa* and feeding with the probe treated *O. marina*

Acartia tonsa (Dana) was sampled during daytime between 6–9 April 2013 from the dock of the Skidaway Institute of Oceanography, Savannah, Georgia, USA by towing a 200-µm mesh net perpendicularly from the bottom to surface. The content of the cod end was transported immediately to the laboratory, where adult females were sorted out for the experiments by pipetting under a dissecting microscope. Individual females were kept in 20 mL polystyrene vessels (Sample cup 722060, Dynalon Labware, Rochester, New York, USA used in experiments **I** and **II**) or 2 mL polystyrene well plates (MultiDish 150628, Nalgene Nunc, Penfield, New York, USA used in experiment **III**) filled with filtered dock water (0.7 µm, GF/F Whatman, Clifton, NJ, USA). Females were either kept on un-incubated control food or treated with 10 µM TAMRA-PUA, TAMRA-SA or TAMRA-N$_3$ pre-incubated *O. marina* cultures (see above). The final cell density/carbon content of *O. marina* for experiment **I** was adjusted to 313 cells mL^{-1}/161 µg C L^{-1} for TAMRA-PUA and TAMRA-SA and 625 cells mL^{-1}/323 µg C L^{-1} for TAMRA-N$_3$ and controls. For experiment **II** 313 cells mL^{-1}/161 µg C L^{-1} and for **III** 714 cells mL^{-1}/369 µg C L^{-1} were used. Vessels and wells were kept dark by a cover of aluminium foil to reduce growth of remaining *D. tertiolecta* and incubated in the climate chamber at 22°C for 5 to 6 h (**I**), 20 h (**II**) or 29 h (**III**). The feeding period was ended by replacing the medium containing *O. marina* with filtered dock water four times using a pipette. Thereafter copepods were either sampled immediately (experiment **I** for TAMRA-N$_3$ and non-treated algae) or the copepods were left to starve in the prey free dock water for 40 min (experiment **I** for TAMRA-PUA and TAMRA-SA treated copepods) before sampling. All copepods were starved for 2.5 h in experiment **II** or 1 h in experiment **III** before sampling. The copepods were sampled and fixed by placing them in a bottom plate of an Utermöhl sedimentation chamber containing filtered dock water and glutaraldehyde (final concentration 0.3%).

Fluorescence microscopy

Fluorescence and bright field images were taken with an Olympus IX-50 inverted epifluorescence microscope (Tokyo, Japan) equipped with a 100-W mercury burner and a 1.4 MP colour CCD microscopy camera (M14, by Lumenera, Ottawa, Ontario, Canada). The Olympus filter cube U-MNG (NG) was used with a 530–550 nm excitation filter, a DM 570 nm dichroic mirror, and a BA 590 nm barrier filter. The microscope's magnification is 2.5, either 4x (UPlan Fl 4x) or 10x (UPlan Fl 10x phase) objectives were used to observe copepods. Unless otherwise indicated epifluorescence pictures of *A. tonsa* were taken with 500 ms exposure time.

Bright field images were transferred into monochrome pictures and processed with Adobe Photoshop CS6 regarding tonal correction. For overlays of fluorescence and bright field images, the black channel of each fluorescence image was removed and selective color settings were optimized, whereby the same routine and settings were applied to all images. All unmodified pictures are available in Folder S1.

Results and Discussion

Design of the probe and control substances

Previous work showed that the activity of PUAs is highly structure specific. While a series of medium size $\alpha,\beta,\gamma,\delta$-
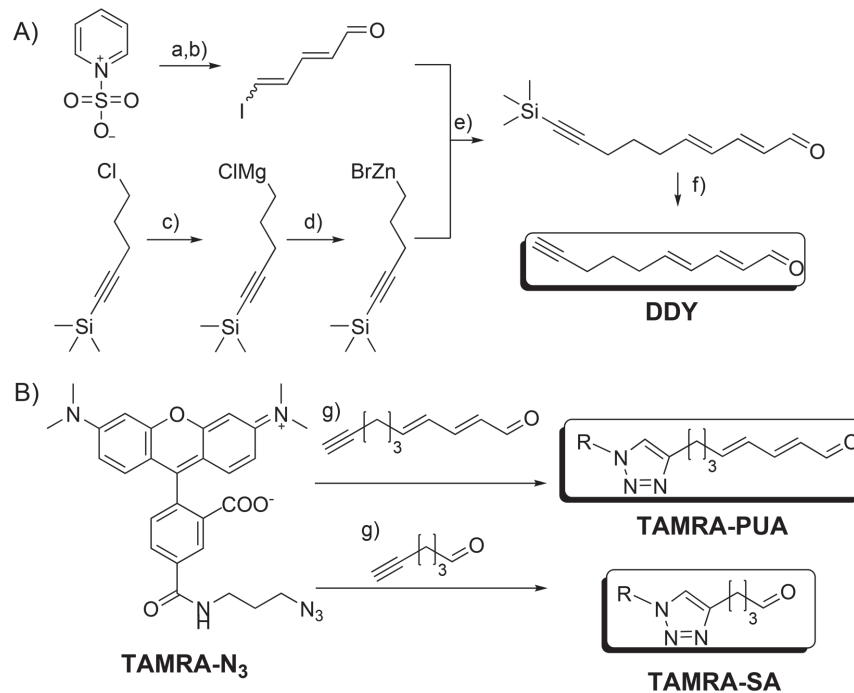
Figure 1. Synthesis of TAMRA-PUA and TARMA-SA. A) Synthesis of DDY, conditions: a) KOH, H_2O, 22% yield; b) 1.2 equ. PPh_3, 1.2 equ. I_2, CH_2Cl_2, 55% yield; c) 3.2 equ. Mg, $C_2H_4Br_2$, THF, d) 1.2 equ. $ZnBr_2$, THF; e) 0.06 equ. $Pd(PPh_3)_4$, THF, 28 to 30% yield; f) 1.2 equ. TBAF, THF, H_2O, 30% yield; B) Synthesis of the probes, conditions: g) tris[(1-benzyl-1H-1,2,3-triazol-4-yl)methyl]amine), sodium ascorbate, copper sulfate, 68% and 77% yield. R = 5-N-propylcarbamoyl tetramethylrhodamine. For detailed experimental procedures and product characterization see Information S1.
doi:10.1371/journal.pone.0112522.g001

unsaturated aldehydes tested showed activity, SAs were completely inactive even at elevated concentrations. Interestingly, activity of α,β,γ,δ-unsaturated aldehydes was not determined by the polarity of the terminus thus offering a potential site for structural manipulation [25,27]. We therefore developed a probe containing a C10 α,β,γ,δ-unsaturated aldehyde structure element linked at the terminus with the well-established and commercially available fluorophore tetramethylrhodamine (TAMRA) (Figure 1). The approach offers the possibility to localize TAMRA-PUA and other TAMRA containing molecules by fluorescence microscopy

without interfering with the active structural element. For control experiments we synthesized a probe with similar structure only modifying the aldehyde head group. By exchanging the α,β,γ,δ-unsaturated aldehyde motive with a saturated aldehyde structure we obtained the probe TAMRA-SA modeled after the inactive structures [27]. The corresponding fluorescent azide (TAMRA-N_3) was monitored in control experiments to exclude that accumulation due to the structure of the fluorophore itself occurs in the copepods.
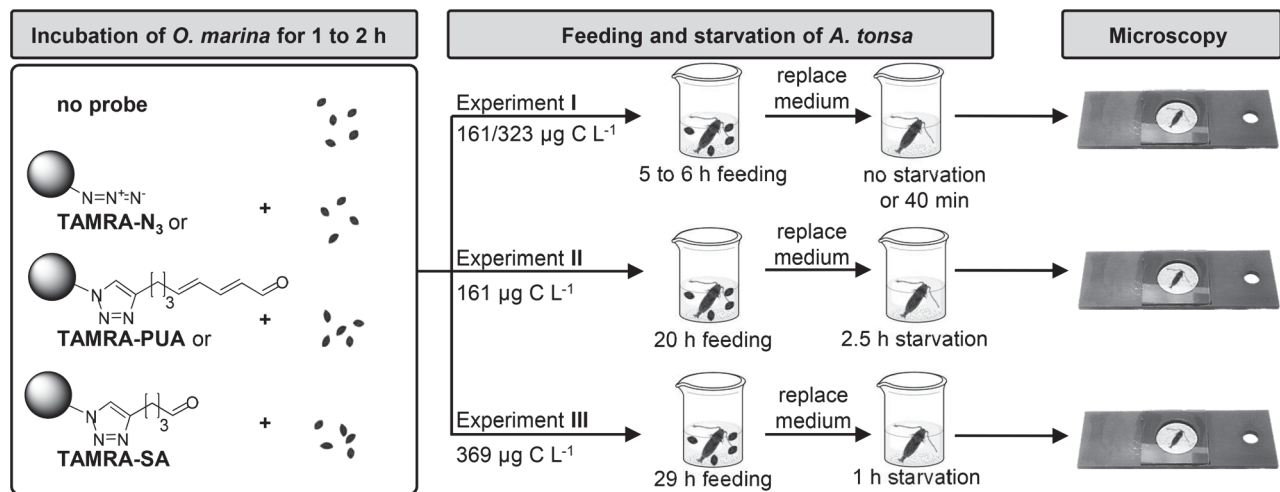
Figure 2. Schematic representation of the experimental set-up. In experiment I incomplete defecation was observed, experiment III was only performed with TAMRA-SA and TAMRA-N_3.
doi:10.1371/journal.pone.0112522.g002
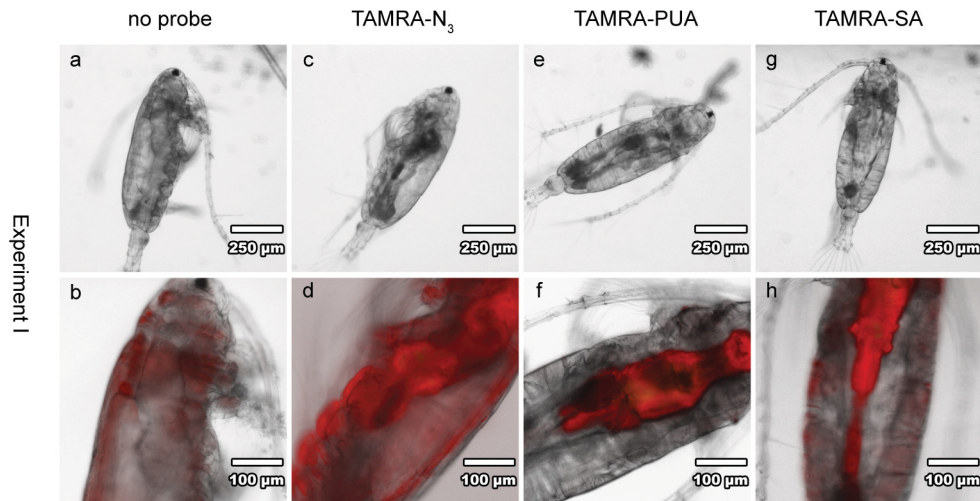
Figure 3. Overview about feeding experiment I with *A. tonsa*. Copepods were fed for 5 h on non-treated (**a**, **b**) *O. marina* or on TAMRA-N$_3$ (**c**, **d**) loaded *O. marina* (323 µg C L^{-1}) without starvation. Copepods fed for 6 h with TAMRA-PUA (**e**, **f**) or TAMRA-SA (**g**, **h**) pre-treated *O. marina* (161 µg C L^{-1}) and starved for 40 min still showed gut fluorescence. First line (**a**, **c**, **e**, **g**): light microscopy images; second line (**b**, **d**, **f**, **h**): overlay light microscopy and epifluorescence images.
doi:10.1371/journal.pone.0112522.g003

Feeding procedure and defecation of *A. tonsa*

Previous experiments showed that PUAs can be delivered on the food algae *P. minimum* to the copepod *C. helgolandicus*. If this dinoflagellate is incubated in a PUA solution in seawater it adsorbs some of the compounds and delivers them if added as a food source to the copepods [7]. In pilot experiments we loaded 10 µM TAMRA-PUA on *P. minimum* and delivered it to *A. tonsa*. Unfortunately, the strong autofluorescence of *P. minimum* interfered with the detection of the TAMRA fluorescence (see Figure S1). It was thus impossible to distinguish between TAMRA and chlorophyll fluorescence. To overcome this limitation we reasoned that a heterotrophic food source that does not contain any photosynthetic pigments could act as a shuttle of the probe. The heterotrophic dinoflagellate *O. marina* is known to be a good food source for *A. tonsa* (reviewed in [28]) and the first experiments demonstrated that TAMRA-PUA can be loaded on this prey (Figure S2). The dinoflagellate *O. marina* was fed with the diatom *D. tertiolecta*. To avoid interference of the pigments of the prey alga, six days before the onset of feeding experiments, *O. marina* cultures were transferred into the dark to arrest growth of the algae. Remaining algae were removed from the culture by predation of *O. marina*. Before the experiments were conducted, it was verified by microscopy that the *D. tertiolecta* cell count was significantly lower than that of *O. marina*, a criterion indicating sufficient suppression of algal autofluorescence. Before conducting the final experiments, preliminary treatments were performed to determine optimum probe-concentration and incubation times. In the experiments shown, one *O. marina* culture was split in four equal parts and either incubated for 1 h (experiments **II**, **III**) or 2 h (**I**) with 10 µM TAMRA-PUA, 10 µM TAMRA-SA or 10 µM TAMRA-N$_3$. The schematic overview of the experiments is presented in Figure 2. One control received no treatment.

Single individuals of *A. tonsa* females were sorted into filtered dock water and pre-treated or control *O. marina* cultures were added to give final cell densities between 313 cells ml^{-1} and 714 cells ml^{-1}. After feeding for 5 to 29 h, the *O. marina* containing medium was replaced by filtered dock water. Copepods were either sampled directly or starved for up to 2.5 h before sampling.

Immediately after sampling fluorescence microscopy was conducted to reveal the localization of the probes within the animals.

We first checked for the effect of defecation and washing of copepods (experiment **I**) to minimize fluorescence on the surface of copepods or in the digestive tract that might interfere with a possible detection of TAMRA-accumulation in copepod tissue (Figure 3). Without starvation a high and unspecific fluorescence was observed if copepods were incubated with TAMRA-N$_3$ (Figure 3d). This might result from unspecific adsorption of the fluorescent dye to the surface of the copepods. This unspecific fluorescence could be eliminated within a 1 to 2.5 h starvation and washing time in fresh medium (Figure 3, Figure 4 and Figure 5). Also the observed fluorescence in the stomach and gut area of the copepods could be reduced significantly by 1 to 2.5 h starvation (and defecation). Earlier reports indicated reduced fluorescence of photopigments of food algae in *A. tonsa* after 120 min starvation to ca. 5% of initial values [29]. Indeed, only minor TAMRA-N$_3$ fluorescence was observed in the gut after this period indicating that the unmodified fluorophore does not behave significantly different compared to food pigments (Figure 4d and Figure 5a). Copepods fed *O. marina* that was not incubated with a fluorophore did not show any signal in the digestive tract. This indicates a successful elimination of autofluorescence of *O. marina* food algae (Figure 4b). Remaining fluorescence in the digestive tract thus originates from TAMRA derivatives and not the autofluorescence of *D. tertiolecta*.

Uptake and localization of TAMRA-PUA

When copepods were fed for brief periods of 5 to 6 h on TAMRA-PUA and TAMRA-SA pre-treated *O. marina* cells as food source and a starvation of 40 min was allowed (Figure 2), enrichment of fluorescence was mainly detected in the gut (Figure 3f, h). These probes remained longer in the digestive tract in comparison to TAMRA-N$_3$. Assuming a clearance of ca. 80% of gut fluorescence from pigmented food algae after 40 min [29], remaining fluorescence would likely be due to residual TAMRA-loaded food. Also the increased hydrophobicity of the aldehyde-probes might be responsible for longer residual times in the gut. However, since we aimed to elucidate the localization of PUAs
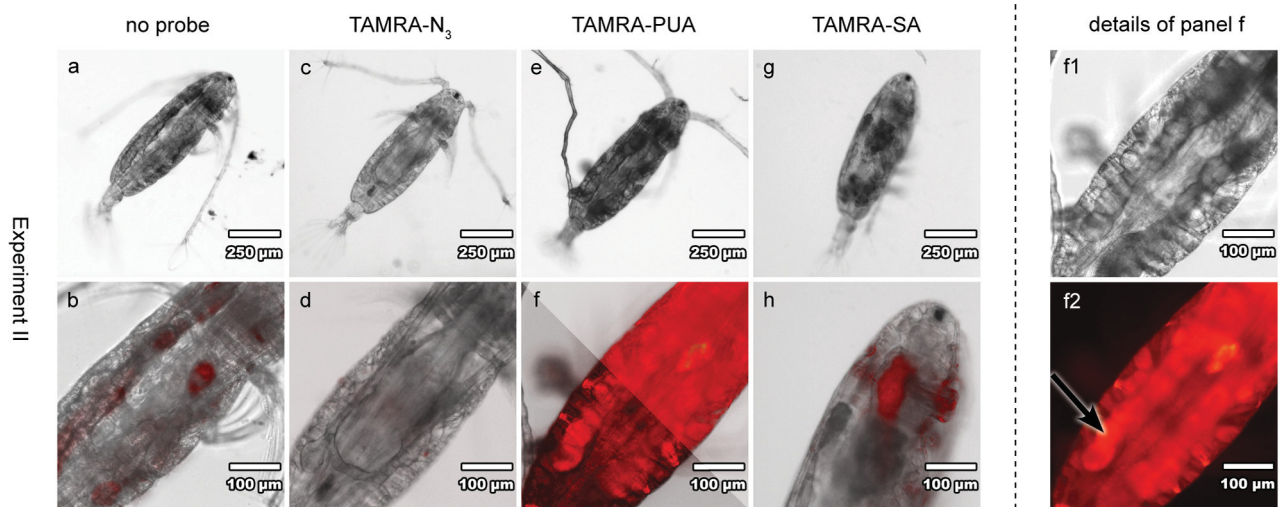
Figure 4. Overview about feeding experiment II with *A. tonsa*. Copepods were fed for 20 h on pre-treated or non-treated *O. marina* (161 µg C L^{-1}) followed by 2.5 h starvation. Strong fluorescence of the TAMRA-PUA treated copepod (**e**, **f**, **f1**, **f2**) is observed, the arrow indicates high accumulation of TAMRA-PUA in gonad tissue (**f2**). First line (**a**, **c**, **e**, **g**, **f1**): light microscopy images; second line (**b**, **d**, **f**, **h**): overlay light microscopy and epifluorescence images; **f2**: epifluorescence image. Overlay image **f** is bisected – right section: with routine applied to all other fluorescence pictures, left section: changed settings for selective colour correction.
doi:10.1371/journal.pone.0112522.g004

within the copepod tissue, we chose longer feeding and defecation times in the subsequent experiments. For optimization, we incubated *A. tonsa* under different conditions, e.g. copepod feeding and starvation times as well as food carbon content. A starvation time of at least 1 h usually enabled more complete defecation and offered the possibility to observe areas of probe accumulation without interfering fluorescent gut content.

Most intensive tissue fluorescence in TAMRA-PUA treated copepods was reached with condition **II** (161 µg C L^{-1}, 20 h feeding time and 2.5 h starvation) (Figure 4f, f2). With remarkable selectivity, the probe accumulated preferentially in the gonads (Figure 4f2, arrow). This accumulation supports the activity of PUAs as antiproliferative metabolites. The targeted delivery of these reactive metabolites to the reproductive organs explains observation that diatom rich diets cause oocyte degradations characterised by cell fragmentation, presence of apoptotic bodies and degradation of cytoplasm in *Calanus helgolandicus* [9]. In that study histological and cytological observations on gonads and oocyte development stages in *C. helgolandicus* were performed and several mechanisms as well as other factors besides PUA content of the diet were postulated to cause adverse effects in

copepod oocyte maturation. A targeted delivery of active metabolites at least partially explains the observed selectivity of adverse effects. Our finding thus provides an explanation for how PUAs can be teratogenic to copepods without any other obvious harmful effect on the feeding adults [30]. Accumulation might be facilitated by covalent reactions of the DD analogue TAMRA-PUA since DD acts as electrophile: PUAs are known to be attacked by nucleophiles, such as amine or thiol groups of proteins [31,32] or amine groups of DNA [33–35]. Such reactions lead to modifications of enzymes that might lead to dysfunctions, functional alterations and thus interference with molecular functions and biological processes. DNA modifications might disturb transcription and translation. In addition, DD enhances oxidative stress which causes DNA breaks [36].

Uptake and localization of TAMRA-SA

Experimental setup **III** with increased carbon content of 369 µg C L^{-1}, increased copepod feeding time of 29 h and 1 h starvation showed an accumulation of TAMRA-SA in the lipid sac of a female (Figure 5b, b2 arrow). TAMRA-SA is the most nonpolar of all tested substances and therefore incorporation in the lipid sac of
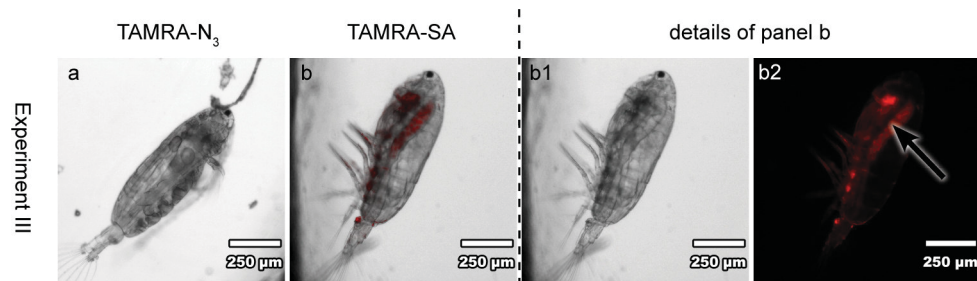
Figure 5. Feeding experiment III with *A. tonsa*. Copepods were fed for 29 h with TAMRA-N$_3$ (**a**, exposure time 1.5 s) or TAMARA-SA (**b**, **b1**, **b2** exposure time 500 ms) pre-treated *O. marina* (369 µg C L^{-1}) and starved for 1 h. The arrow indicates high accumulation of TAMRA-SA in the lipid sac (**b2**). **a**, **b**: overlay light microscopy and epifluorescence images; **b1**: light microscopy image; **b2** epifluorescence image.
doi:10.1371/journal.pone.0112522.g005

A. tonsa might be caused by its physicochemical properties. This result is in agreement with the fact that copepods store part of their food lipids in a lipid sac for energy supply and reproduction [37]. The results indicate that there are different accumulation behaviours of PUAs and SAs besides the physicochemical similarities of these molecules. PUAs enrich in gonads, where they probably interfere with enzyme activity and physiological functions resulting in their teratogenic activity. In contrast, their saturated non-toxic counterparts seem to be enclosed in the lipid sac for storage.

Conclusion

In this study we introduce the delivery and use of molecular probes designed to monitor the action of PUAs in copepods. We provide evidence for a targeted localization of a PUA-derived molecular probe in the gonads of *A. tonsa*. These effects could be responsible for PUAs' selective teratogenic action. We also show that a probe derived from an inactive SA accumulates in the lipid bodies thereby further supporting the notion of selectivity of PUAs.

Supporting Information

Figure S1 Bright field and epifluorescence images of *Prorocentrum minimum*. Algae cells were treated without (**a**, **b**) and with 10 μm TAMRA-PUA after 1 h (**c**, **d**) and 22 h (**e**, **f**) incubation time. For epifluorescence images the exposure time was 405 ms. Cells were measured with an Olympus HX-60 equipped with an U-MSWG filter cube containing an BP 480–550 nm

excitation filter, a DM 570 nm dichroic mirror and an BA 590 nm emission filter combined with a Retiga 1300 camera.
(TIF)

Figure S2 Bright field and epifluorescence images of *Oxyrrhis marina*. Cells were treated without (**a**, **b**, **c**) and with 10 μm TAMRA-PUA after 19 h (**d**, **e**, **f**) incubation time. For epifluorescence images the exposure time was 200 ms (**b**, **e**) or 405 ms (**c**, **f**). The cells were measured as described for Figure S1.
(TIF)

Folder S1 Unmodified light microscopy and epifluorescence images of *A. tonsa*.
(ZIP)

Information S1 Experimental procedures and characterization data of synthetic products.
(DOCX)

Author Contributions

Conceived and designed the experiments: SW JN GP. Performed the experiments: SW JN. Analyzed the data: SW JN GP. Contributed reagents/materials/analysis tools: SW. Wrote the paper: SW JN GP.

References

1. Mauchline J (1998) Advances in Marine Biology, Vol. 33: The Biology of Calanoid Copepods. Amsterdam: Elsevier.
2. Paffenhöfer G-A (2002) An assessment of the effects of diatoms on planktonic copepods. Mar Ecol Prog Ser 227: 305–310.
3. Ianora A, Poulet SA, Miralto A (2003) The effects of diatoms on copepod reproduction: a review. Phycologia 42: 351–363.
4. Caldwell G (2009) The influence of bioactive oxylipins from marine diatoms on invertebrate reproduction and development. Mar Drugs 7: 367–400.
5. Ianora A, Miralto A (2010) Toxigenic effects of diatoms on grazers, phytoplankton and other microbes: a review. Ecotoxicol 19: 493–511.
6. Pohnert G (2005) Diatom/copepod interactions in plankton: The indirect chemical defense of unicellular algae. ChemBioChem 6: 1–14.
7. Ianora A, Miralto A, Poulet SA, Carotenuto Y, Buttino I, et al. (2004) Aldehyde suppression of copepod recruitment in blooms of a ubiquitous planktonic diatom. Nature 429: 403–407.
8. Miralto A, Barone G, Romano G, Poulet SA, Ianora A, et al. (1999) The insidious effect of diatoms on copepod reproduction. Nature 402: 173–176.
9. Poulet SA, Cueff A, Wichard T, Marchetti J, Dancie C, et al. (2007) Influence of diatoms on copepod reproduction. III. Consequences of abnormal oocyte maturation on reproductive factors in *Calanus helgolandicus*. Mar Biol 152: 415–428.
10. Koski M, Wichard T, Jónasdóttir S (2008) "Good" and "bad" diatoms: development, growth and juvenile mortality of the copepod *Temora longicornis* on diatom diets. Mar Biol 154: 719–734.
11. Wichard T, Poulet SA, Boulesteix A-L, Ledoux JB, Lebreton B, et al. (2008) Influence of diatoms on copepod reproduction. II. Uncorrelated effects of diatom-derived α,β,γ,δ-unsaturated aldehydes and polyunsaturated fatty acids on *Calanus helgolandicus* in the field. Prog Oceanogr 77: 30–44.
12. Poulet SA, Wichard T, Ledoux JB, Lebreton B, Marchetti J, et al. (2006) Influence of diatoms on copepod reproduction. I. Field and laboratory observations related to *Calanus helgolandicus* egg production. Mar Ecol Prog Ser 308: 129–142.
13. Jónasdóttir S, Dutz J, Koski M, Yebra L, Jakobsen H, et al. (2011) Extensive cross-disciplinary analysis of biological and chemical control of *Calanus finmarchicus* reproduction during an aldehyde forming diatom bloom in mesocosms. Mar Biol 158: 1943–1963.
14. Jónasdóttir SH, Kiørboe T (1996) Copepod recruitment and food composition: Do diatoms affect hatching success? Mar Biol 125: 743–750.
15. Dutz J, Koski M, Jónasdóttir SH (2008) Copepod reproduction is unaffected by diatom aldehydes or lipid composition. Limnol Oceanogr 53: 225–235.
16. Poulet SA, Laabir M, Ianora A, Miralto A (1995) Reproductive response of *Calanus helgolandicus*. I. Abnormal embryonic and naupliar development. Mar Ecol Prog Ser 129: 85–95.
17. Pohnert G (2000) Wound-activated chemical defense in unicellular planktonic algae. Angew Chem Int Ed 39: 4352–4354.
18. Wichard T, Gerecht A, Boersma M, Poulet SA, Wiltshire K, et al. (2007) Lipid and fatty acid composition of diatoms revisited: Rapid wound-activated change of food quality parameters influences herbivorous copepod reproductive success. ChemBioChem 8: 1146–1153.
19. Buttino I, De Rosa G, Carotenuto Y, Mazzella M, Ianora A, et al. (2008) Aldehyde-encapsulating liposomes impair marine grazer survivorship. J Exp Biol 211: 1426–1433.
20. Walter TC, Boxshall G (02 Apr 2014) WoRMS: *Acartia (Acanthacartia) tonsa* Dana, 1849. World of Copepods database. Available: http://www.marinespecies.org/aphia.php?p=taxdetails&id=345943. Accessed 16 July 2014.
21. Gonzalez G (2013) Animal Diversity Web: *Acartia tonsa*. Available: http://animaldiversity.ummz.umich.edu/accounts/Acartia_tonsa/#309995C3-86C0-4B6A-B33A-4CA4E5DCB74A. Accessed 16 July 2014.
22. Sommer U (2009) Copepod growth and diatoms: Insensitivity of *Acartia tonsa* to the composition of semi-natural plankton mixtures manipulated by silicon:nitrogen ratios in mesocosms. Oecologia 159: 207–215.
23. Ianora A, Poulet SA, Miralto A, Grottoli R (1996) The diatom *Thalassiosira rotula* affects reproductive success in the copepod *Acartia clausi*. Mar Biol 125: 279–286.
24. Barglow KT, Cravatt BF (2007) Activity-based protein profiling for the functional annotation of enzymes. Nat Meth 4: 822–827.
25. Adolph S, Bach S, Blondel M, Cueff A, Moreau M, et al. (2004) Cytotoxicity of diatom-derived oxylipins in organisms belonging to different phyla. J Exp Biol 207: 2935–2946.
26. Guillard RL (1975) Culture of phytoplankton for feeding marine invertebrates. In: Smith W, Chanley M, editors. Culture of Marine Invertebrate Animals: Springer US. pp. 29–60.
27. Adolph S, Poulet SA, Pohnert G (2003) Synthesis and biological activity of α,β,γ,δ-unsaturated aldehydes from diatoms. Tetrahedron 59: 3003–3008.
28. Yang Z, Jeong HJ, Montagnes DJS (2011) The role of *Oxyrrhis marina* as a model prey: current work and future directions. J Plankton Res 33: 665–675.
29. Kiørboe T, Tiselius PT (1987) Gut clearance and pigment destruction in a herbivorous copepod, *Acartia tonsa*, and the determination of in situ grazing rates. J Plankton Res 9: 525–534.
30. Paffenhöfer G-A, Ianora A, Miralto A, Turner JT, Kleppel GS, et al. (2005) Colloquium on diatom-copepod interactions. Mar Ecol Prog Ser 286: 293–305.
31. Zhu X, Tang X, Zhang J, Tochtrop GP, Anderson VE, et al. (2010) Mass spectrometric evidence for the existence of distinct modifications of different proteins by 2(*E*),4(*E*)-decadienal. Chem Res Toxicol 23: 467–473.

32. Sigolo CAO, Di Mascio P, Medeiros MHG (2007) Covalent modification of cytochrome *c* exposed to *trans*, *trans*-2,4-decadienal. Chem Res Toxicol 20: 1099–1110.

33. Carvalho VM, Asahara F, Di Mascio P, Arruda Campos IPd, Cadet J, et al. (2000) Novel 1, N^6-etheno-2'-deoxyadenosine adducts from lipid peroxidation products. Chem Res Toxicol 13: 397–405.

34. Loureiro APM, Di Mascio P, Gomes OF, Medeiros MHG (2000) *trans*, *trans*-2,4-Decadienal-induced 1, N^2-etheno-2'-deoxyguanosine adduct formation. Chem Res Toxicol 13: 601–609.

35. Loureiro APM, Arruda Campos IPd, Gomes OF, Di Mascio P, Medeiros MHG (2004) Structural characterization of diastereoisomeric ethano adducts derived from the reaction of 2'-deoxyguanosine with *trans*, *trans*-2,4-decadienal. Chem Res Toxicol 17: 641–649.

36. Young S-C, Chang LW, Lee H-L, Tsai L-H, Liu Y-C, et al. (2010) DNA damages induced by *trans*, *trans*-2,4-decadienal (*tt*-DDE), a component of cooking oil fume, in human bronchial epithelial cells. Environ Mol Mutag 51: 315–321.

37. Lee RF, Hagen W, Kattner G (2006) Lipid storage in marine zooplankton. Mar Ecol Prog Ser 307: 273–306.

Supporting Information S1: Experimental procedures and characterization data of synthetic products.

Accumulation of polyunsaturated aldehydes in the gonads of the copepod _Acartia tonsa_ revealed by tailored fluorescent probes

Stefanie Wolfram[1], Jens C. Nejstgaard[2,3] and Georg Pohnert[1]

1 Institute for Inorganic and Analytical Chemistry, Friedrich Schiller University, Lessingstr. 8, 07743 Jena, Germany,

2 Skidaway Institute of Oceanography, 10 Ocean Science Circle, Savannah, GA 31411, USA,

3 Department of Experimental Limnology, Leibniz-Institute of Freshwater Ecology and Inland Fisheries (IGB), Department 3 Experimental Limnology, Alte Fischerhütte 2, 16775 Stechlin, Germany

Synthetic procedures

General remarks

All chemicals were purchased as reagent grade or better and used without further purification. If necessary, reactions were performed under argon. Commercially available dry solvents were employed. Diethyl ether and tetrahydrofuran (THF) contained butylhydroxytoluene as peroxidation inhibitor. Column chromatography was carried out on Merck silica gel (0.04 – 0.063 mesh). Thin layer chromatography (TLC) was performed with TLC silica gel 60 F_{254} plates from Merck. TLC spots were visualized by irradiation of the TLC plate with UV radiation (254 nm) or by dipping in Seebach reagent (2.5 g phosphomolybdic acid and 1 g cer(IV)sulfate dissolved in 65 ml water, slowly acidified by dropwise addition of 6 ml concentrated sulfuric acid). Preparative HPLC was performed with a Shimadzu LC-8A system using a SPD-10AV UV/VIS detector and a LiChro CART® 250-10 Purospher® column (RP C18, endcapped, 5 μm particle size) with solvent A, (water, containing 2 % methanol (v/v)) and solvent B (methanol) using the following program: 0.1 min, 98% A; within 4.9 min to 30% A; within 15.0 min to 0% A; for 7 min, 0% A; within 1 min to 98% A; for 10 min 98% A; flow 4 mL min^{-1}.

5-Iodo-penta-2*E*,4*E*/*Z*-dienal
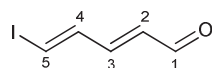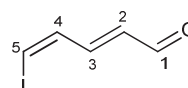
isomer a   isomer b

5-Iodo-penta-2*E*,4*E*/*Z*-dienal was synthesized according to Soullez et *al.* as isomeric mixture with a 4*E*:4*Z* ratio of 52:48; spectroscopic data are identical as described in the literature [1].

isomer a

^{1}H-NMR (600 MHz, CDCl$_3$) δ (ppm) = 6.15 (dd; ^{3}J = 15.41 Hz; ^{3}J = 7.70 Hz; 1H; H-C2); 6.97 (dd; ^{3}J = 15.41 Hz; ^{3}J = 11.00 Hz; 1H; H-C3); 7.16 (d; ^{3}J = 14.31; 1H; H-C5); 7.32 (dd; ^{3}J = 14.30 Hz; ^{3}J = 11.00 Hz; 1H; H-C4); 9.58 (d; ^{3}J = 7.70; 1H; H-C1)

^{13}C-NMR (50 MHz, CDCl$_3$) δ (ppm) = 92.0 (C5); 131.1 (C2); 143.2 (C4); 149.5 (C3); 193.2 (C1)

GC/EI-MS *m/z* (relative intensity) = 51 (31); 52 (32); 53 (33); 81 (100); 82 (13); 127 (19); 179 (7); 208 (12)

HR-EI-TOF-MS *m/z* = 207.9389 (M$^{+\bullet}$); calculated (C$_5$H$_5$IO) m/z = 207.9385

isomer b

^{1}H-NMR (600 MHz, CDCl$_3$) δ (ppm) = 6.37 (dd; ^{3}J = 15.41 Hz; ^{3}J = 8.25 Hz; 1H; H-C2); 7.01-7.05 (m; 2H; H-C4+H-C5); 7.23-7.29 (m; 1H; H-C3); 9.70 (d; ^{3}J = 8.25; 1H; H-C1)

^{13}C-NMR (50 MHz, CDCl$_3$) δ (ppm) = 95.0 (C5); 134.9 (C2); 136.6 (C4); 149.7 (C3); 193.5 (C1)

GC/EI-MS *m/z* (relative intensity) = 51 (30); 52 (29); 53 (29); 81 (100); 82 (13); 127 (18); 179 (5); 209 (4)

HR-EI-TOF-MS *m/z* = 207.9393 (M$^{+\bullet}$); calculated (C$_5$H$_5$IO) m/z = 207.9385

5-Trimethylsilylpent-4-yne-magnesiumchloride
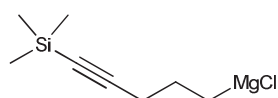
3.2 equ. pelleted magnesium were etched with 4% hydrochloric acid, rinsed with deionized water to neutral pH, rinsed with acetone several times and dried in vaccum/argon using the Schlenk technique. The magnesium was baked out in vacuum using a heat gun. In an argon atmosphere THF (0.1 mL per 1 mM magensium) and a solution of 1.0 equ. of 5-chloro-1-trimethylsilylpent-1-yne in THF (1.0 mL per 1 mM 5-chloro-1-trimethylsilylpent-1-yne) were added. Grignard reaction was

initiated by dropwise adding a maximum of 2 equ. 1,2-dibromoethane. The suspension was refluxed for 2-4 hours with stirring; conversion was checked by GC-MS. The reaction mixture was used *in situ* for metal exchange to trimethylsilylpent-4-yne-zinc(II)bromide on the same day.

5-Trimethylsilylpent-4-yne-zinc(II)bromide
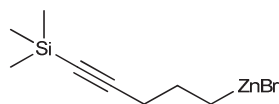
Trimethylsilylpent-4-yne-zinc(II)bromide was synthesized according to Adolph et *al.* [2]. The suspension was allowed to settle down before further transformation of the supernatant on the same day.

(2*E*,4*E*)-10-(Trimethylsilyl)decadien-9-ynal
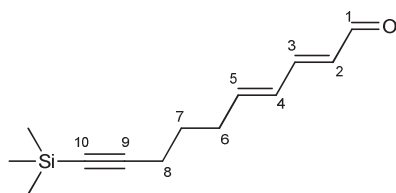
In an argon atmosphere 0.06-0.07 equ. tetrakis(triphenylphosphine)palladium(0) were added to 1.0 equ. of the mixture of isomers 5-Iodo-penta-2*E*,4*E/Z*-dienal in THF (1 mL per 0.1 mmol). 3.1 to 5.0 equ. of the clear solution of 5-trimethylsilylpent-4-yne-zinc(II)bromide were added. The reaction was hydrolyzed after 5 to 10 min and extracted 3 times with diethyl ether. The combined organic phases were washed with brine and dried with $MgSO_4$. Column chromatography was utilized with petrol ether/diethyl ether (4/1, v/v). A light yellow oil was obtained with 28 to 30% yield; it contained approximately 5% of the *2E,4Z* isomer analyzed by GC-MS.

^{1}H-NMR (400 MHz, $CDCl_3$) δ (ppm) = 0.14 (s; 9H; $SiC(CH_3)_3$); 1;65 (quin; ^3J = 7.32 Hz; 2H; H-C7); 2.26 (t; ^3J = 6.95 Hz; 2H; H-C8); 2.33 (m; 2H; H-C6); 6.08 (dd; ^3J = 15.00 Hz; ^3J = 7.68 Hz; 1H; H-C2); 6.25 (dt; ^3J = 15.00 Hz; ^3J = 6.59 Hz; 1H; H-C5); 6.34 (dd; ^3J = 15.37 Hz; ^3J = 10.25 Hz; 1H; H-C4); 7.07 (dd; ^3J = 15.37 Hz; ^3J = 10.25 Hz; 1H; H-C3); 9.53 (d; ^3J = 8.05 Hz; 1H; H-C1)

^{13}C-NMR (100 MHz, $CDCl_3$) δ (ppm) = 0.11 ($SiC(CH_3)_3$); 19.3 (C8); 27.3 (C7); 32.0 (C6); 85.4 (C9); 106.3 (C10); 129.3 (C4); 130.4 (C2); 145.7 (C5); 152.3 (C3); 193.8 (C1)

GC/EI-MS *m/z* (relative intensity) = 67 (7); 73 (100);74 (10); 75 (27); 79 (13); 81 (27); 91 (21); 96 (7);

109 (7); 115 (12); 116 (11); 117 (10); 128 (7); 129 (21); 130 (10); 131 (34); 147 (8); 192 (7);205 (7); 219 (7)

HR-EI-TOF-MS m/z = 205.1051 ([M-CH$_3$]$^+$); calculated (C$_{12}$H$_{17}$OSi) m/z = 205.1049; (no radical cation of entire substance visible)

2*E*,4*E*-Decadien-9-ynal
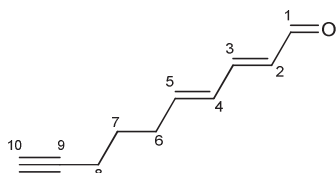
20 mg (0.091 mmol) (2*E*,4*E*)-10-(trimethylsilyl)decadien-9-ynal were dissolved in 4 mL THF and cooled to 0°C. After adding 0.11 mL (0.11 mmol) of a 1.0 M tetra-n-butylammoniumfluoride solution the solution was stirred till complete turnover (verified by TLC) followed by hydrolyzation and extraction (3 times with diethyl ether). The combined organic phases were washed with brine and dried with MgSO$_4$. Column chromatography was utilized with petrol ether/diethyl ether (5/1, v/v) and a light yellow oil was obtained with 30% yield. The product contains approximately 5% of the 2*E*,4*Z* isomer (analyzed by GC-MS).

^{1}H-NMR (400 MHz, CDCl$_3$) δ (ppm) = 1.70 (quin; ^{3}J = 7.32 Hz; 2H; H-C7); 1.98 (t; ^{4}J = 2.56 Hz; 1H; H-C10); 2.24 (td; ^{3}J = 6.95 Hz; ^{3}J = 2.56 Hz; 2H; H-C8); 2.36 (m; 2H; H-C6); 6.09 (dd; ^{3}J = 15.37 Hz; ^{3}J = 7.68 Hz; 1H; H-C2); 6.25 (dt; ^{3}J = 15.00 Hz; ^{3}J = 6.95 Hz; 1H; H-C5); 6.36 (dd; ^{3}J = 15.00 Hz; ^{3}J = 10.61 Hz; 1H; H-C4); 7.08 (dd; ^{3}J = 15.37 Hz; ^{3}J = 10.61 Hz; 1H; H-C3); 9.54 (d; ^{3}J = 8.05 Hz; 1H; H-C1)

^{13}C-NMR (100 MHz, CDCl$_3$) δ (ppm) = 17.9 (C8); 27.3 (C7); 31.9 (C6); 69.0 (C10); 83.6 (C9); 129.4 (C4); 130.5 (C2); 145.4 (C5); 152.3 (C3); 193.8 (C1)

GC/EI-MS m/z (relative intensity) = 63 (16); 65 (19); 66 (12); 67 (14); 77 (33); 78 (28); 79 (61); 80 (26); 81 (100); 91 (85); 92 (15); 107 (13); 108 (23); 115 (14); 117 (21); 119 (34)

HR-EI-TOF-MS 148.0890 (M$^{+\bullet}$); calculated (C$_{10}$H$_{12}$O): 148.0888

5-Hexynal
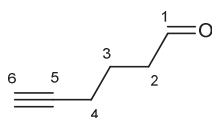
5-Hexynal was synthesized from 5-hexynol according to the general protocol for Swern oxidation [3] and purified by rectification. A colorless oil was obtained with 50% yield. The spectroscopic data are identical to the literature [4].

1H-NMR (400 MHz, CDCl$_3$) δ (ppm) = 1.85 (quin; ^{3}J = 6.95 Hz; 2H; H-C3); 1.98 (t; ^{4}J = 2.38 Hz; 1H; H-C6); 2.27 (td; ^{3}J = 7.20 Hz; ^{4}J = 2.56 Hz; 2H; H-C4); 2.61 (t; ^{3}J = 6.83 Hz; H-C2); 9.81 (s; 1H; H-C1)

13C-NMR (100 MHz, CDCl$_3$) δ (ppm) = 17.8 (C4); 20.8 (C3); 42.5 (C2); 69.3 (C6); 83.1 (C5); 201.7 (C1)

5-[3-Azidopropylcarbamoyl]-2-[6-(dimethylamino)-3-(dimethylimino)-3*H*-xanthene-9-yl]benzoate (TAMRA-N$_3$)
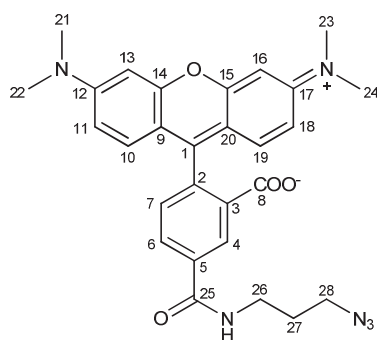
TAMRA-N₃ was synthesized according to Richter et al.; spectroscopic data are identical to the literature [5].

1H-NMR (600 MHz, CD$_3$OD) δ (ppm) = 1.95 (quin; ^{3}J = 6.60 Hz; 2H; H-C27); 3.28 (s; 12H; H-C21+H-C22+H-C23+H-C24); 3.47 (t; ^{3}J = 6.60 Hz; 2H; H-C28); 3.54 (t; ^{3}J = 6.60 Hz; 2H; H-C26); 6.91 (d; ^{4}J = 2.20 Hz; 2H; H-C13+H-C16); 7.02 (dd; ^{3}J = 9.90 Hz; ^{4}J = 2.20 Hz; 2H; H-C11+ H-C18); 7.23 (d; ^{3}J = 9.35 Hz; 2H; H-C10+H-C19); 7.39 (d; ^{3}J = 8.25 Hz; 1H; H-C7); 8.08 (dd; ^{3}J = 7.70 Hz; ^{4}J = 2.20 Hz; 1H; H-C6); 8.56 (d; ^{4}J = 2.20 Hz; 1H; H-C4)

LC-MS (ESI positive mode) m/z = 513 [M+H]$^+$, 535 [M+Na]$^+$

2-(6-(Dimethylamino)-3-(dimethyliminio)-3*H*-xanthene-9-yl)-5-(3-(4-((4*E*,6*E*)-8-xoxoocta-4,6-dienyl)-1*H*-1,2,3-triazol-1-yl)propylcarbamoyl)benzoate (TAMRA-PUA)
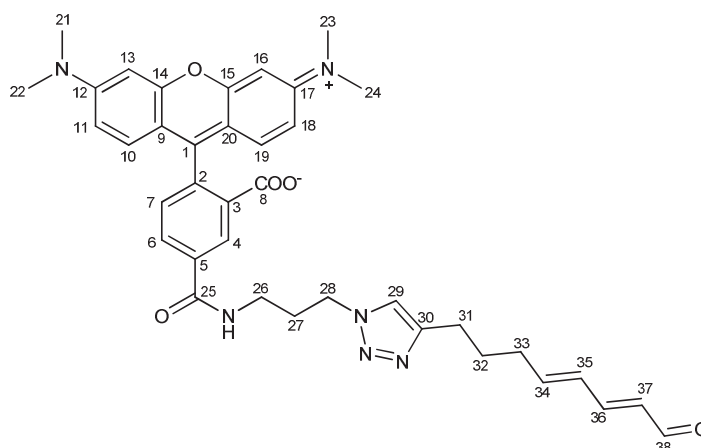
5.3 mg (0.036 mmol) 2*E*,4*E*-decadien-9-ynal and 12.8 mg (0.025 mmol) **TAMRA-N₃** were mixed with 6.0 mg (0.011 mmol) tris[(1-benzyl-1*H*-1,2,3-triazol-4-yl)methyl]amine) (TBTA), 4.7 mL phosphate buffered saline, 0.3 mL *tert*-butanol and 6 mL DMSO. 32 µL of a 1.0 M sodium ascorbate solution (0.032 mmol) and 21 µL of a 0.30 M copper sulfate solution (0.006 mmol) were added with stirring. After 8 hours the mixture was loaded on a C18 cartridge (Chromabond®, C18, endcapped, MACHEREY-NAGEL) for solid phase extraction. The column was washed with water and eluted with methanol. The crude product was diluted with deionized water and purified via preparative HPLC. The solvent was removed under reduced pressure yielding in 11.3 mg (0.017 mmol, 68 %) dark red crystals.

¹H-NMR (600 MHz, CD₃OD) δ (ppm) = 1.86 (quin; ^3J = 7.30 Hz; 2H; H-C32); 2.28 (m; 2H; H-C33); 2.31 (quin; ^3J = 6.60 Hz; 2H; H-C27); 2.74 (t; ^3J = 7.70 Hz; 2H; H-C31); 3.29 (s; 12H; H-C21+H-C22+H-C23+H-C24); 3.51 (t; ^3J = 6.60 Hz; 2H; H-C26); 4.52 (t; ^3J = 6.60 Hz; 2H; H-C28); 6.08 (dd; ^3J = 15.41 Hz; ^3J = 8.25 Hz; 1H; H-C37); 6.38-6.46 (m; 2H; H-C34+H-C35); 6.93 (d; ^4J = 2.20 Hz; 2H; H-C13+H-C16); 7.02 (dd; ^3J = 9.90 Hz; ^4J = 2.20 Hz; 2H; H-C11+H-C18); 7.24 (d; ^3J = 9.35 Hz; 2H; H-C10+ H-C19); 7.27 (dd; ^3J = 15.41 Hz; ^3J = 9.35 Hz; 1H; H-C36); 7.37 (d; ^3J = 7.70 Hz; 1H; H-C7); 7.86 (s; 1H; H-C29); 8.05 (d; ^3J = 7.70 Hz; 1H; H-C6); 8.54 (s; 1H; H-C4); 9.48 (d; ^3J = 7.70 Hz; H-C38)

LC-MS (ESI positive mode) m/z = 331 [M+2H]²⁺; 661 [M+H]⁺; 683 [M+Na]⁺

2-(6-(Dimethylamino)-3-(dimethyliminio)-3*H*-xanthene-9-yl)-5-(3-(4-(4-oxobutyl)-1*H*-1,2,3-triazol-1-yl)propylcarbamoyl)benzoate (TAMRA-SA)
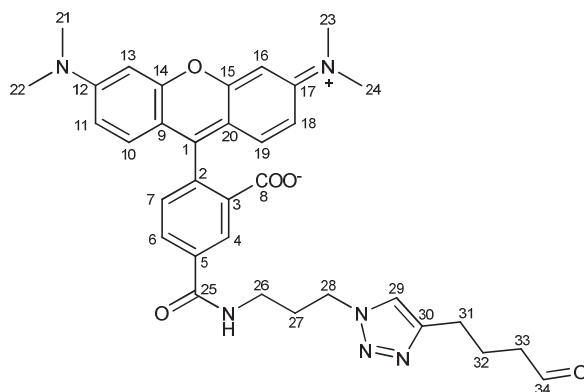

5.0 mg (0.052 mmol) 5-hexynal and 11.1 mg (0.022 mmol) **TAMRA-N₃** were mixed with 3.0 mg (0.006 mmol) TBTA, 5 mL *tert*-butanol, 1 mL DMSO and 5 mL deionized water. 132 µL of a 1.0 M sodium ascorbate solution (0.132 mmol) and 126 µL of a 0.050 M copper sulfate solution (0.006 mmol) were added with stirring. After stirring over night the solvent was removed under reduced pressure, the residue was partly dissolved in 1 mL methanol and 9 ml deionized water and purified via preparative HPLC, the remaining residue mainly contained TBTA and was discarded. The solvent was removed under reduced pressure yielding in 10.2 mg (0.017 mmol, 77 %) dark red crystals.

¹H-NMR (600 MHz, CD₃OD) δ (ppm) = 1.55-1.67 (m; 2H); 1.72-1.79 (m; 2H); 2.27 (quin; ^3J = 6.64 Hz; 2H); 2.71 (t; ^3J = 7.14 Hz; 2H); 3.27 (s; 12H); 3.49 (t; ^3J = 6.99 Hz; 2H); 4.48-4.53 (m; 3H); 6.91 (d; ^4J = 2.35 Hz; 2H); 7.01 (dd; ^3J = 9.77 Hz; ^4J = 2.67 Hz; 2H); 7.24 (d; ^3J = 10.04 Hz; 2H); 7.35 (d; ^3J = 7.58; 1H); 7.83 (s; 1H); 8.06 (dd; ^3J = 7.86 Hz; ^4J = 1.85; 1H); 8.52 (d; ^4J = 1.64; 1H)

LC-MS (ESI positive mode) m/z = 305 [M+2H]²⁺; 609 [M+H]⁺; 631 [M+Na]⁺

References

1. Soullez D, Ple G, Duhamel L (1997) ω-Halogeno polyenals: preparation and application to a one-pot synthesis of polyenals from carbonyl compounds. J Chem Soc, Perkin Trans 1: 1639–1646.

2. Adolph S, Poulet SA, Pohnert G (2003) Synthesis and biological activity of $\alpha,\beta,\gamma,\delta$-unsaturated aldehydes from diatoms. Tetrahedron 59: 3003–3008.

3. Schwetlick K (2009) Organikum. Weinheim: Wiley-VCH.

4. Amoroso JW, Borketey LS, Prasad G, Schnarr NA (2010) Direct acylation of carrier proteins with functionalized β-lactones. Organic Letters 12: 2330-2333.

5. Richter P, Weißflog J, Wielsch N, Svatoš A, Pohnert G (2013) Functionalized bis-enol acetates as specific molecular probes for esterases. ChemBioChem 14: 2435-2438.
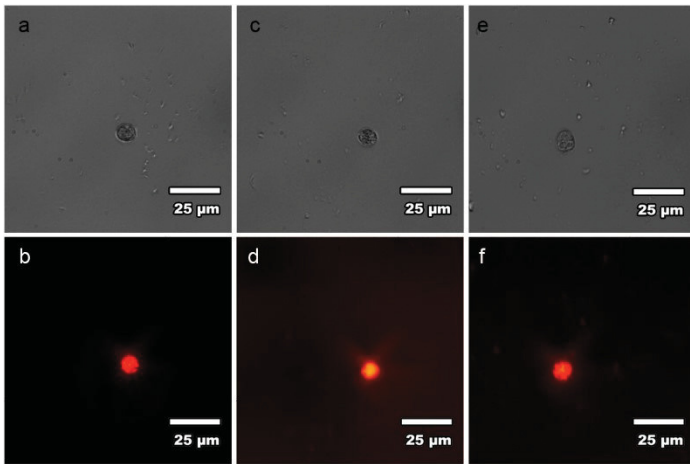
Fig S1
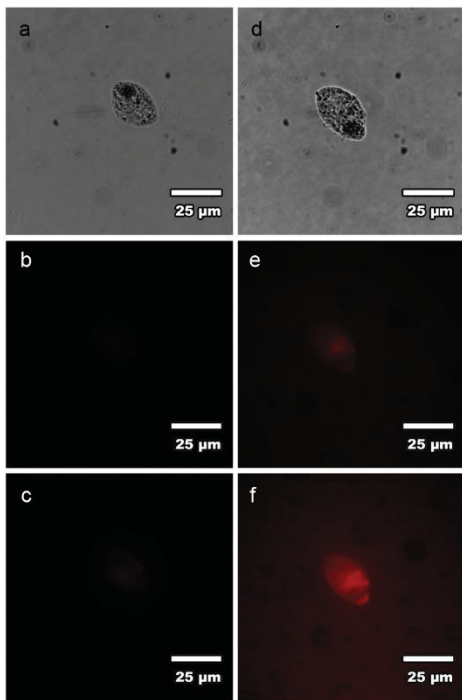
Fig S2

4.4   Manuscript D

A small azide-modified thiazole-based reporter molecule for fluorescence and mass spectrometric detection

Stefanie Wolfram, Hendryk Würfel, Stefanie H Habenicht, Christine Lembke, Phillipp Richter, Eckhard Birckner, Rainer Beckert, Georg Pohnert

BEILSTEIN JOURNAL OF ORGANIC CHEMISTRY

A small azide-modified thiazole-based reporter molecule for fluorescence and mass spectrometric detection

Stefanie Wolfram[1], Hendryk Würfel[2], Stefanie H. Habenicht[2], Christine Lembke[1], Phillipp Richter[1], Eckhard Birckner[3], Rainer Beckert[2] and Georg Pohnert[*1]

Full Research Paper

`Open Access`

Address:
[1]Institute for Inorganic and Analytical Chemistry, Friedrich Schiller University, Lessingstr. 8, 07743 Jena, Germany, [2]Institute of Organic Chemistry and Macromolecular Chemistry, Friedrich Schiller University, Humboldtstr. 10, 07743 Jena, Germany and [3]Institute for Physical Chemistry, Friedrich Schiller University, Helmholtzweg 4, 07743 Jena, Germany

Email:
Georg Pohnert[*] - Georg.Pohnert@uni-jena.de

* Corresponding author

Abstract

Molecular probes are widely used tools in chemical biology that allow tracing of bioactive metabolites and selective labeling of proteins and other biomacromolecules. A common structural motif for such probes consists of a reporter that can be attached by copper(I)-catalyzed 1,2,3-triazole formation between terminal alkynes and azides to a reactive headgroup. Here we introduce the synthesis and application of the new thiazole-based, azide-tagged reporter 4-(3-azidopropoxy)-5-(4-bromophenyl)-2-(pyridin-2-yl)thiazole for fluorescence, UV and mass spectrometry (MS) detection. This small fluorescent reporter bears a bromine functionalization facilitating the automated data mining of electrospray ionization MS runs by monitoring for its characteristic isotope signature. We demonstrate the universal utility of the reporter for the detection of an alkyne-modified small molecule by LC–MS and for the visualization of a model protein by in-gel fluorescence. The novel probe advantageously compares with commercially available azide-modified fluorophores and a brominated one. The ease of synthesis, small size, stability, and the universal detection possibilities make it an ideal reporter for activity-based protein profiling and functional metabolic profiling.

Introduction

Fluorescent dyes are widely used for detection and monitoring in the fields of chemistry, biochemistry, molecular biology, medicine and material sciences. Due to sensitive and selective detection methods and unproblematic toxicology they have almost completely replaced radioactive tags. Widely used repre-
sentatives include dansyl chloride, fluoresceins, rhodamines and boron-dipyrromethenes (BODIPYs) [1]. Dansyl chloride, with a maximum UV–vis absorption at 369 nm, is one of the first extrinsic fluorescent dyes introduced in this field and is still widely used in protein labeling [2]. Later, fluoresceins and

rhodamines found applications in this area as well because of advantageous UV–vis absorption maxima (480–600 nm) and more bathochromic emission wavelengths (510–615 nm) [3].

A successful class of fluorophores also used for probing in life science comprises the heterocyclic thiazoles. This structural element can be found in commercial products, such as thiazole orange, SYBR® Green I or TOTO®, which are, e.g., used for DNA labeling. In these compounds the thiazole ring is part of a benzothiazole. We set out to minimize the structural complexity of the fluorophores to achieve higher atom economy and reduce the interaction with biomacromolecules. In this context it was critical to realize that the thiazole moiety itself can also act as a fluorophore, especially the class of 4-hydroxythiazoles [4,5]. 4-Hydroxythiazoles are now becoming commercially available but are also easily accessible by synthesis with a broad range of substitution patterns. Substantial manipulations of the UV–vis excitation and emission wavelengths of these compounds are thus possible [6].

The design of molecular probes based on fluorophores requires the attachment of the fluorescent reporter to bio(macro)molecules or synthetic probes. Especially "click chemistry", introduced by Sharpless and coworkers in 2001 [7], is a widely used strategy to attach fluorophores covalently to other molecules. Among "click" reactions the Cu(I)-catalyzed azide–alkyne cycloaddition (CuAAC) is often considered as the prototypical transformation [7-9]. Due to the mild conditions and the use of aqueous solvents it is an efficient tool for bioorthogonal chemistry even inside of living systems [10]. One application of this concept for functional analysis of proteins is the activity-based protein profiling (ABPP) [11,12]. This proteomic strategy uses small probes designed to target active members of enzyme families [13]. These are often based on natural products to investigate their protein targets and eventually their mode of action [14,15]. ABPP probes contain two structural units: (1) a reactive group that reacts with the protein target and (2) a reporter unit for detection which could be, e.g., a fluorophore, a MS-tag, biotin or a combination of these [16,17]. For in vivo or in situ applications the alkyne (or azide) modified reactive group is usually applied to living organisms and after cell lysis the reporter is introduced by CuAAC [16]. Fluorophore tagged proteins can then be visualized by gel electrophoresis [17].

Besides fluorescence detection, mass spectrometry (MS) is also suited for the monitoring of tagged biological samples. Several probes have been designed for use with liquid chromatography–mass spectrometry (LC–MS). The probes attach covalently to target functional groups like amines, aldehydes/ketones, carboxylic acids and enhance their detection limit in LC–electrospray ionization (ESI) MS. This can be achieved by

introduction of charged species like ammonium or phosphonium for ionization in the positive mode [18-20]. Bromine [19,21,22] or chlorine [23] containing tags were also introduced as they generate a unique isotopic pattern and therefore enhance recognition and identification of labeled small molecules. These specific isotopic patterns also enable data processing by cluster analysis [19] or other algorithms for an automated structure mining [24,25].

Here we introduce the rational design, synthesis and application of a small thiazole-based, azide-tagged reporter molecule that supports universally, fluorescence, UV and MS detection. We thoroughly characterize its reactivity and utility with different detection methods and compare it with common commercially available fluorophores. As proof of principle protein and amino acid labeling with an alkyne containing reactive probe according to the ABPP concept is introduced using a new reporter molecule.

Results and Discussion
Design of the reporter
We aimed to combine high UV absorption and fluorescence with the possibility of unambiguous mass spectrometric detection (LC–ESIMS) in one reporter molecule. An azide functionality guarantees compatibility with widely applicable CuAAC approaches, that are, for instance, used in the field of ABPP where fluorescent reporter azides act as part of protein probes. To avoid the need for expensive detection systems for in-gel fluorescence we adjusted the excitation and emission wavelengths of the reporter to basic laboratory documentation equipment (365 nm UV-transilluminator, digital camera and a low cost commercial UV filter). Introduction of at least one atom with characteristic isotopic pattern like bromine or chlorine is necessary for a unique mass spectrometric detection of labeled substances. However, introduction of these heavy atom substituents in a fluorophore is challenging since it often results in decreased fluorescence due to intersystem crossing [26]. When working with reversed-phase LC–MS not only a specific isotopic pattern but also balanced polarity of the reporter is required. Addition of a nonpolar reporter shifts the retention time of polar analytes in reversed-phase chromatography to higher values. This is especially advantageous in the detection of small polar analytes [23,27]. On the other hand the polarity of the reporter needs to be high enough to work with biological samples in aqueous solution. Ideally a pH-independent fluorescence should guarantee for unbiased detection in tissues or under variable analytical conditions. In the light of our detailed knowledge of luminescence properties of pyridylthiazoles we considered this compound class to be ideally suited for the above mentioned tasks [28]. Based on previous considerations on the luminescent properties of pyridylthiazoles we decided to

synthesize 4-(3-azidopropoxy)-5-(4-bromophenyl)-2-(pyridin-2-yl)thiazole (BPT, **1**, Figure 1) as target molecule fulfilling the above mentioned requirements.
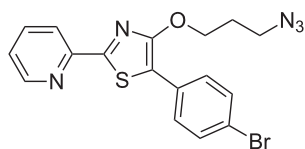
Figure 1: Structure of the reporter molecule BPT (**1**).

Synthesis

The synthesis of the azide-bearing fluorophore starts with a Hantzsch thiazole formation employing pyridine-2-carbothio-amide (**2**) and ethyl 2-bromo-2-(4-bromophenyl)acetate (**3**) (Scheme 1). The cyclization reaction leads, under basic catalysis in moderate yield (ca. 50%), to 5-(4-bromophenyl)-2-(pyridin-2-yl)thiazol-4-ol (**4**). This derivative of the 4-hydroxy-thiazole family was already synthesized by Beckert et al. in a study focusing on the fluorescence properties of 4-hydroxythia-zoles [29]. It exhibits an intense bathochromic shift of the UV–vis absorption when deprotonated at the 4-hydroxy position. The reactive 4-hydroxy position is alkylated employing 1-bromo-3-chloropropane in acetone, yielding the chloropropyl ether **5** in a good yield (85%). The chlorine in compound **5** is subsequently exchanged using an excess of sodium azide in DMF at 80 °C for several hours, leading to the organic azide **1** in good yield (83%).

The thioamide **2** bears an electron-withdrawing substituent in form of a 2-pyridyl moiety, which is important for an efficient fluorescence of the final product [6]. The α-bromoester **3** bears a bromine atom at the 4-position of the phenyl ring, which is introduced to facilitate MS detection.

For comparison, we also synthesized and tested a bromine modified dansyl derivative *N*-(3-azidopropyl)-6-bromo-5-(di-methylamino)naphthalene-1-sulfonamide (BNS, **6**, Figure 2). Dansyl chloride is brominated according to the literature [30] to produce 6-bromo-5-(dimethylamino)naphthalene-1-sulfonyl chloride (**7**) and subsequently treated with 3-azidopropan-1-amine to provide the fluorescence/MS tag **6**.
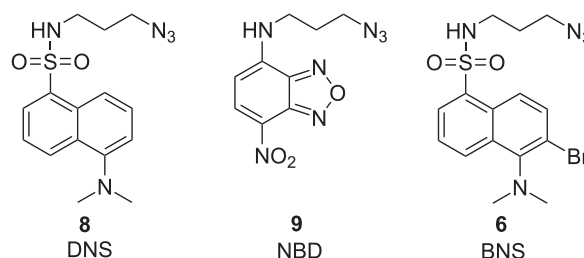
Figure 2: Structure of the tested azide-modified standard fluorophores DNS (**8**) and NBD (**9**) and the bromine modified DNS system **6**.

Characterization of BPT (**1**) and comparison with other azide modified fluorophores

We characterized the new thiazole reporter BPT (**1**) regarding its absorption and emission properties as well as its quantum
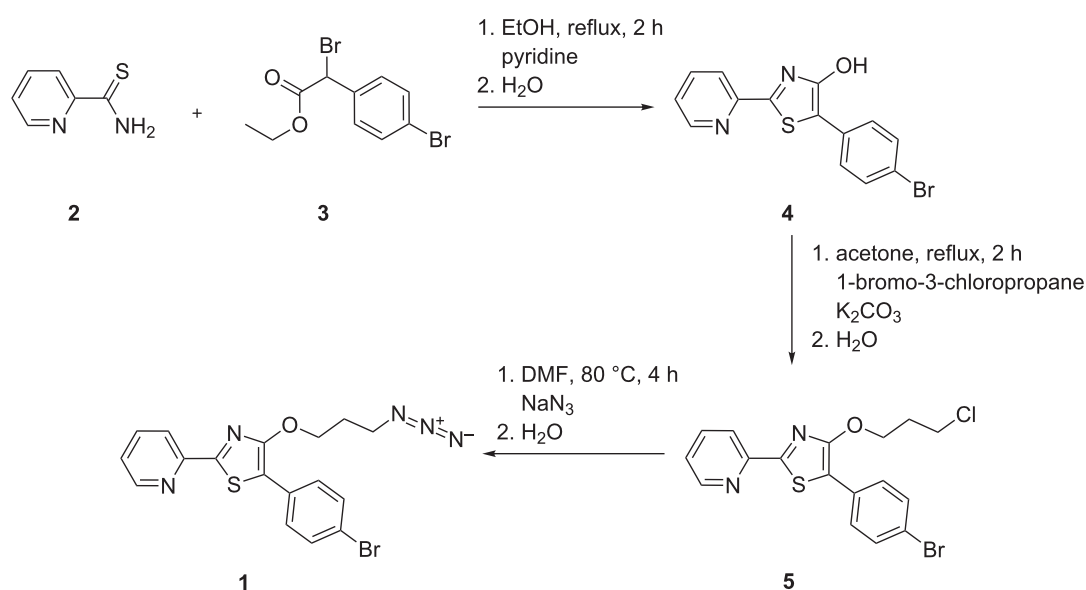
Scheme 1: Synthesis of the azide-bearing 4-hydroxythiazole derivative **1**.

yield and compared it with other commercially available fluorophores of similar size (Figure 2). We chose *N*-(3-azidopropyl)-5-(dimethylamino)naphthalene-1-sulfonamide (DNS, **8**) with a fluorophore system exhibiting a large stokes shift [1] suitable for fluorescence detection with UV filters. Derivatization with dansyl chloride is used for labeling of primary and secondary amines or phenols resulting in enhanced ESI signals and shifted retention times of labeled polar analytes in reversed-phase LC [27]. For comparison with BPT (**1**) we also introduced bromine into the aromatic system of DNS (**8**) to receive BNS (**6**). Furthermore, we utilized *N*-(3-azidopropyl)-7-nitrobenzo[*c*][1,2,5]oxadiazol-4-amine (NBD, **9**), a cheap fluorophore previously used for probes [1,31] or as fluorescent tag [32,33] (Figure 2).

UV–vis spectra of all substances were recorded in an aqueous solution containing 20% THF (v/v) (Figure 3) and their molar absorption coefficients ε at their absorption maxima ($\lambda_{abs,max}$) were calculated (Table 1). Notably, introduction of bromine into DNS (**8**) decreases the molar absorption coefficient more than twice and makes the resulting compound BNS (**6**) unsuitable for excitation with an UV transilluminator whereas BPT (**1**) offers a very good absorbance at 365 nm, a standard UV excitation wavelength.

We then recorded fluorescence spectra of all fluorophores and determined fluorescence quantum yields Φ (Table 1). To characterize BPT (**1**) in a non-interacting solvent we used cyclohexane resulting in an emission maximum of 444 nm and a quantum yield of Φ = 0.96. In an aqueous solution containing 20% THF (v/v) the maximum of emission ($\lambda_{em,max}$) is shifted to 455 nm (Figure 4). The quantum yield of BPT (**1**) in this solution is Φ = 0.87 which makes it convenient for fluorescence detection in aqueous media, e.g., for biological applications. In contrast, the quantum yield of BNS (**6**) in 80% water/20% THF (v/v) was below 0.03 and rendering it inappropriate for this purpose.
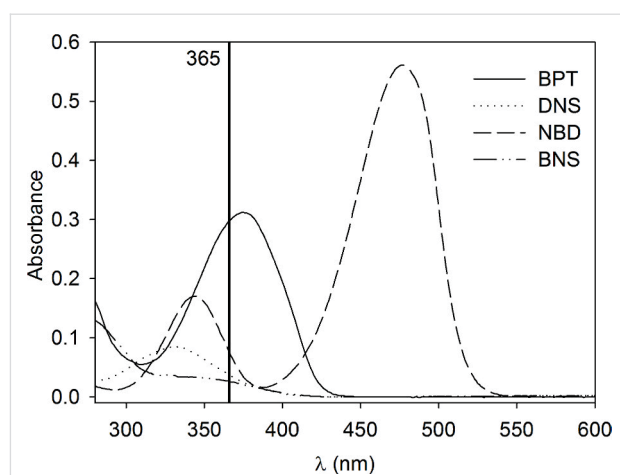
Figure 3: UV–vis spectra of 20 μM solutions of the azide modified fluorophores BPT (**1**), DNS (**8**), NBD (**9**) and BNS (**6**) in THF/water (20:80; v/v).
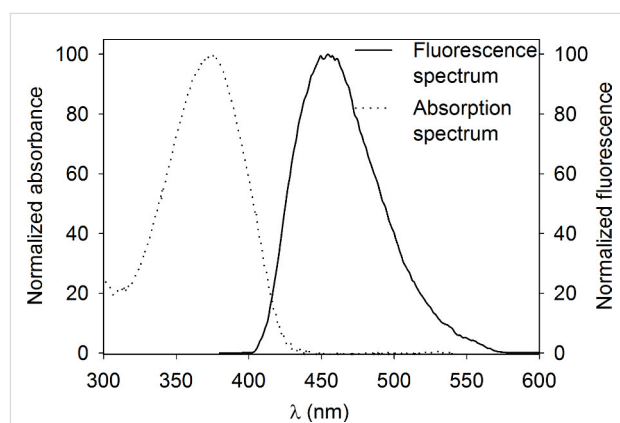
Figure 4: Normalized absorbance and fluorescence of BPT (**1**) in 20% THF/80% water (v/v), excitation at 374 nm.

The UV properties allow UV detection after LC separation as could be shown by ultra-performance liquid chromatography (UPLC) coupled to a photodiode array detector using the

Table 1: Spectral properties of BPT (**1**), DNS (**8**), NBD (**9**) and BNS (**6**) in THF/water (20:80; v/v).

	BPT (**1**)	DNS (**8**)	NBD (**9**)	BNS (**6**)
$\lambda_{abs,max}$ [nm]	374 (376[a])	331	344/477	327
ε [L/(mol cm)]	15.5×10^3	4.3×10^3	8.5×10^3 [b]$/28.1 \times 10^3$	1.9×10^3
$\lambda_{em,max}$ [nm]	455 (444[a])	546	545	550
Φ[c]	0.87 (0.96[a])	n.d.	0.51[d]	<0.03
Lit. ε [L/(mol cm)]		4.2×10^3 [e,f]	22.1×10^3 [d]	
Lit. $\lambda_{em,max}$ [nm]		506 nm[e,g], 520 nm[e,f]	524 nm[d]	

[a]In cyclohexane; [b]at 344 nm (which is a local maximum of NBD), since we excite fluorescently labeled biomolecules in gels with a 365 nm UV transilluminator this region is of crucial importance; [c]quantum yield, [d]in ethanol [45]; [e]solvent not specified; [f]from [46]; [g]from [47]; n.d. - not determined; Lit. - values found in literature.

solvents A (water/acetonitrile/formic acid 98:2:0.1; v/v/v) and B (acetonitrile/0.1% formic acid; v/v). The peaks of equimolar amounts were integrated at their absorption maxima resulting in the highest integrated peak area for NBD (**9**) followed by BPT (**1**) (Figure 5A). BPT is the least polar substance among the tested fluorophores and elutes at 90% B (Table 2). Polar analytes are often poorly retained in reversed-phase chromatography [23]. Thus, after CuAAC BPT (**1**) will shift retention times of polar analytes to higher values as it is achieved with other labeling reagents like dansyl chloride [27] or *p*-chlorophenylalanine containing tags [23]. Nevertheless, BPT (**1**) shows sufficient water solubility when working in aqueous solutions with low amounts of organic co-solvent. For instance during implementation of CuAAC we use 3.5% DMSO and 4.5% *t*-BuOH in our protocol which ensures solubility of BPT (**1**).

Table 2: Solvent composition at time of elution of BPT (**1**), DNS (**8**), NBD (**9**) and BNS (**6**) measured with C18-UPLC–ESIMS using a linear gradient of solvents A (water/acetonitrile/formic acid 98:2:0.1; v/v/v) and B (acetonitrile/0.1% formic acid; v/v) and solvent composition and masses of imines **11**–**14** formed in a model reaction between L-lysine and DDY (**10**) followed by CuAAC with the different reporter molecules.

reporter	comp. B (%)	imine	comp. B (%)	*m/z*[a]
BPT (**1**)	90	**11**	33	691.19
DNS (**8**)	58	**12**	20	609.31
NBD (**9**)	49	**13**	24	539.26
BNS (**6**)	74	**14**	31	687.22

[a]Calculated monoisotopic masses; comp. - solvent composition.

UPLC–ESIMS measurements were employed to characterize ionization properties of the fluorophores (Figure 5B). In posi-

tive mode BPT (**1**) gives a slightly higher peak area than DNS (**8**). Derivatization with dansyl chloride has been previously introduced as an ionization enhancing procedure for LC–ESIMS. Thereby increased linear responses of tested amino acids by over two orders of magnitude compared to underivatized samples were observed [27]. Interestingly, the novel BPT (**1**) is even superior to the established DNS (**8**) but introduced the additional benefit of a characteristic isotope pattern. Ionization of the brominated dansyl system BNS (**6**) resulted in a clearly lower intensity response. In negative mode ionization of BPT (**1**) is not adequate (data not shown).

Taken together in the comparison of all four fluorophores BPT (**1**) has superior properties for detection if fluorescence, UV absorption and MS properties are concerned.

Visualization of small molecules by mass spectrometric detection

To demonstrate the universal application possibilities, we next coupled reporter molecules with a synthetic reactive group as commonly used in ABPP approaches. The alkyne-modified (2*E*,4*E*)-deca-2,4-dien-9-ynal (DDY, **10**) served as reactive group. DDY (**10**) mimics the natural product 2,4-decadienal that is produced by some diatoms as potential chemical defense metabolite against their grazers [34]. Structure-activity tests have revealed that 2,4-decadienal can be modified in the alkyl terminus without loss of function [35]. Thus the alkyne modified α,β,γ,δ-unsaturated aldehyde **10** can serve as a tool for the elucidation of the mode of action of the compound class of polyunsaturated aldehydes. DDY (**10**) was initially transformed with L-lysine to form an imine before CuAAC was performed with the four azides BPT (**1**), DNS (**8**), NBD (**9**) and BNS (**6**). After one hour of incubation with lysine the respective reporter, the ligand 1-(1-benzyltriazol-4-yl)-*N*,*N*-bis[(1-benzyltriazol-4-
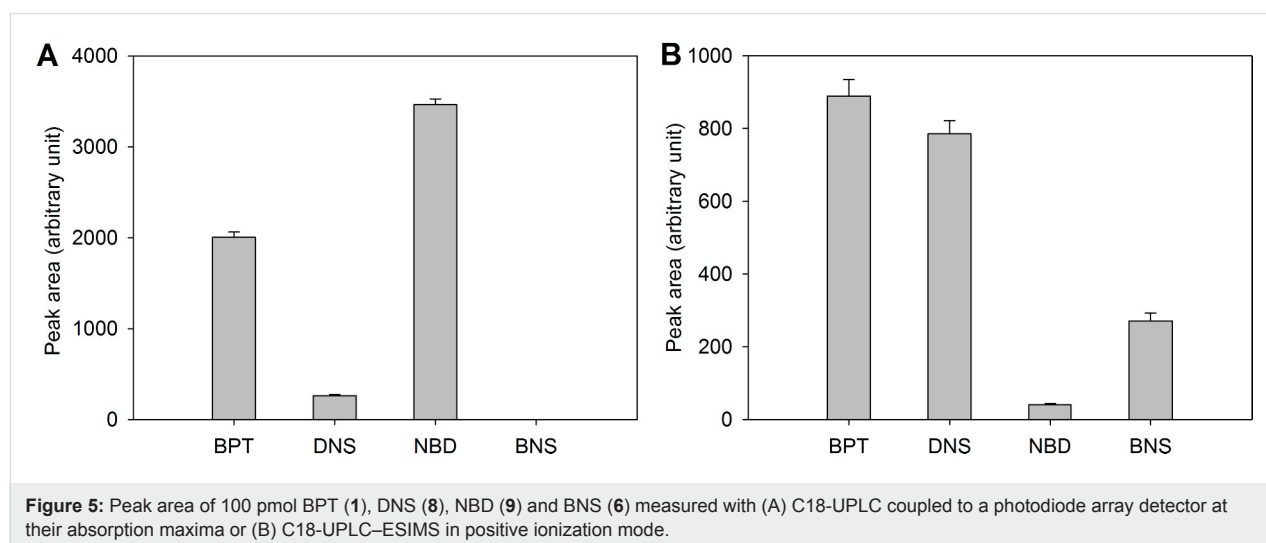
Figure 5: Peak area of 100 pmol BPT (**1**), DNS (**8**), NBD (**9**) and BNS (**6**) measured with (A) C18-UPLC coupled to a photodiode array detector at their absorption maxima or (B) C18-UPLC–ESIMS in positive ionization mode.

yl)methyl]methanamine (TBTA), sodium ascorbate and a copper sulfate solution were added and incubated for another hour (Figure 6). All four reactions were performed with identical molar amounts of the reagents. After centrifugation products were characterized with LC–ESIMS in positive mode (Table 2, Figure 7).

Mass spectra in Figure 7 show clearly that most intensive signals can be obtained with the novel reporter BPT (**1**). BPT (**1**) is thus transformed efficiently in the CuAAC reaction and the products such as **11** can be detected with high sensitivity using LC–MS.

Besides the coupling product of BPT (**11**) only the low fluorescent **14** shows unique isotopic patterns caused by the two isotopes ^{79}Br and ^{81}Br. This enables identification of tagged analytes even in complex samples. Introduction of bromine substituents does not only affect the isotopic pattern of analytes but also increases ionization and the detection limit of small metabolites [36] and peptides [37]. In addition, introduction of Br or Cl by labeling allows the application of cluster analysis [19] or other software [38] as computational tools to identify probe-reactive analytes out of complex mixtures even of unknown mass.

Visualization of proteins by in-gel fluorescence detection

In a model reaction we tested the suitability of BPT (**1**) and the other reporters for in-gel fluorescence detection of labeled proteins. Since DDY is universally reactive against proteins, we chose arbitrary a catalase from bovine liver as target protein that was reacted with DDY (**10**).

After addition and incubation of DDY (**10**) with the catalase, we applied CuAAC with the four fluorophores. The products were then separated by sodium dodecyl sulfate polyacrylamide gel electrophoresis (SDS-PAGE) and visualized by in-gel fluorescence detection (Figure 8). BPT/DDY gives the brightest signal whereas intensities of DNS/DDY and BNS/DDY-labeled catalase are clearly lower. The lowest signal was emitted by NBD/DDY/catalase, which is probably due to very low fluorescence quantum yields reported for NBD derivatives of primary amines in water [39]. Furthermore, NBD (**9**) is not suitable for standard SDS-PAGE (12% gels) as the dye smears and therefore potentially covers fluorescent signals of proteins of lower masses.

The novel probe has further implications since a combination of fluorescence and mass tagging might prove beneficial in proteomics studies. Mass tags containing bromine [24,37,40,41] and chlorine [24,38] have been reported in proteomics related applications. Additionally, bromine containing tags called isotope-differentiated binding energy shift tags (IDBEST™) were designed to introduce a mass-defect in peptides for better sequence coverage of proteins [25,42]. The reporter molecule BPT (**1**) contains bromine and tagged proteins can thus easily be identified with both, fluorescent and MS techniques.

Conclusion

We introduce the azide-modified thiazole-based reporter molecule BPT (**1**) with superior properties for fluorescence, UV and MS detection compared to other common reporters. BPT (**1**) can be easily synthesized and attached to terminal alkyne-modified molecules via CuAAC. We show model experiments that demonstrate the suitability of the molecule in labeling small
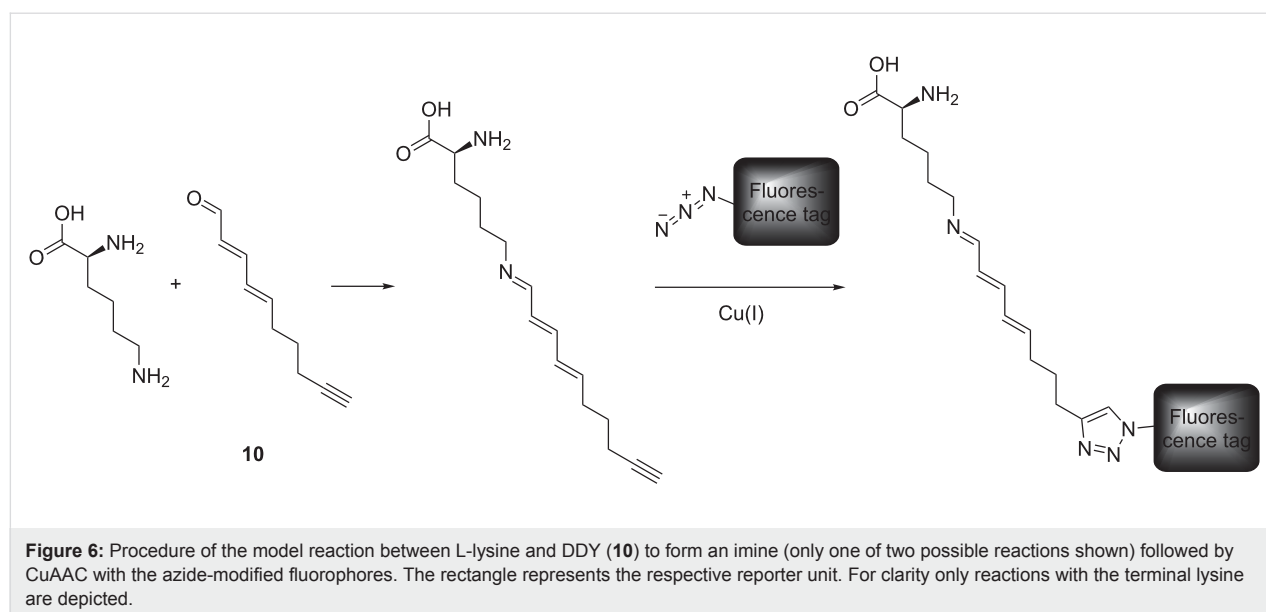
Figure 6: Procedure of the model reaction between L-lysine and DDY (**10**) to form an imine (only one of two possible reactions shown) followed by CuAAC with the azide-modified fluorophores. The rectangle represents the respective reporter unit. For clarity only reactions with the terminal lysine are depicted.

Figure 7: Mass spectra of labeled L-lysine/DDY (**10**)/fluorophore conjugates **11** (containing BPT), **12** (containing DNS), **13** (containing NBD) and **14** (containing BNS) measured in ESI positive mode (S/N: signal to noise ratio after reaction of equal molar amounts of reagents).
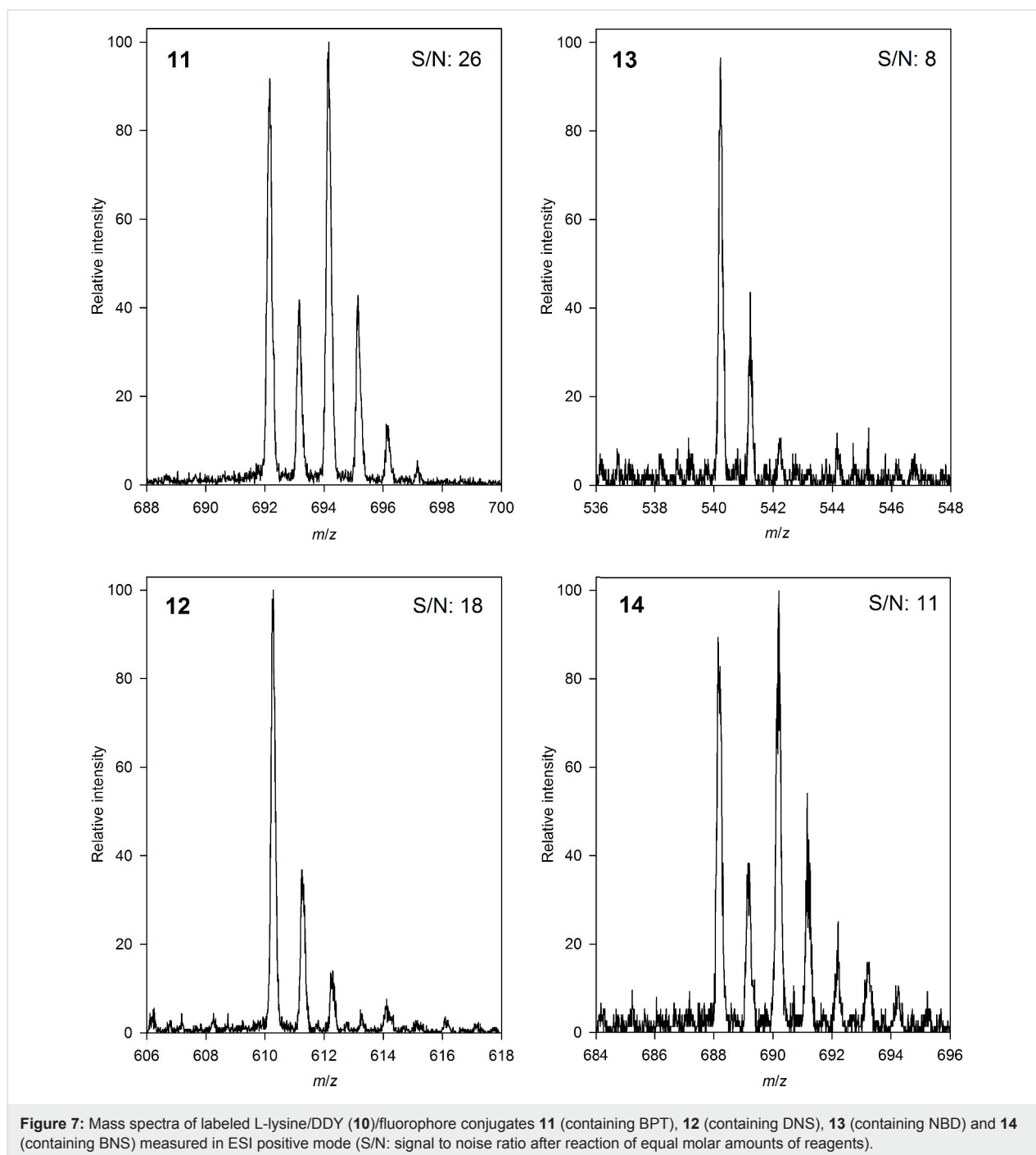
molecules and in ABPP investigations. Fluorescence and MS offer orthogonal opportunities for detection and make this reporter a universal tool for targeting molecules of different sizes and properties.

Experimental
Synthesis
Experimental details are available in Supporting Information File 1.

Sample preparation and measurements
UV–vis and fluorescence spectroscopy
Solutions of each fluorophore in THF/water (20 µM, 20:80; v/v) were prepared out of 5 mM stock solutions in DMSO. UV–vis spectra were recorded with a GENESYS™ 10 S spectrophotometer (Thermo Fischer Scientific Inc., Waltham, MA, USA) with 10 mm quartz cells. Quantum yields were obtained as described in [43] using quinine sulfate in 0.05 M sulfuric acid as fluorescent standard with a Varian Cary 500 spectropho-

Figure 8: Fluorescent labeling of catalase treated with DDY (**10**) followed by CuAAC with all four reporter molecules and in-gel fluorescence detection at 365 nm. Equivalent amounts of protein were labeled and loaded on the gel. (Protein ladder masses in kDa).
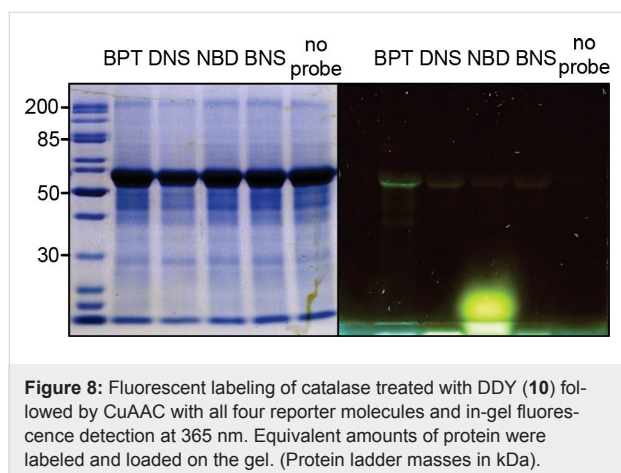
tometer (Varian Inc., Palo Alto, CA, USA) in combination with a Luminescence Spectrophotometer LS 50 (Perkin Elmer, Waltham, MA, USA). For DNS (**8**) and NBD (**9**) emission maxima were obtained with a FP-6500 (Jasco, Tokyo, Japan) spectrofluorimeter.

LC–ESIMS and UV–vis detection

For LC–MS measurements we used an Acquity™ Ultraperformance LC (Waters, Milford, MA, USA) coupled to a Waters 996 PDA detector and a Q-Tof microMS (Waters Micromass, Manchester, England). A Kinetex C18 reversed-phase column (2.1 mm × 50 mm, 1.7 µm particle size, Phenomenex, Torrance, CA, USA) was used. For UV detection and ionization in positive and negative mode 10 µL of 10 µM solutions of each fluorophore in water containing 5% DMSO were injected. For model reactions between DDY (**10**) and lysine followed by CuAAC, 5 µL were injected.

Incubation with DDY (**10**) and CuAAC

For L-lysine: L-Lysine (30 µL 1 mM, prepared from a 50 mM stock in water) were added to 1.47 mL methanol followed by 4 µL (0.13 mM) of DDY (**10**) (prepared from a 50 mM stock in DMSO) and mixed on a vortex mixer. 132 µL of this solution were transferred to a 1.5 mL Eppendorf tube (Eppendorf AG, Hamburg, Germany) and the following substances were added (procedure adapted from [16]): 3 µL (0.1 mM) of BPT (**1**) or the other reporter molecules (5 mM stock in DMSO), 9 µL (0.1 mM) TBTA solution (1.7 mM stock in DMSO/*tert*-butanol, 1:4, v/v) and 3 µL (20 mM) freshly prepared ascorbic acid solution (1.00 M in water). Samples were vortexed and 1 µL (1 mM) copper(II) sulfate solution (from a 50 mM stock solution in water) was added. Samples were vortexed again, centrifuged after one hour and measured by UPLC–MS.

For catalase from bovine liver: Catalase from bovine liver (2.5 mg) was dissolved in 1 mL phosphate buffer (59.0 mM

Na_2HPO_4, 7.6 mM KH_2PO_4, pH 7.6) and 2 µL (0.01 mM) of DDY (**10,** 5 mM stock in DMSO) were added. The sample was incubated for one hour. 44 µL of this solution were transferred to an Eppendorf tube and the following substances were added (procedure adapted from [16]): 1 µL (0.1 mM) of BPT (**1**) or the other reporter molecules (5 mM stock in DMSO), 3 µL (0.1 mM) TBTA solution (1.7 mM stock in DMSO/*tert*-butanol, 1:4, v/v) and 1 µL (20 mM) of a freshly prepared ascorbic acid solution (1.00 M in water). Samples were vortexed and 1 µL (1 mM) copper(II) sulfate solution (50 mM in water) was added. Samples were vortexed again and stored on ice for 1 hour.

SDS-PAGE and in-gel fluorescence detection

Aliquots (10 µL) of each pre-incubated catalase (9 µL of untreated catalase and 1 µL of deionized water) were mixed with 10 µL of 2× loading buffer [44] and heated to 95 °C for 6 min. A protein ladder (PageRuler unstained protein ladder, Thermo Scientific) and 15 µL of each sample were loaded on a 12% SDS mini gel and separated in a Mini-Protean® Tetra gel cell (Bio-Rad, Herculas, CA, USA) by applying 80 V for 30 min followed by 180 V for 65 min. A fluorescent picture was taken at 365 nm irradiation using a UV transilluminator (Bio-Rad, UV star), a PowerShot A640 camera (Canon, Tokyo, Japan) and a commercially available UV filter (HMC Hoya Multi-Coated Filter, Hoya, Tokyo, Japan). The gel was stained with RAPIDstain™ (G-Biosciences, St. Louis, MO, USA).

Supporting Information

Supporting Information File 1

Synthetic procedures and characterization data of synthetic compounds.
[http://www.beilstein-journals.org/bjoc/content/supplementary/1860-5397-10-258-S1.pdf]

Acknowledgements

References

1. Sadaghiani, A. M.; Verhelst, S. H. L.; Bogyo, M.
Curr. Opin. Chem. Biol. **2007,** *11,* 20–28.
doi:10.1016/j.cbpa.2006.11.030

2. Weber, G. *Biochem. J.* **1952,** *51,* 155–167.

3. Lakowicz, J. R. *Principles of fluorescence spectroscopy,* 3rd ed.; Springer: New York, USA, 2006.

4. Calderón-Ortiz, L. K.; Täuscher, E.; Leite Bastos, E.; Görls, H.; Weiß, D.; Beckert, R. *Eur. J. Org. Chem.* **2012,** 2535–2541. doi:10.1002/ejoc.201200140

5. Täuscher, E.; Calderón-Ortiz, L.; Weiß, D.; Beckert, R.; Görls, H. *Synthesis* **2011,** 2334–2339. doi:10.1055/s-0030-1260670

6. Täuscher, E. Beiträge zur Chemie der 4-Hydroxy-1,3-Thiazole. Ph.D. Thesis, University of Jena, Jena, Germany, 2012.

7. Kolb, H. C.; Finn, M. G.; Sharpless, K. B. *Angew. Chem., Int. Ed.* **2001,** *40,* 2004–2021. doi:10.1002/1521-3773(20010601)40:11<2004::AID-ANIE2004>3.0.CO ;2-5

8. Lutz, J.-F.; Zarafshani, Z. *Adv. Drug Delivery Rev.* **2008,** *60,* 958–970. doi:10.1016/j.addr.2008.02.004

9. Le Droumaguet, C.; Wang, C.; Wang, Q. *Chem. Soc. Rev.* **2010,** *39,* 1233–1239. doi:10.1039/b901975h

10. Lim, R. K. V.; Lin, Q. *Sci. China: Chem.* **2010,** *53,* 61–70. doi:10.1007/s11426-010-0020-4

11. Speers, A. E.; Adam, G. C.; Cravatt, B. F. *J. Am. Chem. Soc.* **2003,** *125,* 4686–4687. doi:10.1021/ja034490h

12. Uttamchandani, M.; Li, J.; Sun, H.; Yao, S. Q. *ChemBioChem* **2008,** *9,* 667–675. doi:10.1002/cbic.200700755

13. Evans, M. J.; Cravatt, B. F. *Chem. Rev.* **2006,** *106,* 3279–3301. doi:10.1021/cr050288g

14. Gersch, M.; Kreuzer, J.; Sieber, S. A. *Nat. Prod. Rep.* **2012,** *29,* 659–682. doi:10.1039/c2np20012k

15. Böttcher, T.; Pitscheider, M.; Sieber, S. A. *Angew. Chem., Int. Ed.* **2010,** *49,* 2680–2698. doi:10.1002/anie.200905352

16. Speers, A. E.; Cravatt, B. F. *Chem. Biol.* **2004,** *11,* 535–546. doi:10.1016/j.chembiol.2004.03.012

17. Sieber, S. A.; Cravatt, B. F. *Chem. Commun.* **2006,** 2311–2319. doi:10.1039/b600653c

18. Suzuki, Y.; Tanji, N.; Ikeda, C.; Honda, A.; Ookubo, K.; Citterio, D.; Suzuki, K. *Anal. Sci.* **2004,** *20,* 475–482. doi:10.2116/analsci.20.475

19. Barry, S. J.; Carr, R. M.; Lane, S. J.; Leavens, W. J.; Monté, S.; Waterhouse, I. *Rapid Commun. Mass Spectrom.* **2003,** *17,* 603–620. doi:10.1002/rcm.957

20. Barry, S. J.; Carr, R. M.; Lane, S. J.; Leavens, W. J.; Manning, C. O.; Monté, S.; Waterhouse, I. *Rapid Commun. Mass Spectrom.* **2003,** *17,* 484–497. doi:10.1002/rcm.933

21. Li, M.; Kinzer, J. A. *Rapid Commun. Mass Spectrom.* **2003,** *17,* 1462–1466. doi:10.1002/rcm.1064

22. Paulick, M. G.; Hart, K. M.; Brinner, K. M.; Tjandra, M.; Charych, D. H.; Zuckermann, R. N. *J. Comb. Chem.* **2006,** *8,* 417–426. doi:10.1021/cc0501460

23. Carlson, E. E.; Cravatt, B. F. *J. Am. Chem. Soc.* **2007,** *129,* 15780–15782. doi:10.1021/ja0779506

24. Palaniappan, K. K.; Pitcher, A. A.; Smart, B. P.; Spiciarich, D. R.; Iavarone, A. T.; Bertozzi, C. R. *ACS Chem. Biol.* **2011,** *6,* 829–836. doi:10.1021/cb100338x

25. Hall, M. P.; Ashrafi, S.; Obegi, I.; Petesch, R.; Peterson, J. N.; Schneider, L. V. *J. Mass Spectrom.* **2003,** *38,* 809–816. doi:10.1002/jms.493

26. Valeur, B. *Molecular Fluorescence: Principles and Applications;* Wiley-VCH: Weinheim, 2001. doi:10.1002/3527600248

27. Guo, K.; Li, L. *Anal. Chem.* **2009,** *81,* 3919–3932. doi:10.1021/ac900166a

28. Grummt, U.-W.; Weiss, D.; Birckner, E.; Beckert, R. *J. Phys. Chem. A* **2007,** *111,* 1104–1110. doi:10.1021/jp0672003

29. Täuscher, E.; Weiß, D.; Beckert, R.; Görls, H. *Synthesis* **2010,** 1603–1608. doi:10.1055/s-0029-1219759

30. Kinsey, B. M.; Kassis, A. I. *Nucl. Med. Biol.* **1993,** *20,* 13–22. doi:10.1016/0969-8051(93)90132-E

31. Schmidinger, H.; Birner-Gruenberger, R.; Riesenhuber, G.; Saf, R.; Susani-Etzerodt, H.; Hermetter, A. *ChemBioChem* **2005,** *6,* 1776–1781. doi:10.1002/cbic.200500013

32. Bostic, H. E.; Smith, M. D.; Poloukhtine, A. A.; Popik, V. V.; Best, M. D. *Chem. Commun.* **2012,** *48,* 1431–1433. doi:10.1039/c1cc14415d

33. Novotný, J.; Pospěchová, K.; Hrabálek, A.; Čáp, R.; Vávrová, K. *Bioorg. Med. Chem. Lett.* **2009,** *19,* 6975–6977. doi:10.1016/j.bmcl.2009.10.047

34. Pohnert, G. *ChemBioChem* **2005,** *6,* 946–959. doi:10.1002/cbic.200400348

35. Adolph, S.; Poulet, S. A.; Pohnert, G. *Tetrahedron* **2003,** *59,* 3003–3008. doi:10.1016/S0040-4020(03)00382-X

36. LeBlanc, A.; Shiao, T. C.; Roy, R.; Sleno, L. *Rapid Commun. Mass Spectrom.* **2010,** *24,* 1241–1250. doi:10.1002/rcm.4507

37. Hernandez, H.; Niehauser, S.; Boltz, S. A.; Gawandi, V.; Phillips, R. S.; Amster, I. J. *Anal. Chem.* **2006,** *78,* 3417–3423. doi:10.1021/ac0600407

38. Goodlett, D. R.; Bruce, J. E.; Anderson, G. A.; Rist, B.; Pasa-Tolic, L.; Fiehn, O.; Smith, R. D.; Aebersold, R. *Anal. Chem.* **2000,** *72,* 1112–1118. doi:10.1021/ac9913210

39. Al-Dirbashi, O.; Kuroda, N.; Nakashima, K. *Anal. Chim. Acta* **1998,** *365,* 169–176. doi:10.1016/S0003-2670(97)00675-2

40. Miyagi, M.; Nakao, M.; Nakazawa, T.; Kato, I.; Tsunasawa, S. *Rapid Commun. Mass Spectrom.* **1998,** *12,* 603–608. doi:10.1002/(SICI)1097-0231(19980529)12:10<603::AID-RCM204>3.0. CO;2-0

41. Yang, Y.-Y.; Grammel, M.; Raghavan, A. S.; Charron, G.; Hang, H. C. *Chem. Biol.* **2010,** *17,* 1212–1222. doi:10.1016/j.chembiol.2010.09.012

42. Hall, M. P.; Schneider, L. V. *Expert Rev. Proteomics* **2004,** *1,* 421–431. doi:10.1586/14789450.1.4.421

43. Crosby, G. A.; Demas, J. N. *J. Phys. Chem.* **1971,** *75,* 991–1024. doi:10.1021/j100678a001

44. Laemmli, U. K. *Nature* **1970,** *227,* 680–685. doi:10.1038/227680a0

45. Key, J. A.; Cairo, C. W. *Dyes Pigm.* **2011,** *88,* 95–102. doi:10.1016/j.dyepig.2010.05.007

46. Data sheet: Dansyl azide, Dec 02, 2010, Jena, Germany. http://www.jenabioscience.com/images/c45d35de70/CLK-FA016.pdf (accessed Jan 19, 2014).

47. Deiters, A.; Cropp, T. A.; Mukherji, M.; Chin, J. W.; Anderson, J. C.; Schultz, P. G. *J. Am. Chem. Soc.* **2003,** *125,* 11782–11783. doi:10.1021/ja0370037

License and Terms

Supporting Information

for

A small azide-modified thiazole-based reporter molecule for fluorescence and mass spectrometric detection

Stefanie Wolfram[1], Hendryk Würfel[2], Stefanie H. Habenicht[2], Christine Lembke[1], Phillipp Richter[1], Eckhard Birckner[3], Rainer Beckert[2] and Georg Pohnert*[1]

Address: [1]Institute for Inorganic and Analytical Chemistry, Friedrich Schiller University, Lessingstr. 8, 07743 Jena, Germany and [2]Institute of Organic Chemistry and Macromolecular Chemistry, Friedrich Schiller University, Humboldtstr. 10, 07743 Jena, Germany and [3]Institute for Physical Chemistry, Friedrich Schiller University, Helmholtzweg 4, 07743 Jena, Germany

Email: Georg Pohnert* - Georg.Pohnert@uni-jena.de

* Corresponding author

Synthetic procedures and characterization data

of synthetic compounds

Synthetic procedures

General methods

All chemicals were purchased as reagent grade or better and used without further purification. If necessary reactions were performed under argon. Commercially available dry solvents were employed. Diethyl ether and tetrahydrofuran (THF) contained butylhydroxytoluene as peroxidation inhibitor. Column chromatography was carried out on Merck silica gel (0.04–0.063 mesh). TLC was performed with TLC silica gel 60 F_{254} plates from Merck. TLC spots were visualized by irradiation of the TLC plate with UV radiation (254 nm) or by dipping in Seebach reagent (2.5 g phosphomolybdic acid and 1 g cer(IV) sulfate dissolved in 65 mL water and slowly acidified by dropwise addition of 6 ml concentrated sulfuric acid).

5-(4-Bromophenyl)-2-(pyridin-2-yl)thiazol-4-ol (4)
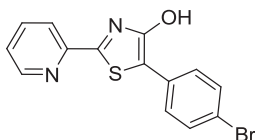
Starting from pyridine-2-carbothioamide (**2**) and ethyl 2-bromo-2-(4-bromophenyl) acetate (**3**) the compound was synthesized according to literature [1].

^{1}H NMR (400 MHz, DMSO-d_6): δ (ppm) 11.64 (s, 1H, OH), 8.62 (d, 1H, ArH), 8.03-7.90 (m, 2H, ArH), 7.72 (d, 2H, ^3J = 8.6 Hz, ArH), 7.58 (d, 2H, ^3J = 8.6 Hz, ArH), 7.50-7.45 (m, 1H, ArH).

^{13}C NMR (100 MHz, DMSO-d_6): δ (ppm) 160.7, 158.9, 149.8, 149.5, 137.4, 131.4, 131.0, 127.7, 124.7, 118.8, 118.2, 109.0.

MS (EI): *m/z* 333.9 [42%] M+2, 331.9 [42%] M, 263.9 [29%], 218.9 [100%], 200.7 [58%].

HRMS: *m/z* calculated: 331.9619, found: 331.9617.

5-(4-Bromophenyl)-4-(3-chloropropoxy)-2-(pyridine-2-yl)thiazole (5)
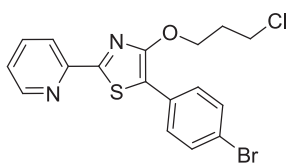
In a 100 mL Erlenmeyer flask 0.81 g (2.4 mmol) **4**, 0.5 g (3.6 mmol) K_2CO_3 and 0.3 mL (3.0 mmol) 1-bromo-3-chloropropane were stirred in 20 mL DMF at r.t. for 6 h. The mixture was poured in 200 mL of water and extracted with $CHCl_3$ (3 x 50 mL). The extracts were combined, washed with saturated K_2CO_3 solution and water, dried over $MgSO_4$ and evaporated in vacuum to obtain a bright yellow solid. The compound was recrystallized from heptane/$CHCl_3$ to obtain light yellow crystals in 85% yield.

^{1}H NMR (250 MHz, $CDCl_3$): δ (ppm) 8.59 (d, 1H, ^4J = 4.6 Hz, ArH), 8.11 (d, 1H, ^3J = 7.9 Hz, ArH), 7.73-7.85 (m, 1H, ArH), 7.62 (d, 2H, ^3J = 8.6 Hz, ArH), 7.50 (d, 2H, ^3J = 8.6 Hz, ArH), 7.25-7.35 (m, 1H, ArH), 4.68 (t, 2H, ^3J = 6.0 Hz, CH_2), 3.75 (t, 2H, ^3J = 6.4 Hz, CH_2), 2.32 (quin, 2H, ^3J = 6.1 Hz, CH_2).

^{13}C NMR (63 MHz, $CDCl_3$): δ (ppm) 160.9, 159.0, 150.9, 149.4, 137.0, 131.8, 130.6, 128.3, 124.4, 120.5, 119.1, 113.6, 67.1, 41.6, 32.5.

MS (EI): m/z 409.9 [40%] M+2, 407.9 [28%] M, 333.9 [16%], 331.9 [16%], 263.9 [30%], 218.9 [100%].

HRMS: m/z calculated: 407.9699, found: 407.9698.

4-(3-Azidopropoxy)-5-(4-bromophenyl)-2-(pyridine-2-yl)thiazole (BPT, 1)
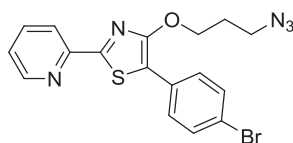
In a 100 mL round bottom flask 0.84 g (2.1 mmol) **5**, 0.27 g (4.1 mmol) NaN$_3$ and 20 mL dimethyl formamide were stirred for 4 h at 80 °C. The cooled mixture was poured into 100 mL of water and extracted with CH$_2$Cl$_2$ (3 x 50 mL). The combined extracts were washed with water (100 mL) and dried over MgSO$_4$. The solvent was removed in vacuum and the product, bright yellow crystals, was dried with a vacuum pump for several hours (83% yield).

^{1}H NMR (250 MHz, CDCl$_3$): δ (ppm) 8.59 (d, 1H, ^4J = 4.6 Hz, ArH), 8.10 (d, 1H, ^3J = 7.9 Hz, ArH), 7.73-7.85 (m, 1H, ArH), 7.63 (d, 2H, ^3J = 8.6 Hz, ArH), 7.50 (d, 2H, ^3J = 8.6 Hz, ArH), 7.27-7.36 (m, 1H, ArH), 4.62 (t, 2H, ^3J = 6.1 Hz, CH$_2$), 3.53 (t, 2H, ^3J = 6.7 Hz, CH$_2$), 2.14 (quin, 2H, ^3J = 6.3 Hz, CH$_2$).

^{13}C NMR (63 MHz, CDCl$_3$): δ (ppm) 160.9, 158.9, 150.9, 149.4, 137.0, 131.8, 130.6, 128.3, 124.4, 120.5, 119.1, 113.6, 67.3, 48.4, 29.0.

MS (EI): m/z 417.0 [28%] M+2, 415.0 [28%] M, 333.9 [50%], 331.9 [50%], 200.7 [100%].

HRMS m/z calculated: 415.0103, found: 415.0096.

LC/MS (ESI, positive mode) m/z 416.0 [M+H]$^+$.

N-(3-Bromopropyl)-7-nitrobenzo[c][1,2,5]oxadiazol-4-amine
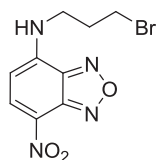
The substance was synthesized according to Key and Cairo [2].

^{1}H NMR (400 MHz, D$_3$COD): δ (ppm) 8.43 (d, 1H, ^3J = 8.8 Hz, ArH), 6.30 (d, 1H, ^3J = 8.8 Hz, ArH), 3.63 (m, 2H, CH$_2$-NH), 3.51 (t, 2H, ^3J = 6.0 Hz, CH$_2$-Br), 2.23 (quin, 2H, ^3J = 7.0 Hz, CH$_2$).

^{13}C NMR (100 MHz, D$_3$COD): δ (ppm) 146.6, 145.9, 145.5, 138.3, 123.5, 99.9, 43.2, 32.4, 31.0.

N-(3-Azidopropyl)-7-nitrobenzo[*c*][1,2,5]oxadiazol-4-amine (NBD, 9)
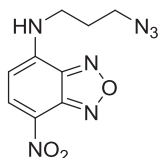
9 was synthesized according to Key and Cairo [2].

^{1}H NMR (400 MHz, CDCl$_3$): δ (ppm) 8.48 (d, 1H, ^3J = 8.4 Hz, ArH), 6.50 (m, 1H, NH), 6.21 (d, 1H, ^3J = 8.8 Hz, ArH), 3.63 (q, 2H, ^3J = 6.2 Hz, CH$_2$-NH), 3.58 (t, 2H, ^3J = 6.2 Hz, CH$_2$-N$_3$), 2.07 (quin, 2H, ^3J = 6.6 Hz, CH$_2$).

^{13}C NMR (100 MHz, CDCl$_3$): δ (ppm) 144.3, 143.8, 143.6, 136.4, 124.4, 98.7, 49.1, 41.56, 27.7.

LC/MS (ESI, positive mode) *m*/*z* 264.1 [M+H]$^+$.

N-(3-Azidopropyl)-5-(dimethylamino)naphthalene-1-sulfonamide (DNS, 8)
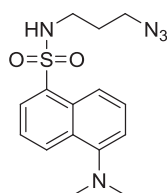
The synthesis of DNS was conducted with 5-(dimethylamino)naphthalene-1-sulfonyl chloride and 3-azidopropan-1-amine adapted from [3] who synthesized *N*-(2-azidoethyl)-5-(dimethylamino)naphthalene-1-sulfonamide. The crude product was purified by column chromatography using petroleum ether/ethyl acetate (2/1, v/v) and dried under reduced pressure resulting in 79% yield.

^{1}H NMR (400 MHz, CDCl$_3$): δ (ppm) 8.55 (d, 1H, ^3J = 8.5 Hz, ArH), 8.28 (d, 1H, ^3J = 8.6 Hz, ArH), 8.26 (dd, 1H, ^3J = 7.3 Hz, ^4J = 1.5 Hz, ArH), 7.51-7.59 (m, 2H,

ArH), 7.19 (d, 1H, ^3J = 7.3 Hz, ArH), 5.06 (m, 1H, NH), 3.25 (t, 2H, ^3J = 6.6 Hz, CH$_2$-N$_3$), 2.98 (q, 2H, ^{3}J = 6.2 Hz, N-CH$_2$), 2.89 (s, 6H, CH$_3$), 1.64 (quin, 2H, ^3J = 6.6 Hz, CH$_2$).

^{13}C NMR (101 MHz, CDCl$_3$): δ (ppm) 152.1, 134.3, 130.6, 129.9, 129.7, 129.5, 128.5, 123.2, 118.5, 115.2, 48.7, 45.4, 40.7, 28.7.

LC/MS (ESI, positive mode) m/z 334.2 [M+H]$^+$.

6-Bromo-5-(dimethylamino)naphthalene-1-sulfonyl chloride (7)
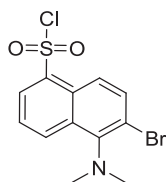
Starting form 5-dimethylamino-1-naphthalenesulfonyl chloride (dansyl chloride) the product was synthesized according to literature [4].

^{1}H NMR (600 MHz, CDCl$_3$): δ (ppm) 8.80 (d, 1H, ^3J = 8.3 Hz, ArH), 8.46 (d, 1H, ^3J = 8.8 Hz, ArH), 8.37 (dd, 1H, ^3J = 7.2 Hz, ^4J = 1.1 Hz, ArH), 7.87 (d, 1H, ^3J = 8.8 Hz, ArH), 7.65 (t, 1H, ^3J = 7.7 Hz, ArH), 3.04 (s, 6H, CH$_3$).

^{13}C NMR (151 MHz, CDCl$_3$): δ (ppm) 148.2, 139.9, 136.1, 134.9, 133.6, 129.5, 127.7, 124.6, 122.5, 122.1, 42.6.

LC/MS (ESI, positive mode) m/z 348.0 [M+H]$^+$.

N-(3-Azidopropyl)-6-bromo-5-(dimethylamino)naphthalene-1-sulfonamide (BNS, 6)
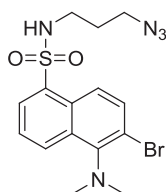
166 mg (0.48 mmol) 6-Bromo-5-(dimethylamino)naphthalene-1-sulfonyl chloride (**7**) were treated with 70 µl (0.71 mmol) 3-azidopropan-1-amine and 123 µL (0.89 mmol) triethylamine in 40 mL CH_2Cl_2. After stirring over night the solvent was removed under reduced pressure. The product was isolated by column chromatography with petrol ether/ethyl acetate 2/1, (v/v) and a yellow oil was obtained with 93% yield.

^{1}H NMR (400 MHz, $CDCl_3$): δ (ppm) 8.64 (d, 1H, $^3J = 8.5$ Hz, ArH), 8.33 (d, 1H, $^3J = 8.8$ Hz, ArH), 8.27 (dd, 1H, $^3J = 7.3$ Hz, $^4J = 1.2$ Hz, ArH), 7.74 (d, 1H, $^3J = 9.5$ Hz, ArH), 7.60 (dd, 1H, $^3J = 8.8$ Hz, $^3J = 7.2$ Hz, ArH), 4.89 (t, 1H, $^3J = 6.3$ Hz, NH), 3.30 (t, 2H, $^3J = 6.5$ Hz, CH_2-N_3), 3.03 (s, 6H, CH_3), 3.01 (q, 2H, $^3J = 6.4$ Hz, N-CH_2), 1.68 (quin, 2H, $^3J = 6.4$ Hz, CH_2).

^{13}C NMR (100 MHz, $CDCl_3$): δ (ppm) 148.1, 135.9, 134.7, 133.8, 131.0, 130.0, 128.4, 124.9, 122.7, 121.3, 48.8, 42.6, 40.8, 28.8.

LC/MS (ESI, positive mode) m/z 412.1 $[M+H]^+$.

(2*E*,4*E*)-deca-2,4-dien-9-ynal (DDY, 10)
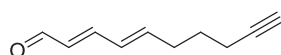
10 was synthesized as described elsewhere [5].

References

1.   Täuscher, E.; Weiß, D.; Beckert, R.; Görls, H. *Synthesis* **2010,** 1603-1608.
2.   Key, J. A.; Cairo, C. W. *Dyes Pigm.* **2011,** *88*, 95-102.
3.   Rogers, S. A.; Bero, J. D.; Melander, C. *ChemBioChem* **2010,** *11*, 396–410.
4.   Kinsey, B. M.; Kassis, A. I. *Nucl. Med. Biol.* **1993,** *20*, 13-22.
5.   Wolfram, S.; Nejstgaard, J.; Pohnert, G *PLOSone*, in press.

Mass spectra of synthetic compounds
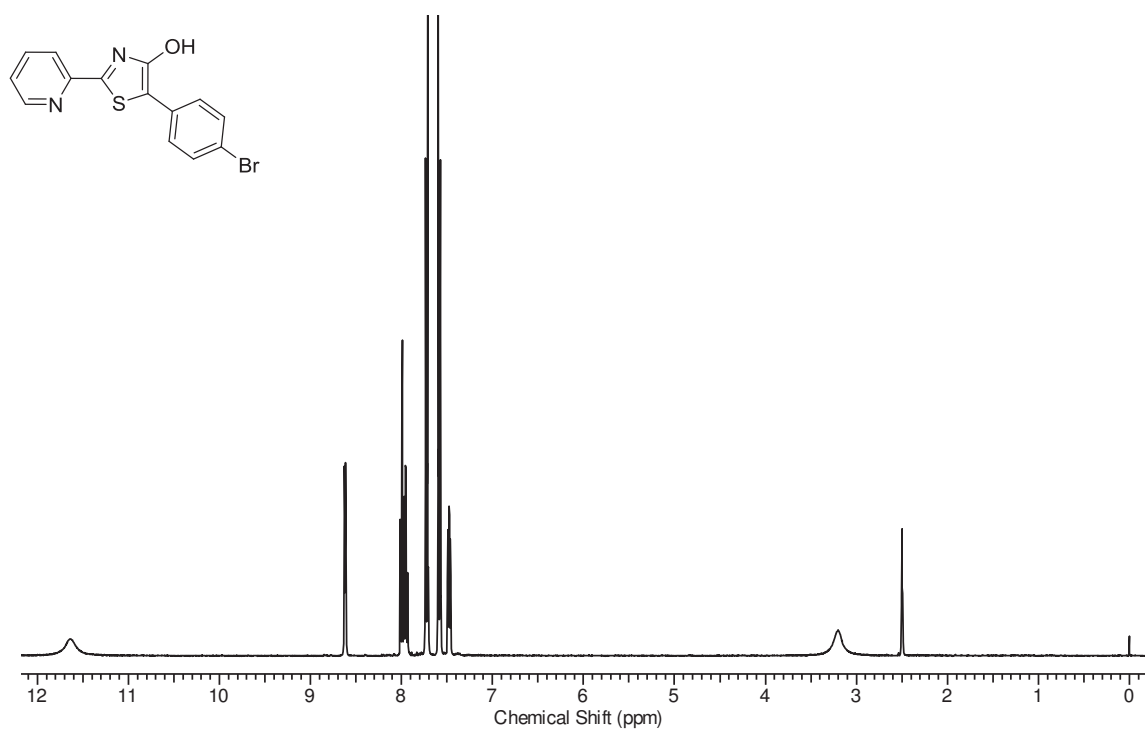
Figure 1: ^{1}H NMR spectrum of compound **4**.
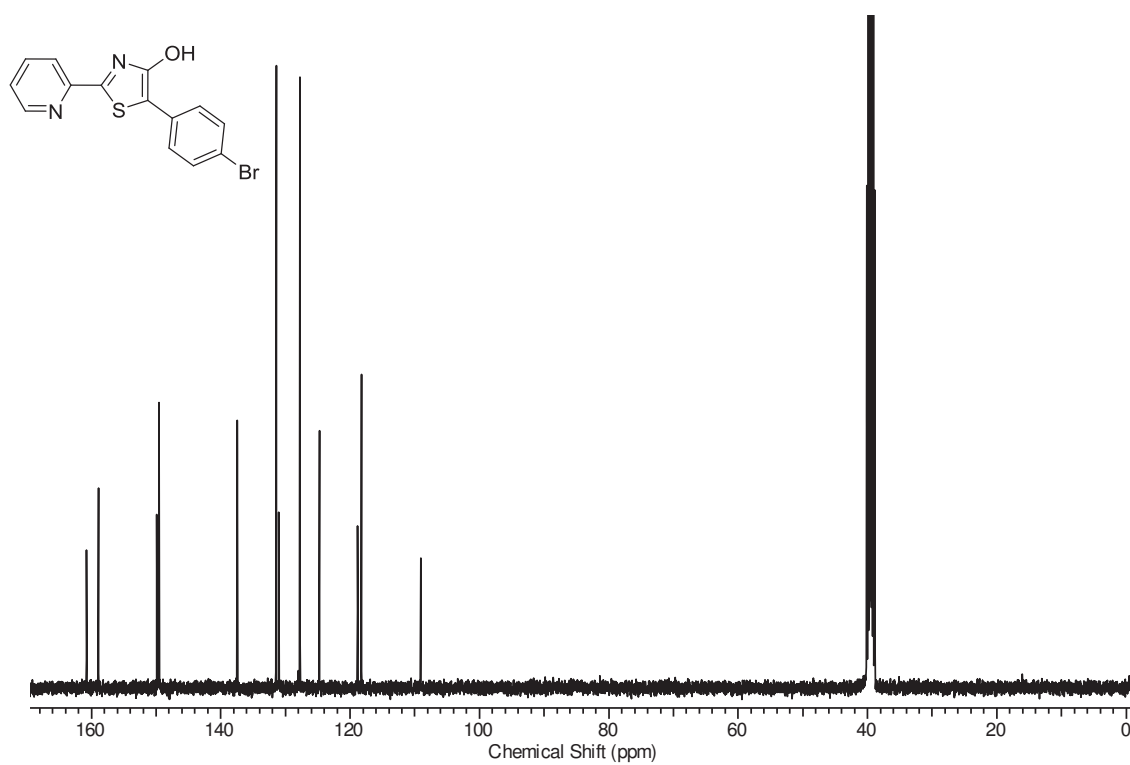
Figure 2: ^{13}C NMR spectrum of compound **4**.
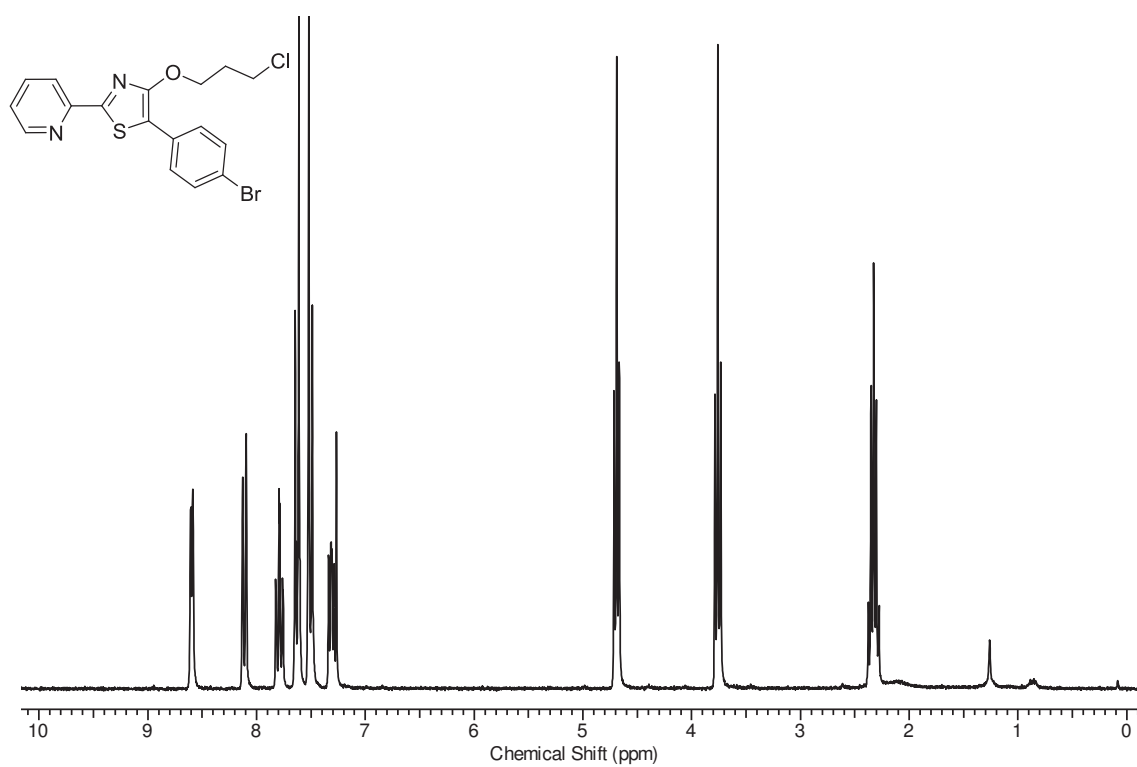
Figure 3: ^{1}H NMR spectrum of compound **5**.
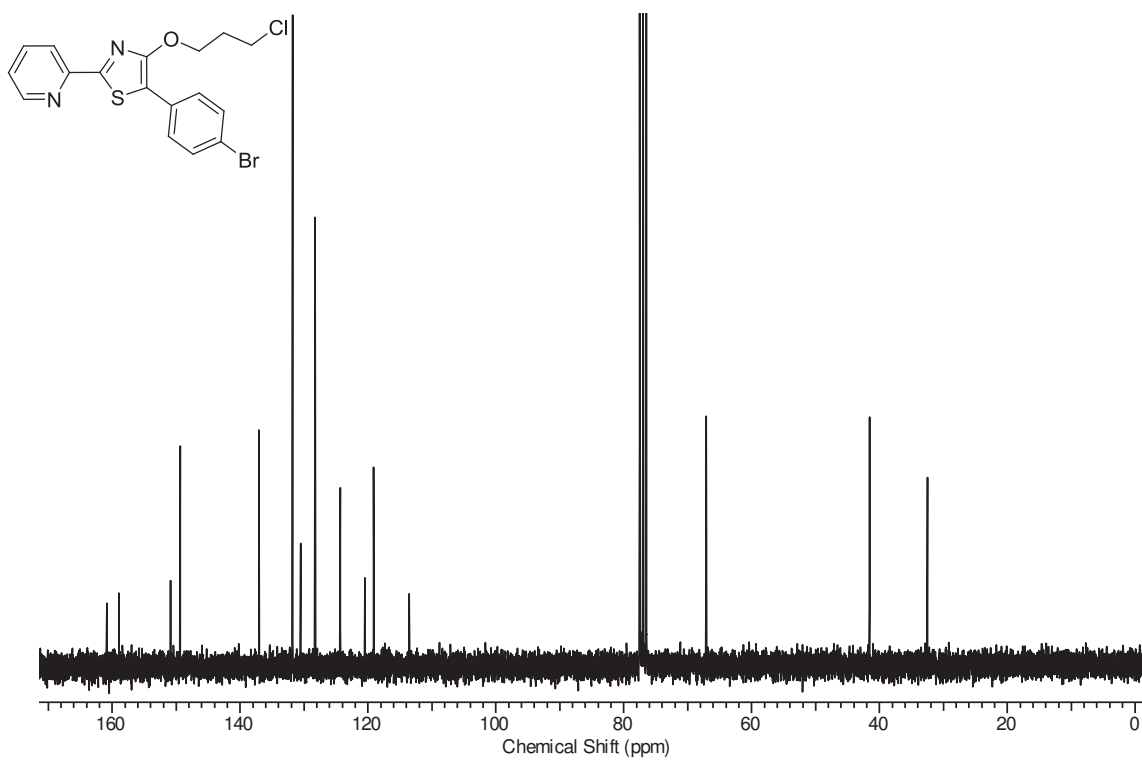
Figure 4: ^{13}C NMR spectrum of compound **5**.
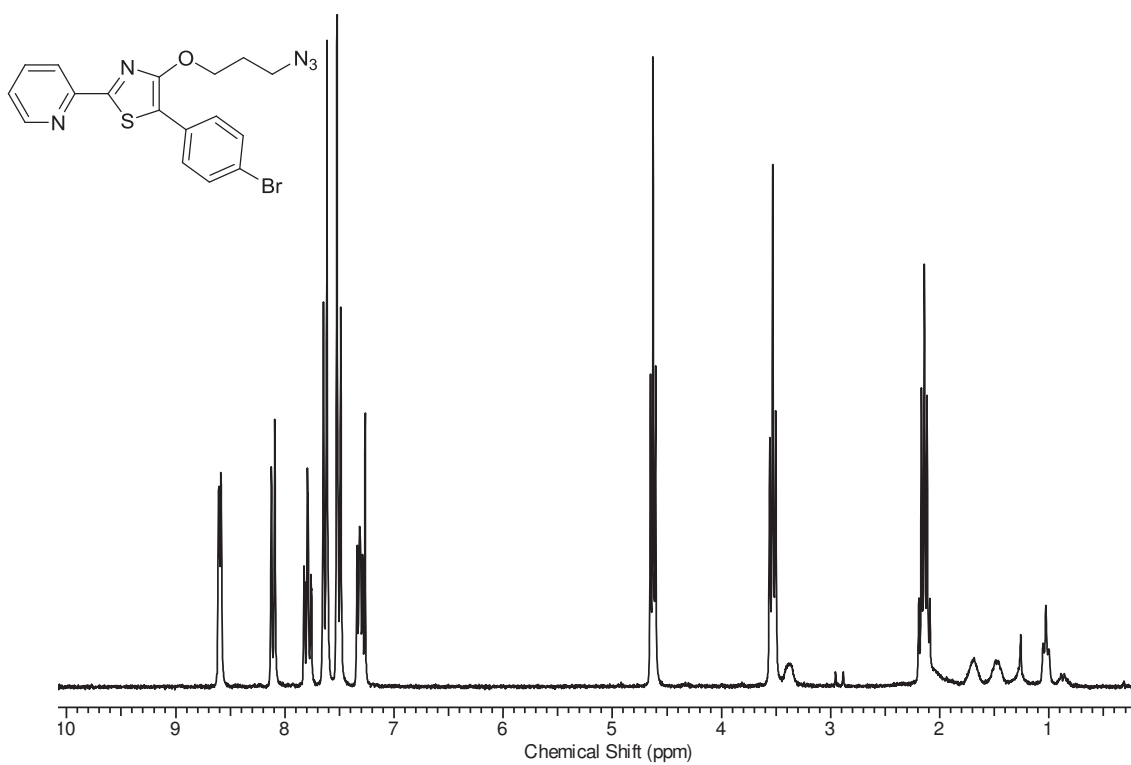
Figure 5: ^{1}H NMR spectrum of compound **1**.
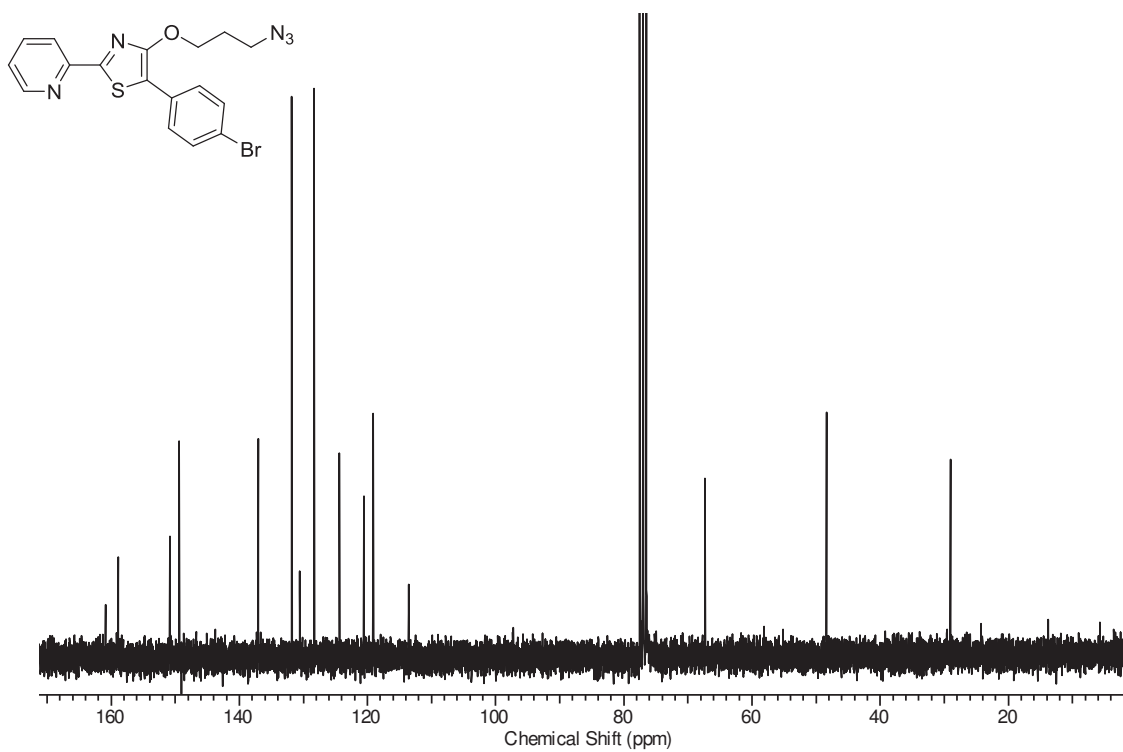
Figure 6: ^{13}C NMR spectrum of compound **1**.
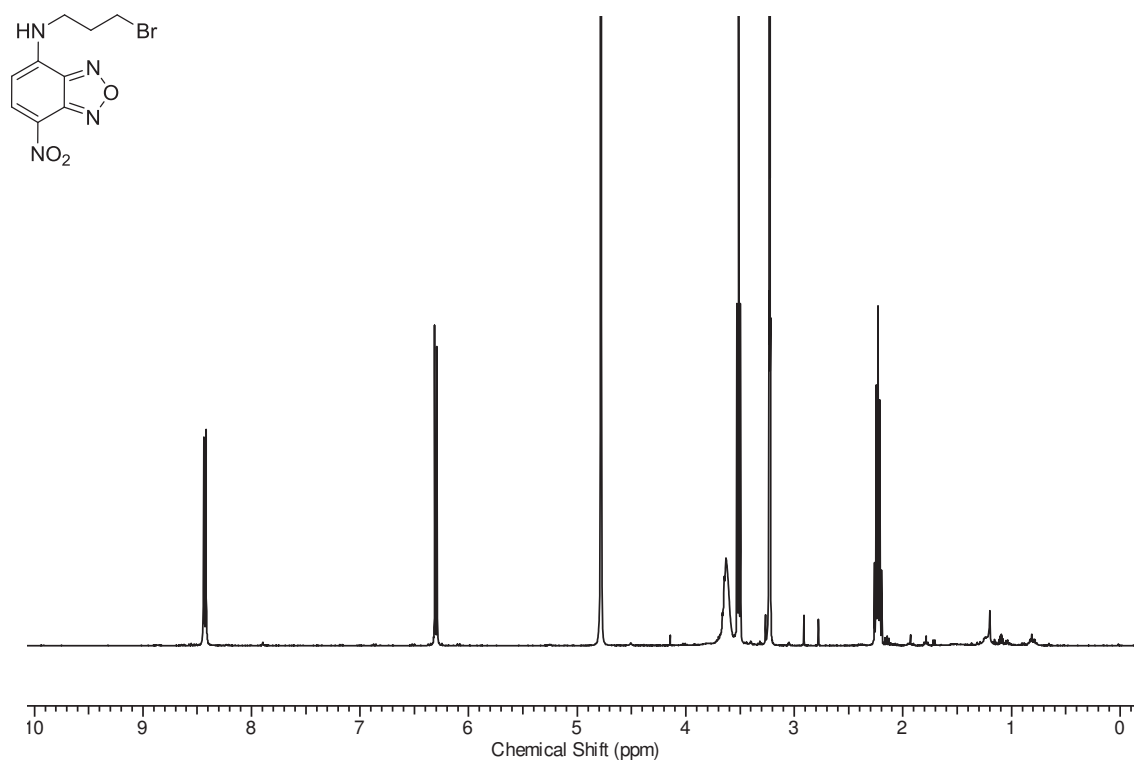
Figure 7: ^{1}H NMR spectrum of *N*-(3-bromopropyl)-7-nitrobenzo[*c*][1,2,5]oxadiazol-4-amine.
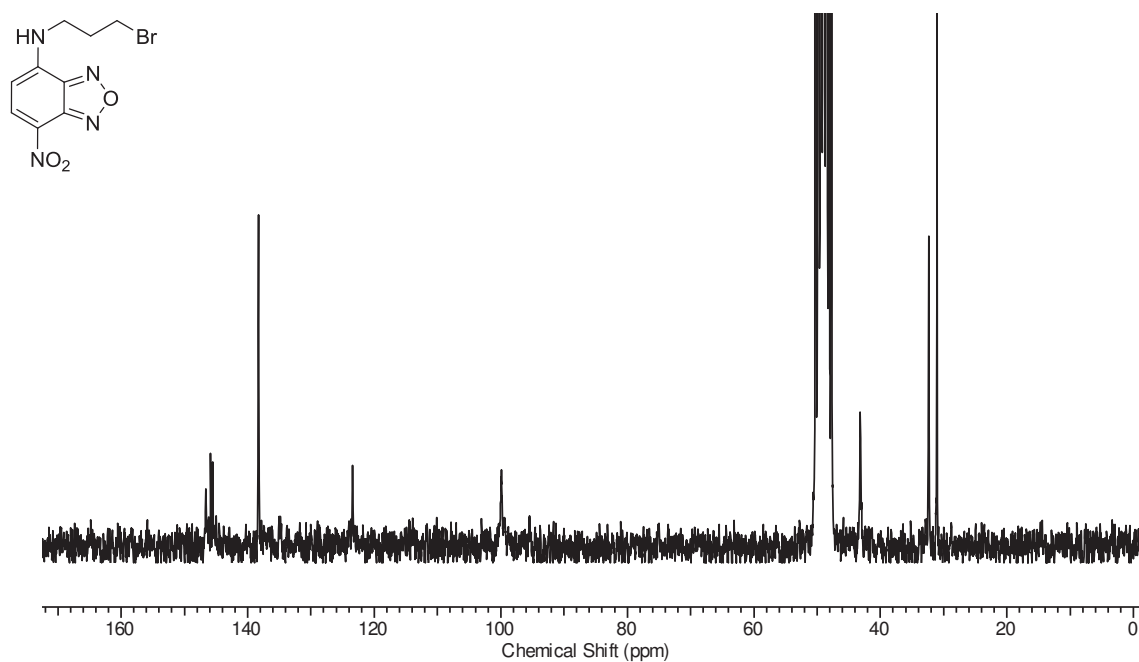
Figure 8: ^{13}C NMR spectrum of *N*-(3-bromopropyl)-7-nitrobenzo[*c*][1,2,5]oxadiazol-4-amine.
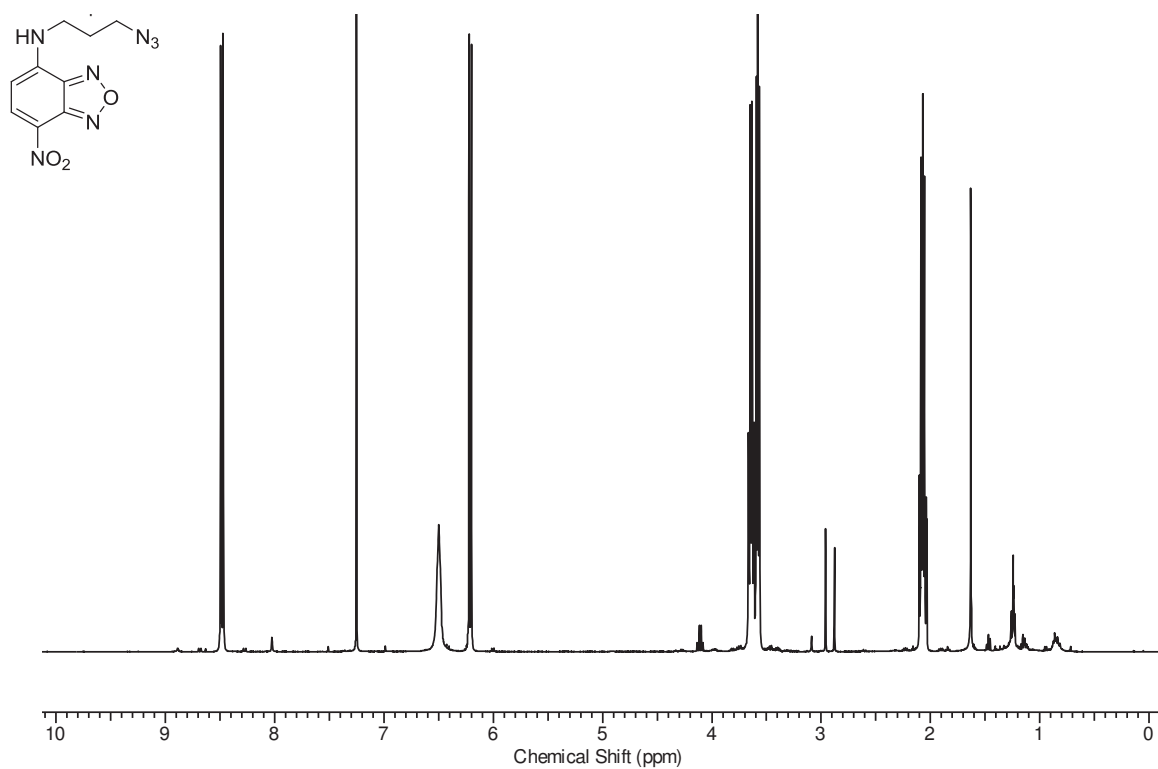
Figure 9: ^{1}H NMR spectrum of compound **9**.
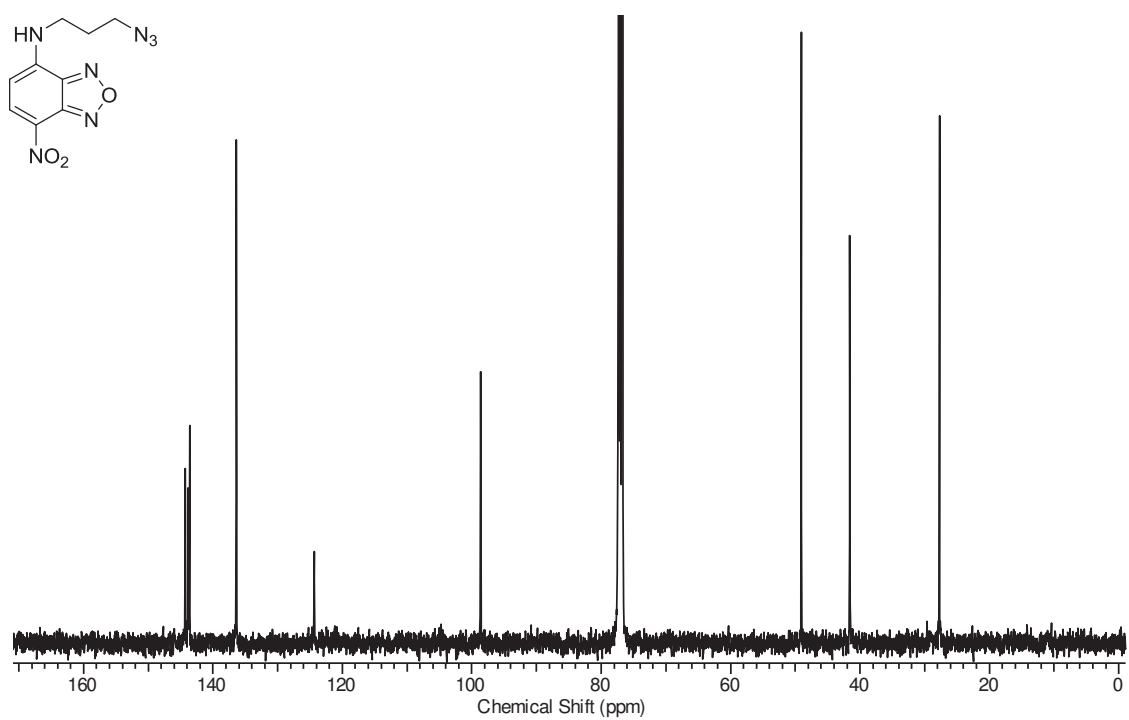
Figure 10: ^{13}C NMR spectrum of compound **9**.
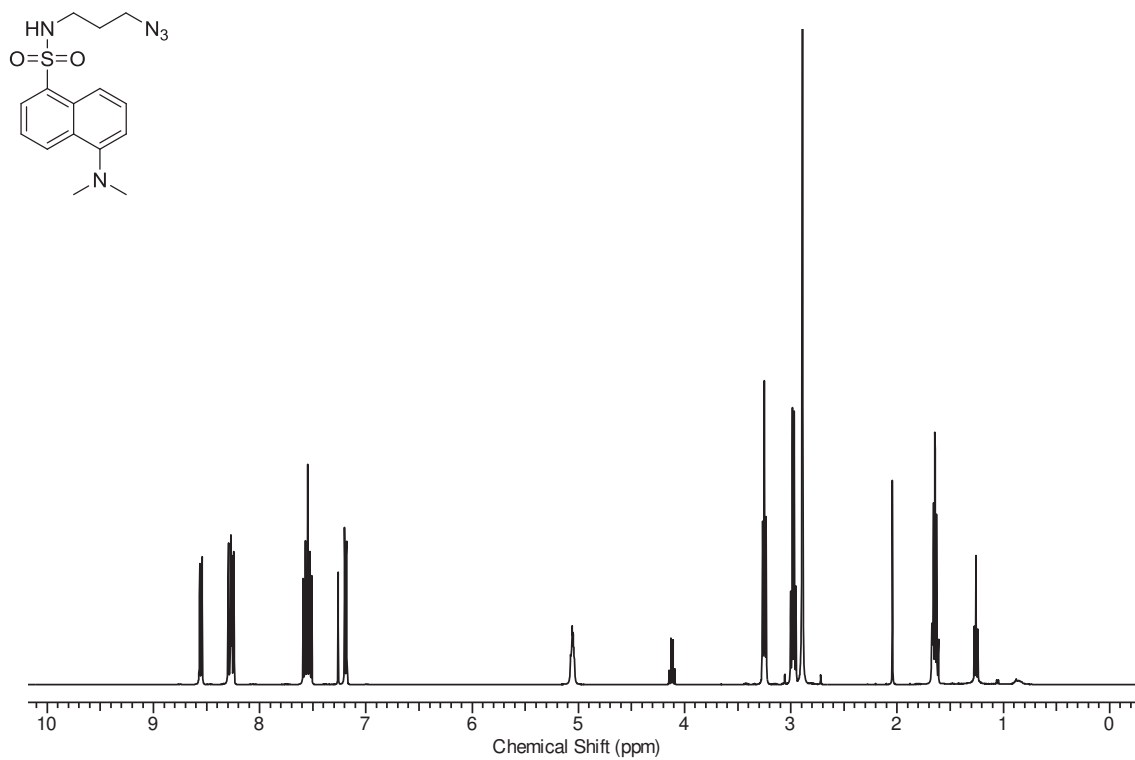
Figure 11: ^{1}H NMR spectrum of compound **8**.
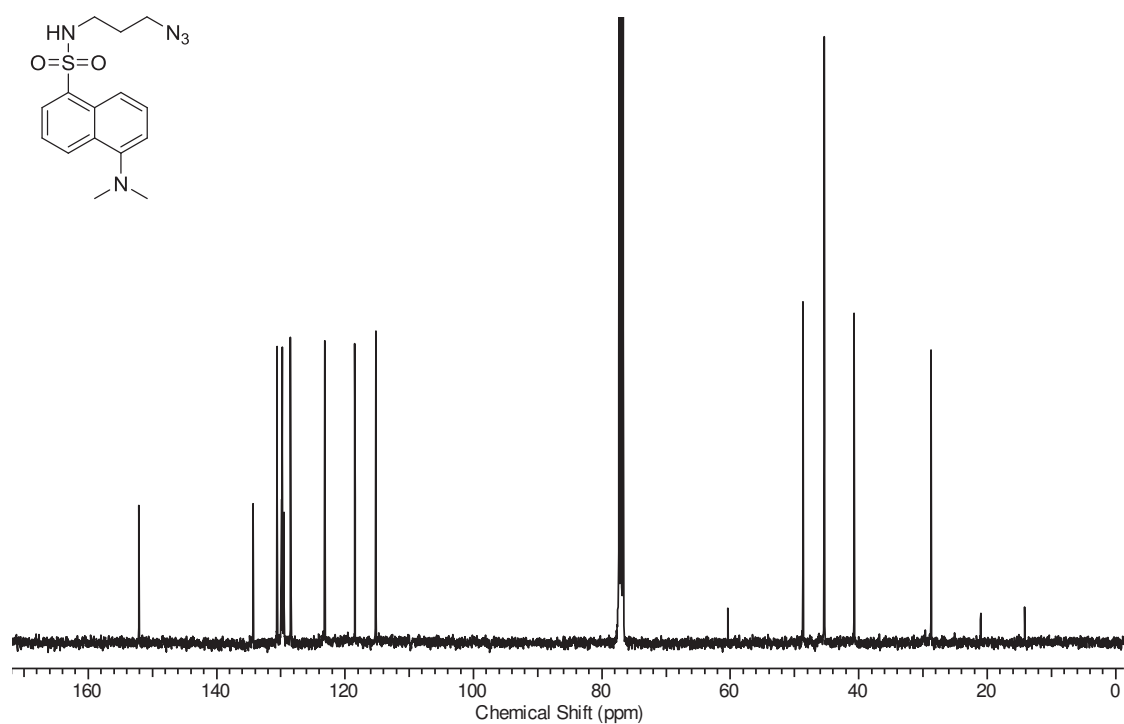
Figure 12: ^{13}C NMR spectrum of compound **8**.
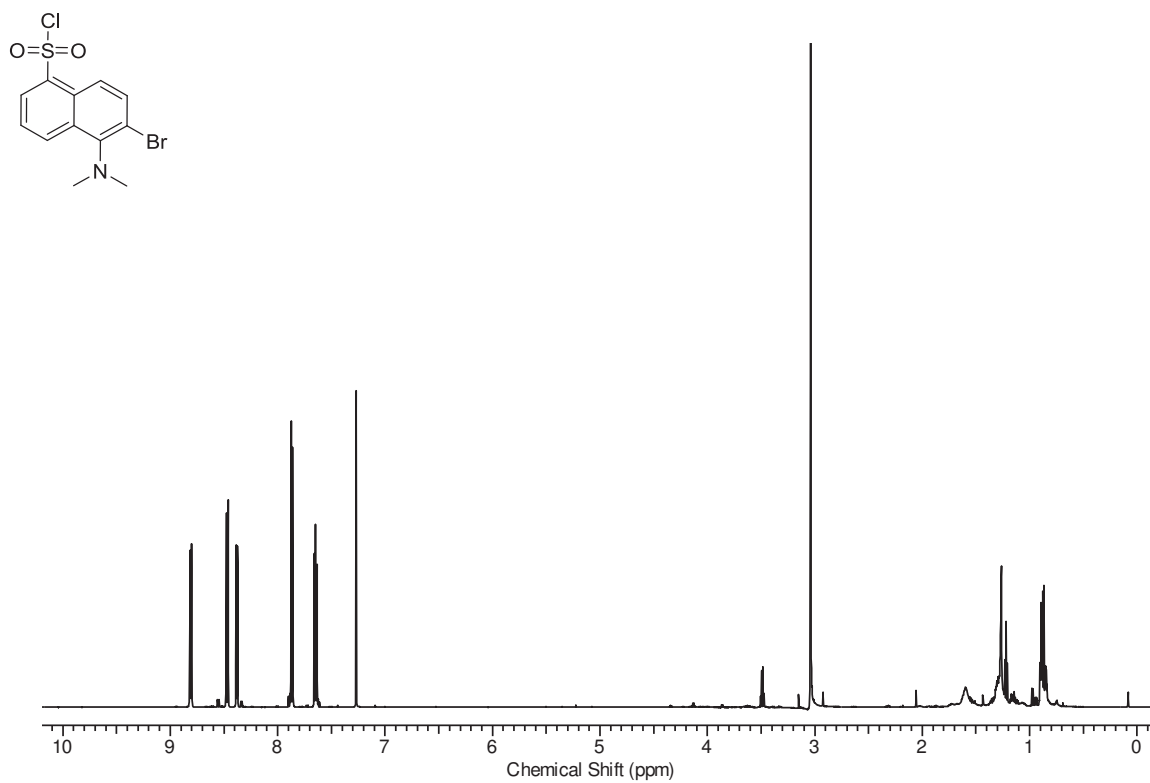
Figure 13: ^{1}H NMR spectrum of compound **7**.
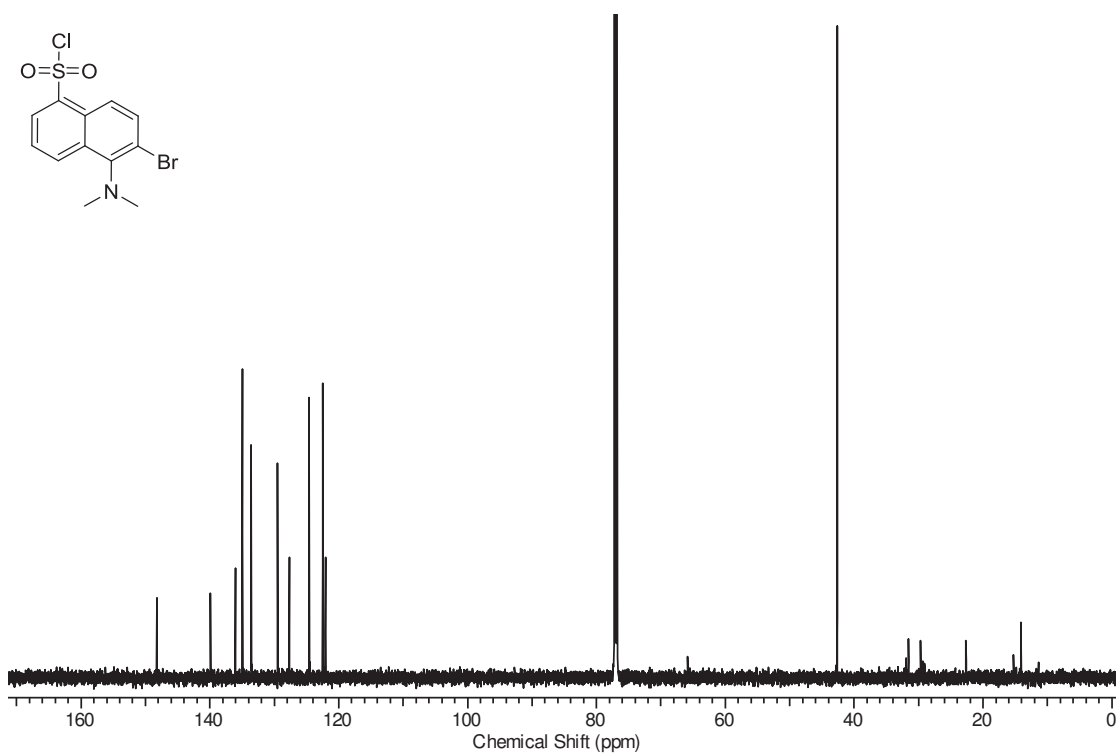
Figure 14: ^{13}C NMR spectrum of compound **7.**

S14
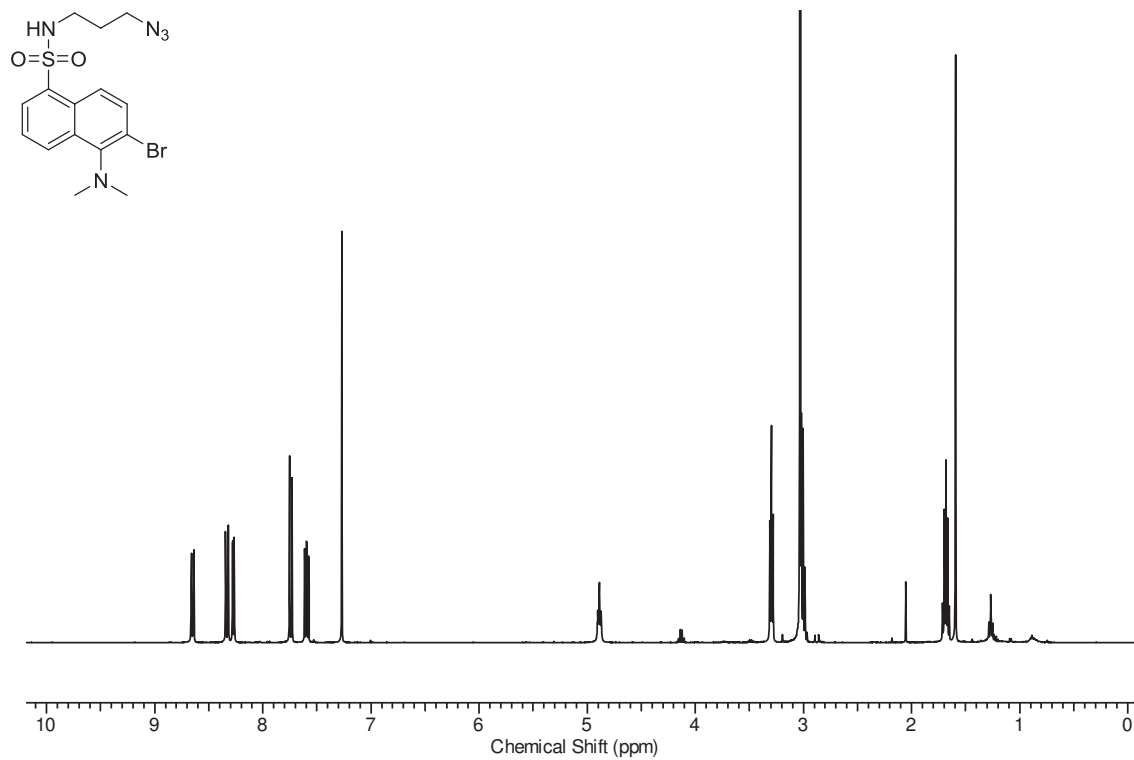
Figure 15: ^{1}H NMR spectrum of compound **6**.
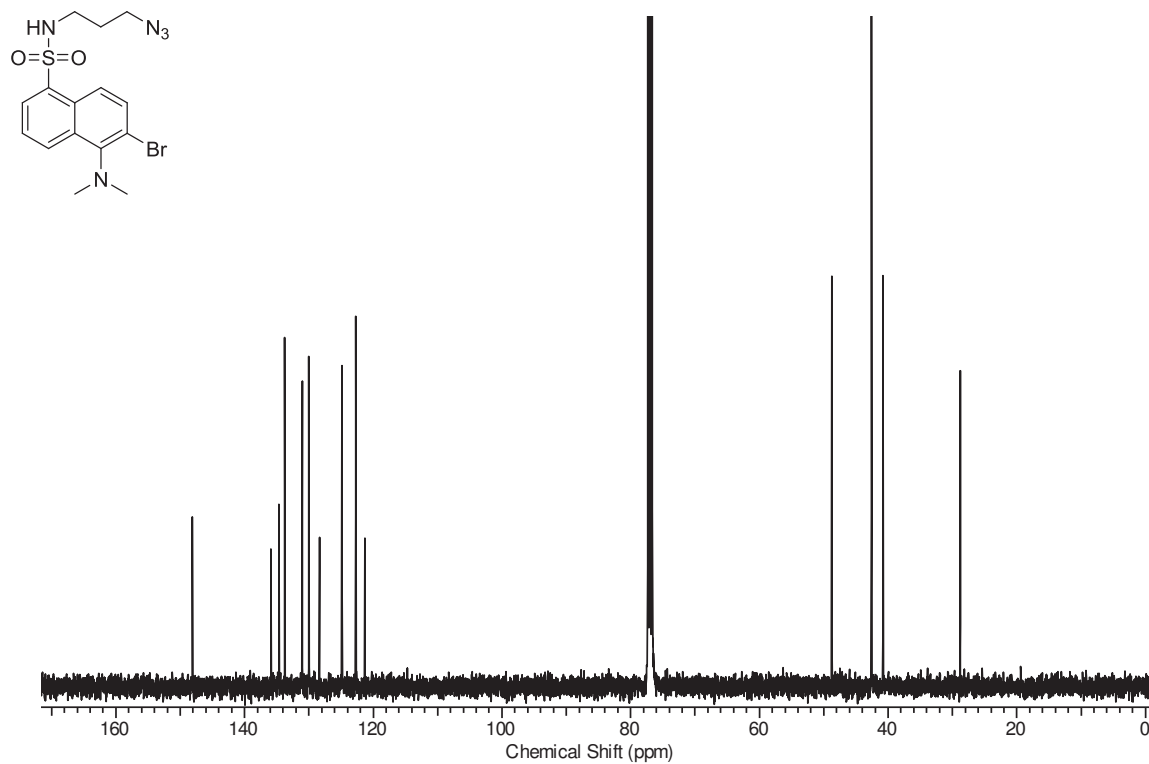
Figure 16: ^{13}C NMR spectrum of compound **6**.
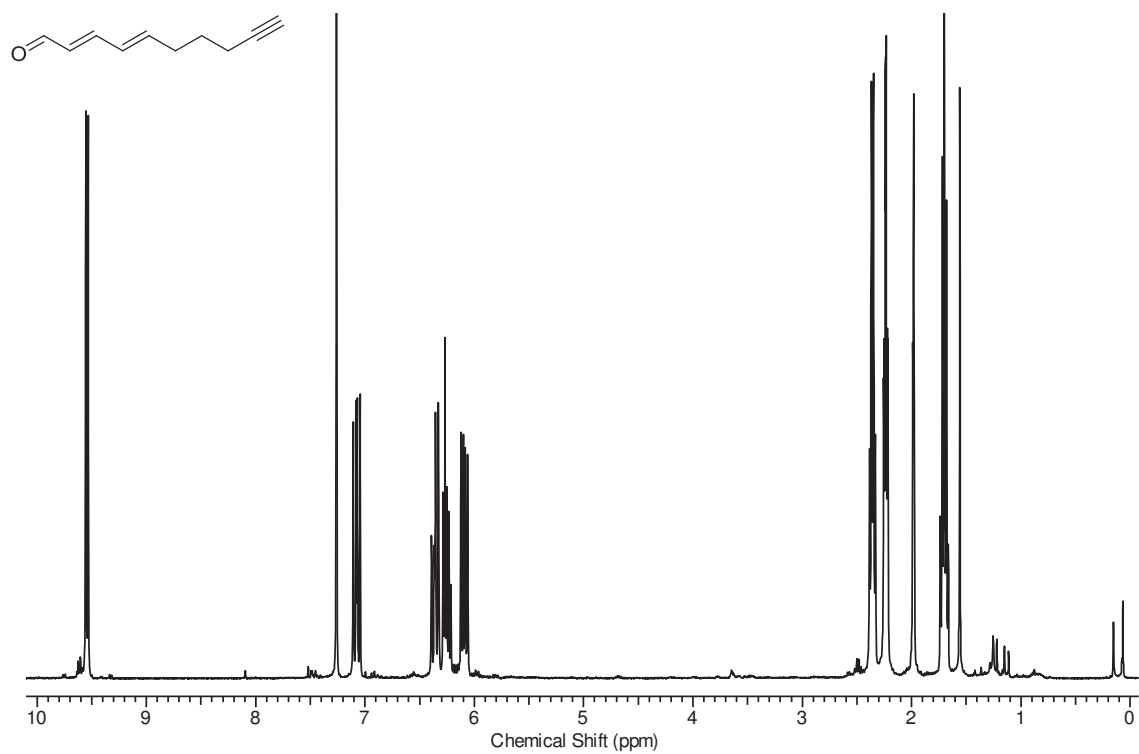
Figure 17: ^{1}H NMR spectrum of compound **10**.
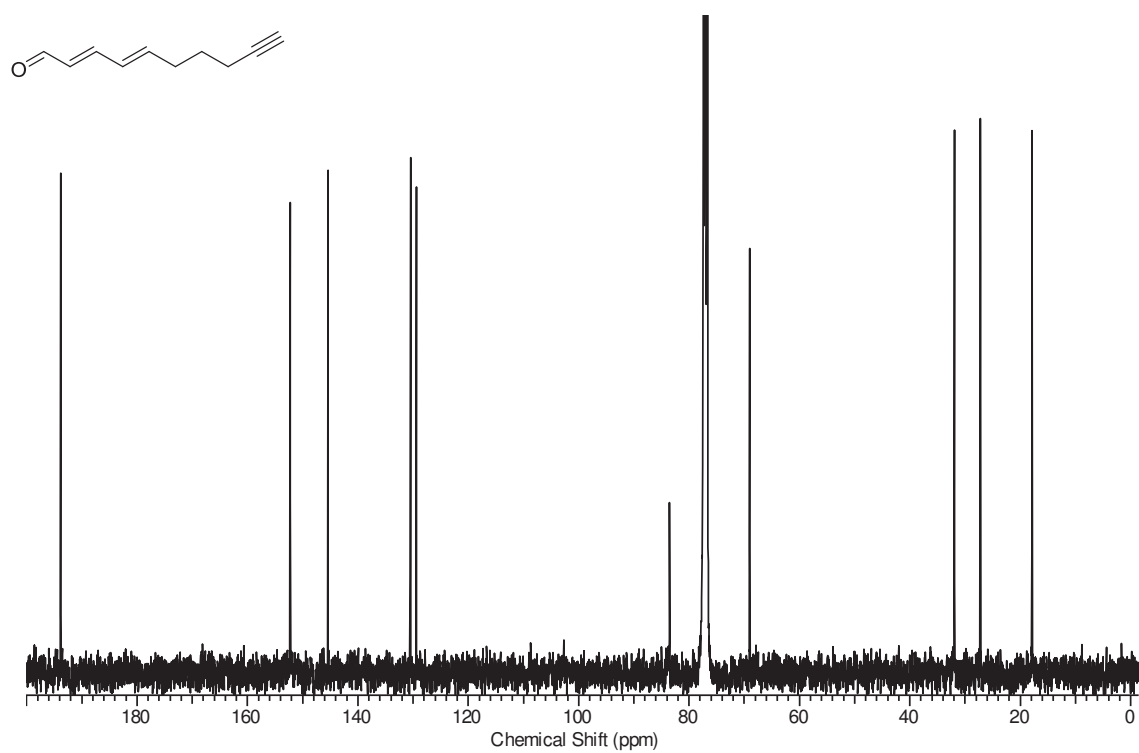
Figure 18: ^{13}C NMR spectrum of compound **10**.

S16

5   DISCUSSION

Diatoms are abundant and important biological components in the oceans. They produce a plethora of metabolites. Among them, fatty acid-derived polyunsaturated aldehydes (PUAs) that belong to the class of oxylipins have been made responsible for "*one of the most fundamental and long-recognized interactions in the sea, which is that between diatoms and copepods*" [149]. A body of literature demonstrates evidence for negative impacts of PUAs and PUA-producing diatoms on the reproduction of copepods. Besides PUAs' role in grazer defense, they have also been suggested as info- and allelochemicals in shaping plankton communities, but all ecological roles were questioned as well (reviewed in [21,55], see chapter 1.2.2). In contrast to their biological functions, uptake and underlying mechanistic effects of these oxylipins are only poorly understood. The little available information about the mode of action includes interference of PUAs with intracellular calcium signaling, cytoskeletal stability, and/or induction of apoptosis (reviewed in [55], see chapter 1.2.3).

To contribute to this topic, I followed a targeted approach to track the fate of PUAs by means of molecular probes. My work reveals uptake and target molecules of these substances in model organisms in the marine plankton and thus promotes understanding of mechanistic effects of PUAs. Furthermore, I developed a bioorthogonal reporter molecule for labeling of alkyne-modified small molecules and (bio)macromolecules that can be utilized to study related questions like detoxification. Quantification of dissolved PUAs and production of these metabolites upon algal cell damage in a mesocosm study provide explanation for unusual outcomes of grazing experiments and contribute to the limited availability of dissolved PUA values in field and close-to-field conditions.

5.1   Quantification of PUAs in a mesocosm study and their impact on grazing experiments

Algal populations are controlled by predation of herbivores that belong to micro- and mesozooplankton[XI]. Mesocosm experiments offer a beautiful possibility to study such marine trophic relationships between grazers and primary producers in a close-to-field scenario. In particular, dilution grazing experiments are the most commonly used method to estimate phytoplankton

---

[XI] **Microzooplankton** are a group of heterotrophic and mixotrophic planktonic organisms between 20 and 200 µm in size (e.g., dinoflagellates, ciliates, copepod larvae etc.), whereas **mesozooplankton** are planktonic animals in the size range of 0.2 to 20 mm and constitute of copepods [150].

growth by microzooplankton grazing [151]. We hypothesized that unusual outcomes of dilution grazing experiments such as negative estimates for grazing [151,152] might be caused by bioactive metabolites like PUAs (**Manuscript A**), which have been previously shown to affect phytoplankton growth and zooplankton reproduction (see chapter 1.2.2).

In a mesocosm experiment in Raunefjord, Norway, we observed a bloom of the frequently co-occurring diatom *Skeletonema marinoi* (former name *Skeletonema costatum* [153]) that produces 2*E*,4*Z*-heptadienal (HD), 2*E*,4*Z*-octadienal (OD), and 2*E*,4*Z*,7*Z*-octatrienal (OT) and the onset of a bloom of the prymnesiophyte *Phaeocystis pouchetii* that is a 2*E*,4*E/Z*-decadienal (DD) producer [154] (Figure 9, **Manuscript A**). The mesocosm setup consisted of 10 m^3 floating enclosures filled with sea water that contained the natural, local plankton community.

For quantification of PUAs, I adapted a well-established derivatization protocol using *O*-2,3,4,5,6-pentafluorobenzyl (PFB) hydroxylamine to form the corresponding PFB oximes followed by identification with gas chromatography coupled to mass spectrometry (GC-MS) [25,155]. Dissolved metabolites were adsorbed by solid phase extraction. PUAs are also released upon wounding of diatoms, which activates an enzyme cascade (see chapter 1.2.1). To quantify this potential of algal cells to produce PUAs (referred as particulate PUAs), collected cells were freeze-thawed resulting in a cell burst. The applied method enabled *in situ* trapping of PUAs with PFB hydroxylamine in the phytoplankton matrix without interfering with enzymatic reactions [155].

Compared to the previous introduced Wittig-derivatization of volatile PUAs for nuclear magnetic resonance spectroscopy and GC-MS-based identification [156], the PFB oxime derivatization provides a quantitative method, is suitable for high sample throughput, requires only little equipment on the sampling site, and offers appropriate sensitivity for field and mesocosm studies [155] (e.g., 10 pmol for a dissolved PUA in 1 L sample volume [25]). Alternative GC-MS-based methods to detect PUAs comprise for example headspace extraction by using a closed-loop stripping device [27] or solid phase microextraction (SPME) [20] that needs no sample derivatization but suffers from low reproducibility [50,157].

In **Manuscript A**, I used electron impact ionization to ionize and fragment the PFB oximes after chromatographic separation. Utilization of chemical ionization electron capture would even increase sensitivity by two orders of magnitude [155]. Lately, a liquid chromatography coupled to mass spectrometry (LC-MS)-based method using atmospheric pressure chemical ionization for direct PUA quantification without derivatization was developed in our lab (unpublished data).

In **Manuscript A**, we demonstrated that dilution experiments in mesocosm and lab experiments can be distorted by inhibition of phytoplankton growth most likely caused by PUAs. In a typical dilution method, the net growth rates (phytoplankton growth including grazing) of undiluted and with filtered sea water diluted samples are measured. Inhibitory PUAs that can be released

during filtration of sea water caused by cell damage probably reduced phytoplankton growth in diluted treatments; thus, the central assumption that the instantaneous growth (that is growth without grazing) is unaffected by the phytoplankton concentration, whereas grazing is density-dependent and increases with higher phytoplankton density due to higher encounter rates with microzooplankton [151], was violated. This resulted in an underestimation of microzooplankton grazing (**Manuscript A**). This observation might be relevant as well for other allelochemicals, especially in dense algal blooms.
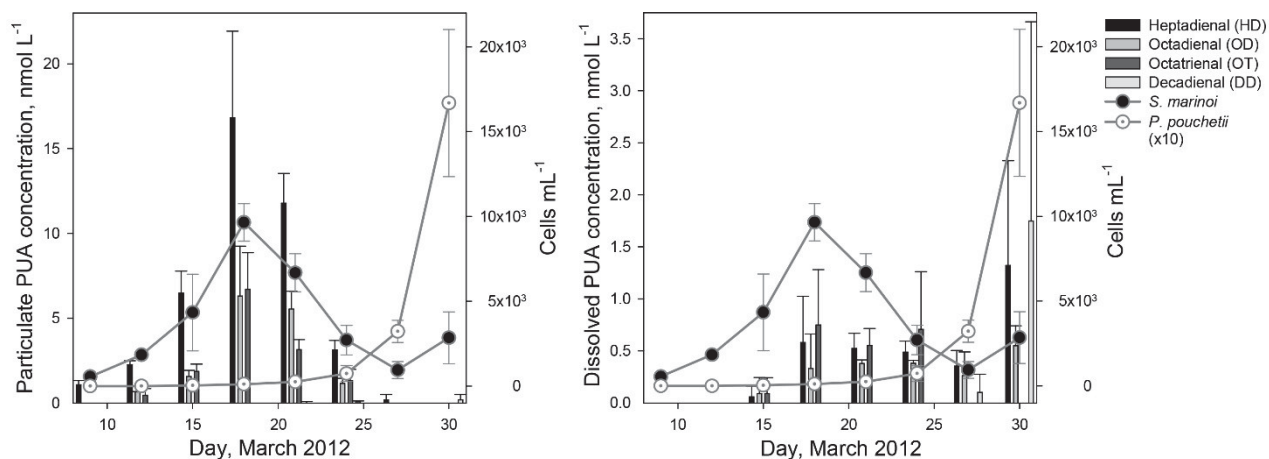
Figure 9.   **Abundance of *S. marinoi* and colonial *P. pouchetii* cells as well as particulate (left) and dissolved PUA concentrations (right) during a mesocosm experiment in March 2012 at the Norwegian National Mesocosm Center, Espegrend.** PUA values and cell counts are averages ± standard deviations of the three nitrate and phosphate (16 μM and 1 μM final concentrations) enriched enclosures. Particulate PUA concentrations (HD, OD, and OT) correlate with the *S. marinoi* bloom. The high dissolved HD and OD concentrations on day 30 can be attributed to cell lysis during decline of *S. marinoi*; this pattern was also observed in [158]. Data for **Manuscript A** were only collected in one of the three nitrate and phosphate enriched mesocosm enclosures.

The use of a carbon cellulose filter for filtration of sea water for dilution experiments removed dissolved organic material including PUAs and resulted in a reduced or eliminated phytoplankton growth inhibition in mesocosm and intraspecific algal growth inhibition in lab experiments (**Manuscript A**). However, the use these filters should only be an additional treatment to identify problems in the dilution protocol since dissolved PUAs and other metabolites that belong to the sample (and are not produced during the filtration process) are captured. Investigations of the underestimation of microzooplankton grazing received less attention before, most of the literature addressed the origin of overestimation (e.g., by release of microzooplankton in the absence of mesozooplankton) [159]. Thus, our study provides guidelines for future evaluation of grazing by utilizing supplementary experiments.

Knowledge of naturally occurring PUA concentrations as observed during this mesocosm experiment (Figure 9) helps to evaluate the significance of laboratory experiments, which often suffer from unnaturally high PUA concentrations (e.g., [22,56]), and their ecological relevance. In

addition, laboratory experiments alone are not always sufficient to describe oxylipin bioactivity and can give different outcomes compared to field studies ([160,161], reviewed in [21]).

Release of PUAs into the water by intact cells was firstly demonstrated by Vidoudez and Pohnert [69] in 2008, who demonstrated that lab cultures of *S. marinoi* exudate PUAs in the late stationary phase, and later also transferred these results to mesocosm and field studies [25,70,146,161]. PUA occurrence in the sea water can result from an active release process or from liberation upon cell lysis [69,146]. Maximum dissolved values of HD and OD each of approximately 0.12 nM were detected during a *S. marinoi* bloom in the Adriatic Sea [25]. During the mesocosm study (**Manuscript A**) we detected higher maximum values of HD (0.58 ± 0.44 nM, 0.06 ± 0.05 fmol cell^{-1}, day 18) and OD (0.38 ± 0.04 nM, 0.06 ± 0.01 fmol cell^{-1}, day 21) (Figure 9, amount per cell is not shown), whereas an induced *S. marinoi* bloom in a mesocosm experiment at the same site gave up to 6.8 nM dissolved HD (1.3 fmol cell^{-1}) in the stationary phase [70], a maximum value that was also observed during a cruise in the Northern Adriatic Sea [146]. These data demonstrate the variability of PUAs (**Manuscript A**, [70]) and support their presumed ecological roles in intra-population signaling and interspecies interactions since concentrations of distinct dissolved PUAs are associated with growth phase changes of *S. marinoi* blooms (**Manuscript A**, [70]) as well as phytoplankton growth inhibition (**Manuscript A**).

Diatoms can benefit from perceiving sublethal concentrations of PUAs since these induce resistance to further doses [69,71]. This offers an advantage compared to competing species [71], but PUAs can also act self-inhibitory to the producing algae above a certain threshold (**Manuscript A**, [69]). An influence of PUAs on bacteria and viruses [71] as suggested before under lab conditions [60,76] could not be confirmed in a previous mesocosm study [161]. However, a much higher PUA liberation (micromolar range) by sinking particles as they appear during decaying diatom blooms even stimulated bacterial growth in a study and contributed to the bacterial initiated remineralization of particles with potential implications for the global carbon cycle [162].

In contrast to release of oxylipins by intact algae or sinking particles, particulate PUA production after cell disruption as it occurs during grazing is well studied and leads to high local PUA concentrations (e.g., approximately 28 nM HD plus OD (35 fmol cell^{-1} of *S. marinoi*) in the Adriatic Sea [25] vs. 23 nM (5 fmol cell^{-1}, day 18) in the presented mesocosm experiment (Figure 9)). These values, which might be locally even higher (e.g., in the gastrointestinal tract of copepods), may cause severe reproduction consequences in copepods (see chapter 1.2.2) like shown before for *Temora stylifera* and *Calanus helgolandicus* fed with giant liposomes containing 19 nM and 23 nM DD [59].

Interestingly, the ratio of HD to OD was not larger than four in particulate and dissolved PUA quantification (Figure 9) and thus fits to laboratory experiments with *S. marinoi* monocultures [69], whereas in a comparable mesocosm study on the same site the particulate HD/OD ratio was at least 25/1 [70]. The delayed bloom of *P. pouchetti* (**Manuscript A**, Figure 9) was the most

noticeable difference compared to simultaneous blooms of these species in [70] without major presence of other algae in both mesocosm experiments. This potentially points towards a regulation of the PUA ratio, maybe as response to DD produced by *P. pouchetii*. An allelopathic effect of DD on *S. costatum* [28] that might also affect the PUA production ratio was shown before in laboratory studies. On the other hand, effects of nutrient limitation [163] and a more complex interaction based on diverse exudated metabolites of other plankton that cause a physiological response in the receiving alga, demonstrated for example during non-contact co-culturing of *S. costatum* and *Thalassiosira rotula* [164], are possible causes.

5.2   Probe design and uptake of a PUA-derived probe in planktonic organisms

The biological effects of PUAs have been documented by simple but often time-consuming measurements like cell counts, observation of copepod egg production, or microscopic inspection of morphology. Over time, a series of methodological advancements have contributed to a first understanding of the mode of action of these metabolites [56,94,95] (see chapter 1.2.3) and their biosynthesis [19] (see chapter 1.2.1). Current fluorescence-based techniques like terminal deoxynucleotidyl transferase-mediated deoxyuridine triphosphate nick-end labeling (TUNEL) [56,95] and DNA labeling with bromodeoxyuridine (BrdU) followed by incubation with fluorescent BrdU antibodies [94] indicated PUA-induced apoptosis in sea urchin and copepod embryos. Moreover, assessment of egg viability was shown by fluorescent probes (e.g., fluorescein diacetate, SYTOX Green) in *C. helgolandicus* [165]). However, all methods do not visualize direct uptake and localization of PUAs.

In a targeted approach I addressed direct uptake of PUAs in marine plankton by using molecular probes and fluorescence microscopy (**Manuscript B** and **Manuscript C**). The demand to apply tailored methods was already discussed in 2002 during a colloquium of 37 scientists that aimed towards a comprehensive understanding of the diatom-copepod interaction: "*A major task in the near future will be the development of chemical analytical methods that will allow us to investigate processes in the copepod gut and tissue, in order to evaluate the possible uptake and distribution of reactive aldehydes towards target molecules, cells and organs*" [149].

Like shown above, fluorescent probes have become valuable tools to study structural and functional changes in cells and organisms. I also chose a fluorescence-based approach and a molecular probe designed according to activity-based protein profiling (ABPP). This technique uses small-molecule activity-based probes (ABPs) that contain functional moieties based on natural products or substrates and inhibitors of enzyme classes [122], which covalently react with target molecules. Compared to their primary applications to determine active protein targets by mass spectrometry, ABPs have been also but less frequently used for optical imaging [108,130,166].

The PUA-derived probe is based on DD, which is the best studied metabolite of the group of PUAs with available data for structure-activity relationship [51]. DD has become a model aldehyde for studying the effects of oxylipins on marine plankton [167]. The synthetic C10 α,β,γ,δ-unsaturated aldehyde 2*E*,4*E*-decadien-9-ynal (DDY, Figure 10) functions as reactive group (RG) and is linked at the terminus with the well-established, cell permeable, and commercially available fluorophore tetramethylrhodamine (TAMRA) [168,169] as reporter molecule to form the ABP TAMRA-PUA (Figure 10). This structural manipulation of the alkyl side chain of DD without interfering with the active α,β,γ,δ-unsaturated aldehyde structural element was justified by the fact that the bioactivity of PUAs only partially depends on the polarity of the side chain and is even present in α,β-unsaturated aldehydes, whereas saturated counterparts are almost biologically inactive [51,60].

To compare uptake behavior of unsaturated and saturated aldehydes I coupled 5-hexynal (SA) to TAMRA-N$_3$ and received TAMRA-SA (Figure 10). As an additional control, the fluorescent azide TAMRA-N$_3$ (Figure 10) was used.
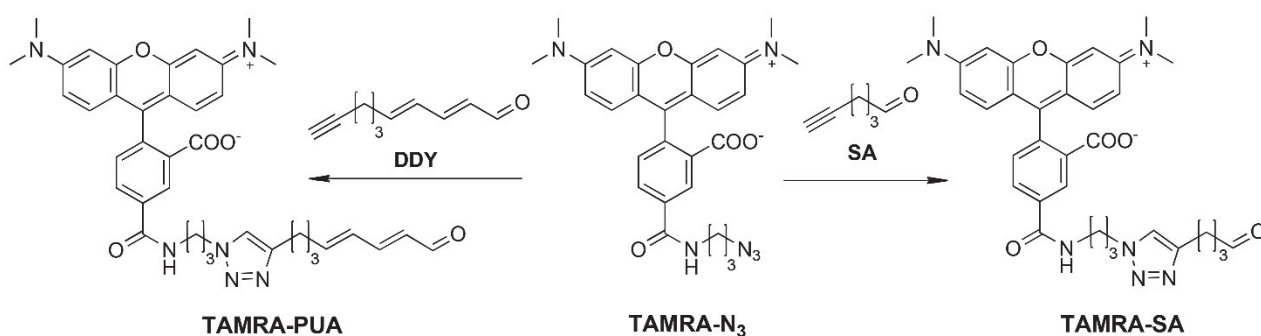
Figure 10. Overview of the probe components, the probe TAMRA-PUA, and the control TAMRA-SA. The synthesis of TAMRA-N$_3$, DDY, and TAMRA-PUA were introduced in my diploma thesis [147] and are presented in **Manuscript C** with slight modifications.

Phaeodactylum tricornutum has become a central model for molecular and cellular studies of diatom biology [170]. It releases polar oxo-acids [23] that also bear the α,β,γ,δ-unsaturated aldehyde motive and was shown to be a highly inhibitory alga to larval development of *C. helgolandicus* [171]. Vardi *et al.* [71] studied effects of DD on *P. tricornutum* and suggested a DD-mediated cell-to-cell signaling. When exposed to 33 μM of this oxylipin, *P. tricornutum* initiated a nitric oxide (NO) burst that resulted from an increased intracellular calcium concentration [71]. At a lower concentration of 10 μM, DD did not affect *P. tricornutum* [71] but different other algae [75] regarding cell membrane permeability of the dye SYTOX Green.

At this concentration we showed for the first time an uptake and accumulation of a DD derivative (TAMRA-PUA) in algal cells of *P. tricornutum* (**Manuscript B**). TAMRA-PUA distributed over almost the entire cells whereas the saturated aldehyde probe TAMRA-SA did not substantially accumulate. Treatment with the control TAMRA-N$_3$ could not be significantly distinguished from

untreated cells so that we can exclude accumulation of the probes in the organisms due to the structure of the fluorophore itself.

The high reactivity of the α,β,γ,δ-unsaturated aldehydes can explain the ability of TAMRA-PUA to enrich in the whole cell without intracellular compartmentation: the electrophilic Michael acceptor probably covalently reacts with nucleophilic moieties of cellular components like proteins [86,87], DNA [88,89,172], or small peptides [84], which will be addressed later (chapter 5.3). This may reduce exfiltration of TAMRA-PUA (**Manuscript B**).

The results indicate that cell walls and membranes do not represent a barrier for PUAs. Furthermore, these aldehydes did not preferentially covalently react with specific components within the membrane like receptors [173] in *P. tricornutum* since no increased membrane fluorescence was detected (Fig 4 in **Manuscript B**).

However, an uptake mechanism for PUAs, as it has been observed earlier for glucose by transporters in the same alga [174], cannot be deduced from the experimental findings. Besides transporters, other mechanisms like passive diffusion, vesicle-mediated transport, or metabolization that enable substances to cross the membrane are known [173].

Our results visualize for the first time that PUA analogs are taken up in cells (**Manuscript B**) to exert their activity in marine plankton. This is also consistent with previous findings by Adolph *et al.* [60], who gave evidence that penetration through membranes is a prerequisite for PUAs' bioactivity. They conducted a clarifying experiment on DD uptake in the yeast *Saccharomyces cerevisiae*, which is almost insensitive to PUAs. Only mutants with increased cell wall and/or plasma membrane permeability were affected by DD compared to wild-type cells [60].

Diatoms produce PUAs as defense metabolites against their main predators, the copepods (see chapter 1.2.2). Biological effects of PUA-producing diatom diets on copepod reproduction in field and laboratory studies include reduced fertility and egg hatching success as well an impaired development and malformations of the offspring (reviewed in [21,43,55]). Visualization of uptake and distribution of PUAs in copepods is central for unraveling the insidious effects of these oxylipins. However, the design of uptake studies needs to be more sophisticated than with single-celled algae mainly due to the restricted transfer of dyes through the chitinous exoskeleton [175] and needs consideration of the following aspect: PUA production starts seconds after wounding of diatoms in the feeding organs of the predators [20,44]; to mimic this natural feeding, delivery of PUAs needs to be involved in an active feeding process of the copepod. Because of these challenges only a few studies have addressed direct effects of PUAs on copepods. Buttino *et al.* [59] developed a feeding protocol with giant liposomes, which they used to encapsulate DD. Ianora *et al.* [56] incubated the dinoflagellate *Prorocentrum minimum* with DD, which was then delivered to *C. helgolandicus* females for three days. At about 10 µM pretreatment concentration none of the hatched larvae reached adulthood [56].

On the basis of this lethal concentration and feeding procedure, we introduced a feeding protocol for copepods to visualize uptake and distribution of probes (**Manuscript C**). It includes the carrier organism *Oxyrrhis marina* that delivers the PUA-derived probe TAMRA-PUA and controls to the copepod *Acartia tonsa.* This calanoid copepod occurs in a wide geographical range, from low temperature to subtropical areas [176], and was used as model organism since it is easy to cultivate and very efficient in transforming ingested material to eggs [177].

A common limitation in fluorescence microscopy is interference of the probe fluorescence with autofluorescence of the observed cells and tissue. This photon attenuation can be overcome by probes that use fluorophores with emission at the near infrared (NIR) region [178], but one has to make sure that cellular uptake of the fluorophore is still guaranteed and appropriate filter sets for fluorescence microscopy are available. In our study, the microscopic system was suitable for TAMRA but not NIR fluorescence detection. Unfortunately, autofluorescence of *P. minimum*, which was initially chosen as carrier organism for the DD-derived probe after Ianora *et al.* [56], strongly overlapped with TAMRA fluorescence (**Manuscript C**). Therefore we replaced *P. minimum* with the heterotrophic *O. marina*, which does not contain any photosynthetic pigments. However, to grow *O. marina* it was fed with the diatom *Dunaliella tertiolecta* whose fluorescence signal also interferes with that of TAMRA. To overcome this issue, *O. marina* cultures were kept in dark a few days before the copepod feeding experiments to arrest the growth of *D. tertiolecta*. The dinoflagellate *O. marina* absorbed TAMRA-PUA and the controls TAMRA-SA and TAMRA-N$_3$ and delivered them if added as food source to *A. tonsa*.

Unspecific fluorescence of the exoskeleton of copepods can occur during fluorescence staining (e.g., with TUNEL [59]). Within **Manuscript C** we introduce a method development to reduce unspecific fluorescence of TAMRA (monitored by TAMRA-N$_3$) on the surface and in the digestive tract of the copepods, which we overcame by starvation accompanied with defecation and washing of the copepods before fluorescence microscopy.

Optimization of the food carbon content as well as feeding and starvation times offered the possibility to observe probe accumulation in the copepod tissue: TAMRA-PUA selectively enriched in the gonads of a female *A. tonsa* (**Manuscript C**). Previously, Poulet *et al.* [64,179] showed that inhibitory compounds of diatoms caused cell fragmentation, formation of apoptotic bodies, and degradation of cytoplasm probably by accumulation in oocytes and gonads of the copepod *C. helgolandicus*. This accumulation might be possible by diffusion of metabolites between the gut epithelium and the closely located ovary [55]. Also copepod females of *C. helgolandicus* and *T. stylifera* fed with DD-loaded liposomes for several days displayed apoptotic gonadal tissue indicated by TUNEL staining [59]. These observations of changed ovarian architectures are at least partially explainable by the targeted delivery of the PUA probe. The remarkable selectivity of TAMRA-PUA accumulation in the gonads of *A. tonsa* (**Manuscript C**)

supports PUAs' activity as anti-proliferative metabolites and explains their role as teratogens in copepod reproduction without being harmful to the adult organisms [149].

A longer incubation period with higher *O. marina* cell densities demonstrated accumulation of TAMRA-SA in the lipid sac of a female. This observation was probably promoted by an increased ingestion rate due to the higher amount of the feeding dinoflagellate and thus carbon content in the medium [180]. Saturated aldehydes have similar properties, but are slightly less polar compared to PUAs, which probably caused accumulation in this storage area of the copepod. This result is able to explain why saturated aldehydes are biologically inactive [60].

Fluorescence microscopy has also been applied in the field of ABPP to target specific enzyme activities [181]. A general drawback, also existing in our study, is that one cannot distinguish between the signal of the ABP bound to a protein and the unbound probe. More sophisticated techniques circumvent this problem. Blum *et al.* [182] incorporated a fluorescence quencher in the RG of a cysteine protease probe that carried a fluorescent reporter tag. When this non-fluorescent probe covalently reacted with the target protease, the quencher-containing side chain was removed resulting in the formation of a fluorescently labeled protease that was monitored in real-time in a human cancer cell line [182] and later also in mice [166]. Besides utilizing fluorescence quenching, differences in fluorescence polarization between covalently probe-inhibited enzymes including serine hydrolases [183], arginine methyltransferases [184], and others [185] and the free ABPs were exploited.

5.3   Target identification of PUAs in planktonic organisms

Motivated by the accumulation of TAMRA-PUA in organisms revealed by fluorescence micros-copy (**Manuscript B** and **Manuscript C**) and reactivity of PUAs and other α,β-unsaturated alde-hydes with certain isolated proteins (**Manuscript D**, [86,87]), with proteins in cell lysates of a cancer cell line [78], and with model peptides in *in silico* studies [84], we followed a proteomic approach to study target proteins of PUAs in diatoms (**Manuscript B**). We chose again the DD-affected *P. tricornutum* as it is a diatom with sequenced genome [148], which facilitates protein identification. A screening of proteins that were covalently modified by PUAs in marine plankton has never been conducted before, but is an important step to unravel putative targets and to deduce mechanisms of action of these metabolites.

Two-step ABPP offers a method to study covalent interactions of minimally modified natural products with their targets in living organisms [122] (see chapter 1.3.1). After adding the DD-derived RG DDY to the biological system, we established a washing protocol to remove unbound DDY as well as salts, which interfere with 2D gel electrophoresis. We then lysed the cells and introduced the reporter TAMRA-N$_3$ by bioorthogonal Cu(I)-catalyzed azide-alkyne cycloaddition

(CuAAC) (Figure 7, bottom). Analytical platforms for ABPP (see chapter 1.3.2) often include enrichment of labeled proteins by biotin with (strept)avidin. After on-bead tryptic digestion, release of probe-labeled proteins needs harsh elution conditions and is frequently problematic [130], whereas enrichment of TAMRA-labeled proteins by anti-TAMRA-antibodies [186] bound to beads (after [187]) was tested unsuccessfully (data not shown). Other techniques like tandem orthogonal proteolysis (TOP) [117] are difficult to establish due to their complexity; furthermore, they use specific non-fluorescent reporter units that are not applicable for other purposes. Finally, difference gel electrophoresis (DIGE) [188] was chosen for protein identification within 2D gels. This high resolution technique visualized fluorescence of ABP-labeled proteins and unperturbed proteins prelabeled with a dye of different excitation and emission wavelengths compared to TAMRA and thus enabled exact protein location within each gel.

Sodium dodecyl sulfate polyacrylamide gel electrophoresis (SDS-PAGE, referred as 1D gel electrophoresis) is usually conducted for fast screening of fluorescent probe-labeled proteins in ABPP [107]. In a two-step ABPP with living *P. tricornutum* cells and TAMRA-N$_3$ as fluorescent reporter, DDY enabled labeling of proteins in a 1D gel (S2 Fig in **Manuscript B**), whereas the less reactive SA, for which only a few covalently labeled proteins have been reported [189,190], did not show any fluorescent band in accordance with uptake experiments (**Manuscript B**). Also in pharmaceutical screening, high quality probes and molecules together with structurally similar but inactive control partners are highly recommended as standard for target identification [191].

In consequence of the wide spectrum of physiological responses of plankton to PUAs, Adolph *et al*. suggested a non-specific chemical reactivity against biomolecules [60]. However, we only found a restricted amount of putative protein targets in the proteome of *P. tricornutum* (**Manuscript B**). This moderate labeling is in accordance with previous studies where DD was attacked by specific nucleophilic sites of proteins [86]. Although α,β-unsaturated aldehydes can be part of non-directed probes to target reactive nucleophilic moieties in proteins, natural product-derived ABPs like cinnamic aldehyde derivatives inhibited protein targets in a selective, stable manner [122].

Based on the identified target proteins of DDY in *P. tricornutum* (Table 1 in **Manuscript B**), PUAs may interfere with several metabolic pathways connected to autotrophic energy generation and conversion. Delivery of excitation energy between photosystem I and II by the light harvesting complex (LHC) [192] might be perturbed by covalently modified fucoxanthin chlorophyll *a/c* proteins. We identified four of these proteins; whereas one *Lhcx* gene product contributes to photoprotection, three *Lhcf* gene products are responsible for capturing photons (reviewed in [193]). A previously observed reduction in photosystem efficiency in *T. rotula* [74] and a transgenic *P. tricornutum* [97] by DD may be explained mechanistically by our results.

In the process of photosynthesis, the phosphorylation of adenosine diphosphate and inorganic phosphate to adenosine triphosphate (ATP) in the presence of protons moving down an electro-

chemical gradient across the membrane is used to store the energy of sunlight [194]. Among the PUA targets, we identified two probe-labeled ATP synthase subunits: ATP synthase subunit alpha (gene name *AtpA*) and ATP synthase subunit beta (gene name *AtpB*). Both belong to the extrinsic catalytic sector, CF1 of the chloroplastic ATP synthase [195]. Additionally, ATP synthases are located in the mitochondrial inner membrane. Changes in the spatial appearance of the subunits due to covalent modification might prohibit their incorporation in the ATP synthase enzyme complex with adverse consequences (e.g., the absence of the mitochondrial beta-subunit (gene name *Atp2*) in the green alga *Chlamydomonas reinhardtii* for example diminished mitochondrial respiration since the assembly of the ATP synthase complex could not be achieved [196]).

Within the Calvin cycle, the light-independent pathway of photosynthesis, we found as well two putative targets that might interfere with the energy household of *P. tricornutum*: the phospho-ribulokinase (PRK) and the ribulose-phosphate-3-epimerase (RPE). The latter catalyzes the reaction of D-xylulose 5-phosphate to D-ribulose 5-phosphate in the Calvin cycle and the pentose phosphate pathway in a reversible manner [197]. The product D-ribulose 5-phosphate is transformed to D-ribulose 1,5-bisphosphate by PRK under ATP consumption. D-ribulose 1,5-bisphosphate exclusively acts as acceptor for CO_2 in photosynthetic carbon assimilation [198]. PRK is part of a multi-enzyme complex and only active in its reduced form, in which certain cysteines do not form an intramolecular disulfide bridge [199]. If PUAs covalently react with those active thiols or other nucleophilic centers, spatial changes and loss of enzyme activities are possible. The ability for covalent alkylations of PRK with partial loss of functionality has already been demonstrated in different organisms [200,201].

The redox state of cysteines in PRK can be regulated by thioredoxin. Among the putative targets, we also found a predicted protein with a thioredoxin domain (accession No. B7FNS4). A modification of this predicted enzyme by PUAs may additionally interfere with redox homeostasis. Interestingly, cinnamic aldehyde that also bears a conjugated aldehyde covalently inhibited thioredoxin reductases [202]. Like thioredoxin, this oxidoreductase comprises a redox-active disulfide bond, which provides a point of attack for Michael acceptors in its reduced form.

Our data also provide a hint for labeled cytochrome *c* (accession No. A0T0C6, B5Y578) (Table S1 in **Manuscript B**) and thus overlap with a previous study by Sigolo *et al.* [87]. They found covalently DD-labeled cytochrome *c* that influenced the charge of the molecule and promoted structural and functional changes probably leading to impaired mitochondrial electron transport and apoptosis induction by release into the cytosole [87].

Complementary biological and chemical biology approaches will be essential to build sufficient confidence in targets [191]. Target protein identification can be performed by protein-specific fluorescent antibodies (e.g., by affinity enrichment of proteins labeled with a biotin-containing two-step ABP and subsequent western blot analysis). Enzyme-specific activity assays of cell lysates or recombinant proteins (e.g., produced by molecular cloning and gene expression in host

organisms followed by purification) can be performed to demonstrate restricted or loss of function after PUA incubation in a dose-dependent manner. Furthermore, those recombinant proteins labeled with the probe should be used as controls for liquid chromatography/tandem mass spectrometry (LC-MS/MS) analysis [116]. RNA interference and gene knockout of the putative target protein-encoding genes that match the PUA-induced phenotype [203] are further tools to confirm the target. However, these techniques are not yet established for diatoms. Only *P. tricornutum* has previously been shown to be accessible for targeted mutagenesis and gene insertion [204]. This species may allow generation of mutants lacking the specific amino acid of a target protein that is responsible for covalent bond formation with the reactive group of an ABP. Absence of labeling *in vivo* would confirm the labeling site. However, a previous precise identification of the labeling site of the target protein is necessary. This should include a reduction step prior to proteolysis to prevent reversible reactions and/or consecutive reactions [85]. In **Manuscript B**, the labeling site for fluorescent proteins could be assigned in some cases: it was mostly ascribed to lysine, which mainly underwent imine formation with the probe. This was also confirmed in a model investigation with lysine (**Manuscript D**).

Our results indicate that several important pathways involved in the energy household of *P. tricornutum* are specifically affected by PUAs (**Manuscript B**). However, no specific receptors of PUAs that mediate signal transduction like identified for the α,β-unsaturated aldehyde 4-hydroxy-2-nonenal (HNE) [205] or hints of covalent targeting of enzymes responsible for metabolic degradation of PUAs (see chapter 1.2.3) were found.

Besides putative target proteins in *P. tricornutum*, I also detected promising fluorescently labeled proteins (data not shown, experimental conditions are as in **Manuscript B**) after *in vivo* two-step ABPP of the green alga *Dunaliella tertiolecta*, which probably perceives PUAs as allelochemical [75]. *In vitro* protein labeling experiments with zooplankton samples mainly containing *C. helgolandicus* resulted in fluorescent proteins in 1D and 2D gels prepared by Seifert [206] that support the susceptibility of copepod proteins for covalent reactions with PUAs [59]. Future studies should investigate if protein target patterns found in *P. tricornutum* overlap with those of other organisms or if biological effects of PUA-induced phenotypes can be assigned to other perturbations.

In addition to covalent modifications, the interactions of natural products with proteins also include weak, non-covalent interactions [111]. These interactions might be visualized in future studies with ABPs containing a photo-reactive cross-linker, which enables permanent labeling with proteins in close proximity [111].

Since Gallina *et al.* observed algal species- and molecular weight-dependent differences in PUAs' mode of action regarding NO production [102] and Varrella *et al.* reported PUA-dependent responses on gene regulation in sea urchin embryos [101], also other PUA-derived RGs than DDY

would contribute to the mechanistic understanding of these oxylipins. However, during probe design conjugation of the Michael acceptor with the terminal alkyne must be excluded to avoid altered activity. Unfortunately, efforts to synthesize 2*E*,4-octadien-7-ynal analogous to DDY [147] via a Negishi-type cross coupling and another route, which also couples C3 and C5 synthons, failed during the diploma thesis of Pfeifer-Leeg [207].

Also other oxylipins like fatty acid hydroxides and epoxy alcohols (Figure 4) or simply polyunsaturated fatty acids (PUFAs) were suspected to mediate biological effects [45,57] and may be translated to RGs for future ABPP to assign their influence and mechanisms.

In contrast to covalent reactions of proteins, transcriptional responses are less intermediate. They do not necessarily involve a covalent interaction of the electrophile and represent another path to study effects of electrophiles [78] (Figure 11). A few transcriptomic studies on the influence of PUAs or PUA-producing diatoms on planktonic organisms are available [97-101]. Induction of cytoskeletal instability, a mode of action of PUAs classified by Caldwell [55] was supported by regulation of gene expression in the sea urchin *Paracentrotus lividus* [101] and confirmed in the diatom *C. helgolandicus* [98]. Expression of mRNA of tubulins, which form the building blocks of microtubules, one of the active components of the cytoskeleton, was downregulated in response to a diet of the PUA-producing *S. costatum* compared to a control in *C. helgolandicus* [98].

Also our dataset provides one predicted protein of the cell division protein FtsZ family (accession No. B7FUQ1) structurally similar with tubulins that indicates a direct PUA action. However, this putative target was only found in one of the three 2D gels besides other proteins (Table S1 in **Manuscript B**) and requires additional proof.
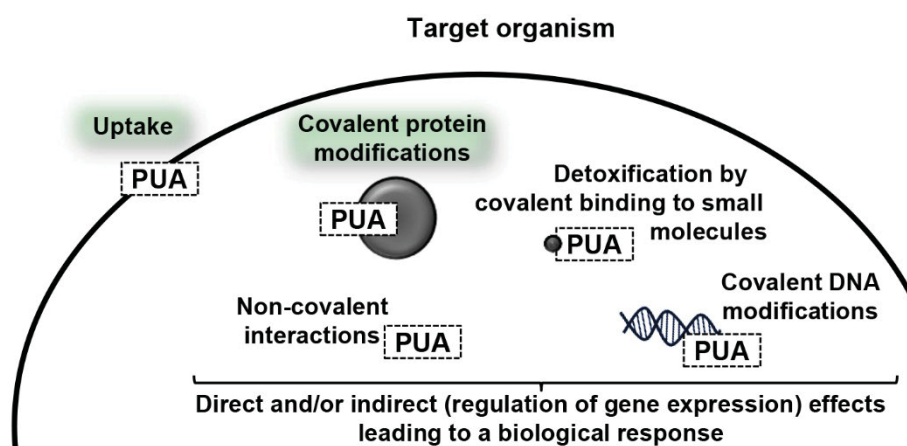
Figure 11. Possible consequences of PUA uptake in organisms. Organisms take up PUAs that may react covalently with proteins ([86,87], **Manuscript B** for *P. tricornutum*), DNA [81,89], and other nucleophilic metabolites like small molecules [84] or interact non-covalently [81]. The sum of direct effects (e.g., protein dysfunction and blocked replication caused by covalent protein and DNA modifications, detoxification by small molecules) and indirect effects like gene expression regulation caused by perturbed biological processes in consequence of covalent and non-covalent interactions results in the PUA-induced phenotype [78]. The highlighted fields were successfully investigated in this thesis.

Because of the rather unspecific chemical reactivity of α,β-unsaturated aldehydes, one would generally not consider them as drugs for pharmaceutical purpose. This reactivity makes identification of the mechanisms of action more difficult [208] compared to other natural products that highly specifically and selectively bind to targets, which are mainly proteins [116].

The influence of PUAs on planktonic organisms has to be seen as a combination of target effects (Figure 11). This is supported by different putative target proteins in *P. tricornutum* (**Manuscript B**) and affected expression patterns of different target genes in copepods and sea urchins having roles in e.g., development, differentiation, stress response, apoptosis regulation, detoxification, and defense [98,99,101]. Whereas direct effects can be linked to covalent bond formations (e.g., with proteins) that immediately interfere with biological processes (e.g., due to protein dysfunction), indirect effects like regulation of gene expression (e.g., of signal transduction genes due to stress reactions [101]) might be the response of affected biological pathways and processes by covalent and non-covalent interactions. However, linking these interactions on a molecular level with cellular and physiological processes and even ecological consequences is a key topic in understanding the activity of oxylipins.

In an exemplary study, the link between direct protein modifications and altered transcription pathways based on direct effects and via signal transduction pathways has been established for HNE, a toxic and well-studied α,β-unsaturated aldehyde, on a human colon cancer cell line [78]. In this cell line, the heat shock factor 1 (HSF1) that is a transcription factor and normally kept in an inactive complex by heat shock proteins (Hsp) was released out of the complex and thus activated by HNE adduct formation with Hsp70 and Hsp90. Subsequently, HSF1-mediated gene expression induced a few genes relevant in protection against electrophilic stress (e.g., antiapoptotic Bd-2 proteins) [78].
Our data set does not provide evidence of a Hsp target that points towards a similar mechanism of action like HNE. However, the concept of systems analysis illustrates that connection of covalently modified proteins and gene regulation, which might be also extended by DNA modifications, has the powerful potential to make the complex mechanisms of action of the investigated electrophiles even more accessible than the separate view of target genes and proteins [78].

Electrophiles are known to form covalent bonds with nucleic acids, their best studied targets, that block replication [78] and may induce apoptosis of cells that were seriously affected [55]; motivated by the fact that even covalent DD modifications with purified nucleotides and DNA are known [88,89] (Figure 11), I also addressed DNA as target. Only recently, even electrophilic ABPs for detection of RNA were introduced by McDonald *et al.* [209]. In the course of this study, catalytic RNAs of an archaebacterium covalently bound to an epoxide-containing ABP [209].
Following the concept of two-step ABPP for proteins (**Manuscript B**), I also transferred the technique to find modified DNA in the copepods *C. helgolandicus* and *A. tonsa in vivo.* According

to the previously established feeding protocols (**Manuscript C**, [56]), the carrier organisms *P. minimum*, *Rhodomonas salina*, or *O. marina* were labeled with DDY and used as food source for copepods. After feeding and starvation, copepods were lysed, genomic DNA (gDNA) was extracted, and CuAAC was applied to introduce TAMRA-N$_3$ (analogues experimental conditions are described in [210]). Besides this *in vivo* (Figure 12, lane 4) also *in vitro* studies, in which DDY was added to the extracted gDNA (Figure 12, lane 2), failed probably because of unfavorable CuAAC conditions and H$_2$O$_2$ formation that may have caused DNA degradation [211].

Also Lembke did not observe any gDNA fluorescence in systematic *in vivo* and *in vitro* two-step incubation experiments with gDNA of *P. tricornutum* in her master thesis; she tested different CuAAC conditions while facing the same problems of DNA degradation [210]. Remarkably, also the simplest try to label isolated gDNA of different origin with TAMRA-PUA was not successful (Figure 12, lane 3 for *C. helgolandicus*; see [210] for experimental details).

1	DNA ladder
2	*in vitro*: **DDY**, **TAMRA-N$_3$**
3	*in vitro*: **TAMRA-PUA**
4	*in vivo*: **DDY**, **TAMRA-N$_3$**
5	control

Agarose gel prior to nucleic acid staining   Agarose gel treated with GelRed™
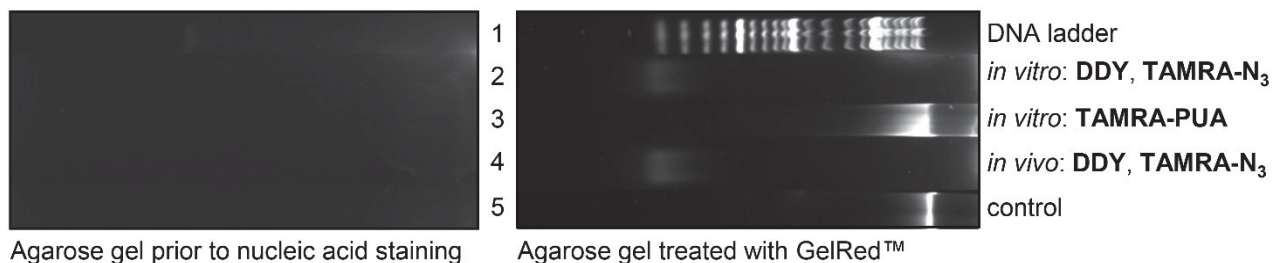
Figure 12. DNA labeling experiments with *C. helgolandicus*. In-gel fluorescence detection was conducted before (left) and after staining of the agarose gel with the nucleic acid dye GelRed™ (right), no labeling experiment resulted in TAMRA-fluorescence. *C. helgolandicus* was fed for 3 days on *R. salina,* copepods were starved, and gDNA was extracted (lane 5). *In vitro* experiments with addition of 100 µM DDY to this sample followed by CuAAC with TAMRA-N$_3$ revealed non-fluorescent, degraded gDNA (lane 2), whereas addition of 100 µM TAMRA-PUA (lane 3) resulted in non-fluorescent gDNA with weak signs of degradation. The result of an *in vivo* experiment with *R. salina* preincubated with 100 µM DDY and fed to copepods followed by copepod starvation, gDNA extraction, and CuAAC (lane 4) is similar to degraded DNA in the *in vitro* experiment. Experimental conditions were conducted as described in [210] and **Manuscript C**. (Abbreviations – CuAAC: Cu(I)-catalyzed azide-alkyne cycloaddition; gDNA: genomic DNA)

In conclusion, we found no evidence of a stable, covalent labeling of DNA. However, inappropriate experimental conditions, fluorescence signals below the detection limit, the lack of enrichment of probably labeled DNA as conducted with ABPs for RNA labeling by McDonald *et al.* [209], or simply absence of covalent labeling can explain missing fluorescence signals in agarose gels.

The absence of in-gel fluorescence in DNA labeling experiments is also explainable by protection mechanisms. The PUA-producing *S. costatum* for example is known to be comparatively resistant to PUAs [75]; this species also withstood two-step ABPP with DDY without recognizable fluorescence in 1D gels (data not shown) [147].

Efficient protection mechanisms maybe linked to the inability of PUAs or related oxylipins to enter cells [60] or to detoxification of PUAs (e.g., by aldehyde dehydrogenases, by general pathways in protection against electrophiles, or by small peptides like glutathione (see chapter

1.2.3)). In my diploma thesis, I demonstrated complete turnover of glutathione with DDY in an aqueous buffer within minutes [147]. However, attempts to study detoxification products in an approach similar to two-step ABPP by using DDY and TAMRA-N$_3$ failed. Therefore, *P. tricornutum* and *S. costatum* were incubated with DDY (as described in **Manuscript B**) or *C. helgolandicus* was fed with DDY-preincubated *O. marina* (as described in **Manuscript C**). TAMRA-N$_3$ was introduced after sonication (as described in **Manuscript B**), proteins were removed by precipitation with acetonitrile, and the samples were analyzed by LC-MS and a photodiode array detector. However, no small molecules that were covalently linked to the ABP could be identified (data not shown) because of the limited detection possibilities of TAMRA restricted to UV-Vis absorption in this approach. To overcome this issue, additional detection strategies are necessary, which are addressed in the next section.

5.4   Reporter tag development for multiple detection possibilities

Fluorescent, bioorthogonal reporters are a widely distributed tool in chemical biology (e.g., in two-step ABPP as shown before (**Manuscript B**)) since they can be easily attached to the complementary handle without interfering with other molecules. Besides fluorescence, also mass spectrometry offers a powerful detection method. Tags that contain bromine and chlorine for small and biomacromolecule labeling offer a characteristic isotopic pattern (e.g., ^{79}Br and ^{81}Br are abundant in almost equal amounts) and can help to locate tagged molecules (see chapter 1.3.3) [136-139,141,143-145].

Following the concepts of fluorescence and mass spectrometric detection strategies we introduced the synthesis and application of a small, azide tagged reporter for bioorthogonal connection to terminal alkynes via CuAAC. The molecule 4-(3-azidopropoxy)-5-(4-bromophenyl)-2-(pyridin-2-yl)thiazole (BPT) supports fluorescence and UV detection based on the well investigated ethers of the 4-hydroxy pyridylthiazol basic chromophore [212] as well as mass spectrometric detection monitored by the characteristic isotopic pattern of bromine (**Manuscript D**).

The high quantum yields in nonpolar to aqueous environments containing only little amounts of organic solvent offer a wide application range (e.g., in-gel fluorescence detection of proteins, LC coupled to UV-Vis and fluorescence detectors). Thereby, intersystem crossing often caused by heavy atoms [213] did not substantially reduce fluorescence in contrast to a dansyl molecule brominated at the naphthalene aromatic system (**Manuscript D**).

To circumvent the need of expensive lab equipment for fluorescence detection (e.g., in 1D and 2D gels) and to perform experiments with plankton on the sampling site without transfer of equipment, we adjusted excitation and emission wavelengths of BPT to standard laboratory devices (365 nm UV-transilluminator, digital camera, and a simple, commercial UV filter), which are available in most laboratories.

In a model reaction, the arbitrary chosen protein catalase was labeled with DDY and connected via CuAAC with different reporter molecules. BPT revealed superior fluorescence compared to fluorophore azides of the commonly used dansyl and 4-nitrobenzo[*c*][1,2,5]oxadiazole systems (**Manuscript D**).

Previously, dansyl chloride has been introduced as derivatization agent for enhanced electrospray ionization (ESI) of polar metabolites containing amine or phenolic hydroxyl groups [214] in positive ionization mode; linear responses of tested amino acids were increased by over two orders of magnitude compared to non-derivatized samples [214]. BPT is even superior to the established dansyl system, which was shown in a model reaction with lysine and DDY to form an imine and subsequent CuAAC with BPT or the above mentioned fluorophore azides followed by LC-MS measurements (**Manuscript D**). Besides detection, BPT enhanced recognition of the labeled substance by introduction of a characteristic isotopic pattern. As dansyl chloride and other derivatization reagents [141,145,214], BPT also increases retention of polar metabolites in reversed phase chromatography and thus gives additional, orthogonal information to identify labeled molecules.

For small molecules like BPT-labeled lysine, location within the LC-MS chromatogram was easily done by isotope cluster analysis (incorporated within the MassLynx™ software) with fixed mass ratios [141]. However, automated identification of BPT-labeled peptides of the model catalase with this tool was not applicable, because of the decreasing bromine influence on the isotopic pattern with increasing molecular mass. Therefore, pattern-searching algorithms that have already been developed for peptide identification with certain bromine and chlorine reagents [136,139] could be tailored for BPT together with bioinformaticians to improve automated data mining. Additionally, consideration of an introduced mass-defect in peptides caused by bromine could improve sequence coverage of proteins, which has already been demonstrated with isotope-differentiated binding energy shift tags (IDBEST™) [215].

Besides BPT's use as reporter in model reactions (**Manuscript D**) and in in-gel fluorescence detection with plankton samples on-site and in the lab [206,210], its orthogonal detection possibilities probably could make it a suitable reporter to identify detoxification products of PUAs by LC-MS in future studies. Preliminary experiments with *P. tricornutum* revealed no PUA-labeled small molecules in a two-step incubation procedure (data not shown, procedure similar to methods described in **Manuscript B** with additional protein precipitation); however, further method development to optimize experimental conditions of CuAAC due to minor formation of unidentified side products is necessary.

Halogenated metabolites in algae and other organisms occur rarely [216,217] compared to total cellular substances and will not severely interfere with LC-MS approaches; additionally, naturally organobromine compounds may be excluded by lacking BPT fluorescence or at least UV absorption by using the corresponding detectors coupled on-line between LC-MS systems. The outcome

of these detoxification studies with small molecules may contribute to the understanding why some copepods, algae, and bacteria are less inhibited and influenced by PUAs than others [75].

Whereas cytotoxicity of copper and side reactions of CuAAC can preclude or impair some applications (e.g., *in vivo* imaging, DNA labeling due to degradation presented in chapter 5.3), other bioorthogonal coupling reactions like tetrazine ligation via inverse electron-demand Diels-Alder cycloaddition may be more suitable to these requirements [119,121]. If BPT is not applicable for the desired purpose, alternative bioorthogonal coupling sites (Figure 13 B–D) can be incorporated by simply modifying the synthetic procedure (Scheme 1 in **Manuscript D**): after the Hantzsch thiazole reaction to form the 4-hydroxythiazole A (Figure 13), Williamson ether synthesis and additional steps may be used.
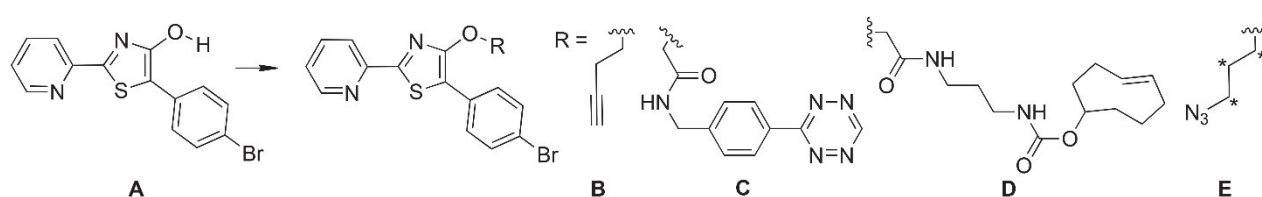
Figure 13. **Potential modifications of BPT that contain a terminal alkyne (B), tetrazine (C), cyclooctene (D), or stable isotopes (E).** *Indicates a ^{13}C isotope.

Other possible synthetic modifications of BPT include incorporation of ^{13}C isotopes in the azidopropyl side chain (e.g., via commercially available ^{13}C$_3$-1-bromo-3-chloropropane and subsequent synthesis of the azide E (Figure 13)) that may enable quantification procedures of samples labeled with the light and heavy form of the reporter similar to already existing approaches for small molecules [214] or proteins (e.g., isotope-coded affinity tags (ICAT))[133,135]. Therefore, one sample labeled with the heavy and another labeled with the light reporter are combined before LC-MS measurements to determine abundances.

Application of BPT and related molecules might be advantageous for diverse biological and mass spectrometric fields. Lots of examples in which artificial chemical entities with bioorthogonal coupling sites were incorporated in biomolecules by using the cell's own biosynthetic machinery (see chapter 1.3.3) are known (e.g., palmitoyltransferases introduced an artificial alkynyl-palmitic acid to cysteine residues in proteins to form *S*-palmitoylation) [119,129].

Besides optical microscopy, BPT would be also applicable for matrix-assisted laser desorption/ ionization (MALDI) imaging. Thereby, BPT-labeled molecules may contribute to the understanding of biological processes orthogonal to optical microscopy. Although MALDI imaging suffers from restricted resolution compared to optical microscopy, it offers the big advantage to characterize and even identify the biological composition of the sample by its mass.

These putative applications demonstrate that BPT is a versatile and developable tool for bioorthogonal coupling and detection.

6   SUMMARY

Diatoms are among the ecologically most significant groups of organisms in the marine environment. Some species produce biologically active polyunsaturated aldehydes (PUAs) during predation by copepods that interfere with the reproduction of these grazers. In addition, PUAs are released by intact cells and have been suggested to act as info- and allelochemicals and to participate in cell-to-cell signaling. However, targets that are covalently modified by these oxylipins have not been reported to date.

The core of this thesis was to address the uptake and covalent targets of PUAs in marine organisms. This study thus aims to contribute to a more fundamental understanding of the mechanisms of action of these oxylipins, which have been poorly investigated so far.

To pursue this goal, I successfully designed and applied molecular probes as well as versatile profiling techniques covering fluorescence microscopy and covalent target investigations in planktonic organisms, all of which were designed after activity-based protein profiling (ABPP) concepts.

As a starting point, I observed PUA-production of the microalgae *Skeletonema marinoi* and *Phaeocystis pouchetii* in a mesocosm study that was designed to discover trophic relations between grazers and primary producers. During this study, I quantified dissolved PUAs as well as PUA production during cell damage (Figure 14, top), which correlated to the cell density of *S. marinoi* during its bloom. The determined concentrations of dissolved PUAs contribute to the so far poorly addressed quantification of these metabolites in field and near-field studies, which are crucial to assess PUAs' ecological roles and significance of laboratory experiments.

Microzooplankton grazing experiments on phytoplankton during mesocosm experiments demonstrated that PUAs, which were probably released during filtration caused by damaged cells, suppressed phytoplankton growth in filtrate-added, diluted treatments. This PUA-triggered diminished growth resulted in an underestimation of grazing by microzooplankton, a process that might be also relevant for other allelochemicals, especially in dense blooms.

To investigate the origin of PUAs' biological functions in plankton, I addressed direct uptake and accumulation of the very potent PUA 2*E*,4*E/Z*-decadienal (DD) in a targeted approach. Therefore, I utilized a molecular probe (TAMRA-PUA) consisting of a C10 α,β,γ,δ-unsaturated aldehyde, linked at the terminus to the well-established tetramethylrhodamine (TAMRA) fluorophore, as well as a newly designed control probe (TAMRA-SA) based on bioinactive saturated aldehydes.

Development of probe-based fluorescence microscopy provided insights into the uptake of PUAs in different planktonic organisms. In the model diatom *P. tricornutum*, which previously gave

evidence for a DD-induced nitric oxide-based intercellular signaling system, passage across the membrane (Figure 14, bottom left) and strong intracellular accumulation without compartmentation of TAMRA-PUA was observed. In contrast, only weak enrichment of TAMRA-SA occurred.
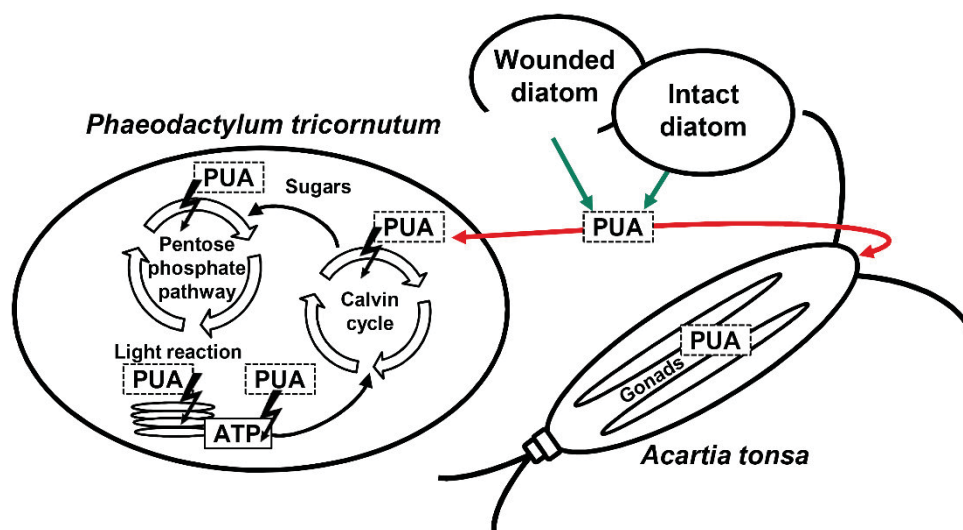
Figure 14: Schematic summary of core results. Firstly, the thesis comprises quantification of dissolved PUAs in sea water and of PUA production during algal cell damage in a mesocosm study (green arrows, top). Secondly, I established incubation protocols (red arrows) of a PUA-derived probe in the diatom *P. tricornutum* (bottom left) and the copepod *A. tonsa* (bottom right) that revealed PUA uptake and accumulation (depicted as PUA). Thirdly, covalent targets of these Michael acceptors were identified by a two-step ABPP approach in *P. tricornutum*; PUAs may interfere with the displayed metabolic pathways and processes in this alga by covalent modification of certain identified proteins (represented by flashes and PUA , bottom left). Finally, a reporter tag, which offers orthogonal detection strategies and can be used for molecular probes, was introduced (not shown). (Abbreviation – ATP: adenosine triphosphate)

Development and successful application of a novel incubation procedure that mimics natural feeding of copepods by carrier organisms for probes revealed a strong accumulation of TAMRA-PUA in the ovaries of *Acartia tonsa* (Figure 14, bottom right). Discernable effects of PUAs on the copepod ovarian architecture have been shown before, but optical visualization of a specific enrichment was displayed for the first time and supports the teratogenic role of PUAs.

The development of a two-step ABPP protocol allowed covalent protein target identification in *P. tricornutum*. Therefore, a C10 α,β,γ,δ-unsaturated aldehyde (DDY), which was slightly modified with an alkyne group at the alkyl terminus, was utilized. This enabled bioorthogonal introduction of the TAMRA fluorophore azide via the well-established Cu(I)-catalyzed azide-alkyne cycloaddition (CuAAC) after cell lysis. 2D gel electrophoresis revealed moderate fluorescent labeling of target proteins that were identified by liquid chromatography/tandem mass spectrometry.

This proteomic survey allowed me to draw a model of potentially influenced key biological pathways and processes by covalent modifications of protein targets with PUAs in *P. tricornutum* (Figure 14, bottom left). Besides proteins functioning in light harvesting and photoprotection as part of the light harvesting complex, subunits of adenosine triphosphate synthases were found as targets. Furthermore, phosphoribulokinase that supplies Calvin cycle intermediates for further

CO_2 assimilation and ribulose-phosphate-3-epimerase that also functions in the Calvin cycle as well as in the reverse pentose phosphate pathway are putative targets.

Future target studies with complementary approaches and additional organisms should be conducted in order to confirm and examine protein targets and affected biochemical pathways.

In addition to proteins, I also addressed covalently modified DNA, which may block replication, and detoxification reactions of PUAs with small molecules. Therefore, I combined the introduced feeding protocol for copepods with a two-step probe incubation procedure; however, it was not possible to detect specific fluorescent copepod DNA.

Moreover, the UV-Vis absorption of the TAMRA reporter was not adequate to screen for covalently probe-modified small molecules in plankton in a two-step application by means of liquid chromatography coupled to mass spectrometry (LC-MS) and a photodiode array detector.

For future investigations of this issue, an azide-containing reporter tag, namely 4-(3-azidopropoxy)-5-(4-bromophenyl)-2-(pyridin-2-yl)thiazole (BPT), was developed and applied. It can be coupled to terminal alkynes via bioorthogonal CuAAC. BPT offers multiple detection possibilities: (I) fluorescence, (II) UV, and (III) mass spectrometric detection by incorporation of bromine. The reporter provides high quantum yields in aqueous to nonpolar environments and the synthetic strategy enables the possibility to introduce other bioorthogonal coupling sites than azides.

Model reactions with an amino acid and a protein modified with the PUA-derived alkyne DDY confirmed reactivity of these Michael acceptors; additionally, they demonstrated superior detection of BPT via LC-MS by utilizing electrospray ionization and in-gel fluorescence detection, compared to two other azide-tagged commercial fluorophores and a bromine/azide-containing one.

In sum, I examined PUA prevalence during a mesocosm study and my research introduces methodological tools to study the fate of oxylipins in plankton. It presents data for an enhanced understanding of mechanisms of action of PUAs: uptake studies illustrate how different organisms perceive PUAs and bioinactive unsaturated aldehydes. Additionally, a moderate number of covalently labeled proteins by the PUA probe in a model diatom revealed new targets and provides insights into possibly affected biological pathways. The development of a reporter enables orthogonal detection possibilities that might be administrable to examine detoxification mechanisms.

PUA-induced phenotypes of marine planktonic organisms have to be seen as sum of covalent reactions with biomolecules, which were illuminated in this work, and non-covalent interactions. Whereas a recently increasing number of studies performed by others are concerned with PUAs' influence on the transcriptome, this work provides the first proteomic approach. Linking PUA interactions on a molecular level with cellular, physiological, and even ecological consequences is a complex, interdisciplinary task and still requires further investigation and should be also widened to a comprehensive understanding of general action of oxylipins. The introduced probes and methods provide valuable and versatile tools to address this superior goal.

7 ZUSAMMENFASSUNG

Diatomeen gehören zu den ökologisch bedeutendsten Organismen im Meer. Einige Arten produzieren polyungesättigte Aldehyde (PUA) während der Prädation durch Copepoden, die die Reproduktion dieser Fraßfeinde beeinträchtigen. Außerdem werden PUA von intakten Zellen abgegeben und es gibt Hinweise auf Funktionen als Info- und Allelochemikalien sowie in der Zell-Zell Signalweiterleitung. Jedoch wurden noch keine kovalent modifizierten Targets dieser Oxylipine publiziert.

Das Ziel meiner Arbeit war es, die Aufnahme und kovalent modifizierte Targetmoleküle der PUA in marinen Organismen zu untersuchen. Diese Arbeit soll damit zum Verständnis der Wirkmechanismen dieser Oxylipine, die bisher nur wenig untersucht worden sind, beitragen.

Um dieses Ziel zu verfolgen, habe ich erfolgreich molekulare Sonden und vielseitige Profilingtechniken konzipiert und angewendet, die sowohl Fluoreszenzmikroskopie als auch kovalente Targetidentifizierungen in planktonischen Organismen umfassen und nach dem aktivitätsbasierten Protein-Profiling (ABPP) und zugehörigen Sonden entworfen wurden sind.

Als Ausgangspunkt habe ich die Bildung von PUA durch die Mikroalgen *Skeletonema marinoi* und *Phaeocystis pouchetii* in einem Mesokosmos-Experiment, das der Untersuchung von trophischen Interaktionen zwischen Fraßfeinden und Primärproduzenten diente, beobachtet.

Während des Versuchs quantifizierte ich die im Meerwasser gelösten und die während der Zerstörung der Algenzellen gebildeten PUA (Abbildung 15, oben), die mit der Zellzahl von *S. marinoi* während ihrer Blüte korrelierten. Die Daten der gelösten PUA tragen zu den bisher wenig verfügbaren Quantifizierungen dieser Metabolite in Feld- und feldähnlichen Experimenten bei, die einen entscheidenden Parameter in der Einschätzung der ökologischen Rolle der PUA und der Aussagekraft von Laborexperimenten darstellen.

Fraßexperimente des Mikrozooplanktons auf das Phytoplankton während des Meskosomos-Versuchs zeigten, dass sich PUA, die wahrscheinlich während des Filtrationsvorganges durch zerstörte Zellen frei wurden, negativ auf das Phytoplanktonwachstum in der mit dem Filtrat verdünnten Probenbehandlung auswirkten. Das durch PUA ausgelöste geringere Phytoplanktonwachstum führte zur Unterschätzung des Fraßverhaltens des Mikrozooplanktons – ein Prozess, der auch für andere Allelochemikalien vor allem in dichten Phytoplanktonblüten relevant sein kann.

Um die Ursache der Bioaktivität von PUA im Plankton zu erforschen, habe ich die direkte Aufnahme und Anreicherung des sehr aktiven 2*E*,4*E/Z*-Decadienal (DD) in einem zielgerichteten Ansatz untersucht. Dabei verwendete ich eine molekulare Sonde (TAMRA-PUA), basierend auf einem

C10 α,β,γ,δ-ungesättigten Aldehyd, welcher am Alkylende an das etablierte Tetramethylrhoda-min (TAMRA)-Fluorophor gebunden ist, sowie eine neu entwickelte Kontrollsonde (TAMRA-SA) auf Basis von biologisch inaktiven gesättigten Aldehyden.

Die Entwicklung von sondenbasierten Fluoreszenzmikroskopie-Protokollen ergab Erkenntnisse über die Aufnahme von PUA im Plankton. In der Modelldiatomee *P. tricornutum*, in der es Hin-weise auf ein DD-induziertes, interzellulares Signalweiterleitungssystem auf Basis von Stickstoff-monoxid gibt, passierte die Sonde TAMRA-PUA die Membran (Abbildung 15, unten links) und verteilte sich gleichförmig in den Zellen, wohingegen TAMRA-SA eine geringere Anreicherung zeigte.
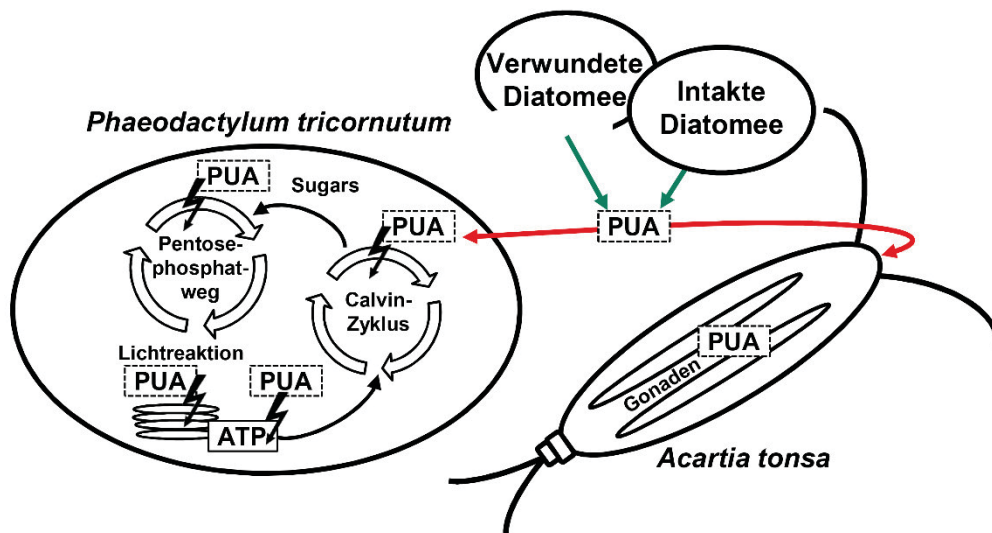
Abbildung 15: Schematische Zusammenfassung der zentralen Ergebnisse. Die Dissertation beinhaltet im ersten Teil die Quantifizierung von im Meerwasser gelösten PUA und die PUA-Bildung während der Zerstörung von Algenzellen in einem Mesokosmos-Experiment (grüne Pfeile, oben). Zweitens habe ich Inkubationsprotokolle (rote Pfeile) einer PUA-abgeleiteten Sonde eingeführt, die die PUA-Aufnahme und -Anreicherung in der Diatomee *P. tricornutum* (unten links) und dem Copepoden *A. tonsa* (unten rechts) demonstrierten (dargestellt als PUA). In einem dritten Ansatz wurden kovalente Targets dieser Michael-Akzeptoren mittels eines zweistufigen ABPP-Ansatzes in *P. tricornutum* identifiziert; PUA beeinträchtigen möglicherweise die abgebildeten Stoffwechsel-prozesse in dieser Alge durch kovalente Modifikationen von bestimmten Proteinen (repräsentiert durch Blitze und PUA , unten links). Schließlich wurde ein Reportermolekül eingeführt, welches orthogonale Detektionsstrategien erlaubt und für molekulare Sonden verwendet werden kann (nicht dargestellt). (Abkürzung: ATP – Adenosintriphosphat)

Die Entwicklung und erfolgreiche Anwendung eines neuen Inkubationsprotokolls für Sonden, welches das natürliche Fraßverhalten der Copepoden mit Hilfe von Trägerorganismen nachahmt, ergab eine starke Anreicherung von TAMRA-PUA in den Ovarien von *Acartia tonsa* (Abbildung 15, unten rechts). Erkennbare Einflüsse von PUA auf die Ovarienstruktur wurden schon vorher ge-zeigt. Die optische Visualisierung dieser Anreicherung gelang jedoch in dieser Arbeit zum ersten Mal und unterstützt die teratogene Wirkung der PUA.

Die Entwicklung eines zweistufigen ABPP-Protokolls ermöglichte die kovalente Proteintargetiden-tifizierung in *P. tricornutum*. Dafür wurde ein C10 α,β,γ,δ-ungesättigtes Aldehyd (DDY), welches mit einem Alkin am Alkylterminus modifiziert wurde, verwendet. Dies ermöglichte die bioortho-gonale Einführung des TAMRA-Fluorophorazids durch die etablierte Cu(I)-katalysierte Azid-Alkin Cycloaddition (CuAAC). Die 2D Gelelektrophorese ergab eine mäßige Anzahl markierter Proteine in *P. tricornutum*, die mit Hilfe der Flüssigkeitschromatographie/Tandem-Massenspektrometrie identifiziert wurden.

Dieser proteomische Ansatz ermöglichte mir das Erstellen eines Modells, welches potentiell beeinflusste Stoffwechselvorgänge in dieser Alge bedingt durch kovalente Modifikationen von Targetproteinen mit PUA darstellt (Abbildung 15, unten links). Neben Proteinen, die im Lichtsam-melkomplex zum Einfangen von Licht und für photoprotektive Vorgänge nötig sind, wurden Un-tereinheiten der Adenosintriphosphat-Synthase als Targets gefunden. Außerdem wurden Phos-phoribulokinase, welches Zwischenprodukte des Calvin-Zyklus für die anschließende CO_2 Auf-nahme bereitstellt, und Ribulosephosphat-3-epimerase, das ebenfalls im Calvin-Zyklus als auch im reversiblen Pentosephosphatweg aktiv ist, gefunden.

Zukünftige Targetstudien mit komplementären Ansätzen und weiteren Organismen sollten durchgeführt werden, um Proteintargets und beeinflusste biologische Prozesse zu bestätigen und aufzuklären.

Neben markierten Proteinen habe ich ebenso kovalente DNA-Modifikationen, die die Replikation behindern können, sowie Detoxifizierungsreaktionen von PUA mit kleinen Molekülen untersucht. Dafür kombinierte ich das Inkubationsprotokoll für Copepoden mit der zweistufigen Sonden-inkubation, jedoch war es nicht möglich, fluoreszierende Copepoden-DNA zu detektieren.

Auch die UV-Vis-Absorption des TAMRA-Reporters war nicht ausreichend für ein Screening von kovalent modifizierten niedermolekularen Verbindungen im Plankton; dafür wendete ich eine zweistufige Sondeninkubation in Kombination mit Flüssigkeitschromatographie, gekoppelt mit Massenspektrometrie (LC-MS), und einen Photodiodenarray-Detektor an.

Für zukünftige, weiterführende Untersuchungen dieses Sachverhaltes wurde ein azidhaltiges Reportermolekül entwickelt, synthetisiert und angewendet. 4-(3-Azidopropoxy)-5-(4-bromophe-nyl)-2-(pyridin-2-yl)thiazol (BPT) kann zu terminalen Alkinen mittels der bioorthogonalen CuAAC gekoppelt werden und ermöglicht verschiedene Detektionsmöglichkeiten: (I) Fluoreszenz-, (II) UV- und (III) massenspektrometrische Detektion durch den Einbau von Brom.

Der Reporter ermöglicht hohe Quantenausbeuten in wässriger sowie unpolarer Umgebung. Die Syntheseroute erlaubt neben der Synthese des Azids auch die Möglichkeit zur Einführung ande-rer bioorthogonaler Kopplungsstellen.

Modellreaktionen mit einer Aminosäure und einem Protein, die mit dem PUA-abgeleitetem Alkin DDY modifiziert worden sind, demonstrierten die Reaktivität der PUA. Diese zeigten außerdem

die, verglichen mit zwei kommerziell erhältlichen azidhaltigen und einem azid-/bromhaltigen Fluorophor, überlegene Detektion von BPT mittels LC-MS und Elektrospray-Ionisierung sowie mittels in-Gel Fluoreszenz.

In meiner Dissertation habe ich das Vorkommen der PUA während eines Mesokosmos-Experiments analysiert. Meine Arbeit stellt methodische Werkzeuge vor, um Oxylipine im Plankton zu untersuchen, und präsentiert Daten zum verbesserten Verständnis der Wirkmechanismen der PUA: Aufnahmeexperimente zeigen, wie verschiedene Organismen PUA und bioinaktive gesättigte Aldehyde wahrnehmen. Die mäßige Anzahl von kovalent modifizierten Proteinen durch die Sonde in einer Modellalge ergab zudem neue potentielle Targets und Einblicke in möglicherweise beeinflusste biologische Prozesse der PUA. Der neu entwickelte Reporter ermöglicht orthogonale Detektionsmöglichkeiten, die hilfreich für die zukünftige Untersuchung von Detoxifizierungsmechanismen sein können.

Der PUA-induzierte Phänotyp von Organismen im marinen Plankton muss als Summe von kovalenten Reaktionen mit Biomolekülen, die in dieser Dissertation beleuchtet worden sind, und nichtkovalenten Interaktionen angesehen werden. Während die in letzter Zeit steigende Anzahl von Studien den Einfluss der PUA auf das Transkriptom untersuchen, stellt diese Arbeit den ersten proteomischen Ansatz dar. Die Verknüpfung von molekularen Interaktionen mit zellulären, physiologischen bis hin zu ökologischen Konsequenzen ist eine komplexe, interdisziplinäre Aufgabe, die weiterer Forschung bedarf und auch auf die allgemeine Wirkung von Oxylipinen ausgeweitet werden sollte. Die hier eingeführten Sonden und Methoden bilden wertvolle und vielfältige Werkzeuge, um dieses übergreifende Ziel zu verfolgen.

8   REFERENCES

1.   Falkowski PG, Katz ME, Knoll AH, Quigg A, Raven JA, Schofield O, et al. The evolution of modern eukaryotic phytoplankton. *Science*. **2004**; *305*(5682):354–360.

2.   Nelson DM, Tréguer P, Brzezinski MA, Leynaert A, Quéguiner B. Production and dissolution of biogenic silica in the ocean: Revised global estimates, comparison with regional data and relationship to biogenic sedimentation. *Global Biogeochem Cycles*. **1995**; *9*(3):359–372.

3.   Atlantik FM (2011). Algal bloom. Available: http://www.atlantic.fm/news/cornwall-news/fifty-mile-long-algae-lurking-off-the-cornish-coast-1319 . Accessed 18 Mar 2011.

4.   Stueber K. (2007). Kunstformen der Natur von Ernst Haeckel, Diatomeen. Available: http://caliban.mpiz-koeln.mpg.de/haeckel/kunstformen/. Accessed 15 Dec 2015.

5.   Nejstgaard JC, Båmstedt U, Bagøien E, Solberg PT. Algal constraints on copepod grazing. Growth state, toxicity, cell size, and season as regulating factors. *ICES J Mar Sci*. **1995**; *52*(3-4):347–357.

6.   Smithonian National Museum of Natural History (March 16, 2012): The World of copepods. Available: http://invertebrates.si.edu/copepod/. Accessed 16 Dec 2015.

7.   Hardy, AC. Fish and Fisheries, Chapters on Whales, Turtles and Animals of the Sea Floor. London: Collins; **1959**.

8.   Hamm CE, Merkel R, Springer O, Jurkojc P, Maier C, Prechtel K, et al. Architecture and material properties of diatom shells provide effective mechanical protection. *Nature*. **2003**; *421*(6925):841–843.

9.   Wolfe GV. The chemical defense ecology of marine unicellular plankton: constraints, mechanisms, and impacts. *Biol Bull*. **2000**; *198*(2):225–244.

10.   Bates SS. Domoic-acid-producing diatoms: another genus added! *J Phycol*. **2000**; *36*(6):978–983.

11.   Mos L. Domoic acid: a fascinating marine toxin. *Environ Toxicol Pharmacol*. **2001**; *9*(3):79–85.

12.   Pohnert G. Chemical defense strategies of marine organisms. *Top Curr Chem*. **2004**; *239*:179–219.

13.   Schwartz ER, Poulin RX, Mojib N, Kubanek J. Chemical ecology of marine plankton. *Nat Prod Rep*. **2016**; *doi:10.1039/C6NP00015K.*

14.   Zimmer RK, Ferrer RP. Neuroecology, chemical defense, and the keystone species concept. *The Biological Bulletin*. **2007**; *213*(3):208–225.

15.   Tammilehto A, Nielsen TG, Krock B, Møller EF, Lundholm N. Induction of domoic acid production in the toxic diatom *Pseudo-nitzschia seriata* by calanoid copepods. *Aquat Toxicol*. **2015**; *159*:52-61.

16.   Selander E, Thor P, Toth G, Pavia H. Copepods induce paralytic shellfish toxin production in marine dinoflagellates. *Proc Roy Soc B*. **2006**; *273*(1594):1673–1680.

17.   Wolfe GV, Steinke M, Kirst GO. Grazing-activated chemical defence in a unicellular marine alga. *Nature*. **1997**; *387*(6636):894–897.

18.   Kathryn LVA, Letise TH. Dimethylsulfide release during macroinvertebrate grazing and its role as an activated chemical defense. *Mar Ecol Prog Ser*. **2003**; *250*:175–181.

19. Pohnert G. Phospholipase A$_2$ activity triggers the wound-activated chemical defense in the diatom *Thalassiosira rotula*. *Plant Physiol*. **2002**; *129*(1):103–111.

20. Pohnert G. Wound-activated chemical defense in unicellular planktonic algae. *Angew Chem Int Ed*. **2000**; *39*(23):4352–4354.

21. Ianora A, Miralto A. Toxigenic effects of diatoms on grazers, phytoplankton and other microbes: a review. *Ecotoxicology*. **2010**; *19*(3):493–511.

22. Miralto A, Barone G, Romano G, Poulet SA, Ianora A, Russo GL, et al. The insidious effect of diatoms on copepod reproduction. *Nature*. **1999**; *402*(6758):173–176.

23. Pohnert G, Lumineau O, Cueff A, Adolph S, Cordevant C, Lange M, et al. Are volatile unsaturated aldehydes from diatoms the main line of chemical defence against copepods? *Mar Ecol Prog Ser*. **2002**; *245*(33–45).

24. Bartual A, Arandia-Gorostidi N, Cózar A, Morillo-García S, Ortega M, Vidal M, et al. Polyunsaturated aldehydes from large phytoplankton of the Atlantic Ocean surface (42°N to 33°S). *Mar Drugs*. **2014**; *12*(2):682–699.

25. Vidoudez C, Casotti R, Bastianini M, Pohnert G. Quantification of dissolved and particulate polyunsaturated aldehydes in the Adriatic Sea. *Mar Drugs*. **2011**; *9*(4):500–513.

26. Wichard T, Poulet SA, Halsband-Lenk C, Albaina A, Harris R, Liu D, et al. Survey of the chemical defence potential of diatoms: Screening of fifty species for α,β,γ,δ-unsaturated aldehydes. *J Chem Ecol*. **2005**; *31*(4):949–958.

27. Wendel T, Jüttner F. Lipoxygenase-mediated formation of hydrocarbons and unsaturated aldehydes in freshwater diatoms. *Phytochem*. **1996**; *41*(6):1445–1449.

28. Hansen E, Eilertsen HC. Do the polyunsaturated aldehydes produced by *Phaeocystis pouchetii* (Hariot) Lagerheim influence diatom growth during the spring bloom in Northern Norway? *J Plankton Res*. **2007**; *29*(1):87–96.

29. Alsufyani T, Engelen AH, Diekmann OE, Kuegler S, Wichard T. Prevalence and mechanism of polyunsaturated aldehydes production in the green tide forming macroalgal genus Ulva (Ulvales, Chlorophyta). *Chem Phys Lipids*. **2014** Oct; *183*:100–109.

30. Akakabe Y, Washizu K, Matsui K, Kajiwara T. Concise synthesis of (8*Z*,11*Z*,14*Z*)-8,11,14-heptadecatrienal, (7*Z*,10*Z*,13*Z*)-7,10,13-hexadecatrienal, and (8*Z*,11*Z*)-8,11-heptadecadienal, components of the essential oil of marine green alga *Ulva pertusa*. *Biosci Biotechnol Biochem*. **2005**; *69*(7):1348–1352.

31. Croisier E, Rempt M, Pohnert G. Survey of volatile oxylipins and their biosynthetic precursors in bryophytes. *Phytochemistry*. **2010**; *71*(5–6):574–580.

32. Ponce De León I, Hamberg M, Castresana C. Oxylipins in moss development and defense. *Frontiers in Plant Science*. **2015**; *6*:483.

33. Boosfeld J, Vitzthum OG. Unsaturated aldehydes identification from green coffee. *J Food Sci*. **1995**; *60*(5):1092–1096.

34. Moshonas MG, Shaw PE. Isolation of *trans,trans*-2,4-decadienal and intermedeol from cold-pressed citrus oils. *J Agric Food Chem*. **1979**; *27*(1):210-211.

35. Andrianarison R-H, Rabinovitch-Chable H, Beneytout JL. Oxodiene formation during the *Vicia sativa* lipoxygenase-catalyzed reaction: Occurrence of dioxygenase and fatty acid lyase activities associated in a single protein. *Biochem Biophys Res Commun*. **1991**; *180*(2):1002-1009.

36. Boevé J-L, Gfeller H, P. Schlunegger U, Francke W. The secretion of the ventral glands in *Hoplocampa* sawfly larvae. *Biochem Syst Ecol*. **1997**; *25*(3):195–201.

37. Cheng L, Roussis V. Sex attractant in the marine insect *Trochopus plumbeus* (Heteroptera: Veliidae): a preliminary report. *Mar Ecol Prog Ser*. **1998**; *170*:83–286.

38.   Glasgow WC, Harris TM, Brash AR. A short-chain aldehyde is a major lipoxygenase product in arachidonic acid-stimulated porcine leukocytes. *J Biol Chem*. **1986**; *261*(1):200–204.

39.   Schieberle P, Grosch W. Potent odorants of the wheat bread crumb differences to the crust and effect of a longer dough fermentation. *Eur Food Res Technol*. **1991**; *192*(2):130–135.

40.   Yoshiwa T, Morimoto K, Sakamoto K, Ishikawa Y, Tokita M, Morita M. Volatile compounds of fishy odor in sardine by simultaneous distillation and extraction under reduced pressure. *Nippon Suisan Gakkaishi*. **1997**; *63*(2):222–230.

41.   Kerler J, Grosch W. Character impact odorants of boiled chicken: changes during refrigerated storage and reheating. *Eur Food Res Technol*. **1997**; *205*(3):232–238.

42.   Chang LW, Lo W-S, Lin P. *Trans,trans*-2,4-decadienal, a product found in cooking oil fumes, induces cell proliferation and cytokine production due to reactive oxygen species in human bronchial epithelial cells. *Toxicol Sci*. **2005**; *87*(2):337–343.

43.   Pohnert G. Diatom/copepod interactions in plankton: The indirect chemical defense of unicellular algae. *ChemBioChem*. **2005**; *6*:1–14.

44.   Wichard T, Gerecht A, Boersma M, Poulet SA, Wiltshire K, Pohnert G. Lipid and fatty acid composition of diatoms revisited: Rapid wound-activated change of food quality parameters influences herbivorous copepod reproductive success. *ChemBioChem*. **2007**; *8*(10):1146–1153.

45.   Fontana A, d'Ippolito G, Cutignano A, Romano G, Lamari N, Massa Gallucci A, et al. LOX-induced lipid peroxidation mechanism responsible for the detrimental effect of marine diatoms on zooplankton grazers. *ChemBioChem*. **2007**; *8*(15):1810–1818.

46.   d'Ippolito G, Tucci S, Cutignano A, Romano G, Cimino G, Miralto A, et al. The role of complex lipids in the synthesis of bioactive aldehydes of the marine diatom *Skeletonema costatum*. *BBA Molecular and cell biology of lipids*. **2004**; *1686*(1–2):100–107.

47.   d'Ippolito G, Romano G, Caruso T, Spinella A, Cimino G, Fontana A. Production of octadienal in the marine diatom *Skeletonema costatum*. *Org Lett*. **2003**; *5*(6):885–887.

48.   d'Ippolito G CA, Tucci S, Romano G, Cimino G, Fontana A. Biosynthetic intermediates and stereochemical aspects of aldehyde biosynthesis in the marine diatom *Thalassiosira rotula*. *Phytochemistry* **2006**; *67*(3):314-322.

49.   Pohnert G, Adolph S, Wichard T. Short synthesis of labeled and unlabeled 6*Z*,9*Z*,12*Z*,15-hexadecatetraenoic acid as metabolic probes for biosynthetic studies on diatoms. *Chem Phys Lipids*. **2004**; *131*:159–166.

50.   Spiteller D, Spiteller G. Identification of toxic 2,4-decadienal in oxidized, low-density lipoprotein by solid-phase microextraction. *Angew Chem Int Ed*. **2000**; *39*(3):583–585.

51.   Adolph S, Poulet SA, Pohnert G. Synthesis and biological activity of α,β,γ,δ-unsaturated aldehydes from diatoms. *Tetrahedron*. **2003**; *59*(17):3003–3008.

52.   Cutignano A, d'Ippolito G, Romano G, Lamari N, Cimino G, Febbraio F, et al. Chloroplastic glycolipids fuel aldehyde biosynthesis in the marine diatom *Thalassiosira rotula*. *ChemBioChem*. **2006**; *7*(3):450–456.

53.   Barofsky A, Pohnert G. Biosynthesis of polyunsaturated short chain aldehydes in the diatom *Thalassiosira rotula*. *Org Lett*. **2007**; *9*(6):1017–1020.

54.   Wichard T, Pohnert G. Formation of halogenated medium chain hydrocarbons by a lipoxygenase/hydroperoxide halolyase-mediated transformation in planktonic microalgae. *J Am Chem Soc*. **2006**; *128*(22):7114–7115.

55.   Caldwell G. The influence of bioactive oxylipins from marine diatoms on invertebrate reproduction and development. *Mar Drugs*. **2009**; *7*(3):367–400.

56.   Ianora A, Miralto A, Poulet SA, Carotenuto Y, Buttino I, Romano G, et al. Aldehyde suppression of copepod recruitment in blooms of a ubiquitous planktonic diatom. *Nature*. **2004**; *429*(6990):403–407.

57.   Leflaive J, Ten-Hage L. Chemical interactions in diatoms: role of polyunsaturated aldehydes and precursors. *New Phytol*. **2009**; *184*(4):794–805.

58.   Ban S, Burns C, Castel J, Chaudron Y, Christou E, Escribano R, et al. The paradox of diatom-copepod interactions. *Mar Ecol Prog Ser*. **1997**; *157*:287–293.

59.   Buttino I, De Rosa G, Carotenuto Y, Mazzella M, Ianora A, Esposito F, et al. Aldehyde-encapsulating liposomes impair marine grazer survivorship. *J Exp Biol*. **2008**; *211*(9):1426–1433.

60.   Adolph S, Bach S, Blondel M, Cueff A, Moreau M, Pohnert G, et al. Cytotoxicity of diatom-derived oxylipins in organisms belonging to different phyla. *J Exp Biol*. **2004**; *207*(17):2935–2946.

61.   Poulet SA, Wichard T, Ledoux JB, Lebreton B, Marchetti J, Dancie C, et al. Influence of diatoms on copepod reproduction. I. Field and laboratory observations related to *Calanus helgolandicus* egg production. *Mar Ecol Prog Ser*. **2006**; *308*:129–142.

62.   Wichard T, Poulet SA, Boulesteix A-L, Ledoux JB, Lebreton B, Marchetti J, et al. Influence of diatoms on copepod reproduction. II. Uncorrelated effects of diatom-derived α,β,γ,δ-unsaturated aldehydes and polyunsaturated fatty acids on *Calanus helgolandicus* in the field. *Prog Oceanogr*. **2008**; *77*(1):30–44.

63.   Jónasdóttir S, Dutz J, Koski M, Yebra L, Jakobsen, HH. Extensive cross-disciplinary analysis of biological and chemical control of *Calanus finmarchicus* reproduction during an aldehyde forming diatom bloom in mesocosms. *Mar Biol*. **2011**; *158*(9):1943–1963.

64.   Poulet S, Cueff A, Wichard T, Marchetti J, Dancie C, Pohnert G. Influence of diatoms on copepod reproduction. III. Consequences of abnormal oocyte maturation on reproductive factors in *Calanus helgolandicus*. *Mar Biol*. **2007**; *152*(2):415–428.

65.   Koski M, Wichard T, Jónasdóttir S. "Good" and "bad" diatoms: development, growth and juvenile mortality of the copepod *Temora longicornis* on diatom diets. *Mar Biol*. **2008**; *154*(4):719–734.

66.   Lauritano C, Romano G, Roncalli V, Amoresano A, Fontanarosa C, Bastianini M, et al. New oxylipins produced at the end of a diatom bloom and their effects on copepod reproductive success and gene expression levels. *Harmful Algae*. **2016**; *55*:221–229.

67.   Jónasdóttir SH, Kiørboe T. Copepod recruitment and food composition: do diatoms affect hatching success? *Mar Biol*. **1996**; *125*(4):743–750.

68.   Dutz J, Koski M, Jónasdóttir SH. Copepod reproduction is unaffected by diatom aldehydes or lipid composition. *Limnol Oceanogr*. **2008**; *53*(1):225–235.

69.   Vidoudez C, Pohnert G. Growth phase-specific release of polyunsaturated aldehydes by the diatom *Skeletonema marinoi*. *J Plankton Res*. **2008**; *30*(11):1305–1313.

70.   Vidoudez C, Nejstgaard JC, Jakobsen HH, Pohnert G. Dynamics of dissolved and particulate polyunsaturated aldehydes in mesocosms inoculated with different densities of the diatom *Skeletonema marinoi*. *Mar Drugs*. **2011**; *9*(3):345–358.

71.   Vardi A, Formiggini F, Casotti R, De Martino A, Ribalet F, Miralto A, et al. A stress surveillance system based on calcium and nitric oxide in marine diatoms. *PLoS Biol*. **2006**; *4*(3):411–419.

72.   d'Ippolito G, Lamari N, Montresor M, Romano G, Cutignano A, Gerecht A, et al. 15S-Lipoxygenase metabolism in the marine diatom *Pseudo-nitzschia delicatissima*. *The New Phytologist*. **2009**; *183*(4):1064–1071.

73. Dicke M, Sabelis MW. Infochemical terminology: Based on cost-benefit analysis rather than origin of compounds? *Funct Ecol*. **1988**; *2*(2):131–139.

74. Casotti R, Mazza S, Brunet C, Vantrepotte V, Ianora A, Miralto A. Growth inhibition and toxicity of the diatom aldehyde 2-*trans*,4-*trans*-decadienal on *Thalassiosira weissflogii* (bacillariophyceae) *J Phycol*. **2005**; *41*(1):7–20.

75. Ribalet F, Berges JA, Ianora A, Casotti R. Growth inhibition of cultured marine phytoplankton by toxic algal-derived polyunsaturated aldehydes. *Aquat Toxicol*. **2007**; *85*(3):219–227.

76. Ribalet F, Intertaglia L, Lebaron P, Casotti R. Differential effect of three polyunsaturated aldehydes on marine bacterial isolates. *Aquat Toxicol*. **2008**; *86*(2):249–255.

77. Lee SE, Park YS. Role of lipid peroxidation-derived α,β-unsaturated aldehydes in vascular dysfunction. *Oxid Med Cell Longev*. **2013**; *doi: 10.1155/2013/629028.*

78. Jacobs AT, Marnett LJ. Systems analysis of protein modification and cellular responses induced by electrophile stress. *Acc Chem Res*. **2010**; *43*(5):673–683.

79. Schwöbel JAH, Koleva YK, Enoch SJ, Bajot F, Hewitt M, Madden JC, et al. Measurement and estimation of electrophilic reactivity for predictive toxicology. *Chem Rev*. **2011**; *111*(4):2562–2596.

80. Böhme A, Thaens D, Schramm F, Paschke A, Schüürmann G. Thiol reactivity and its impact on the ciliate toxicity of α,β-unsaturated aldehydes, ketones, and esters. *Chem Res Toxicol*. **2010**; *23*(12):1905–1912.

81. Koleva YK, Madden JC, Cronin MTD. Formation of categories from structure-activity relationships to allow read-across for risk assessment: Toxicity of α,β-unsaturated carbonyl compounds. *Chem Res Toxicol*. **2008**; *21*(12):2300–2312.

82. Carry FA. Organic chemistry. 4th ed. New York: McGraw-Hill; **2000**.

83. Schwetlick K. Organikum. 21st ed. Weinheim: Wiley-VHC; **2001**.

84. Schwöbel JAH, Wondrousch D, Koleva YK, Madden JC, Cronin MTD, Schüürmann G. Prediction of Michael-type acceptor reactivity toward glutathione. *Chem Res Toxicol*. **2010**; *23*(10):1576–1585.

85. Sayre LM, Lin d, Yuan Q, Zhu X, Tang X. Protein adducts generated from products of lipid oxidation: Focus on HNE and ONE. *Drug Metab Rev*. **2006**; *38*(4):651–675.

86. Zhu X, Tang X, Zhang J, Tochtrop GP, Anderson VE, Sayre LM. Mass spectrometric evidence for the existence of distinct modifications of different proteins by 2(*E*),4(*E*)-decadienal. *Chem Res Toxicol*. **2010**; *23*(3):467–473.

87. Sigolo CAO, Di Mascio P, Medeiros MHG. Covalent modification of cytochrome *c* exposed to *trans*,*trans*-2,4-decadienal. *Chem Res Toxicol*. **2007**; *20*(8):1099–1110.

88. Loureiro APM, de Arruda Campos IP, Gomes OF, Di Mascio P, Medeiros MHG. Structural characterization of diastereoisomeric ethano adducts derived from the reaction of 2'-deoxyguanosine with *trans*,*trans*-2,4-decadienal. *Chem Res Toxicol*. **2004**; *17*(5):641–649.

89. Loureiro APM, Di Mascio P, Gomes OF, Medeiros MHG. *trans*,*trans*-2,4-Decadienal-induced 1,N^2-etheno-2'-deoxyguanosine adduct formation. *Chem Res Toxicol*. **2000**; *13*(7):601–609.

90. Singh M, Kapoor A, Bhatnagar A. Oxidative and reductive metabolism of lipid-peroxidation derived carbonyls. *Chem Biol Interact*. **2015**; *234*:261–273.

91. Boobis AR, Cohen SM, Dellarco V, McGregor D, Meek ME, Vickers C, et al. IPCS framework for analyzing the relevance of a cancer mode of action for humans. *Crit Rev Toxicol*. **2006**; *36*(10):781–792.

92. Carlson EE. Natural products as chemical probes. *ACS Chemical Biology*. **2010**; *5*(7):639–653.

93.   Tosti E, Romano G, Buttino I, Cuomo A, Ianora A, Miralto A. Bioactive aldehydes from diatoms block the fertilization current in ascidian oocytes. *Mol Reprod Dev*. **2003**; *66*(1):72–80.

94.   Hansen E, Even Y, Genevière A-M. The $\alpha,\beta,\gamma,\delta$-unsaturated aldehyde 2-*trans*-4-*trans*-decadienal disturbs DNA replication and mitotic events in early sea urchin embryos. *Toxicol Sci*. **2004**; *81*(1):190–197.

95.   Romano G, Russo GL, Buttino I, Ianora A, Miralto A. A marine diatom-derived aldehyde induces apoptosis in copepod and sea urchin embryos. *J Exp Biol*. **2003**; *206*(19):3487–3494.

96.   Ruocco N, Varrella S, Romano G, Ianora A, Bentley MG, Somma D, et al. Diatom-derived oxylipins induce cell death in sea urchin embryos activating caspase-8 and caspase 3/7. *Aquat Toxicol*. **2016**; *176*:128–140.

97.   Vardi A, Bidle KD, Kwityn C, Hirsh DJ, Thompson SM, Callow JA, et al. A diatom gene regulating nitric-oxide signaling and susceptibility to diatom-derived aldehydes. *Curr Biol*. **2008**; *18*(12):895–899.

98.   Lauritano C, Borra M, Carotenuto Y, Biffali E, Miralto A, Procaccini G, et al. First molecular evidence of diatom effects in the copepod *Calanus helgolandicus*. *J Exp Mar Biol Ecol*. **2011**; *404*(1-2):79–86.

99.   Lauritano C, Carotenuto Y, Miralto A, Procaccini G, Ianora A. Copepod population-specific response to a toxic diatom diet. *PLoS ONE*. **2012**; *7*(10):e47262.

100.   Lauritano C, Borra M, Carotenuto Y, Biffali E, Miralto A, Procaccini G, et al. Molecular evidence of the toxic effects of diatom diets on gene expression patterns in copepods. *PLoS ONE*. **2011**; *6*(10):e26850.

101.   Varrella S, Romano G, Costantini S, Ruocco N, Ianora A, Bentley MG, et al. Toxic diatom aldehydes affect defence gene networks in sea urchins. *PLoS ONE*. **2016**; *11*(2):e0149734.

102.   Gallina AA, Brunet C, Palumbo A, Casotti R. The effect of polyunsaturated aldehydes on *Skeletonema marinoi* (bacillariophyceae): The involvement of reactive oxygen species and nitric oxide. *Mar Drugs*. **2014**; *12*(7):4165–4187.

103.   Gallina AA, Chung C-C, Casotti R. Expression of death-related genes and reactive oxygen species production in *Skeletonema tropicum* upon exposure to the polyunsaturated aldehyde octadienal. *Adv Oceanol Limnol* **2015**; *6*(1/2):13–20.

104.   Gallina AA, Palumbo A, Casotti R. Oxidative pathways in response to polyunsaturated aldehydes in the marine diatom *Skeletonema marinoi* (Bacillariophyceae). *J Phycol*. **2016**:accepted for publication.

105.   Greenbaum D, Medzihradszky KF, Burlingame A, Bogyo M. Epoxide electrophiles as activity-dependent cysteine protease profiling and discovery tools. *Chem Biol*. **2000**; *7*(8):569–581.

106.   Liu Y, Patricelli MP, Cravatt BF. Activity-based protein profiling: The serine hydrolases. *Proc Natl Acad Sci U S A*. **1999**; *96*(26):14694–14699.

107.   Sieber SA, Cravatt BF. Analytical platforms for activity-based protein profiling - exploiting the versatility of chemistry for functional proteomics. *Chem Commun*. **2006**; (22):2311–2319.

108.   Uttamchandani M, Li J, Sun H, Yao SQ. Activity-based protein profiling: New developments and directions in functional proteomics. *ChemBioChem*. **2008**; *9*(5):667–675.

109.   Evans MJ, Cravatt BF. Mechanism-based profiling of enzyme families. *Chem Rev*. **2006**; *106*(8):3279–3301.

110.   Weerapana E, Simon GM, Cravatt BF. Disparate proteome reactivity profiles of carbon electrophiles. *Nat Chem Biol*. **2008**; *4*:405–407.

111. Böttcher T, Pitscheider M, Sieber SA. Natural products and their biological targets: Proteomic and metabolomic labeling strategies. *Angew Chem Int Ed*. **2010**; *49*(15):2680–2698.

112. Speers AE, Cravatt BF. Profiling enzyme activities in vivo using click chemistry methods. *Chem Biol*. **2004**; *11*(4):535–546.

113. Speers AE, Cravatt BF. A tandem orthogonal proteolysis strategy for high-content chemical proteomics. *J Am Chem Soc*. **2005**; *127*(28):10018–10019.

114. Golkowski M, Pergola C, Werz O, Ziegler T. Strategy for catch and release of azide-tagged biomolecules utilizing a photolabile strained alkyne construct. *Org Biomol Chem*. **2012**; *10*(23):4496–4499.

115. Staub I, Sieber SA. β-Lactams as selective chemical probes for the in vivo labeling of bacterial enzymes involved in cell wall biosynthesis, antibiotic resistance, and virulence. *J Am Chem Soc*. **2008**; *130*(40):13400–13409.

116. Sieber SA. Activity-Based Protein Profiling. 1st ed. Berlin, Heidelberg: Springer-Verlag; **2011**.

117. Weerapana E, Speers AE, Cravatt BF. Tandem orthogonal proteolysis-activity-based protein profiling (TOP-ABPP): a general method for mapping sites of probe modification in proteomes. *Nat Protocols*. **2007**; *2*(6):1414–1425.

118. Kolb HC, Finn MG, Sharpless KB. Click chemistry: Diverse chemical function from a few good reactions. *Angew Chem Int Ed*. **2001**; *40*(11):2004–2021.

119. Grammel M, Hang HC. Chemical reporters for biological discovery. *Nat Chem Biol*. **2013**; *9*(8):475–484.

120. Saxon E, Bertozzi CR. Cell surface engineering by a modified Staudinger reaction. *Science*. **2000**; *287*(5460):2007–2010.

121. Lim VRK, Qing L. Bioorthogonal chemistry: a covalent strategy for the study of biological systems. *Science China-Chemistry*. **2010**; *53*(1):61–70.

122. Gersch M, Kreuzer J, Sieber SA. Electrophilic natural products and their biological targets. *Nat Prod Rep*. **2012**; *29*(6):659–682.

123. Staub I, Sieber SA. β-Lactam probes as selective chemical-proteomic tools for the identification and functional characterization of resistance associated enzymes in MRSA. *J Am Chem Soc*. **2009**; *131*(17):6271–6276.

124. Steen H, Mann M. The abc's (and xyz's) of peptide sequencing. *Nat Rev Mol Cell Biol*. **2004**; *5*(9):699–711.

125. Bilbao A, Varesio E, Luban J, Strambio-De-Castillia C, Hopfgartner G, Müller M, et al. Processing strategies and software solutions for data-independent acquisition in mass spectrometry. *Proteomics*. **2015**; *15*(5-6):964–980.

126. Okerberg ES, Wu J, Zhang B, Samii B, Blackford K, Winn DT, et al. High-resolution functional proteomics by active-site peptide profiling. *Proc Natl Acad Sci U S A*. **2005**; *102*(14):4996–5001.

127. Sieber SA, Mondala TS, Head SR, Cravatt BF. Microarray platform for profiling enzyme activities in complex proteomes. *J Am Chem Soc*. **2004** 2; *126*(48):15640–15641.

128. Speers AE, Adam GC, Cravatt BF. Activity-based protein profiling in vivo using a copper(I)-catalyzed azide-alkyne [3 + 2] cycloaddition. *J Am Chem Soc*. **2003**; *125*(16):4686–4687.

129. Prescher JA, Bertozzi CR. Chemistry in living systems. *Nat Chem Biol*. **2005**; *1*(1):13–21.

130. Sadaghiani AM, Verhelst SHL, Bogyo M. Tagging and detection strategies for activity-based proteomics: Proteomics and genomics. *Curr Opin Chem Biol*. **2007**; *11*(1):20–28.

131. Haugland RP. Handbook of fluorescent probes and research products. 9th ed. Eugene: Molecular Probes Inc; **2002**.

132.   Baruch A, Jeffery DA, Bogyo M. Enzyme activity - it's all about image. *Trends Cell Biol*. **2004**; *14*(1):29–35.

133.   Ross PL, Huang YN, Marchese JN, Williamson B, Parker K, Hattan S, et al. Multiplexed protein quantitation in *Saccharomyces cerevisiae* using amine-reactive isobaric tagging reagents. *Mol Cell Proteomics*. **2004**; *3*(12):1154–1169.

134.   Gygi SP, Rist B, Gerber SA, Turecek F, Gelb MH, Aebersold R. Quantitative analysis of complex protein mixtures using isotope-coded affinity tags. *Nat Biotech*. **1999**; *17*(10):994–999.

135.   Weerapana E, Wang C, Simon GM, Richter F, Khare S, Dillon MBD, et al. Quantitative reactivity profiling predicts functional cysteines in proteomes. *Nature*. **2010**; *468*(7325):790–795.

136.   Palaniappan KK, Pitcher AA, Smart BP, Spiciarich DR, Iavarone AT, Bertozzi CR. Isotopic signature transfer and mass pattern prediction (IsoStamp): An enabling technique for chemically-directed proteomics. *ACS Chemical Biology*. **2011**; *6*(8):829–836.

137.   Hernandez H, Niehauser S, Boltz SA, Gawandi V, Phillips RS, Amster IJ. Mass defect labeling of cysteine for improving peptide assignment in shotgun proteomic analyses. *Anal Chem*. **2006**; *78*(10):3417–3423.

138.   Miyagi M, Nakao M, Nakazawa T, Kato I, Tsunasawa S. A novel derivatization method with 5-bromonicotinic acid N-hydroxysuccinimide for determination of the amino acid sequences of peptides. *Rapid Commun Mass Spectrom*. **1998**; *12*(10):603–608.

139.   Goodlett DR, Bruce JE, Anderson GA, Rist B, Pasa-Tolic L, Fiehn O, et al. Protein identification with a single accurate mass of a cysteine-containing peptide and constrained database searching. *Anal Chem*. **2000**; *72*(6):1112–1118.

140.   Suzuki Y, Tanji N, Ikeda C, Honda A, Ookubo K, Citterio D, et al. Design and synthesis of labeling reagents (MS probes) for highly sensitive electrospray ionization mass spectrometry. *Anal Sci*. **2004**; *20*(3):475–482.

141.   Barry SJ, Carr RM, Lane SJ, Leavens WJ, Monté S, Waterhouse I. Derivatisation for liquid chromatography/electrospray mass spectrometry: synthesis of pyridinium compounds and their amine and carboxylic acid derivatives. *Rapid Commun Mass Spectrom*. **2003**; *17*(6):603–620.

142.   Barry SJ, Carr RM, Lane SJ, Leavens WJ, Manning CO, Monté S, et al. Use of S-pentafluorophenyl tris(2,4,6-trimethoxyphenyl)phosphonium acetate bromide and (4-hydrazino-4-oxobutyl) [tris(2,4,6-trimethoxyphenyl)phosphonium bromide for the derivatization of alcohols, aldehydes and ketones for detection by liquid chromatography/electrospray mass spectrometry. *Rapid Commun Mass Spectrom*. **2003**; *17*(5):484–497.

143.   Li M, Kinzer JA. Structural analysis of oligosaccharides by a combination of electrospray mass spectrometry and bromine isotope tagging of reducing-end sugars with 2-amino-5-bromopyridine. *Rapid Commun Mass Spectrom*. **2003**; *17*(13):1462–1466.

144.   Paulick MG, Hart KM, Brinner KM, Tjandra M, Charych DH, Zuckermann RN. Cleavable hydrophilic linker for one-bead-one-compound sequencing of oligomer libraries by tandem mass spectrometry. *J Comb Chem*. **2006**; *8*(3):417–426.

145.   Carlson EE, Cravatt BF. Enrichment tags for enhanced-resolution profiling of the polar metabolome. *J Am Chem Soc*. **2007**; *129*(51):15780–15782.

146.   Ribalet F BM, Vidoudez C, Acri F, Berges J, Ianora A, et al. Phytoplankton cell lysis associated with polyunsaturated aldehyde release in the northern Adriatic Sea. *PLoS ONE*. **2014**; *9*(5):e98727.

147. Wolfram S. Ungesättigte Aldehyde als metabolische Sonden, Friedrich Schiller University, Jena. *diploma thesis*. **2011**.

148. Bowler C, Allen AE, Badger JH, Grimwood J, Jabbari K, Kuo A, et al. The *Phaeodactylum* genome reveals the evolutionary history of diatom genomes. *Nature*. **2008**; *456*(7219):239–244.

149. Paffenhöfer GA, Ianora A, Miralto A, Turner JT, Kleppel GS, Ribera d'Alcalà M, et al. Colloquium on diatom-copepod interactions. *Mar Ecol Prog Ser* **2005**; *286*:293–305.

150. Calbet A. The trophic roles of microzooplankton in marine systems. *ICES J Mar Sci*. **2008**; *65*(3):325–331.

151. Calbet A, Saiz E. Effects of trophic cascades in dilution grazing experiments: from artificial saturated feeding responses to positive slopes. *J Plankton Res*. **2013**; *doi:10.1093/plankt/fbt067.*

152. Stoecker DK, Weigel A, Goes JI. Microzooplankton grazing in the Eastern Bering Sea in summer. *Deep Sea Res Part II: Top Stud Oceanogr*. **2014**; *109*:145–156.

153. Sarno D, Kooistra WHCF, Medlin LK, Percopo I, Zingone A. Diversity in the genus *Skeletonema* (bacillariophyceae). II. An assessment of the taxonomy of *S. costatum*-like species with the description of four new species. *J Phycol*. **2005**; *41*(1):151–176.

154. Hansen E, Ernstsen A, Eilertsen HC. Isolation and characterisation of a cytotoxic polyunsaturated aldehyde from the marine phytoplankter *Phaeocystis pouchetii* (Hariot) Lagerheim. *Toxicol*. **2004**; *199*(2–3):207–217.

155. Wichard T, Poulet SA, Pohnert G. Determination and quantification of α,β,γ,δ-unsaturated aldehydes as pentafluorobenzyl-oxime derivates in diatom cultures and natural phytoplankton populations: application in marine field studies. *J Chromatogr B*. **2005**; *814*(1):155–161.

156. d'Ippolito G, Iadicicco O, Romano G, Fontana A. Detection of short-chain aldehydes in marine organisms: the diatom *Thalassiosira rotula*. *Tetrahedron Lett*. **2002**; *43*(35):6137–6140.

157. Wichard T. Untersuchungen zur Lipoxygenase-vermittelten chemischen Verteidigung: Oxylipine aus Diatomeen und dem Moos *Physcomitrella patens*, Friedrich Schiller University, Jena. *doctoral thesis*. **2006**.

158. Vidoudez C, Nejstgaard JC, Jakobsen HH, Pohnert G. Dynamics of dissolved and particulate polyunsaturated aldehydes in mesocosms inoculated with different densities of the diatom *Skeletonema marinoi*. *Mar Drugs*. **2011**; *9*(3):345–358.

159. Dolan JR, Gallegos CL, Moigis A. Dilution effects on microzooplankton in dilution grazing experiments. *Mar Ecol Prog Ser*. **2000**; *200*:127–139.

160. Gerecht A, Carotenuto Y, Ianora A, Romano A, Fontana A, d'Ippolito A, et al. Oxylipin production during a mesocosm bloom of *Skeletonema marinoi*. *J Exp Mar Biol Ecol*. **2013**; *446*:159–165.

161. Paul C, Reunamo A, Lindehoff E, Bergkvist J, Mausz MA, Larsson H, et al. Diatom derived polyunsaturated aldehydes do not structure the planktonic microbial community in a mesocosm study. *Mar Drugs*. **2012**; *10*(4):775–792.

162. Edwards BR, Bidle KD, Van Mooy BAS. Dose-dependent regulation of microbial activity on sinking particles by polyunsaturated aldehydes: Implications for the carbon cycle. *Proc Natl Acad Sci U S A*. **2015**; *112*(19):5909–5914.

163. Ribalet F, Vidoudez C, Cassin D, Pohnert G, Ianora A, Miralto A, et al. High plasticity in the production of diatom-derived polyunsaturated aldehydes under nutrient limitation: Physiological and ecological implications. *Protist*. **2009**; *160*(3):444–451.

164. Paul C, Barofsky A, Vidoudez C, Pohnert G. Diatom exudates influence metabolism and cell growth of co-cultured diatom species. *Mar Ecol Prog Ser*. **2009**; *389*:61–70.

165. Buttino I, do Espirito Santo M, Ianora A, Miralto A. Rapid assessment of copepod (*Calanus helgolandicus*) embryo viability using fluorescent probes. *Mar Biol*. **2004**; *145*(2):393–399.

166. Blum G, von Degenfeld G, Merchant MJ, Blau HM, Bogyo M. Noninvasive optical imaging of cysteine protease activity using fluorescently quenched activity-based probes. *Nat Chem Biol*. **2007**; *3*(10):668–677.

167. Ianora A, Bentley MG, Caldwell GS, Casotti R, Cembella AD, Engström-Öst J, et al. The relevance of marine chemical ecology to plankton and ecosystem function: An emerging field. *Mar Drugs*. **2011**; *9*(9):1625–1648.

168. Salic A, Mitchison TJ. A chemical method for fast and sensitive detection of DNA synthesis in vivo. *Proc Natl Acad Sci U S A*. **2008**; *105*(7):2415–2420.

169. Cunningham CW, Mukhopadhyay A, Lushington GH, Blagg BSJ, Prisinzano TE, Krise JP. Uptake, distribution and diffusivity of reactive fluorophores in cells: Implications toward target identification. *Mol Pharm*. **2010**; *7*(4):1301–1310.

170. Falciatore A, Bowler C. Revealing the molecular secrets of marine diatoms. *Annu Rev Plant Biol*. **2002**; *53*(1):109–130.

171. Laabir M, Poulet AS, Cueff A, Ianora A. Effect of diet on levels of amino acids during embryonic and naupliar development of the copepod *Calanus helgolandicus*. *Mar Biol*. *134*(1):89–98.

172. Carvalho VM, Asahara F, Di Mascio P, de Arruda Campos IP, Cadet J, Medeiros MHG. Novel 1,N^6-etheno-2'-deoxyadenosine adducts from lipid peroxidation products. *Chem Res Toxicol*. **2000**; *13*(5):397–405.

173. Hacker M, Bachmann K, Messer M. Pharmacology: Principles and Practice. 1st ed; chapter 3: membranes and drug action. San Diego: Academic Press; **2009**.

174. Zheng Y, Quinn A, Sriram G. Experimental evidence and isotopomer analysis of mixotrophic glucose metabolism in the marine diatom *Phaeodactylum tricornutum*. *Microb Cell Fact*. **2013** Nov 14; *12*(1):1–17.

175. Buttino I, Ianora A, Carotenuto Y, Zupo V, Miralto A. Use of the confocal laser scanning microscope in studies on the developmental biology of marine crustaceans. *Microsc Res Tech*. **2003**; *60*(4):458–464.

176. Leandro S, Tiselius P, Queiroga H. Growth and development of nauplii and copepodites of the estuarine copepod *Acartia tonsa* from southern Europe (Ria de Aveiro, Portugal) under saturating food conditions. *Mar Biol*. **2006**; *150*(1):121–129.

177. Tiselius P, Hansen B, Jonsson P, Kiørboe T, Nielsen TG, Piontkovski S, et al. Can we use laboratory-reared copepods for experiments? A comparison of feeding behaviour and reproduction between a field and a laboratory population of *Acartia tonsa*. *ICES J Mar Sci*. **1995**; *52*(3-4):369–376.

178. Rao J, Dragulescu-Andrasi A, Yao H. Fluorescence imaging in vivo: recent advances. *Curr Opin Biotechnol*. **2007**; *18*(1):17–25.

179. Poulet SA, Ianora A, Miralto A, Meijer L. Do diatoms arrest embryonic development in copepods? *Mar Ecol Prog Ser*. **1994**; *111*:79–86.

180. Kiørboe T, Møhlenberg F, Hamburger K. Bioenergetics of the planktonic copepod *Acartia tonsa*: relation between feeding, egg production and respiration, and composition of specific dynamic action *Mar Ecol Prog Ser*. **1985**; *26*:85–87.

181. Willems LI, Overkleeft HS, van Kasteren SI. Current Developments in activity-based protein profiling. *Bioconjugate Chem*. **2014**; *25*(7):1181–1191.

182. Blum G, Mullins SR, Keren K, Fonovic M, Jedeszko C, Rice MJ, et al. Dynamic imaging of protease activity with fluorescently quenched activity-based probes. *Nat Chem Biol*. **2005**; *1*(4):203–209.

183. Bachovchin DA, Brown SJ, Rosen H, Cravatt BF. Identification of selective inhibitors of uncharacterized enzymes by high-throughput screening with fluorescent activity-based probes. *Nat Biotech*. **2009**; *27*(4):387–394.

184. Dillon MBC, Bachovchin DA, Brown SJ, Finn MG, Rosen H, Cravatt BF, et al. Novel inhibitors for PRMT1 discovered by high-throughput screening using activity-based fluorescence polarization. *ACS Chemical Biology*. **2012**; *7*(7):1198–1204.

185. Geurink PP, El Oualid F, Jonker A, Hameed DS, Ovaa H. A general chemical ligation approach towards isopeptide-linked ubiquitin and ubiquitin-like assay reagents. *ChemBioChem*. **2012**; *13*(2):293–297.

186. Thermo Fisher (2011). Anti-Tetramethylrhodamine and Anti-Texas Red Antibodies (PDF). Available: https://tools.thermofisher.com/content/sfs/manuals/mp06397.pdf. Accessed 15 Dec 2010.

187. GE Healthcare Life Sciences (2011). Instruction Protocol (PDF): Protein A Mag Sepharose, Protein G Mag Sepharose. Available: http://www.gelifesciences.com/webapp/wcs/stores/servlet/ProductDisplay?categoryId=11750&catalogId=10101&productId=22287&storeId=11762&langId=-1. Accessed 15 Dec 2010.

188. Waggoner A. Fluorescent labels for proteomics and genomics. *Curr Opin Chem Biol*. **2006**; *10*(1):62–66.

189. Meynier A, Rampon V, Dalgalarrondo M, Genot C. Hexanal and t-2-hexenal form covalent bonds with whey proteins and sodium caseinate in aqueous solution. *Int Dairy J*. **2004**; *14*(8):681–690.

190. O'Keefe SF, Wilson LA, Resurreccion AP, Murphy PA. Determination of the binding of hexanal to soy glycinin and β-conglycinin in an aqueous model system using a headspace technique. *J Agric Food Chem*. **1991**; *39*(6):1022–1028.

191. Blagg J, Workman P. Chemical biology approaches to target validation in cancer. *Curr Opin Pharmacol*. **2014**; *17*:87–100.

192. Liu XD, Shen YG. NaCl-induced phosphorylation of light harvesting chlorophyll a/b proteins in thylakoid membranes from the halotolerant green alga, *Dunaliella salina*. *FEBS Lett*. **2004**; *569*(1-3):337–340.

193. Gundermann K, Schmidt M, Weisheit W, Mittag M, Büchel C. Identification of several sub-populations in the pool of light harvesting proteins in the pennate diatom *Phaeodactylum tricornutum*. *Biochim Biophys Acta*. **2013** Mar; *1827*(3):303–310.

194. Yoshida M, Muneyuki E, Hisabori T. ATP synthase — a marvellous rotary engine of the cell. *Nat Rev Mol Cell Biol*. **2001**; *2*:669–677.

195. Groth G, Strotmann H. New results about structure, function and regulation of the chloroplast ATP synthase (CF_0CF_1). *Physiol Plant*. **1999**; *106*(1):142–148.

196. Lapaille M, Thiry M, Perez E, Gonzalez-Halphen D, Remacle C, Cardol P. Loss of mitochondrial ATP synthase subunit beta (Atp2) alters mitochondrial and chloroplastic function and morphology in *Chlamydomonas*. *Biochim Biophys Acta*. **2010**; *1797*(8):1533–1539.

197. Sprenger GA. Genetics of pentose-phosphate pathway enzymes of *Escherichia coli* K-12. *Arch Microbiol*. **1995**; *164*(5):324–330.

198. Brandes HK, Hartman FC, Lu T-YS, Larimer FW. Efficient expression of the gene for spinach phosphoribulokinase in *Pichia pastoris* and utilization of the recombinant enzyme to

explore the role of regulatory cysteinyl residues by site-directed mutagenesis. *J Biol Chem*. **1996**; *271*(11):6490–6496.

199. Maberly SC, Courcelle C, Groben R, Gontero B. Phylogenetically-based variation in the regulation of the Calvin cycle enzymes, phosphoribulokinase and glyceraldehyde-3-phosphate dehydrogenase, in algae. *J Exp Bot*. **2010**; *61*(3):735–745.

200. Porter MA, Hartman FC. Commonality of catalytic and regulatory sites of spinach phosphoribulokinase: Characterization of a tryptic peptide that contains an essential cysteinyl residue. *Biochemistry*. **1986**; *25*(23):7314–7318.

201. Lebreton S, Graciet E, Gontero B. Modulation, via protein-protein interactions, of glyceraldehyde-3-phosphate dehydrogenase activity through redox phosphoribulokinase regulation. *J Biol Chem*. **2003**; *278*(14):12078–12084.

202. Chew E-H, Nagle AA, Zhang Y, Scarmagnani S, Palaniappan P, Bradshaw TD, et al. Cinnamaldehydes inhibit thioredoxin reductase and induce Nrf2: potential candidates for cancer therapy and chemoprevention. *Free Radical Biol Med*. **2010**; *48*(1):98–111.

203. Schenone M, Dancik V, Wagner BK, Clemons PA. Target identification and mechanism of action in chemical biology and drug discovery. *Nat Chem Biol*. **2013**; *9*(4):232–240.

204. Daboussi F, Leduc S, Maréchal A, Dubois G, Guyot V, Perez-Michaut C, et al. Genome engineering empowers the diatom *Phaeodactylum tricornutum* for biotechnology. *Nat Commun*. **2014**; *5*:3831.

205. Trevisani M, Siemens J, Materazzi S, Bautista DM, Nassini R, Campi B, et al. 4-Hydroxynonenal, an endogenous aldehyde, causes pain and neurogenic inflammation through activation of the irritant receptor TRPA1. *Proceedings of the National Academy of Sciences*. **2007**; *104*(33):13519–13524.

206. Seifert C. Untersuchung von Planktoninteraktionen mit molekularen Sonden: Methoden der Präparation von Proteinproben für die 1D- und 2D-Gelelektrophorese, Friedrich Schiller University, Jena. *bachelor thesis*. **2014**.

207. Pfeifer-Leeg M. Modifizierte Oxylipine als Sonden zur mechanistischen Untersuchung von Planktoninteraktionen, Friedrich Schiller University, Jena. *diploma thesis*. **2012**.

208. Wermuth CG. The Practice of Medicinal Chemistry, Chapter 2: Definitions and objectives, drug activity phases, drug classification systems. 3rd ed. New York: Academic Press; **2008**.

209. McDonald RI, Guilinger JP, Mukherji S, Curtis EA, Lee WI, Liu DR. Electrophilic activity-based RNA probes reveal a self-alkylating RNA for RNA labeling. *Nat Chem Biol*. **2014**; *10*(12):1049–1054.

210. Lembke C. Molecular probes for the elucidation of diatom communication and defense mechanisms, Friedrich Schiller University, Jena. *master thesis*. **2013**.

211. Hong V, Presolski SI, Ma C, Finn MG. Analysis and optimization of copper-catalyzed azide–alkyne cycloaddition for bioconjugation. *Angew Chem Int Ed*. **2009**; *48*(52):9879–9883.

212. Täuscher E. Beiträge zur Chemie der 4-Hydroxy-1,3-Thiazole, Friedrich Schiller University, Jena. *doctoral thesis*. **2012**.

213. Valeur B. Molecular Fluorescence: Principles and Applications. 1st ed. Weinheim-New York-Chichester-Brisbane-Singapore-Toronto: Wiley-VCH; **2001**.

214. Guo K, Li L. Differential ^{12}C-/^{13}C-isotope dansylation labeling and fast liquid chromatography/mass spectrometry for absolute and relative quantification of the metabolome. *Anal Chem*. **2009**; *81*(10):3919–3932.

215. Hall MP, Schneider LV. Isotope-differentiated binding energy shift tags (IDBEST™) for improved targeted biomarker discovery and validation. *Expert Rev Proteomics*. **2004**; *1*(4):421–431.

216.   Paul C, Pohnert G. Production and role of volatile halogenated compounds from marine algae. *Nat Prod Rep*. **2011**; *28*(2):186–195.

217.   Grimvall A, De Leer WB. Naturally-produced organohalogens. Dordrecht, Boston: Kluwer Academic, **1995**.

9 SELBSTSTÄNDIGKEITSERKLÄRUNG

Ich erkläre, dass ich die vorliegende Arbeit selbständig und unter Verwendung der angegebenen Hilfsmittel, persönlichen Mitteilungen und Quellen angefertigt habe.

Pößneck, den

Stefanie Wolfram

10 WEITERE ERKLÄRUNGEN

Erklärung zu den Eigenanteilen der Promovendin sowie der weiteren Doktoranden/ Doktorandinnen als Koautoren an den Publikationen und Zweitpublikationsrechten bei einer kumulativen Dissertation.

Für alle in dieser kumulativen Dissertation verwendeten Manuskripte liegen die notwendigen Genehmigungen der Verlage („Reprint permissions") für die Zweitpublikation vor.

Die Co-Autoren der in dieser kumulativen Dissertation verwendeten Manuskripte sind sowohl über die Nutzung, als auch über die oben angegebenen Eigenanteile (Kapitel 3) der weiteren Doktoranden/Doktorandinnen als Koautoren an den Publikationen und Zweitpublikationsrechten bei einer kumulativen Dissertation informiert und stimmen dem zu.

Die Anteile der Promovendin sowie der weiteren Doktoranden/Doktorandinnen als Co-Autoren an den Publikationen und Zweitpublikationsrechten bei einer kumulativen Dissertation sind in Kapitel 3 aufgeführt.

<div align="center">Pößneck, den</div>

_____

Stefanie Wolfram

Einverständniserklärung des Betreuers

Ich bin mit der Abfassung der Dissertation als publikationsbasiert, d.h. kumulativ, einverstanden und bestätige die vorstehenden Angaben. Eine entsprechend begründete Befürwortung mit Angabe des wissenschaftlichen Anteils der Doktorandin an den verwendeten Publikationen werde ich parallel an den Rat der Fakultät der Chemisch-Geowissenschaftlichen Fakultät richten.

<div align="center">Jena, den</div>

_____

Prof. Dr. Georg Pohnert